

JAERI - M
85-015

POST TEST ANALYSIS OF ROSA-III
DOUBLE-ENDED BREAK TEST RUN 901

February 1985

Hideo NAKAMURA, Yutaka KUKITA, Makoto AKINAGA*
and Kanji TAsAKA

JAERI-Mレポートは、日本原子力研究所が不定期に公刊している研究報告書です。
入手の問い合わせは、日本原子力研究所技術情報部情報資料課（〒319-11茨城県那珂郡東海村）あて、お申しこしてください。なお、このほかに財団法人原子力弘済会資料センター（〒319-11茨城県那珂郡東海村日本原子力研究所内）で複写による実費頒布をおこなっております。

JAERI-M reports are issued irregularly.

Inquiries about availability of the reports should be addressed to Information Division
Department of Technical Information, Japan Atomic Energy Research Institute, Tokai-
mura, Naka-gun, Ibaraki-ken 319-11, Japan.

©Japan Atomic Energy Research Institute, 1985

編集兼発行 日本原子力研究所
印刷 いばらき印刷株式会社

Post Test Analysis of ROSA-III Double-Ended Break Test RUN 901

Hideo NAKAMURA, Yutaka KUKITA, Makoto AKINAGA* and Kanji TASAKA

Department of Nuclear Safety Research,
Tokai Research Establishment, JAERI

(Received January 24, 1985)

The ROSA-III test facility is a volumetrically scaled (1/424) boiling water reactor (BWR) system with an electrically heated core. The purpose of ROSA-III experiment is to study the thermal-hydraulic behavior and the performance of the emergency core cooling system (ECCS) during a postulated loss-of-coolant accident (LOCA) and to provide the data base for the assessment and improvement of reactor safety analysis codes.

RUN 901 was a first ROSA-III experiment with the fourth fuel assembly and assumed a 200% double-ended break at the recirculation pump section line with full ECCS actuation. Post test analyses of RUN 901 were performed with the computer codes RELAP4J and RELAP5/MOD1/001.

The system pressure response calculated with the two codes agreed well with the data. The agreement was also good for the core inlet flow behavior until the beginning of the lower plenum flashing (LPF).

RELAP4J is a fast running code and calculated well the overall behavior of the mixture level in the core. However, the spray water was accumulated in the upper plenum (UP) due to the inability of the code to calculate counter current flow at the upper tie plate (UTP). While spray water was not accumulated in the upper plenum in the experiment.

RELAP5 with an advanced two-phase flow model calculated well the rewetting of the fuel after the LPF and the top-down quench after the uncovering of the whole core. However, the incorporation of a CCFL model and/or the improvement in the interphase drag correlations are necessary to be able to calculate the mixture level behavior more accurately. An

* Nippon Atomic Industry Group Co., Ltd.

appropriate discharge coefficient is also necessary to calculate the break flow accurately with the RELAP5 characteristic analysis break flow model.

Keywords: BWR, ROSA-III, LOCA, 200% Double-ended break, ECCS, RELAP4J, RELAP5/MOD1/001, TRAC-BD1, Analysis, Break Nozzles, Thermal Hydraulic Behavior, Reactor Safety

ROSA - III 両端破断実験 RUN 901 の実験後解析

日本原子力研究所東海研究所安全工学部
中村秀夫・久木田豊・秋永 誠*・田坂完二

(1985年1月24日受理)

ROSA-III実験装置は、電気加熱の模擬炉心を有する、1/424の沸騰水型原子炉(BWR)模擬体系である。実験の目的は、BWRの冷却材喪失事故(LOCA)時の熱水力学の挙動および非常用炉心冷却系(ECCS)の作動特性を調べ、原子炉安全性解析コードの検証および改良に寄与する実験データを提供することである。RUN 901は、4次模擬燃料を用いた最初の実験で、全ECCSの作動を仮定した再循環ポンプ吸込配管の200%両端破断を模擬している。この実験結果を、RELAP 4 J コードおよびRELAP 5/MOD 1/001 コードを用いて解析を行なった。

両算コード共に、系の圧力挙動、下部プレナムフラッシング(LPF)前の炉心入口流量は実験結果と良い一致を示した。

RELAP 4 J コードは計算速度が速く、また、炉心水位挙動を良く計算することができた。しかし、気液二相流挙動、特に上部タイプレートでの気液対向流の計算ができず、実験結果に反してECCS水が上部プレナムに蓄積された。

RELAP 5 コードは、非均質非平衡二相流モデルに依り、LPF後の炉心冷却や炉心露出後の炉心上部からの冷却(top-down quench)を計算することができた。しかし、炉心水位挙動をより正確に計算するためには、気液対向二相流限界(CCFL)モデルを取り入れるか、相間抗力関係式を改良する必要がある。また、正確な破断流計算のために、適当な放出係数が必要である。

* 日本原子力事業(株)

CONTENTS

1. INTRODUCTION	1
2. ROSA-III EXPERIMENT RUN 901	2
2.1 ROSA-III Test Facility	2
2.2 Test Conditions	3
2.3 Test Results	4
3. ANALYSIS OF RUN 901 TEST RESULTS BY RELAP4J	47
3.1 Computer Code	47
3.2 Calculation Model	48
3.3 Comparison with the Experimental Data	49
3.3.1 Pressure Transient	49
3.3.2 Differential Pressure	50
3.3.3 Break Flow	50
3.3.4 Core Flow and Jet Pump Flow	51
3.3.5 Liquid Levels in the Pressure Vessel	52
3.3.6 Fuel Rod Surface Temperature	54
3.4 Conclusions for the RELAP4J Calculations	55
4. ANALYSIS OF RUN 901 TEST RESULTS BY RELAP5/MOD1/001	83
4.1 Computer Code	83
4.2 Calculation Model	84
4.3 Comparison with the Experimental Data	86
4.3.1 Pressure Transient	86
4.3.2 Differential Pressure	87
4.3.3 Break Flow and Jet Pump Flow	88
4.3.4 Core Flow	90
4.3.5 Liquid Levels in the Pressure Vessel	91
4.3.6 Fuel Rod Surface Temperature	92
4.4 Conclusions for the RELAP5/MOD1/001 Calculations	93
5. CONCLUSIONS	150

目 次

1. 緒 言	1
2. ROSA - III 実験 RUN 901	2
2.1 ROSA - III 実験装置	2
2.2 実験条件	3
2.3 実験結果	4
3. RELAP 4J による RUN 901 実験解析	47
3.1 計算コード	47
3.2 計算モデル	48
3.3 実験結果との比較	49
3.3.1 圧 力	49
3.3.2 差 圧	50
3.3.3 破断流	50
3.3.4 炉心流およびジェットポンプ流	51
3.3.5 圧力容器内水位	52
3.3.6 模擬燃料表面温度	54
3.4 RELAP 4J 計算結果に対する結論	55
4. RELAP 5/MOD 1/001 による RUN 901 実験解析	83
4.1 計算コード	83
4.2 計算モデル	84
4.3 実験結果との比較	86
4.3.1 圧 力	86
4.3.2 差 圧	87
4.3.3 破断流およびジェットポンプ流	88
4.3.4 炉心流	90
4.3.5 圧力容器内水位	91
4.3.6 模擬燃料表面温度	92
4.4 RELAP 5/MOD 1/001 計算結果に対する結論	93
5. 結 論	150
謝 辞	151
参考文献	151
付 録 (計算コード入力データリスト)	
A RELAP 4J Case A	152
B RELAP 5/MOD 1/001 Case A	157
C RELAP 5/MOD 1/001 Case C (変更点のみ)	173
D RELAP 5/MOD 1/001 Case E (変更点のみ)	177

List of Tables

Table 2.1	The Primary Characteristics of ROSA-III and BWR/6
Table 2.2	Design Comparison of First through Fourth Fuel Assemblies
Table 2.3	Characteristics of Steam Discharge Line Valves
Table 2.4	Control Sequences for Steam Discharge Line Valves in RUN 901
Table 2.5	Test conditions of Test RUN 901
Table 2.6	Sequence of Events in RUN 901
Table 3.1	Description of Volumes for RELAP4J Model
Table 3.2	Description of Junctions for RELAP4J Model
Table 3.3	Description of Heat Slabs for RELAP4J Model
Table 4.1	Calculation conditions of RELAP5 Analyses
Table 4.2	Description of RELAP5 Components (Volumes and Junctions)
Table 4.3	Description of RELAP5 Components (Heat Structures)

List of Figures

- Fig. 2. 1 ROSA-III Major Components
- Fig. 2. 2 Pressure Vessel Internal Structure
- Fig. 2. 3 Pressure Vessel Instruments Arrangement
- Fig. 2. 4 ROSA-III Piping System
- Fig. 2. 5(a) Heater Rod Arrangement
- Fig. 2. 5(b) Radial Power Distribution
- Fig. 2. 6 Axial Power Distribution
- Fig. 2. 7 Schematic of Steam Line
- Fig. 2. 8 Schematic of Feedwater Line
- Fig. 2. 9 Break Nozzle
- Fig. 2.10 Power Transient
- Fig. 2.11 Lower Plenum Pressure
- Fig. 2.12 Break Upstream Pressure
- Fig. 2.13 Differential Pressure between Lower and Upper Plena
- Fig. 2.14 Differential Pressure between Upper Plenum and Steam Dome
- Fig. 2.15 Differential Pressure between Lower Plenum and Steam Dome
- Fig. 2.16 Lower Downcomer Head
- Fig. 2.17 Differential Pressure between Jet Pump Discharge and Suction
- Fig. 2.18 Differential Pressure between Jet Pump Drive and Suction
- Fig. 2.19 Differential Pressure between MRP Delivery and Suction
- Fig. 2.20 Main Steam Discharge Flow Rate
- Fig. 2.21(a) Feedwater Flow Rate
- Fig. 2.21(b) Feedwater Flow Rate (Expanded Time History)
- Fig. 2.22 HPCS and LPCS Flow Rates
- Fig. 2.23 LPCI Flow Rates
- Fig. 2.24 Core Inlet Flow of Channel A
- Fig. 2.25 Core Inlet Flow of Channel B

- Fig. 2.26 Core Inlet Flow of Channel C
- Fig. 2.27 Core Inlet Flow of Channel D
- Fig. 2.28 Guide Tube Inlet Flow
- Fig. 2.29 Electric Core Power
- Fig. 2.30 Liquid Level in Downcomer
- Fig. 2.31 Liquid Level Transients in Pressure Vessel
- Fig. 2.32 Fuel Rod Surface Temperature A11
- Fig. 2.33 Fuel Rod Surface Temperature A22
- Fig. 2.34 Fuel Rod Surface Temperature A24
- Fig. 2.35 Fuel Rod Surface Temperature A33
- Fig. 2.36 Fuel Rod Surface Temperature B22
- Fig. 2.37 Fuel Rod Surface Temperature C11
- Fig. 2.38 Fuel Rod Surface Temperature C22
- Fig. 2.39 Fuel Rod Surface Temperature C33
- Fig. 2.40 Dryout and Quench Fronts in Channel A
- Fig. 2.41 Dryout and Quench Fronts in Channel C
- Fig. 2.42 Average Fluid Densities at Break
- Fig. 2.43 Momentum Fluxes at Break
- Fig. 2.44 Discharge Flow Rate at Break A (MRP side)
- Fig. 2.45 Discharge Flow Rate at Break B (PV side)
-
- Fig. 3. 1 RELAP4J Nodalization of ROSA-III (Base Case A)
- Fig. 3. 2 RELAP4J Nodalization of ROSA-III (Case B)
(Reduced Case)
- Fig. 3. 3 Initial Flow Distribution of RUN 901
- Fig. 3. 4 Main Steam Discharge Flow Rate
- Fig. 3. 5 Feedwater Flow Rate
- Fig. 3. 6 HPCS + LPCS and LPCI Flow Rate
- Fig. 3. 7 Lower Plenum Pressure
- Fig. 3. 8 Pressure at Break B Upstream (PV Side)
- Fig. 3. 9 Pressure at Break A Upstream (MRP Side)
- Fig. 3.10 Differential Pressure between Lower and Upper Plena

- Fig. 3.11 Differential Pressure between Channel Inlet and Upper Plenum
- Fig. 3.12 Break Flow from Break B (PV side)
- Fig. 3.13 Break Flow from Break A (MRP side)
- Fig. 3.14 Average Fluid Densities at the Break B Upstream
- Fig. 3.15 Average Fluid Densities at the Break A Upstream
- Fig. 3.16 Total Core Inlet Flow through SEO
- Fig. 3.17 Guide Tube Inlet Flow
- Fig. 3.18 Total Core Flow through UTP
- Fig. 3.19 Total Core Flow through LTP
- Fig. 3.20 Total Core Flows through UTP and LTP (Case A)
- Fig. 3.21 Total Core Flows through UTP and LTP (Case B)
- Fig. 3.22 Jet Pump Flow (Intact Loop Side ; Case A)
- Fig. 3.23 Jet Pump Flow (Broken Loop Side ; Case A)
- Fig. 3.24 Jet Pump Flow (Intact Loop Side ; Case B)
- Fig. 3.25 Jet Pump Flow (Broken Loop Side ; Case B)
- Fig. 3.26 Liquid Levels in the Pressure Vessel (Case A)
- Fig. 3.27 Liquid Levels in the Pressure Vessel (Case B)
- Fig. 3.28 Fuel Rod Surface Temperature in Case A
(Average Power Channel)
- Fig. 3.29 Fuel Rod Surface Temperature in Case A
(Peak Power Channel)
- Fig. 3.30 Fuel Rod Surface Temperature in Case B
(Average Power Channel)
- Fig. 3.31 Fuel Rod Surface Temperature in Case B
(Peak Power Channel)
- Fig. 3.32 Heat Transfer Coefficient at Position 1 (Case A)
- Fig. 3.33 Heat Transfer Coefficient at Position 2 (Case A)
- Fig. 3.34 Heat Transfer Coefficient at Position 3 (Case A)
- Fig. 3.35 Heat Transfer Coefficient at Position 4 (Case A)
- Fig. 3.36 Heat Transfer Coefficient at Position 5 (Case A)

- Fig. 3.37 Heat Transfer Coefficient at Position 6 (Case A)
- Fig. 3.38 Heat Transfer Coefficient at Position 7 (Case A)
- Fig. 3.39 Heat Transfer Coefficient at Position 1 (Case B)
- Fig. 4. 1 Nodalization Diagrams of ROSA-III Pressure Vessel for
RELAP5/MOD1/001 Model
- Fig. 4. 2 Nodalization Diagrams of ROSA-III Recirculation Loop
- Fig. 4. 3 Nodalization Diagrams of Simulated Break Nozzles
in Cases D and E
- Fig. 4. 4 Main Steam Discharge Flow Rate
- Fig. 4. 5 Feedwater Flow Rate
- Fig. 4. 6 HPCS Flow Rate
- Fig. 4. 7 LPCS and LPCI Flow Rates (Case C)
- Fig. 4. 8 Lower Plenum Pressure
- Fig. 4. 9 Pressure at Break B Upstream
- Fig. 4.10 Pressure at Break A Upstream
- Fig. 4.11 Differential Pressure between Lower and Upper Plena
- Fig. 4.12 Differential Pressure between Upper Plenum and Steam Dome
- Fig. 4.13 Differential Pressure between Lower Plenum and Steam Dome
- Fig. 4.14 Lower Downcomer Head
- Fig. 4.15 Differential Pressure between MRP1 Delivery and Suction
in Intact Loop
- Fig. 4.16 Differential Pressure between MRP2 Delivery and Suction
in Broken Loop
- Fig. 4.17 Break Flow from Break B (PV side)
- Fig. 4.18 Break Flow from Break A (MRP side)
- Fig. 4.19 Average Fluid Densities at Break B Upstream
- Fig. 4.20 Average Fluid Densities at Break A Upstream
- Fig. 4.21 Jet Pump Flow (Intact Loop ; Case A)
- Fig. 4.22 Jet Pump Flow (Broken Loop ; Case A)
- Fig. 4.23 Jet Pump Flow (Intact Loop ; Case B)

- Fig. 4.24 Jet Pump Flow (Broken Loop ; Case B)
- Fig. 4.25 Jet Pump Flow (Intact Loop ; Case C)
- Fig. 4.26 Jet Pump Flow (Broken Loop ; Case C)
- Fig. 4.27 Jet Pump Flow (Intace Loop ; Case D)
- Fig. 4.28 Jet Pump Flow (Broken Loop ; Case D)
- Fig. 4.29 Jet Pump Flow (Intact Loop ; Case E)
- Fig. 4.30 Jet Pump Flow (Broken Loop ; Case E)
- Fig. 4.31 Liquid and Steam Velocities through Break B (Case A)
- Fig. 4.32 Liquid and Steam Velocities through Break A (Case A)
- Fig. 4.33 Liquid and Steam Velocities through Break B (Case B)
- Fig. 4.34 Liquid and Steam Velocities through Break A (Case B)
- Fig. 4.35 Liquid and Steam Velocities through Break B (Case C)
- Fig. 4.36 Liquid and Steam Velocities through Break A (Case C)
- Fig. 4.37 Liquid and Steam Velocities thorough Break B (Case D)
- Fig. 4.38 Liquid and Steam Velocities through Break A (Case D)
- Fig. 4.39 Liquid and Steam Velocities through Break B (Case E)
- Fig. 4.40 Liquid and Steam Velocities through Break A (Case E)
- Fig. 4.41 Total Flow Rate through SEO, LTP and UTP (Case A)
- Fig. 4.42 Total Flow Rate through SEO, LTP and UTP (Case B)
- Fig. 4.43 Total Flow Rate through SEO, LTP and UTP (Case C)
- Fig. 4.44 Total Flow Rate through SEO, LTP snd UTP (Case D)
- Fig. 4.45 Total Flow Rate through SEO, LTP and UTP (Case E)
- Fig. 4.46 Comparison of Total Flow Rates through SEO
- Fig. 4.47 Fluid Velocities through UTP of Average Power Channel
(Case A)
- Fig. 4.48 Fluid Velocities through UTP of Peak Power Channel
(Case A)
- Fig. 4.49 Fluid Velocities through UTP of Average Power Channel
(Case B)
- Fig. 4.50 Fluid Velocities through UTP of Peak Power Channel
(Case B)

- Fig. 4.51 Fluid Velocities through UTP of Average Power Channel
(Case C)
- Fig. 4.52 Fluid Velocities through UTP of Peak Power Channel
(Case C)
- Fig. 4.53 Fluid Velocities through UTP of Average Power Channel
(Case D)
- Fig. 4.54 Fluid Velocities through UTP of Peak Power Channel
(Case D)
- Fig. 4.55 Fluid Velocities through UTP of Average Power Channel
(Case E)
- Fig. 4.56 Fluid Velocities through UTP of Peak Power Channel
(Case E)
- Fig. 4.57 Estimated Liquid Levels in PV (Cases A, B, D and E)
- Fig. 4.58 Estimated Liquid Levels in PV (Case C)
- Fig. 4.59 Void Fractions in Upper Downcomer (Case C)
- Fig. 4.60 Void Fractions in Lower Downcomer (Case C)
- Fig. 4.61 Void Fractions in Steam Dome (Case C)
- Fig. 4.62 Void Fractions in Upper Plenum and Separator (Case C)
- Fig. 4.63 Void Fractions in Bypass and Guide Tube (Case C)
- Fig. 4.64 Void Fractions in Peak-Power Channel (Case C)
- Fig. 4.65 Void Fractions in Average-Power Channel (Case C)
- Fig. 4.66 Void Fractions in Lower Plenum (Case C)
- Fig. 4.67 Fuel Surface Temperatures (Average-Power Channel)
- Fig. 4.68 Fuel Surface Temperatures (Peak-Power Channel)
- Fig. 4.69 Fuel Surface Temperatures (Average-Power Channel) (Case C)
- Fig. 4.70 Fuel Surface Temperatures (Peak-Power Channel) (Case C)
- Fig. 4.71 CHF and Heat Transfer Rate at Position 1 in Peak-Power
Channel (Case A)
- Fig. 4.72 CHF and Heat Transfer Rate at Position 2 in Peak-Power
Channel (Case A)
- Fig. 4.73 CHF and Heat Transfer Rate at Position 3 in Peak-Power

- Channel (Case A)
- Fig. 4.74 CHF and Heat Transfer Rate at Position 4 in Peak-Power Channel (Case A)
- Fig. 4.75 CHF and Heat Transfer Rate at Position 1 in Peak-Power Channel (Case B)
- Fig. 4.76 CHF and Heat Transfer Rate at Position 2 in Peak-Power Channel (Case B)
- Fig. 4.77 CHF and Heat Transfer Rate at Position 3 in Peak-Power Channel (Case B)
- Fig. 4.78 CHF and Heat Transfer Rate at Position 4 in Peak-Power Channel (Case B)
- Fig. 4.79 CHF and Heat Transfer Rate at Position 1 in Peak-Power Channel (Case C)
- Fig. 4.80 CHF and Heat Transfer Rate at Position 2 in Peak-Power Channel (Case C)
- Fig. 4.81 CHF and Heat Transfer Rate at Position 3 in Peak-Power Channel (Case C)
- Fig. 4.82 CHF and Heat Transfer Rate at Position 4 in Peak-Power Channel (Case C)
- Fig. 4.83 CHF and Heat Transfer Rate at Position 1 in Peak-Power Channel (Case D)
- Fig. 4.84 CHF and Heat Transfer Rate at Position 2 in Peak-Power Channel (Case D)
- Fig. 4.85 CHF and Heat Transfer Rate at Position 3 in Peak-Power Channel (Case D)
- Fig. 4.86 CHF and Heat Transfer Rate at Position 4 in Peak-Power Channel (Case D)
- Fig. 4.87 CHF and Heat Transfer Rate at Position 1 in Peak-Power Channel (Case E)
- Fig. 4.88 CHF and Heat Transfer Rate at Position 2 in Peak-Power Channel (Case E)

Fig. 4.89 CHF and Heat Transfer Rate at Position 3 in Peak-Power Channel (Case E)

Fig. 4.90 CHF and Heat Transfer Rate at Position 4 in Peak-Power Channel (Case E)

Abbreviations

ADS	Automatic Depressurization System
AV	Air Actuation Valve
BWR	Boiling Water Reactor
CCFL	Counter Current Flow Limiting
CV	Control Valve
ECCS	Emergency Core Cooling System
ESF	Engineered Safety Features
Fig.	Figure
FW	Feedwater
FWLF	Feedwater Line Flashing
HPCS	High Pressure Core Spray
JP	Jet Pump
LOCA	Loss-of-Coolant Accident
LP	Lower Plenum
LPCI	Low Pressure Coolant injection
LPCS	Low Pressure Core Spray
LPF	Lower Plenum Flashing
LTP	Lower Tie Plate
LWR	Light Water Reactor
MRP	Main Recirculation pump
MSIV	Main Steam Isolation Valve
MSL	Main Steam Line
OR	Orifice
PCT	Peak Cladding Temperature
PV	Pressure Vessel
ROSA	Rig of Safety Assessment
SEO	Side Entry Orifice
UP	Upper Plenum
UTP	Upper Tie Plate

1. INTRODUCTION

The ROSA (Rig of Safety Assessment)-III program was initiated in 1976 to investigate the thermal-hydraulic behavior of a boiling water reactor (BWR) during a postulated Loss of Coolant Accident (LOCA) and to provide base data to evaluate the predictability of reactor safety analysis codes. The ROSA-III test facility, completed in 1978, consists of a volumetrically scaled (1/424) primary system of a 3800 MW thermal power BWR/6-251 with an electrically heated core and a scaled Emergency Core Cooling System (ECCS).

The objectives of the ROSA-III experimental program are:

- (1) To provide data required for evaluation and improvement of the analytical methods currently used to predict the LOCA transients in large BWRs. The performance of the engineered safety features (ESFs), with particular emphasis on ECCS, and the qualitative margins of safety inherent in performance of the ESFs are of primary interest.
- (2) To identify and investigate any unexpected event(s) or threshold(s) in the response of either the plant or the ESFs and to develop analytical techniques that adequately describe such unexpected behaviors.

The ROSA-III experiment RUN 901⁽¹⁾ conducted on April 8, 1981 was the acceptance test of the fourth fuel assembly⁽²⁾. The test simulated a 200% double-ended break at the suction of the main recirculation pump (MRP) with all of ECCS function as designed.

RUN 901 was the first test using the fourth fuel assembly and also was the first large break test using the downcomer liquid level signals to initiate the main steam isolation valve (MSIV) closure and to actuate high pressure core spray (HPCS), low pressure core spray (LPCS), low pressure core injection (LPCI) and automatic depressurization system (ADS) in the same manner as BWR/6.

This report presents the results of post test analysis of RUN901 conducted with the RELAP4J and RELAP5/MOD1/001 codes. The RELAP4J code is an JAERI improved version of the RELAP4/MOD2 code and is based on the

homogenous and thermodynamically equilibrium two-phase flow models. The RELAP5/MOD1/001 code is a so-called advanced code based on the nonhomogenous nonequilibrium hydrodynamic models. These analyses with RELAP4J and RELAP5/MOD1/001 will make the features of two codes clear.

2. ROSA-III EXPERIMENT RUN901

2.1 ROSA-III Test Facility

The ROSA-III test facility is a volumetrically scaled (1/424) model of a BWR system with four half-length electrically-heated fuel bundles. It is designed to represent the operation of the ESFs (Engineered Safety Features) in commercial BWR systems during a postulated LOCA. The ROSA-III major components, the pressure vessel internal structure, the pressure vessel instruments arrangement and the piping system are shown in Figs. 2.1 through 2.4, respectively. The primary characteristics of the ROSA-III test facility are compared with those of BWR/6 in Table 2.1.

Heater rod arrangement, radial power distribution and axial power distribution are shown in Figs. 2.5(a), 2.5(b) and 2.6, respectively. A 44mm ID side entry orifice (SEO) is installed between the lower plenum and the lower tieplate for each channel of the fourth fuel assembly. The core inlet flow rate through the SEO can be estimated from the differential pressure across the orifice. Comparison of the design of the first through fourth fuel assemblies is shown in Table 2.2. The detailed system description of the ROSA-III with the fourth fuel assembly is given in Reference 2.

Steam is discharged into the atmosphere through the steam line connected to the steam dome. The steam line has three branches as shown in Fig. 2.7. The first branch has a control valve (CV130) to control the steady state steam flow before the initiation of a blowdown. The second branch simulates the (ADS) Automatic Depressurization System. The third branch has an orifice (OR5) to simulate the flow resistance of the steam turbine-generator. Immediately after the break initiation the steam flow

homogeneous and thermodynamically equilibrium two-phase flow models. The RELAP5/MOD1/001 code is a so-called advanced code based on the nonhomogeneous nonequilibrium hydrodynamic models. These analyses with RELAP4J and RELAP5/MOD1/001 will make the features of two codes clear.

2. ROSA-III EXPERIMENT RUN901

2.1 ROSA-III Test Facility

The ROSA-III test facility is a volumetrically scaled (1/424) model of a BWR system with four half-length electrically-heated fuel bundles. It is designed to represent the operation of the ESFs (Engineered Safety Features) in commercial BWR systems during a postulated LOCA. The ROSA-III major components, the pressure vessel internal structure, the pressure vessel instruments arrangement and the piping system are shown in Figs. 2.1 through 2.4, respectively. The primary characteristics of the ROSA-III test facility are compared with those of BWR/6 in Table 2.1.

Heater rod arrangement, radial power distribution and axial power distribution are shown in Figs. 2.5(a), 2.5(b) and 2.6, respectively. A 44mm ID side entry orifice (SEO) is installed between the lower plenum and the lower tieplate for each channel of the fourth fuel assembly. The core inlet flow rate through the SEO can be estimated from the differential pressure across the orifice. Comparison of the design of the first through fourth fuel assemblies is shown in Table 2.2. The detailed system description of the ROSA-III with the fourth fuel assembly is given in Reference 2.

Steam is discharged into the atmosphere through the steam line connected to the steam dome. The steam line has three branches as shown in Fig. 2.7. The first branch has a control valve (CV130) to control the steady state steam flow before the initiation of a blowdown. The second branch simulates the (ADS) Automatic Depressurization System. The third branch has an orifice (OR5) to simulate the flow resistance of the steam turbine-generator. Immediately after the break initiation the steam flow

is switched from the first to the third branch in RUN 901. Then the main steam isolation valve (MSIV) is simulated by AV165 in the third branch. The characteristics and control sequences of the steam discharge line valves are described in Tables 2.3 and 2.4.

The feedwater line supplies the feedwater of temperature of 489 K below the steam separator in the downcomer. Since the feedwater line isolation valve (AV112), which is to be closed after the break initiation, is installed far from the pressure vessel, the feedwater remains in the feedwater line between the pressure vessel and the isolation valve. The schematic of the feedwater line between the pressure vessel and the isolation valve (AV112) is shown in Fig. 2.8.

2.2 Test Conditions

RUN 901 was conducted on April 8, 1981. The test conditions actually obtained in RUN 901 are summarized and compared with the specified test conditions in Table 2.5. RUN 901 simulated a 200 % double-ended break at the recirculation pump suction line with all the ECCS functioned as designed. The break was simulated by a nozzle shown in Fig. 2.9. The core power transient in RUN 901 is shown in Fig. 2.10. The core power was held constant for 7.0 s after the break initiation because of the limited electrical power capacity of the facility. Power history during transient simulated the heat transfer rate from nuclear fuel rod to coolant during a LOCA of a BWR. The transient core power after break is composed of the delayed neutron fission power, the decay power of fission products and actinides, and the stored heat release from the nuclear fuel rod⁽³⁾.

The liquid level signals in the upper downcomer obtained from the water head were used to trip MSIV closure and ECCS actuation as in a BWR/6. The initial L3 liquid level (5.00 m from the bottom of the pressure vessel in the downcomer of the ROSA-III test facility) was defined so that the liquid volume below this level including the jet pump suction pipings scale the liquid volume below the scram L3 level in a BWR/6. The L2 and

L1 liquid levels in the downcomer of ROSA-III were 4.76 m and 4.25 m, respectively. MSIV closure and HPCS actuation were initiated by the L2 signal with time delays of 3 s and 27 s, respectively. LPCS, LPCI and ADS actuation were initiated by the L1 signal with 40 s, 40 s and 120 s time delays, respectively. Time delays of 3 s, 40 s and 120 s, are used in the safety analysis of a BWR⁽⁴⁾. LPCS and LPCI injections were also specified to initiate at system pressures below 2.16 MPa and 1.57 MPa⁽⁴⁾, respectively.

2.3 Test Results

Sequence of major events in RUN 901 are summarized in Table 2.6.

System pressure in the lower plenum is shown in Fig. 2.11, which represents the pressure response in the pressure vessel in RUN 901. The pressure decreased during initial 8 s due to discharge of the coolant from the steam line and the break. The pressure began to recover after the MSIV closure.

The pressure started to drop again after the liquid level in the downcomer lowered to the recirculation line nozzle level at 12.0 s and the volumetric flow rate from the break exceeded the vapor generation rate in the system. When the pressure decreased to the saturation pressure corresponding to the lower plenum fluid temperature at 17 s after the break the Lower Plenum Flashing (LPF) began. Similarly, when the pressure lowered to the saturation pressure of 2.15 MPa corresponding to the feedwater temperature at 64.8 s after the break, the liquid in the feedwater line began to flash. The HPCS, the LPCS, the LPCI and the ADS were initiated at 31.5 s, 65.6 s, 90.9 s and 127.7 s after the break, respectively. However, the ECCS affected the pressure response little.

Steam discharge flow rate is shown in Fig. 2.20. Measuring range of the flow meters are 0.0 kg/s to 1.13 kg/s for a low-range and 0.0 kg/s to 3.00 kg/s for a high-range flow meters, respectively. The steam discharge flow decreased temporarily after the break due to switching over the flow path from the steady flow path to the transient flow path as described before. Steam discharge stopped at 9.2 s after the break because the MSIV

closed and started again at 127.7 s because of the ADS actuation. The anomalous behavior in the ADS steam discharge flow rate was because of error at low flow rate near insensitive range of the flow meter.

Feedwater injection rate is shown in Figs. 2.21(a) and 2.21(b). Figure 2.21(a) shows the flashing in the feedwater line after 64.8 s.

Injection flow rates of HPCS, LPCS and LPCI are shown in Figs. 2.22 and 2.23.

The core inlet flows through the Side Entry Orifice (SEO) of the channels A through D are shown in Fig. 2.24 through 2.27, respectively. The flow decreased rapidly after the break because of the recirculation pump coastdown and the flow stagnated until the LPF initiation. Figure 2.28 shows the flow through the bypass hole which reversed immediately after the break initiation. The flow rate shown in Figs. 2.24 through 2.28 present only a trend in two-phase flow condition after the LPF initiation.

Figure 2.29 shows the transient curves of the electric core power. The core power began to decrease at 7.0 s after the break.

Figure 2.30 shows the liquid level in the downcomer obtained from the downcomer head. Figure 2.30 shows the liquid level in the downcomer which began to drop immediately after break and reached the jet pump suction and the MRP suction line at 10 s and 13 s, respectively. The instantaneous decrease in the lower downcomer collapsed level after the break is probably due to increase in the downward acceleration pressure loss induced by the break. Liquid level transients estimated from the signals of conductivity probes installed in the pressure vessel are shown in Fig. 2.31. The liquid level in the core decreased after the break to Position 3 and temporarily recovered thereafter by the LPF. The liquid level in the core decreased again by the mitigation of the LPF and rapidly dropped temporarily by the Feedwater Line Flashing (FWLF) initiated at 64.8 s after the break. The bottom part of the core was not uncovered. The liquid level began to recover at 70 s after the break because of the mitigation of

the FWLF and accumulation of ECCS water in the core. The reflooding was accelerated by the actuation of LPCI. The liquid level was not formed in the channel inlet chamber since the Counter Current Flow Limiting (CCFL) occurred at the SEO from 17 s to 133 s after the break.

Figures 2.32 through 2.39 show comparison of the surface temperatures of the heater rods A11, A22, A24, A33, B22, C11, C22 and C33 measured at seven elevations in the core, respectively. The dryout and quench front behaviors at the heater rod surfaces in the peak-power channel A and the average-power channel C are compared with the liquid level transient in Figs. 2.40 and 2.41, respectively. Figures 2.40 and 2.41 show that the dryout and quench front behaviours are closely related to the liquid level transients in the core. The early dryout in the upper core before the LPF was caused by a liquid level drop due to decrease in the core inlet flow and resulted in a rapid temperature rise at the heater rod surface due to high core power shortly after the break. The heater rods were rewetted by the LPF and began to dryout again following the liquid level fall due to mitigation of the LPF. The top-down quench was observed because of the CCFL breakdown induced by the FWLF and the LPCS actuation. All heater rods were quenched a little later than the whole core reflooding. The liquid level in the average-power channel dropped temporarily after 115 s because of the CCFL breakdown at SEO.

When the core is reflooded after the LPF as well as after the ECCS actuations the cladding surface temperature, which increased during dryout period, turns around to decrease. Therefore, the PCT, which is the highest cladding surface temperature recorded through the test, is usually observed at the time of reflooding of the fuel surface at some location in the core. The PCT in RUN 901 was 779 K observed at Position 2 of A11 rod 18.5 s after the break and 1.6 s after the LPF initiation.

Average fluid densities at the upstream side of the break A (MRP side break) and the break B (PV side break) are shown in Fig. 2.42. The fluid density through the break A decreased rapidly after the break because of

the flashing in the broken recirculation loop piping between the jet pump drive nozzles and the break. After the liquid level in the downcomer decreased to the recirculation pump suction line, the average fluid densities through the breaks A and B decreased almost to the steam density.

The momentum flux and the discharge flow rate at the breaks A and B are shown in Figs. 2.43 through 2.45. Before the break initiation figures show the steady state flow in the recirculation line because the drag disk flow meters are installed in the recirculation loop. The signal from the drag disk flow meters installed in the upstream side of the PV-side break B became saturated until 38 s after break. The break mass flow transients at the breaks A and B are strongly related to the upstream fluid density. The measured break flow has an uncertainty of as large as ± 20 %.

Table 2.1 Primary Characteristics of BWR-6 and ROSA-III

	BWR-6	ROSA-III	BWR/ROSA
No. of Recirc. Loops	2	2	1
No. of Jet Pumps	24	4	6
No. of Separators	251	1	251
No. of Fuel Assemblies	848	4	212
Active Fuel Length (m)	3.76	1.88	2
Total Volume (m ³)	621	1.42	437
Power (MW)	3800	4.40	864
Pressure (MPa)	7.23	7.23	1
Core Flow (kg/s)	1.54x10 ⁴	36.4	424
Recirculation Flow (l/s)	2970	7.01	424
Feedwater Flow (kg/s)	2060	4.86	424
Feedwater Temp (K)	489	489	1

Table 2.2 Comparison of Fuel Assemblies from the First to the Fourth

	1st	2nd	3rd	4th
Active Core Length (m)		1.880		
Number of Fuel Rods	252	252	248	248
Number of Water Rods	4	4	8	8
Rods Array		8 x 8 square		
Fuel Rod O.D. (mm)	12.52	12.52	12.27	12.27
Fuel Rod Pitch (mm)	16.26	16.26	16.16	16.16
Peaking Factor				
Local P.F.	1.0	1.0	1.0	1.1
Axial P.F.	1.4	1.4	1.4	1.4
Radial P.F.	1.0	1.0	1.4	1.4
Side Entry Orifices				
Number of Holes	48	48	48	4
Diameter (mm)	9.5	6.29	6.5	44.0
Total Area (cm ²)	34.02	14.92	15.93	60.82
Leak Holes				
Number of Holes	8	8	8	8
Diameter (mm)	8.6	7.66	9.2	9.14
Total Area (cm ²)	4.65	3.69	5.32	5.25
Guide Tube Holes				
Number of Holes	4	4	4	4
Diameter (mm)	5.3	4.9	5.12	7.48
Total Area (cm ²)	0.88	0.75	0.82	1.76
Conducted Test RUNs	701	704	731	901
	{	{	{	{
	703	710	7341	
			{	
			801	
			{	
			827	

Table 2.3 Valve Characteristics of Steam Discharge Line

Valve	Close to Open (sec)	Open to Close (sec)
AV165	0.1	1.5
AV168	-	0.1
AV169	0.3	2.0

Orifice	Diameter (mm)	Area (mm ²)
OR3	Not Used	-
OR4	15.5	188.7
OR5	16.8	221.7

Table 2.4 Valve Control Sequence of Steam Discharge Line in RUN 901

Time	t < 0	Break (t=0)	L2 + 3s	L1 + 120s
AV [*] 168	Open	Close	Close	Close
CV 130	Control to maintain steady state pressure			
AV 165	Close	Open	Close	Close
AV 169	Close	Close	Close	Open

* AV ; Air Actuation Valve (Auto)
 CV ; Control Valve (Manual)

Table 2.5 Test Conditions of the ROSA-III Test RUN 901

Parameter	Specified Value	Measured Value
<u>Break Conditions</u>		
Location	Recirculation pump suction	Recirculation pump suction
Type	Double-ended	Double-ended
Break Nozzle Diameter (mm)	26.2/26.2	26.2/26.2
<u>Initial System Conditions</u>		
Steam Dome Pressure (MPa)	7.35	7.29
Lower Plenum Temperature (K)	----	552.0
Lower Plenum Subcooling (K)	----	10.5
Core Inlet Flow Rate (kg/s)	16.0	16.0
Broken Loop Flow Rate (m ³ /s)	----	----
Intact Loop Flow Rate (m ³ /s)	----	----
Core Outlet Quality (%)	----	13.9
Power Level (kW)	(1400+3000)	(1250+2795)
Maximum Linear Heat Rate (kW/m)		
of Channel A	18.5	16.5
of Channel B, C and D	13.2	12.3
Power Curve	Fig. 2.10	Fig. 2.29
Water Level in PV (m)	5.00	5.00
Fuel Assembly	No.4	No.4
<u>Feedwater Conditions</u>		
Temperature (K)	489	489
Flow Rate (kg/s)	Steady state value 2.388	Fig. 2.21
Initiation of line closure (s)	2.0	2.0 (completely close at 3.7 s)

Table 2.5 (Continue)

Parameter	Specified Value	Measured Value
<u>Steam Discharge Conditions</u>		
Steady State Line		
Flow Rate (kg/s)	Steady State Value (2.388)	2.00
Transient Line		
Flow Rate (kg/s)	----	Fig. 2.20
Orifice Diameter (mm)	16.8	16.8
Initiation of line closure		
at Water Level (m)	4.76*	4.3 (7.5 s after break and completely closed at 9.4 s)
with Time Lag (s)	3	
<u>ECCS Conditions</u>		
HPCS		
Injection Location		
	Upper Plenum	Upper Plenum
Initiation		
at Water Level (m)	4.76	
with Time Lag (s)	27	28.3 (31.5s after break at 5.21 MPa in PV)
Coolant Temperature (K)	313	313
Injection Flow Rate (m ³ /s)	6.17×10^{-4} at 6.5 MPa	Fig. 2.22
Injection Duration (s)	1500	Fig. 2.22
LPCS		
Injection Location		
	Upper Plenum	Upper Plenum
Initiated		
at Water Level (m)	4.25 **	
with Time Lag (s)	40	
and at Pressure in PV(MPa)	2.16	2.23 (65.6 s after break)
Coolant Temperature (K)	313	313
Injection Flow Rate (m ³ /s)	1.13×10^{-3}	Fig. 2.22
Injection Duration (s)	1500	Fig. 2.22

* L2 level

** L1 level

Table 2.5 (Continue)

Parameter	Specified Value	Measured Value
<u>ECCS Conditions (Continued)</u>		
LPCI		
Injection Location	Upper Plenum and Core Bypass	Upper Plenum and Core Bypass
Initiated		
at Water Level (m)	4.25	
with Time Lag (s)	4	
and at Pressure in PV(MPa)	1.57	1.61 (90.9s after break)
Coolant Temperature (K)	313	313
Injection Flow Rate (m ³ /s)	3.5×10^{-3}	Fig. 2.23
Injection Duration (s)	1500	Fig. 2.23
<u>ADS Conditions</u>		
Initiation		
at Water Level (m)	4.25	
with Time Lag (s)	120	120.3 (127.7 s after break, 0.79 MPa in PV)
Valve Closing Time (s)	No closure	No closure
Flow Rate (m ³ /s)	----	Fig. 2.20
Orifice Diameter (mm)	15.5	15.5

Table 2.6 Sequence of Events in RUN 901

Time after break (s)	Events
0.0	Break
	Initiate core power control
	Terminate intact loop recirculation pump power (simple coastdown)
	Terminate broken loop recirculation pump power (simple coastdown)
1.2	Initiation of feedwater line valve closure
3.2	Liquid level in downcomer decreased to L2 level
4.0	Closure of feedwater line
7.0	Initiation of core power curve reduction
7.4	Initiation of steam discharge line valve closure
	Liquid level in downcomer decreased to L1 level
9.2	Closure of steam discharge line
9.5	Liquid level in downcomer decreased to jet pump suction nozzle
12.0	Liquid level in downcomer decreased to recirculation pump suction line
17.0	Initiation of lower plenum flashing
31.5	HPCS initiation (at system pressure 5.21 MPa)
64.8	Feedwater line flashing
65.6	LPCS initiation (at system pressure 2.23 MPa)
90.9	LPCI initiation (at system pressure 1.61 MPa)
127.3	Quench of the whole core
128.2	ADS initiation (at system pressure 0.79 MPa)
490	End of data acquisition

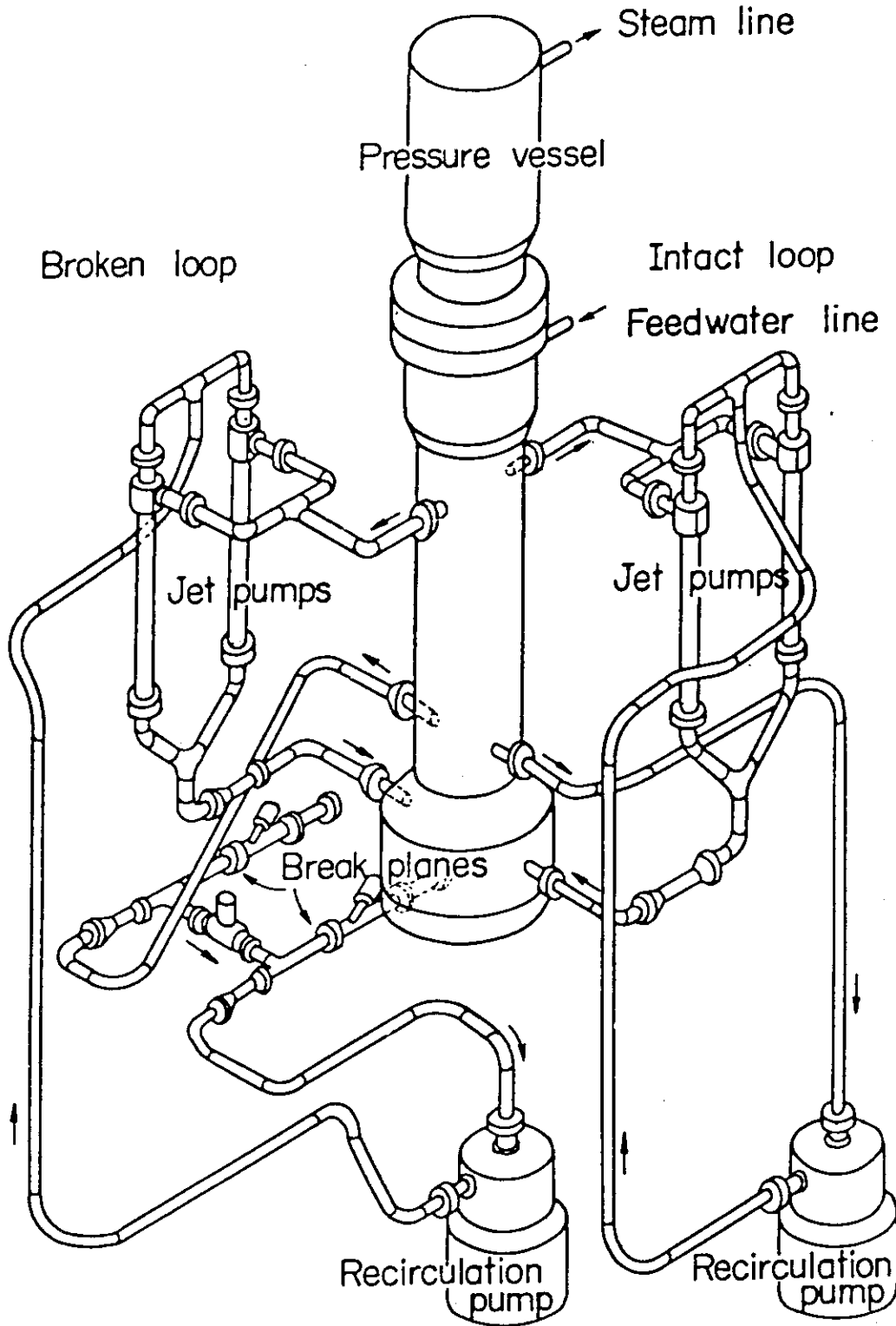


Fig. 2.1 ROSA-III Major Components

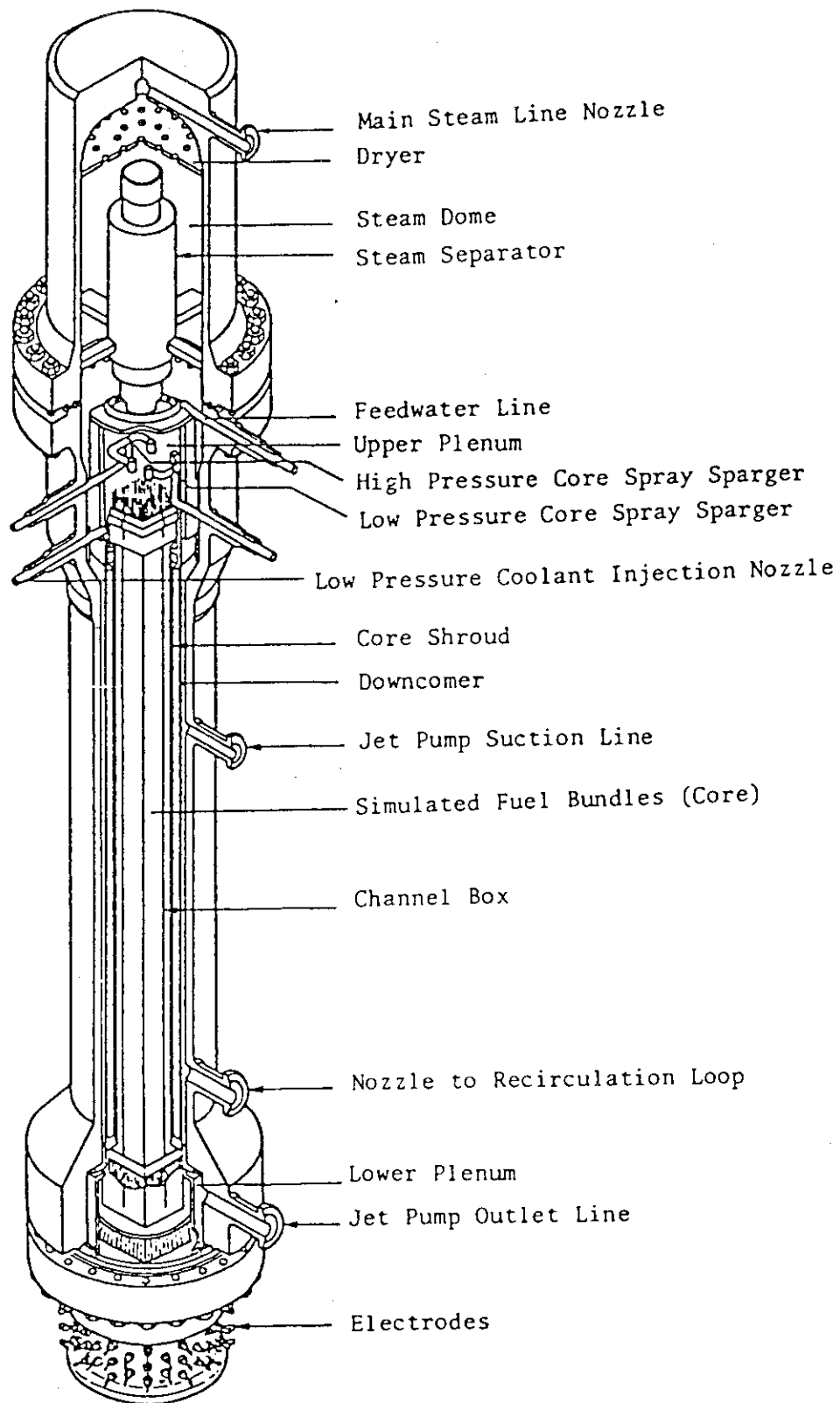


Fig. 2.2 Pressure Vessel Internal Structure

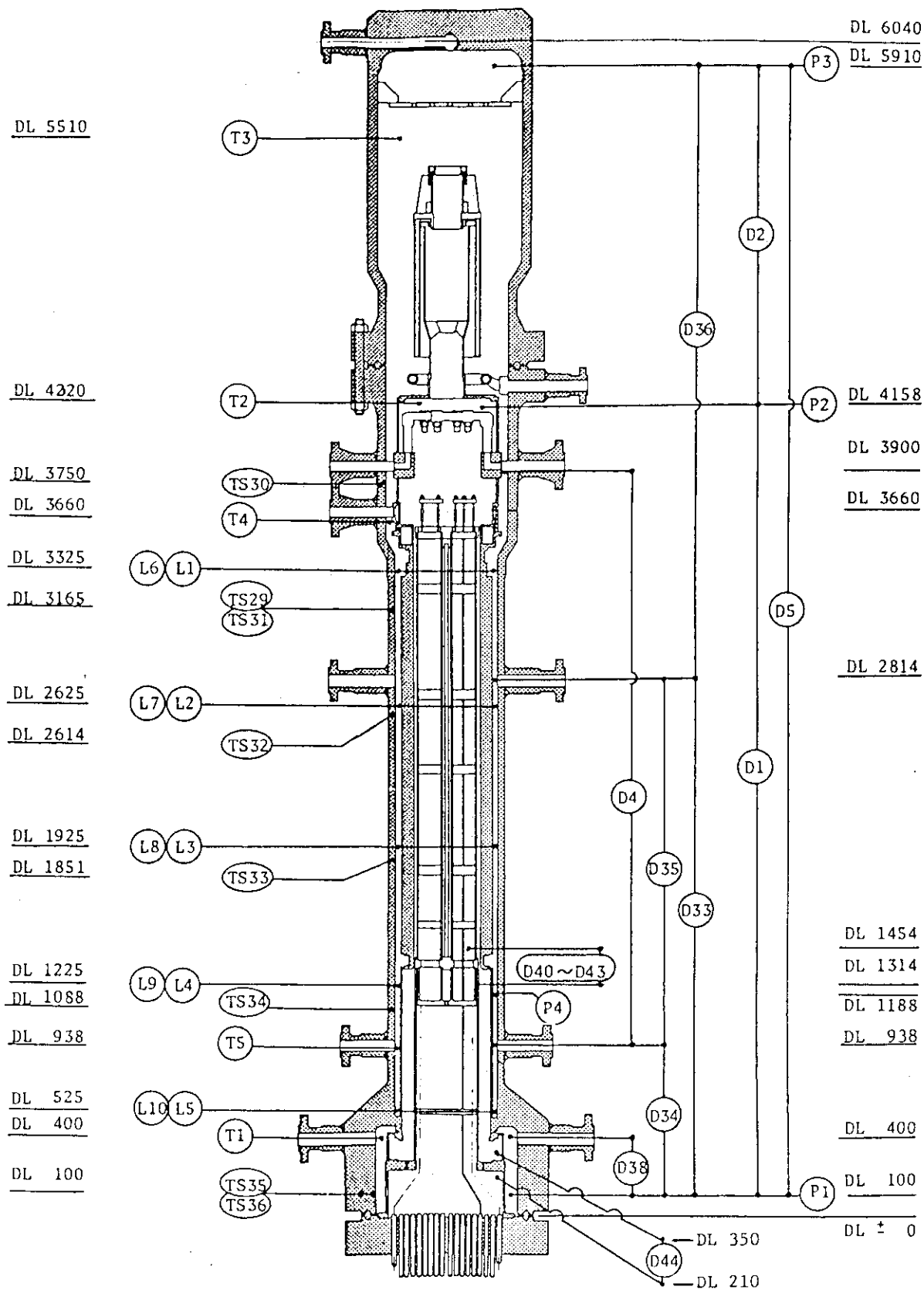
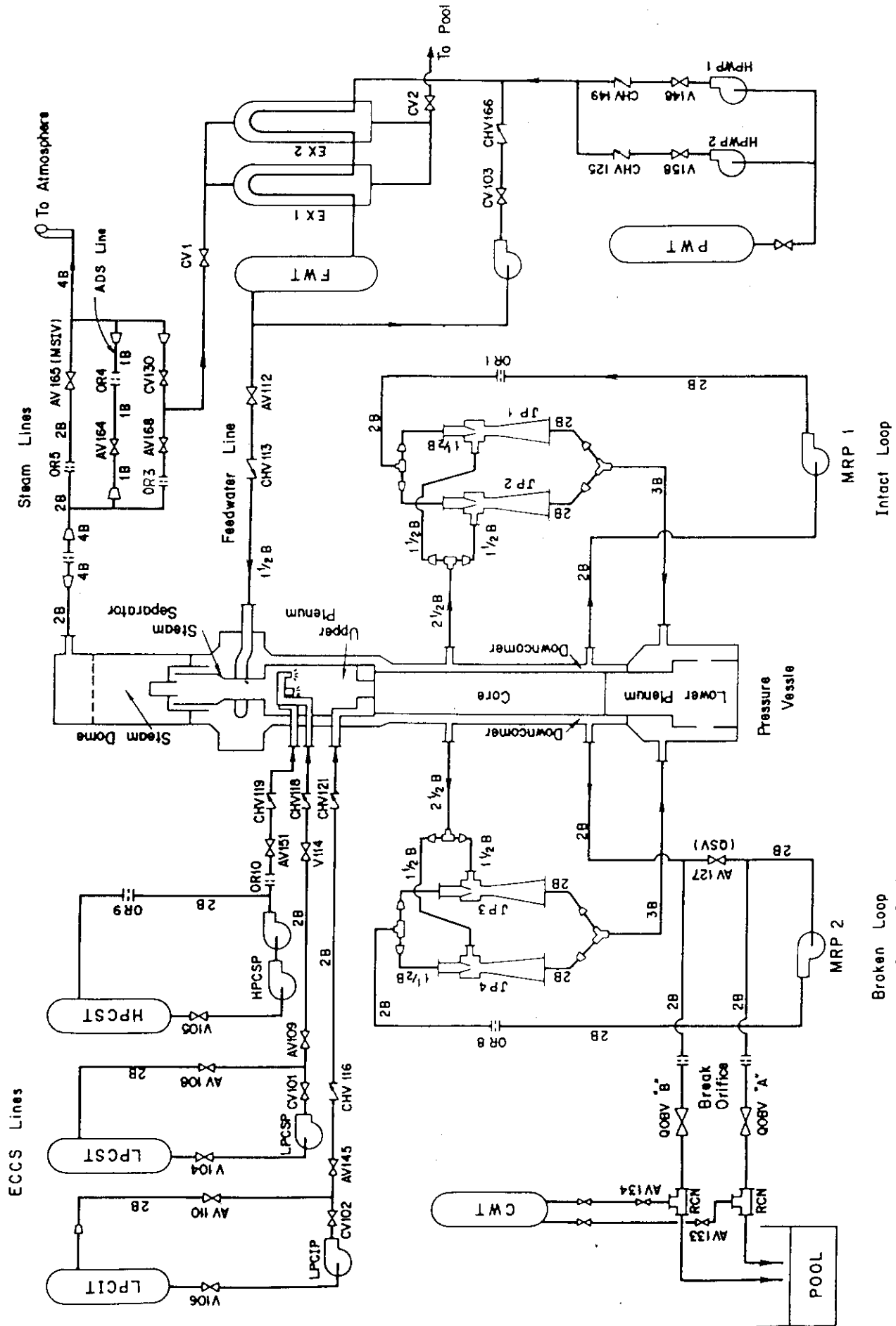
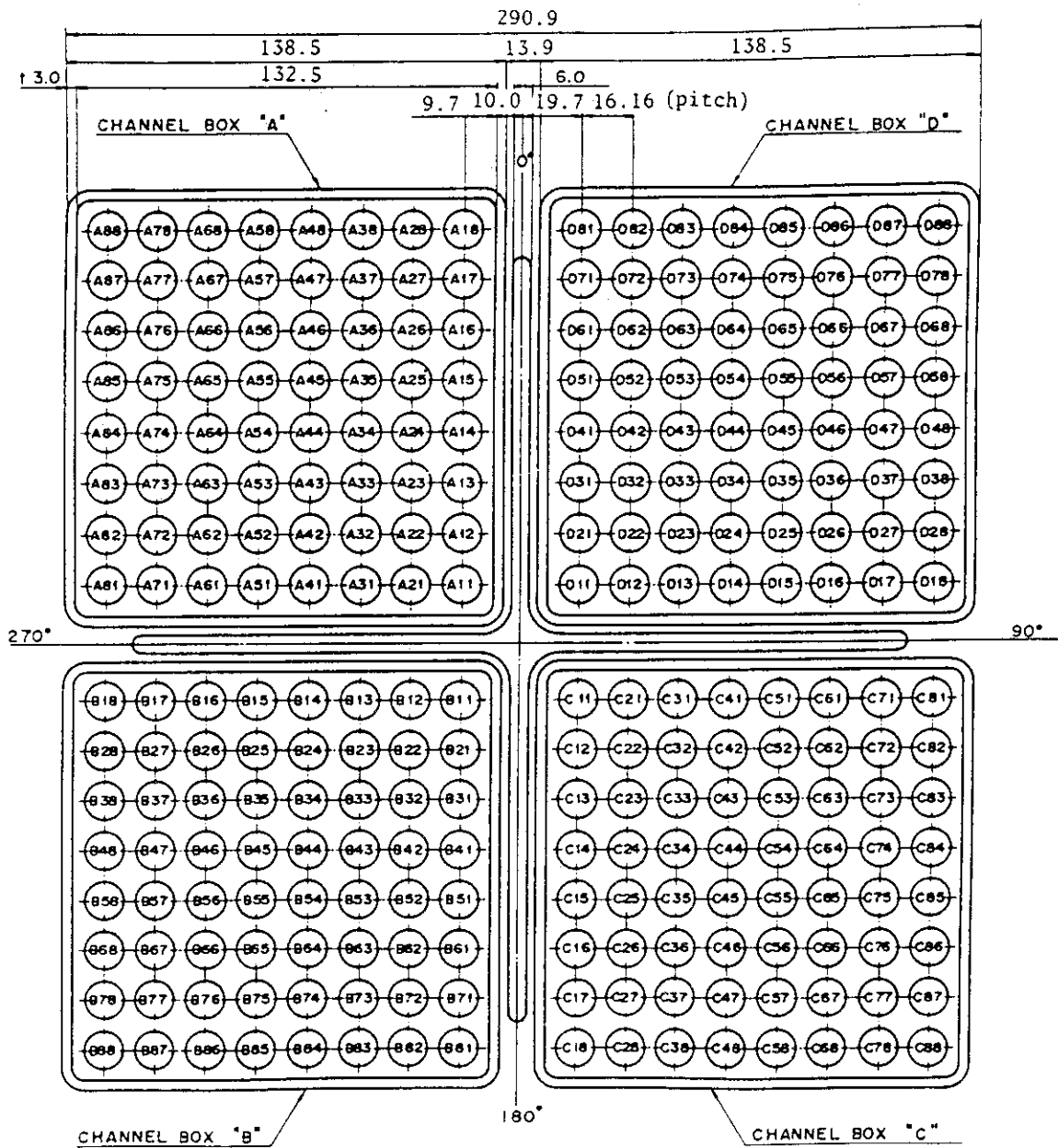


Fig. 2.3 Pressure Vessel Instruments Arrangement



Broken Loop Intact Loop
Fig. 2.4 ROSA-III Piping System



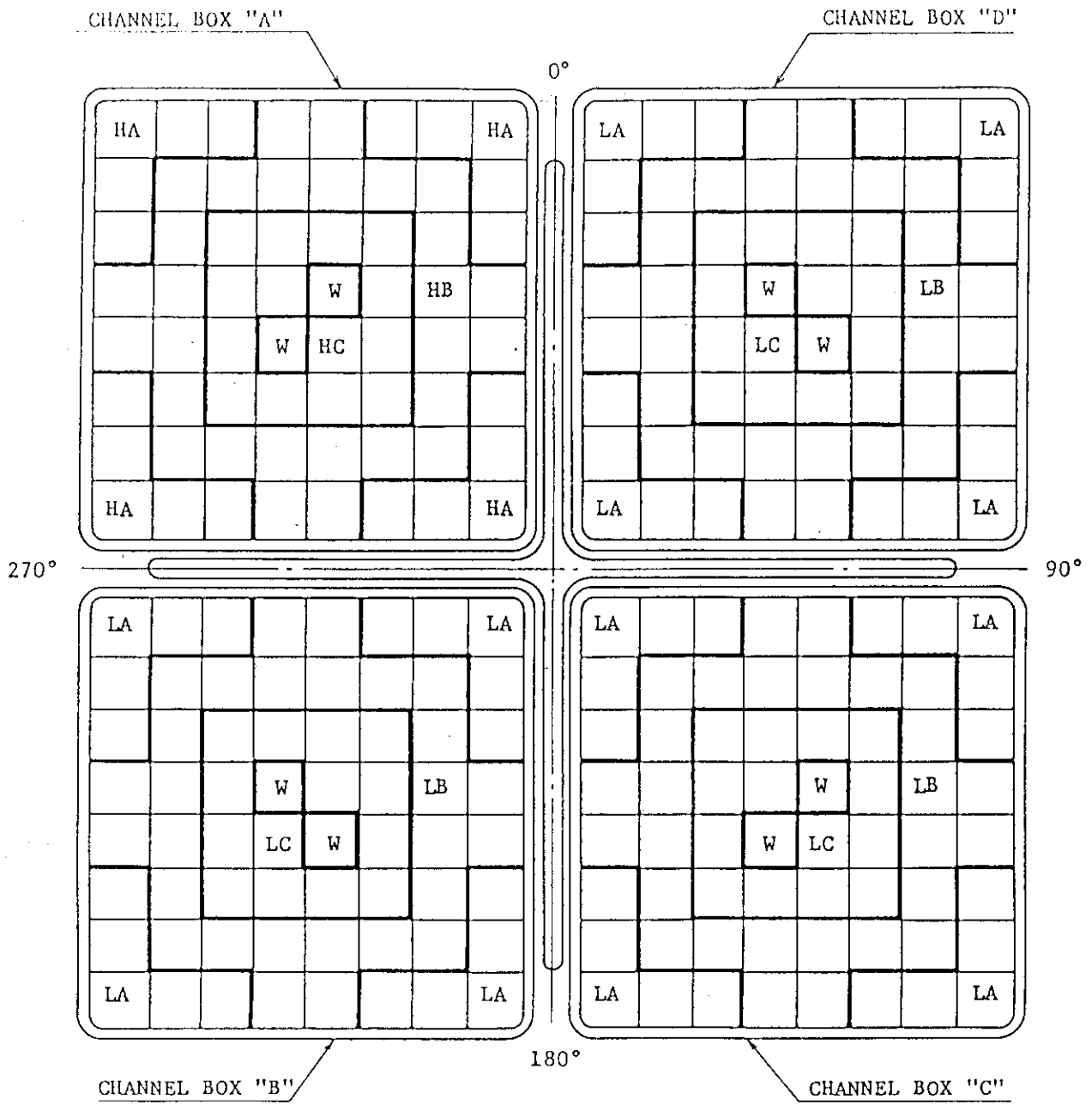
Peaking Factor ; A = 1.4, B, C and D = 1.0

Heater Rod O.D. = 12.27mm

A54, B54, C54 and D54 are water rod simulators with void probes.
O.D. = 15.01mm

A45, B45, C45 and D45 are water rod simulators with thermocouples.
O.D. = 15.01mm

Fig. 2.5 (a) Heater Rod Arrangement

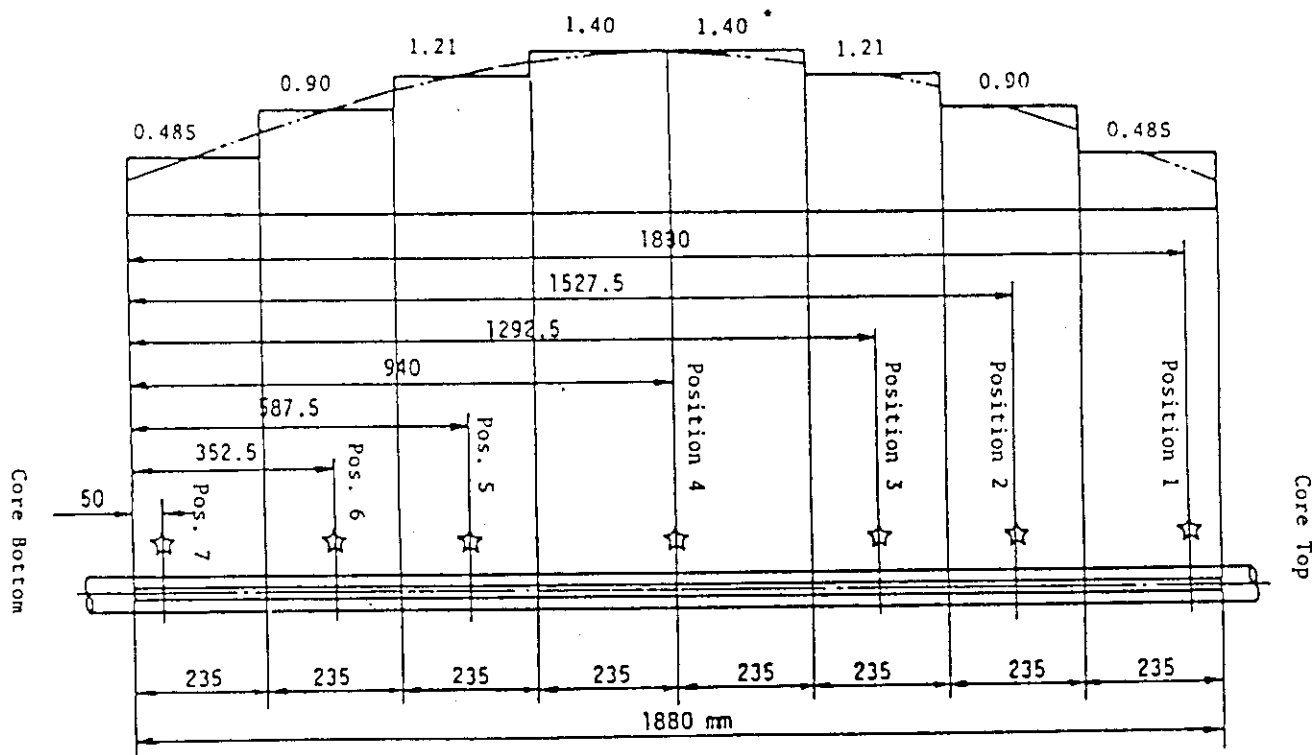


Region	HA	HB	HC	LA	LB	LC	W
Linear Heat Rate (kw/m)*	18.5	16.81	14.41	13.21	12.01	10.29	0.0
Local Peaking factor	1.1	1.0	0.875	1.1	1.0	0.875	0.0
No. of Rods	20	28	14	60	84	42	8

note : Radial Peaking factor is 1.4

* in the case of power = 4.4MW

Fig. 2.5 (b) Radial Power Distribution



☆ indicates position of thermocouple. * Axial Peaking Factor

Fig. 2.6 Axial Power Distribution

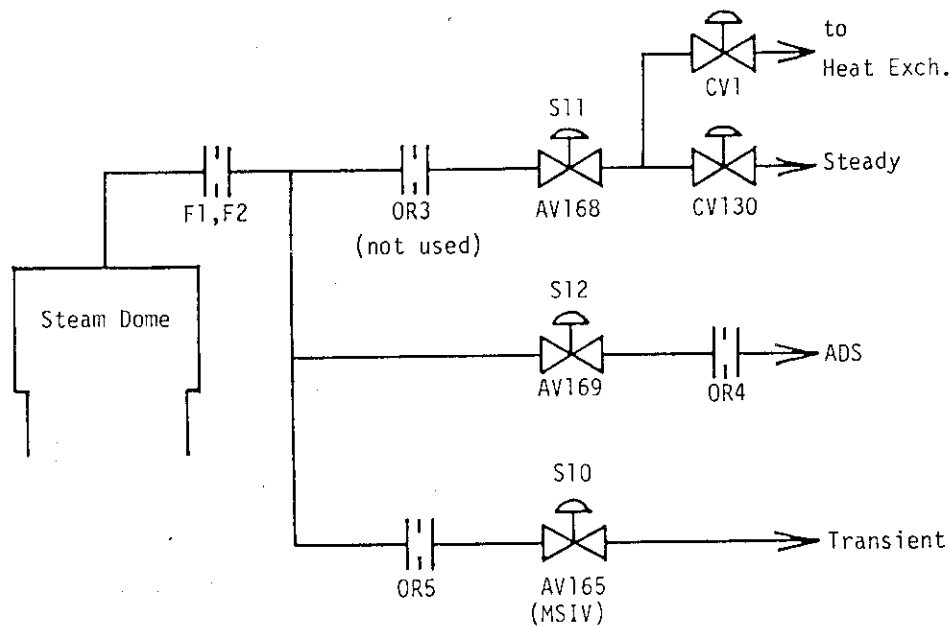


Fig. 2.7 Schematic of Steam Line

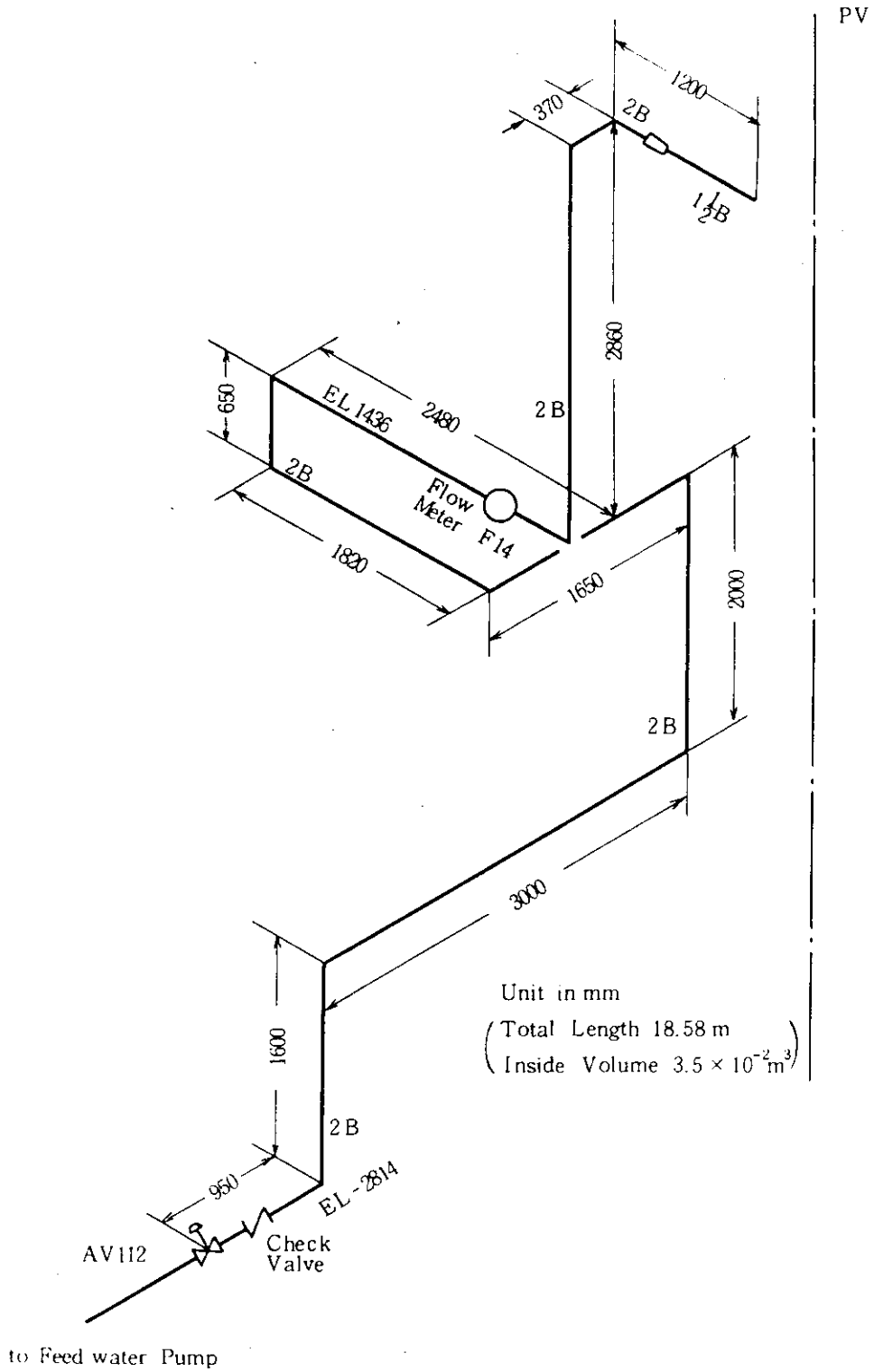
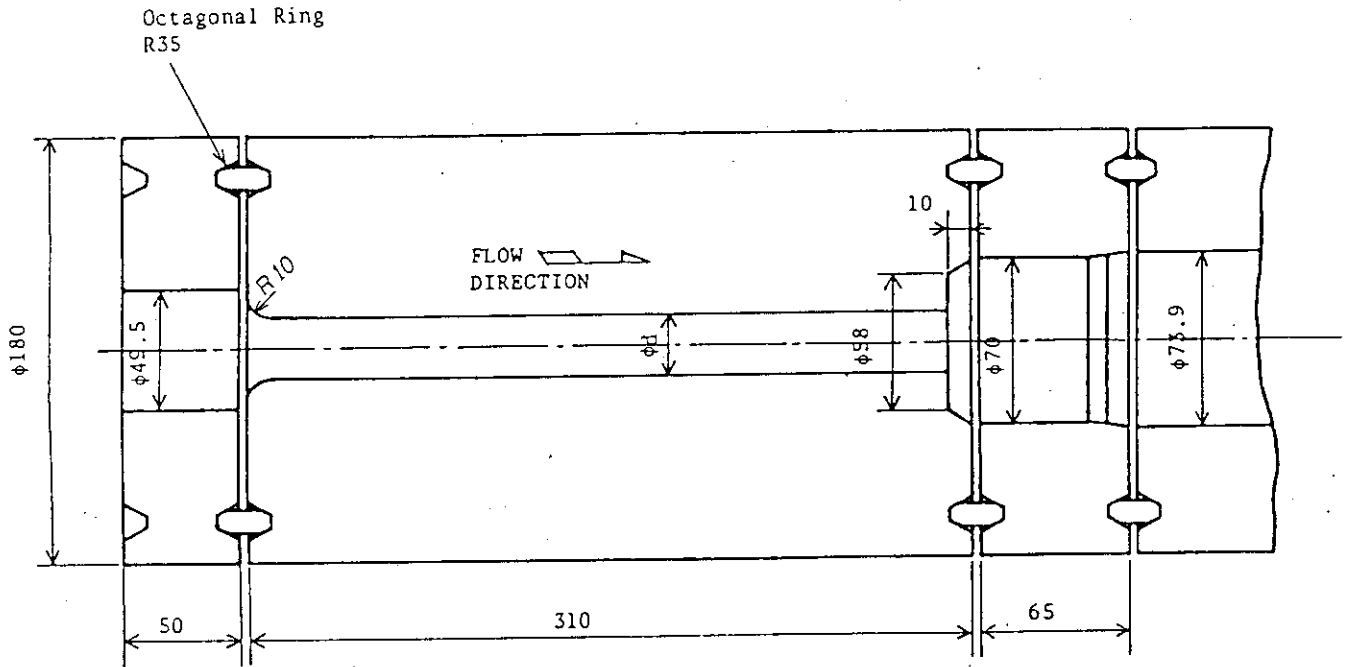


Fig. 2.8 Schematic of Feedwater Line



Material SUS304
Dimension in mm

Break area ratio (%)	d (mm)
100	26.2

Fig. 2.9 Break Nozzle

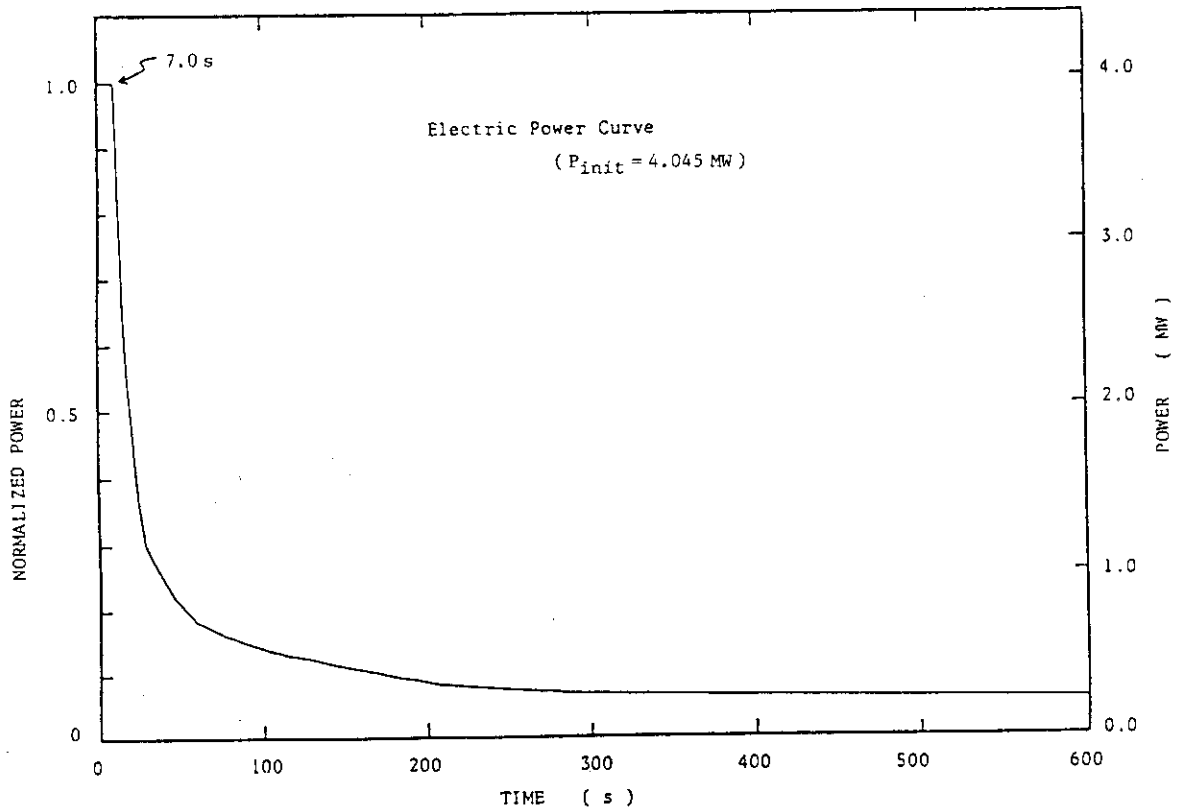


Fig. 2.10 Power Transient

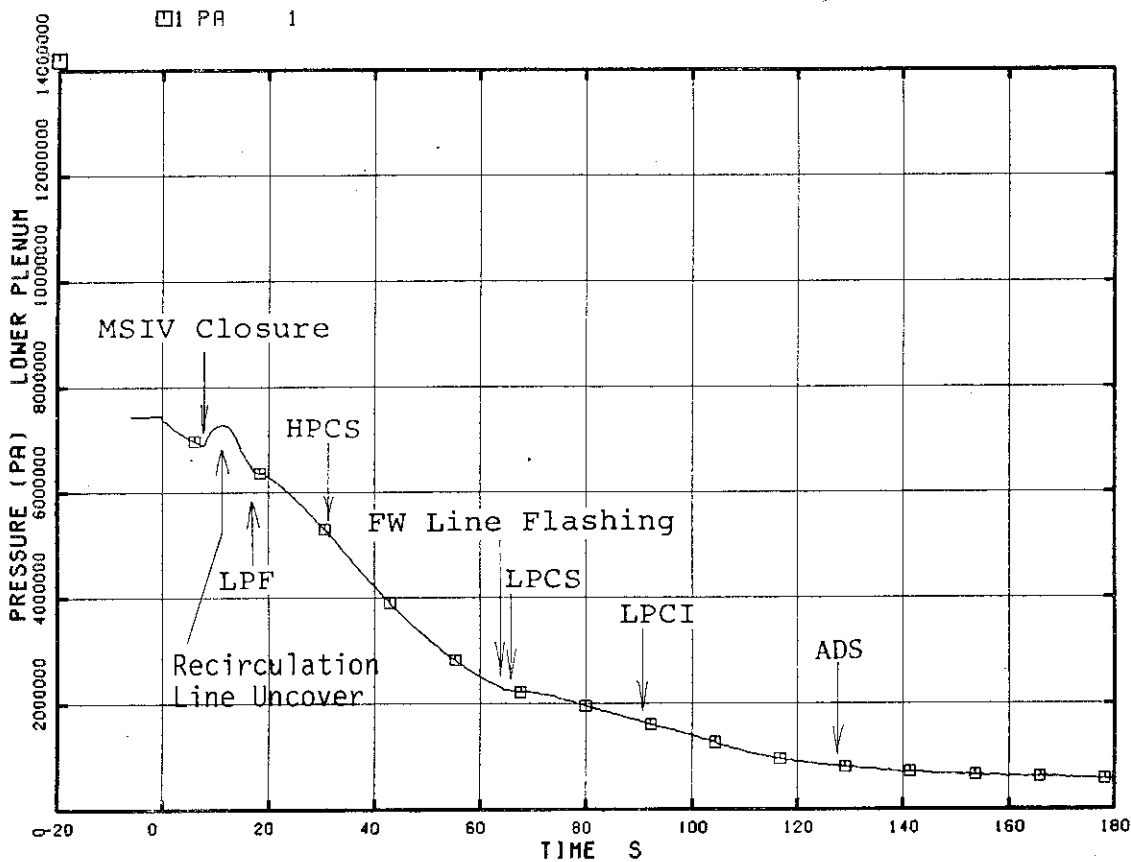


Fig. 2.11 Lower Plenum Pressure

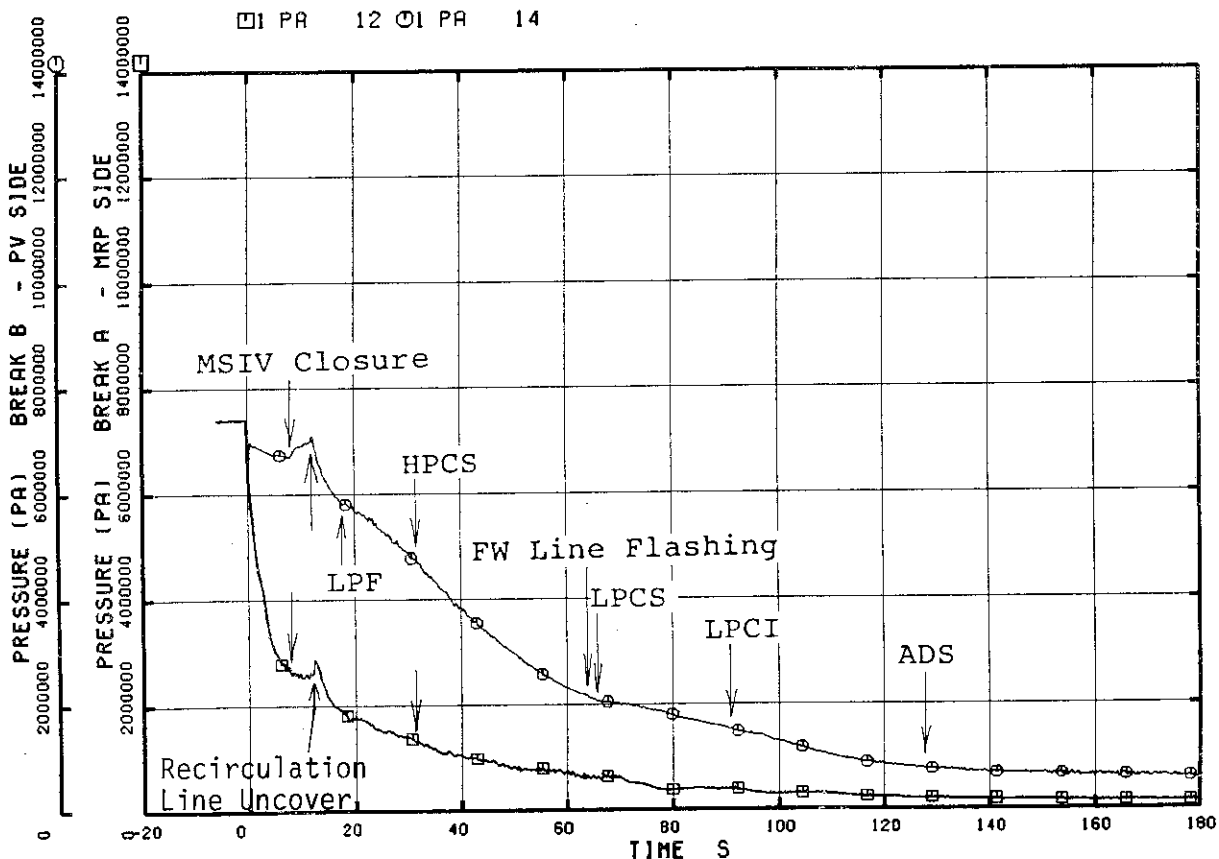


Fig. 2.12 Break Upstream Pressure

□ PD 21

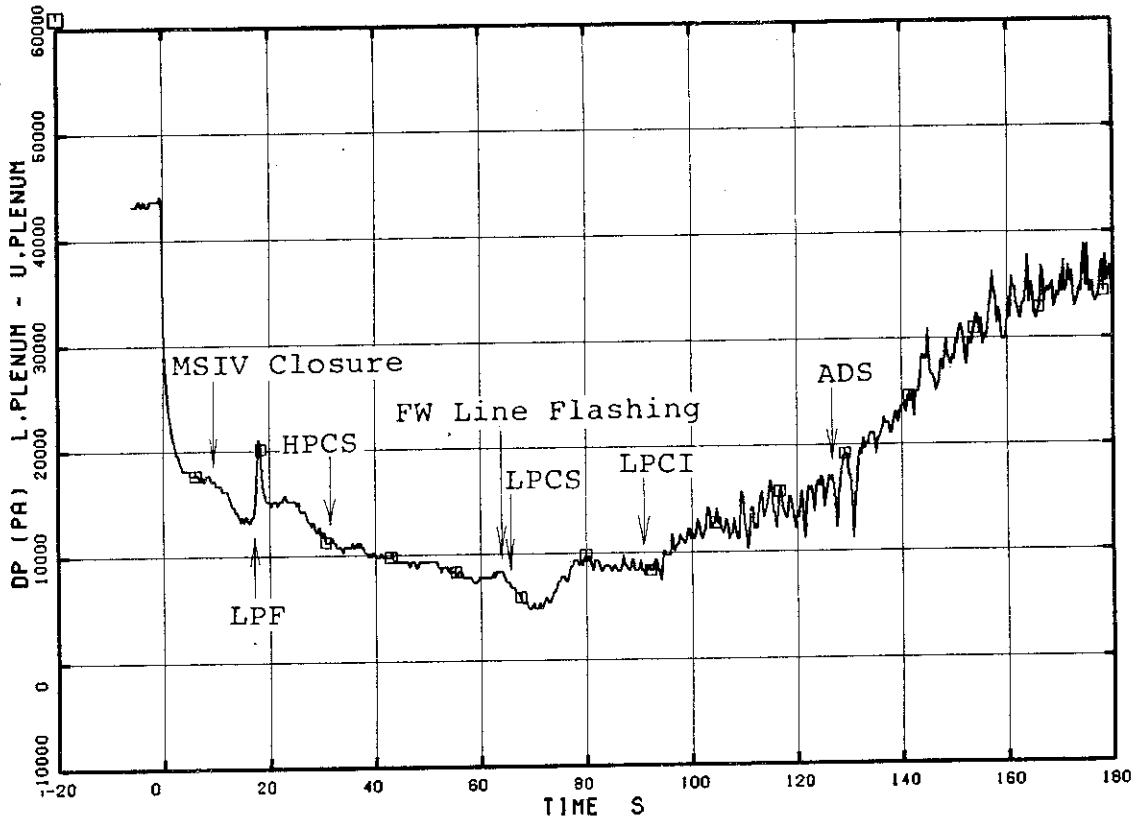


Fig. 2.13 Differential Pressure between Lower and Upper Plena

□ PD 22

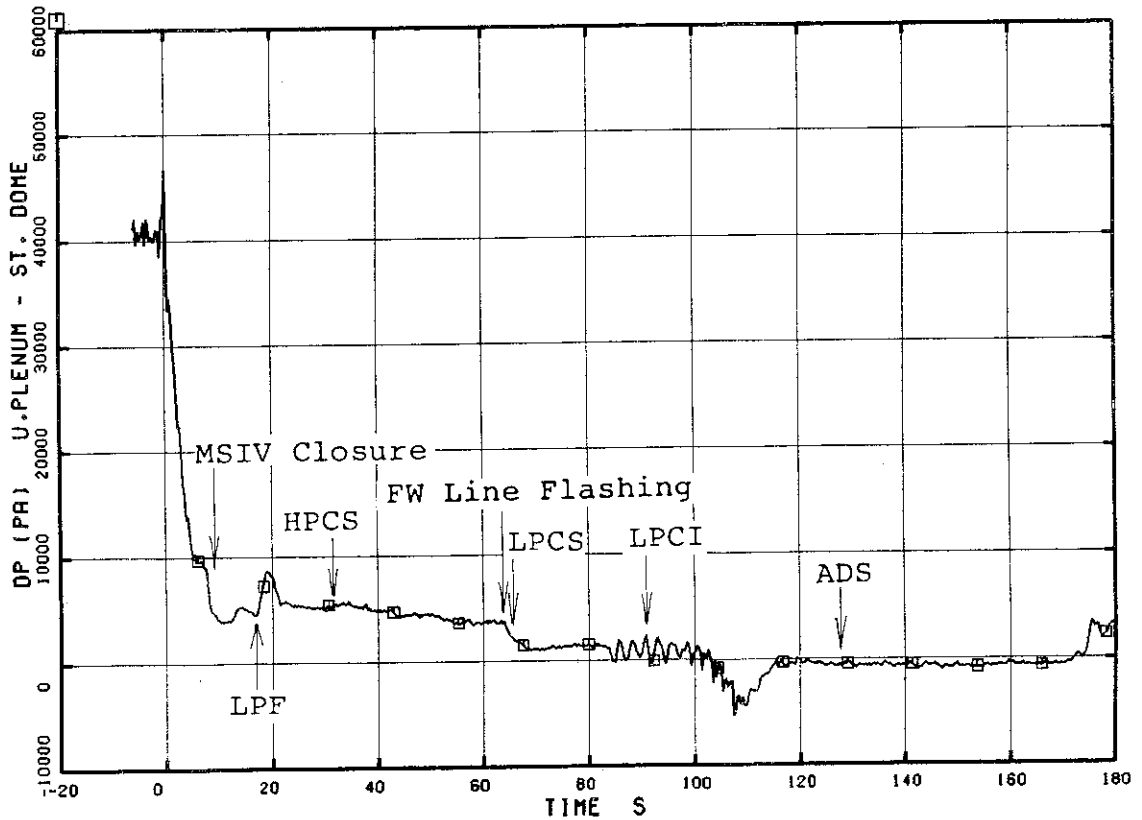


Fig. 2.14 Differential Pressure between Upper Plenum and Steam Dome

□ PD 25

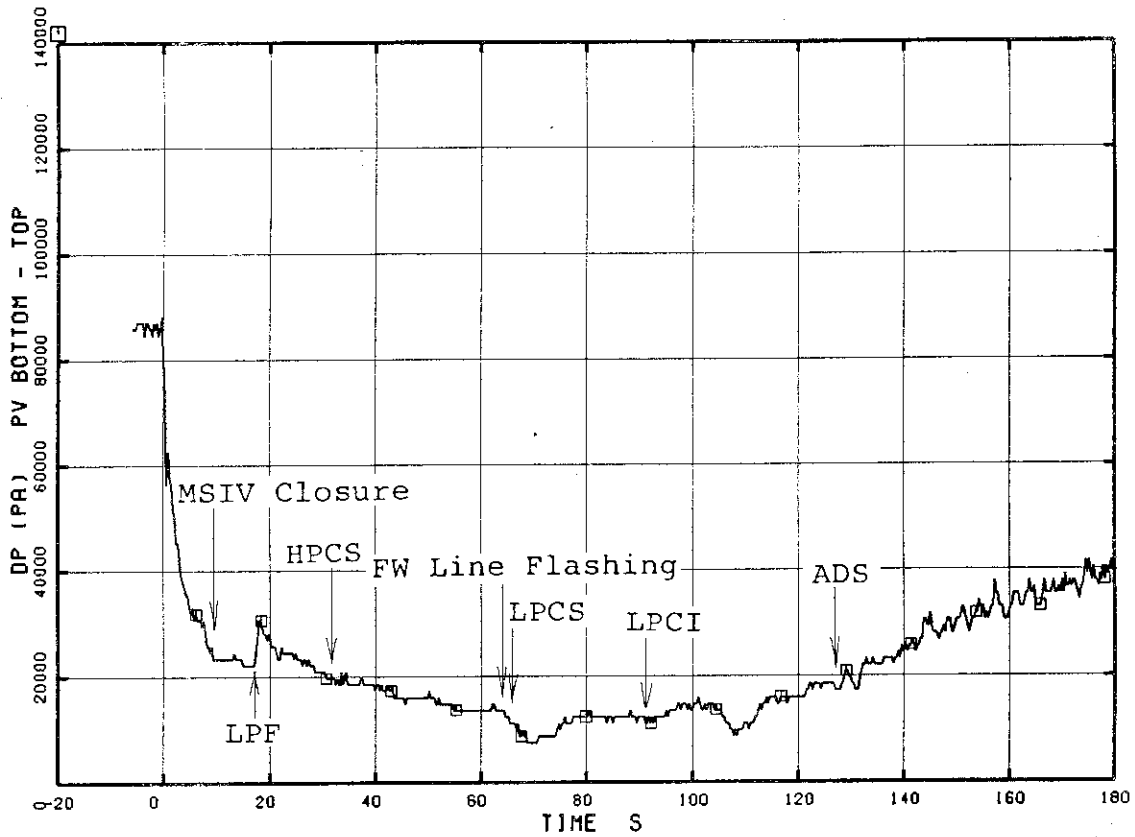


Fig. 2.15 Differential Pressure between Lower Plenum and Steam Dome

□ PD 24

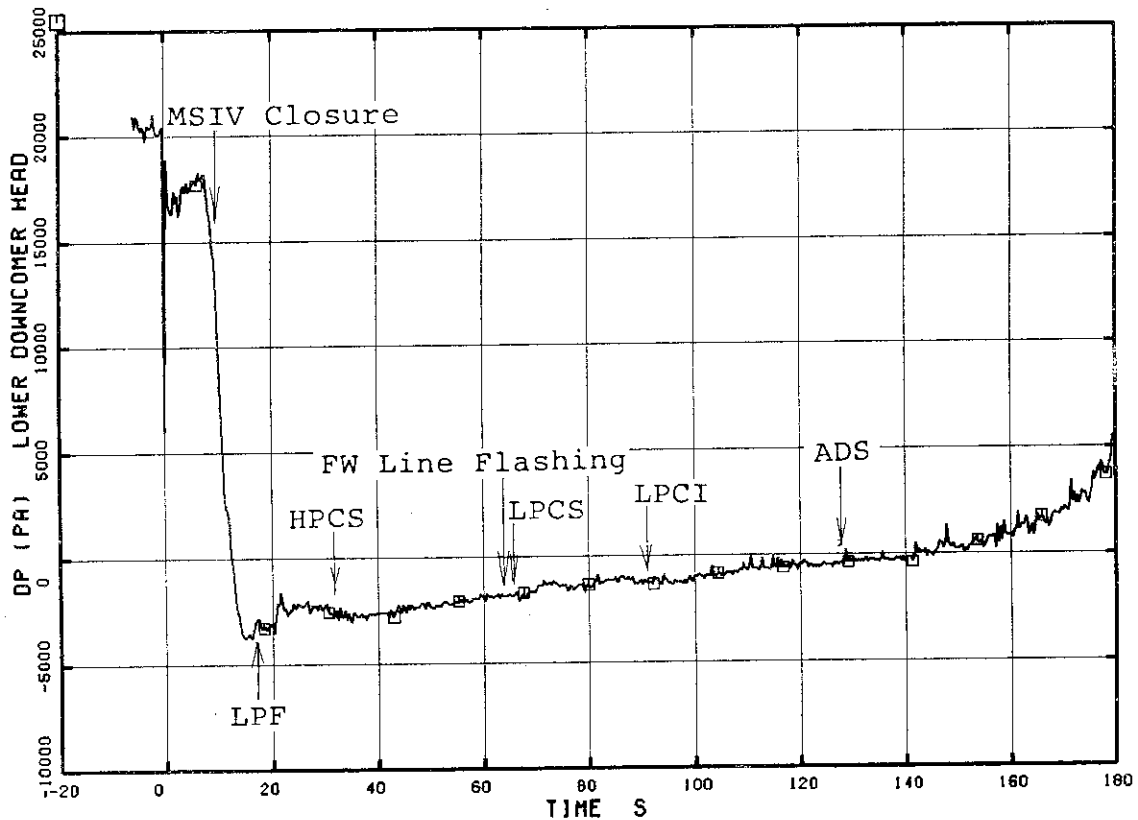


Fig. 2.16 Lower Downcomer Head

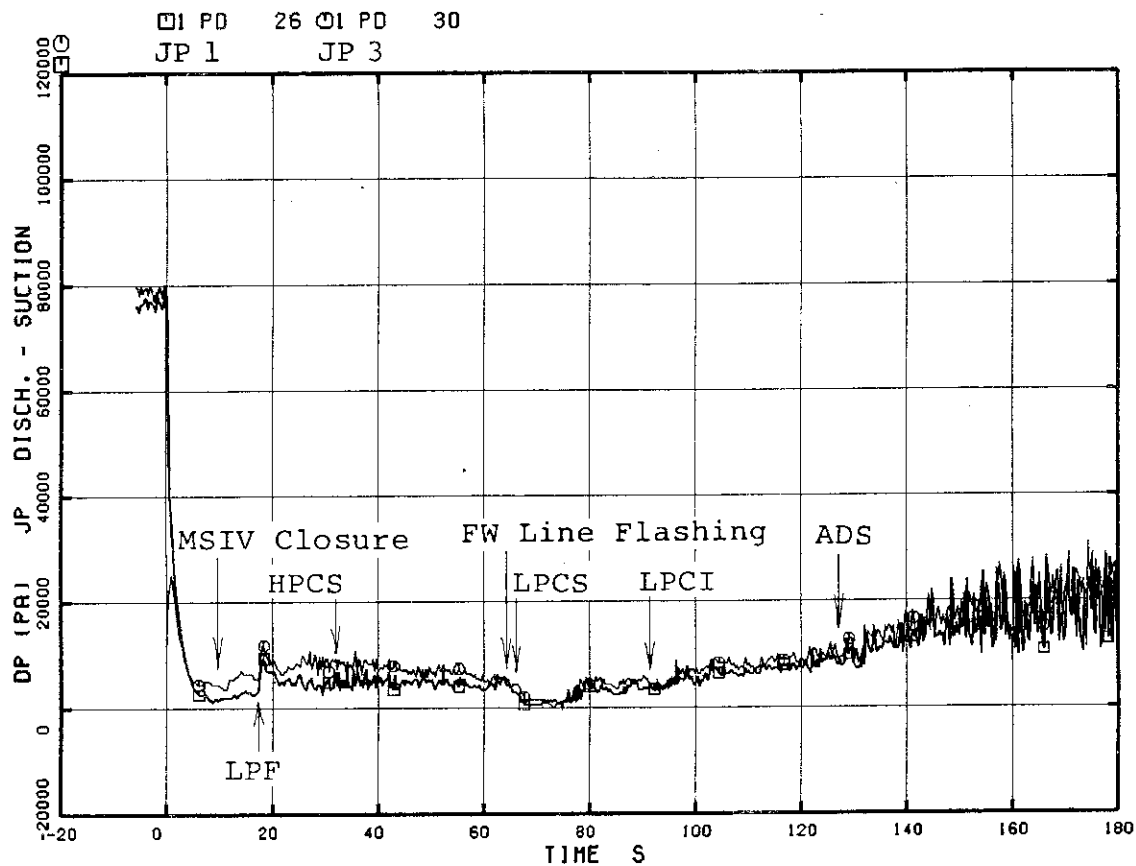


Fig. 2.17 Differential Pressure between Jet Pump Discharge and Suction

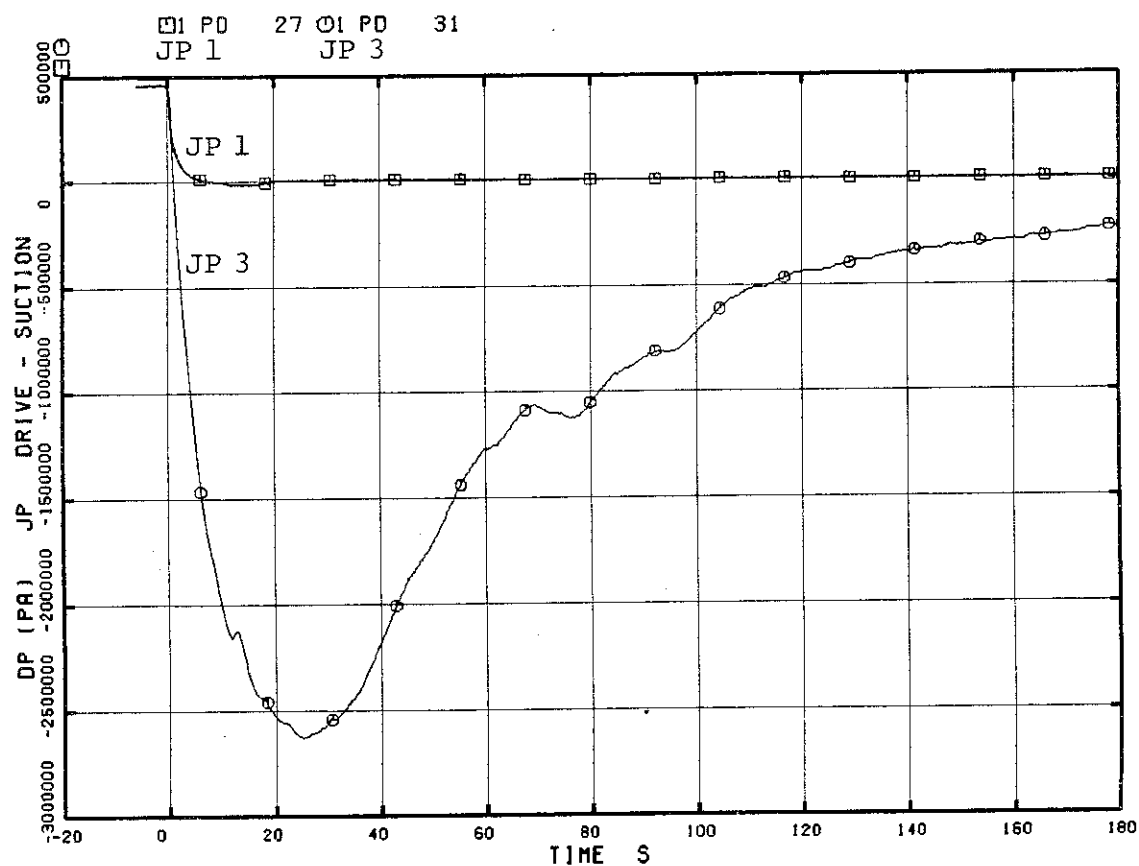


Fig. 2.18 Differential Pressure between Jet Pump Drive and Suction

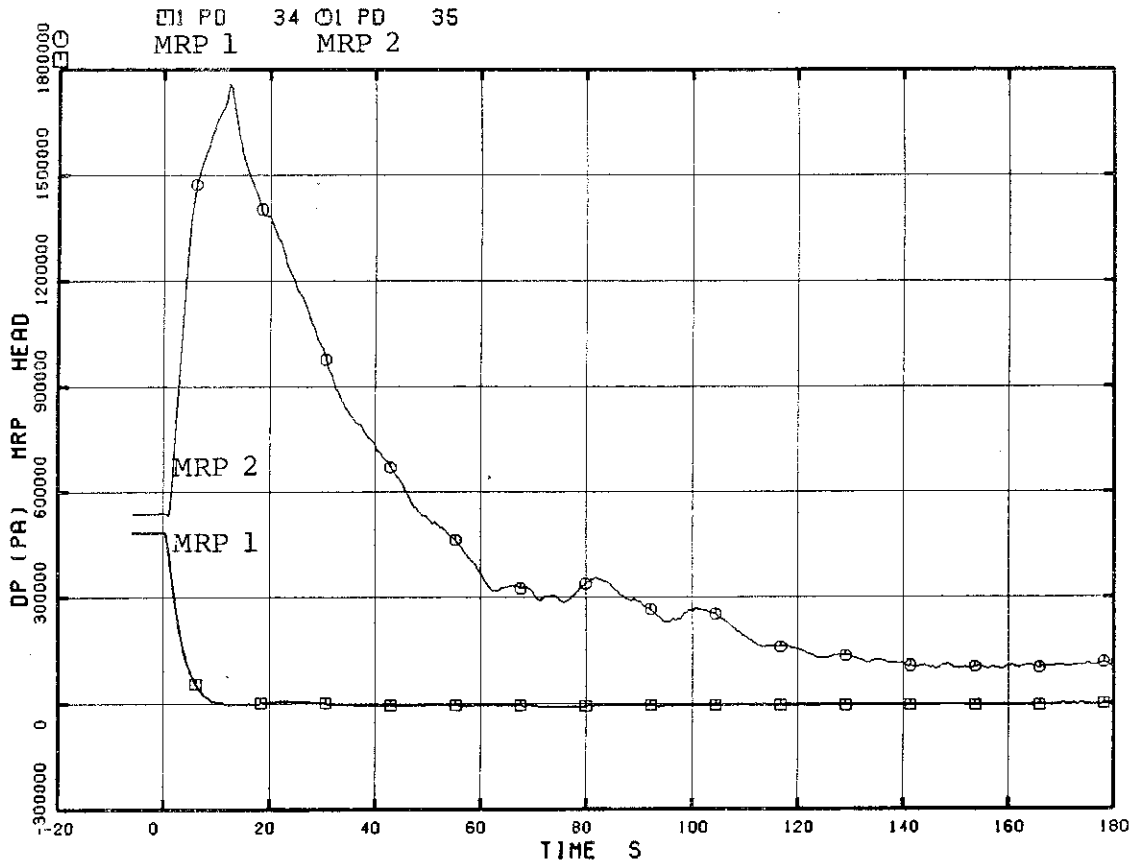


Fig. 2.19 Differential Pressure between MRP Delivery and Suction

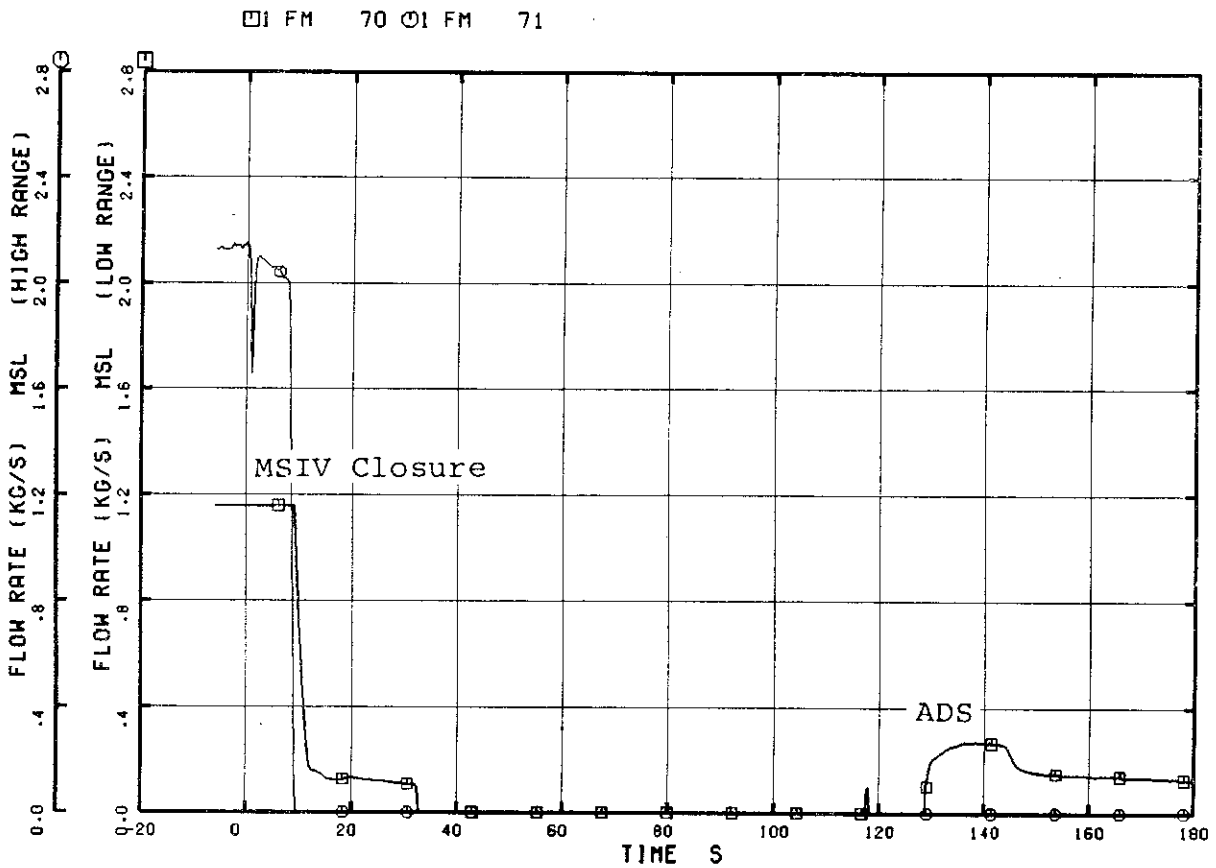


Fig. 2.20 Main Steam Discharge Flow Rate

□ FV 76

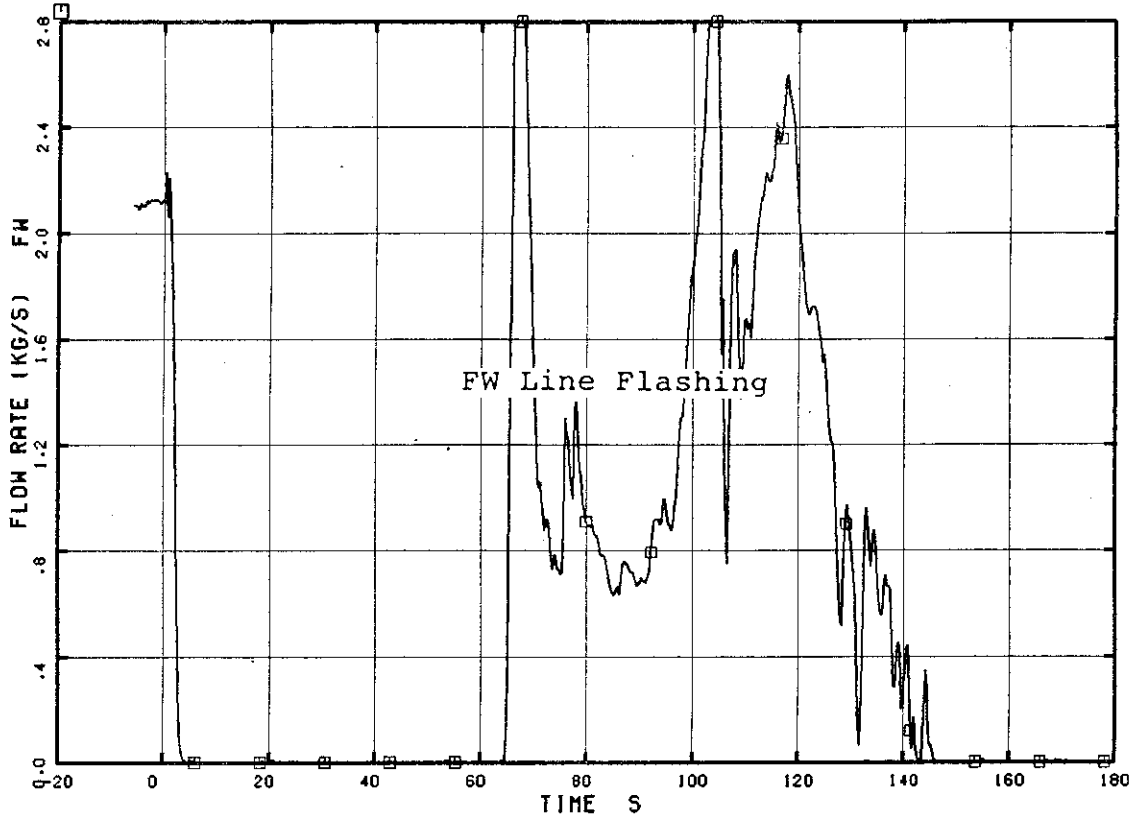


Fig. 2.21(a) Feedwater Flow Rate

□ FV 76

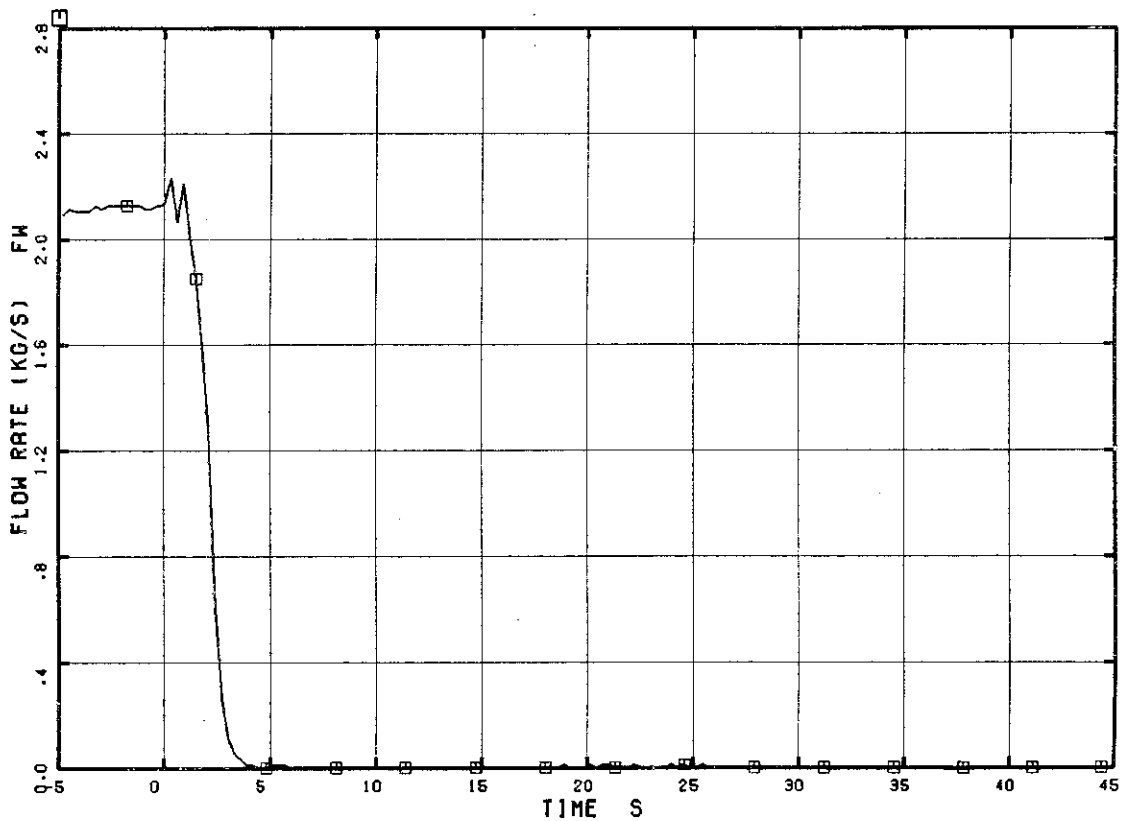


Fig. 2.21(b) Feedwater Flow Rate (Expanded Time History)

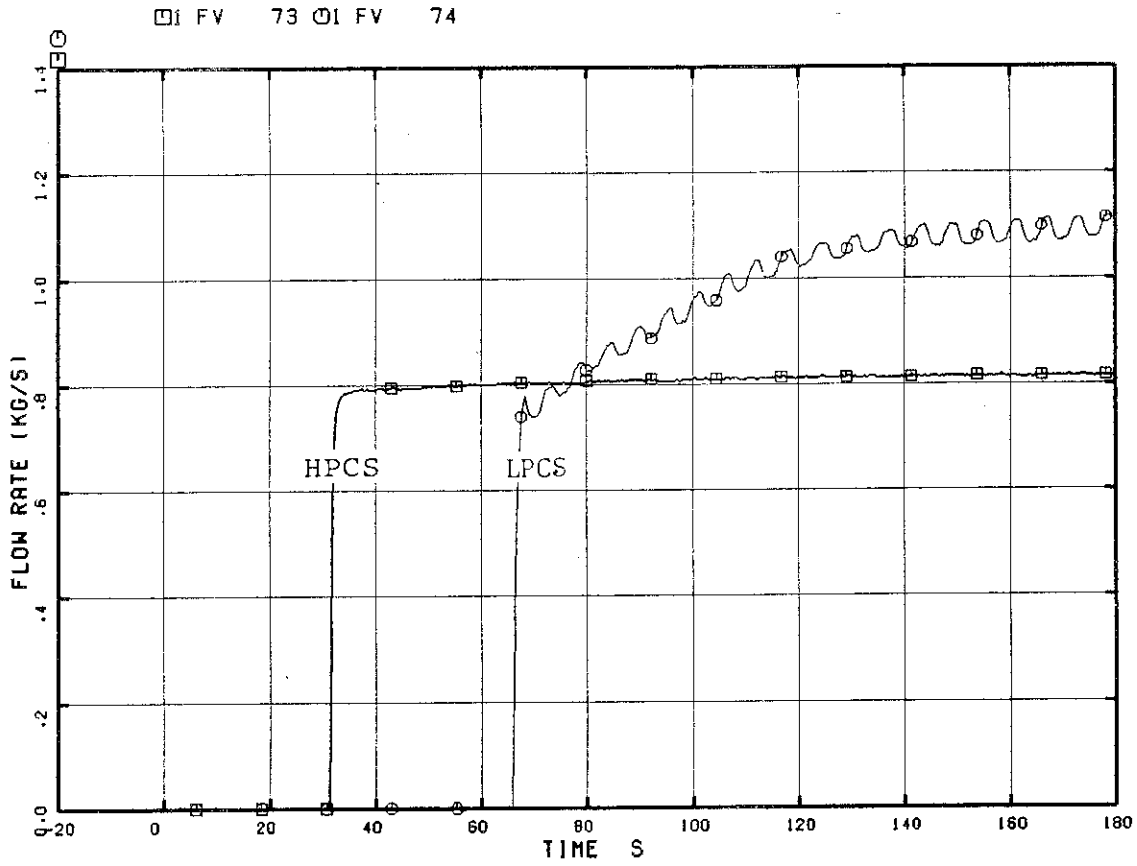


Fig. 2.22 HPCS and LPCS Flow Rates

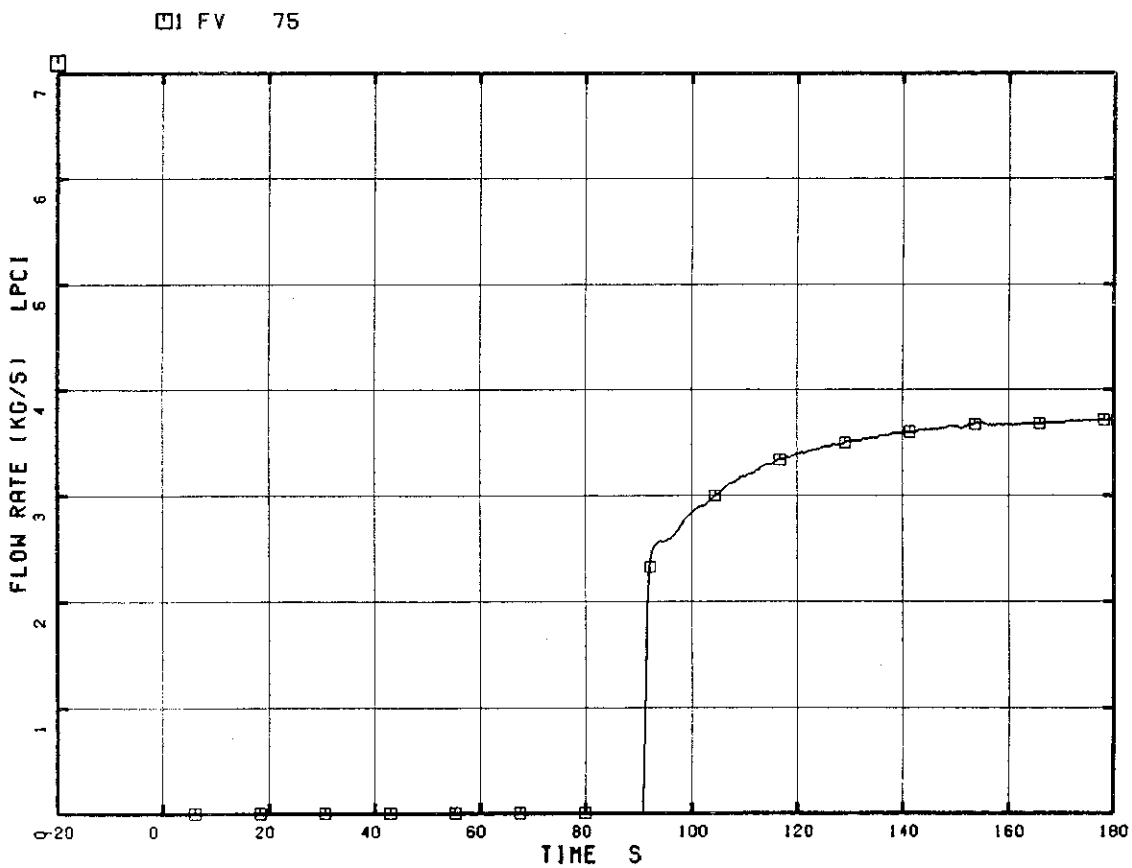


Fig. 2.23 LPCI Flow Rates

□ FM 714

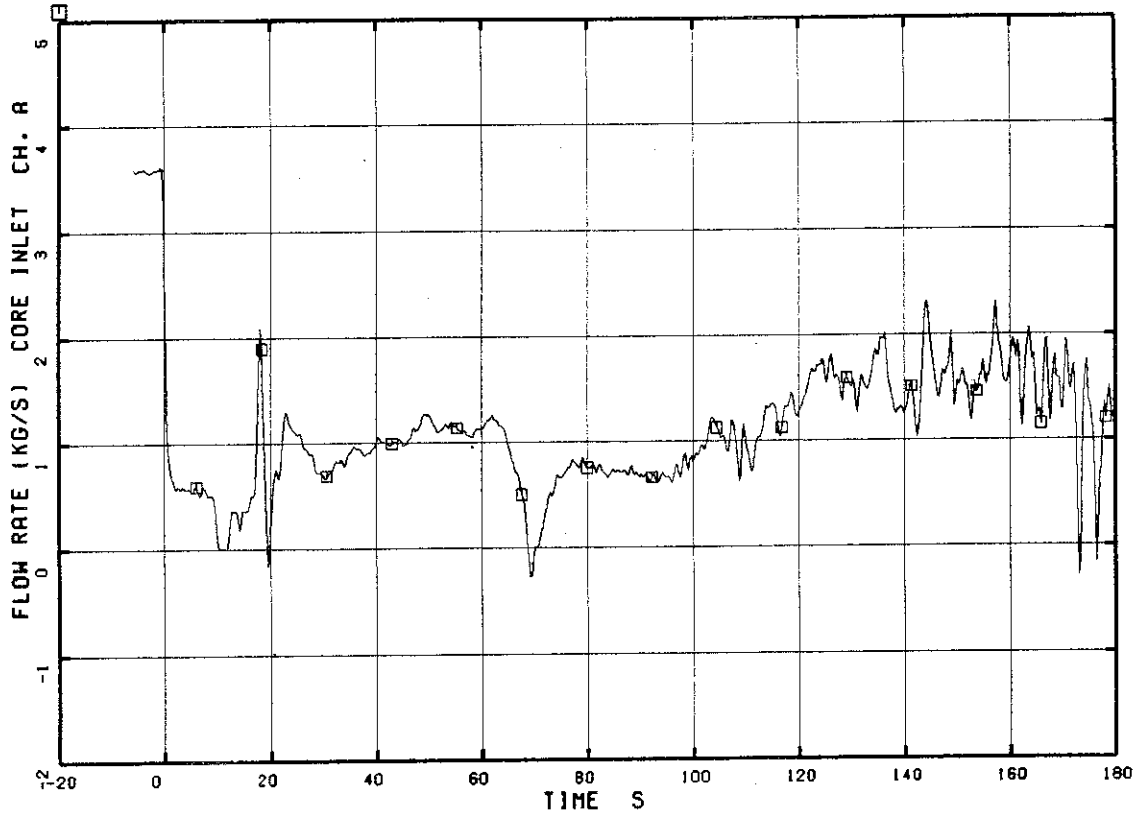


Fig. 2.24 Core Inlet Flow of Channel A

□ FM 715

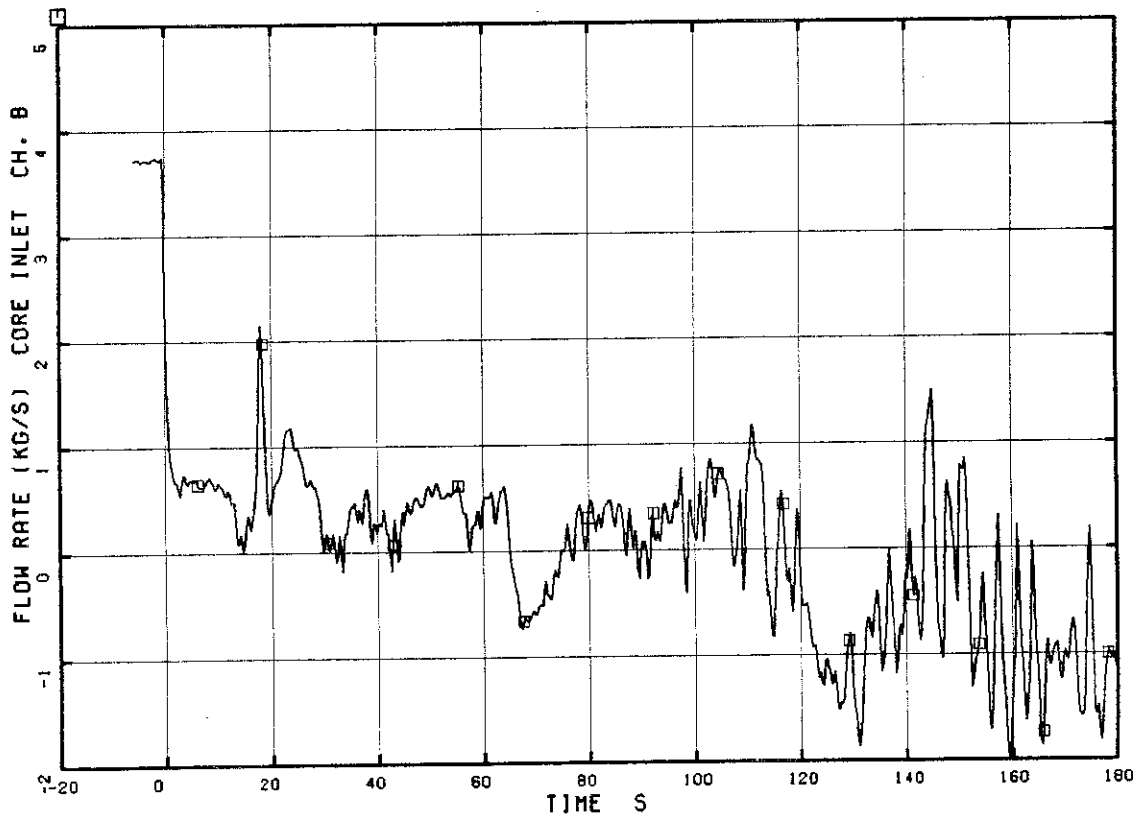


Fig. 2.25 Core Inlet Flow of Channel B

□ FM 716

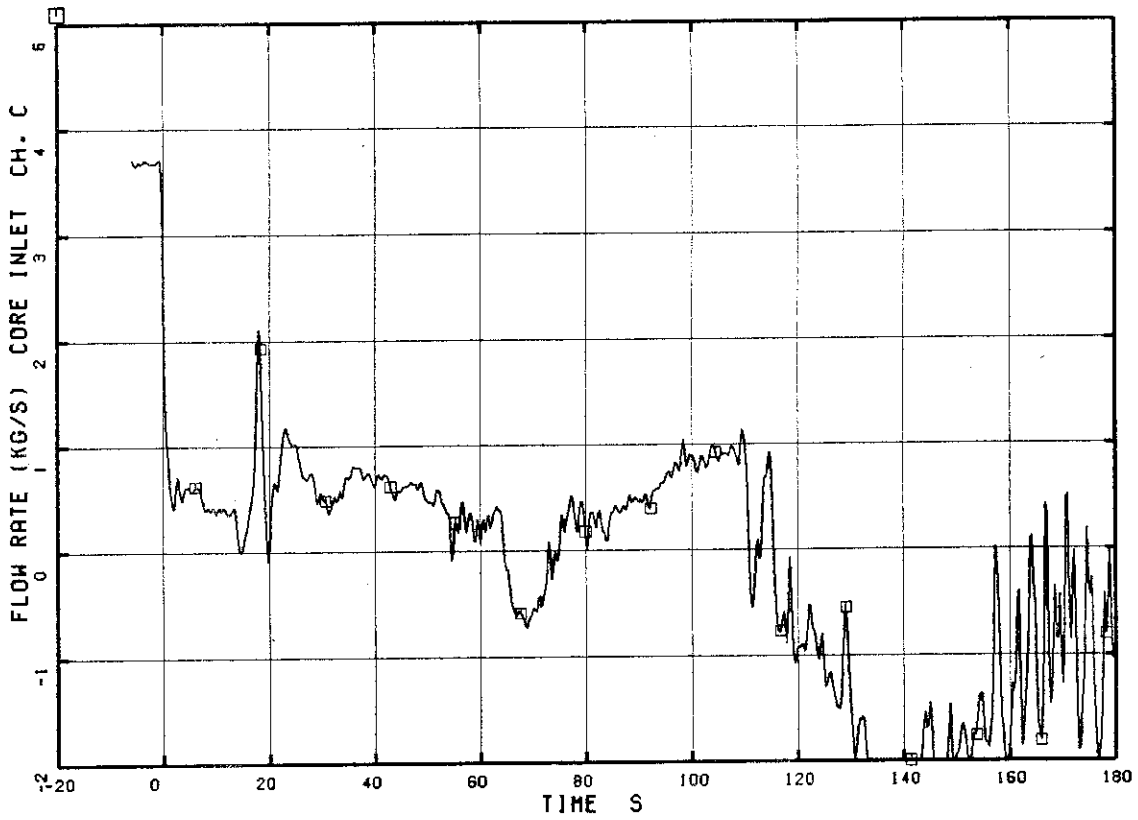


Fig. 2.26 Core Inlet Flow of Channel C

□ FM 717

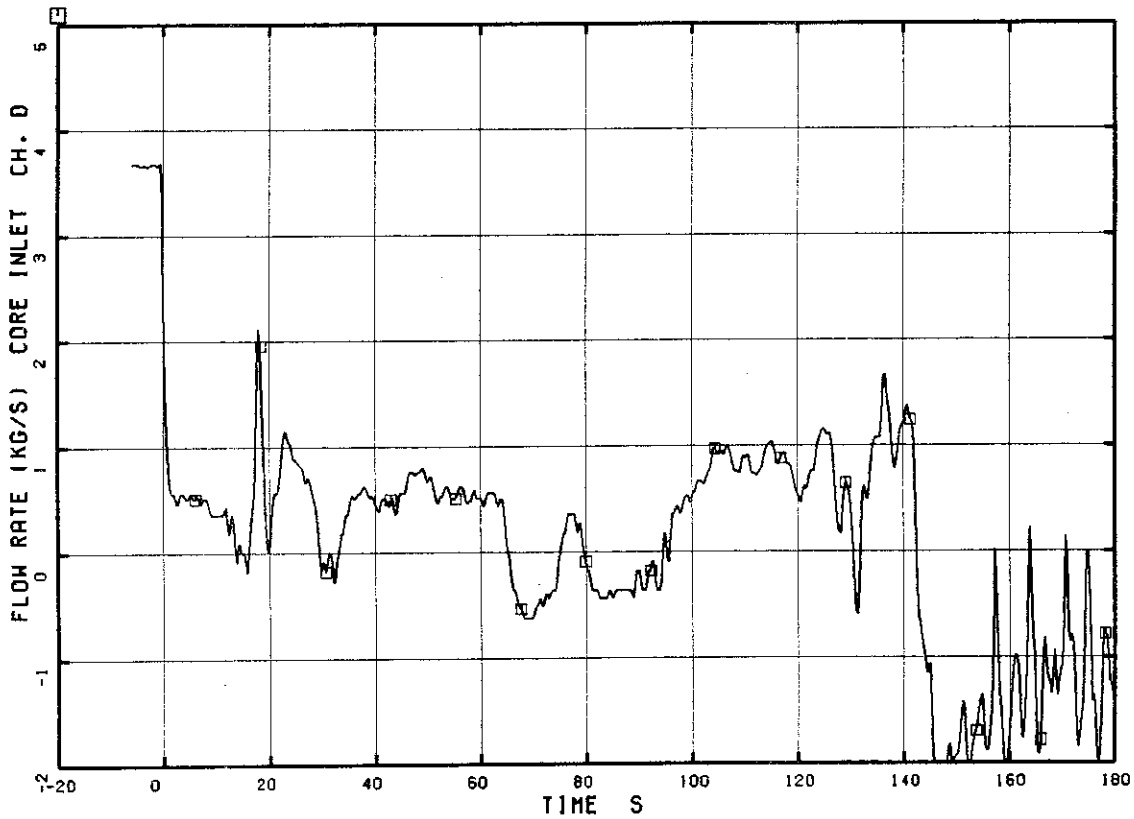


Fig. 2.27 Core Inlet Flow of Channel D

□ FM 718

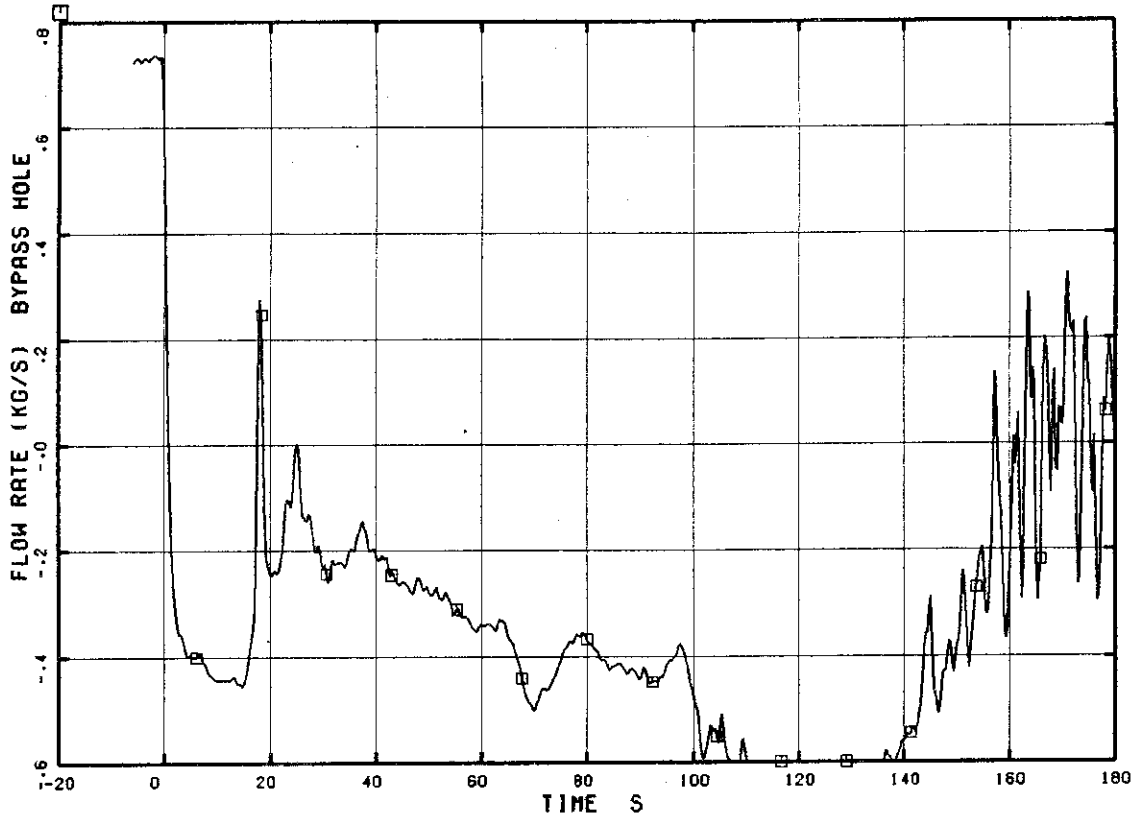


Fig. 2.28 Guide Tube Inlet Flow

□ WE 101 ○ WE 102

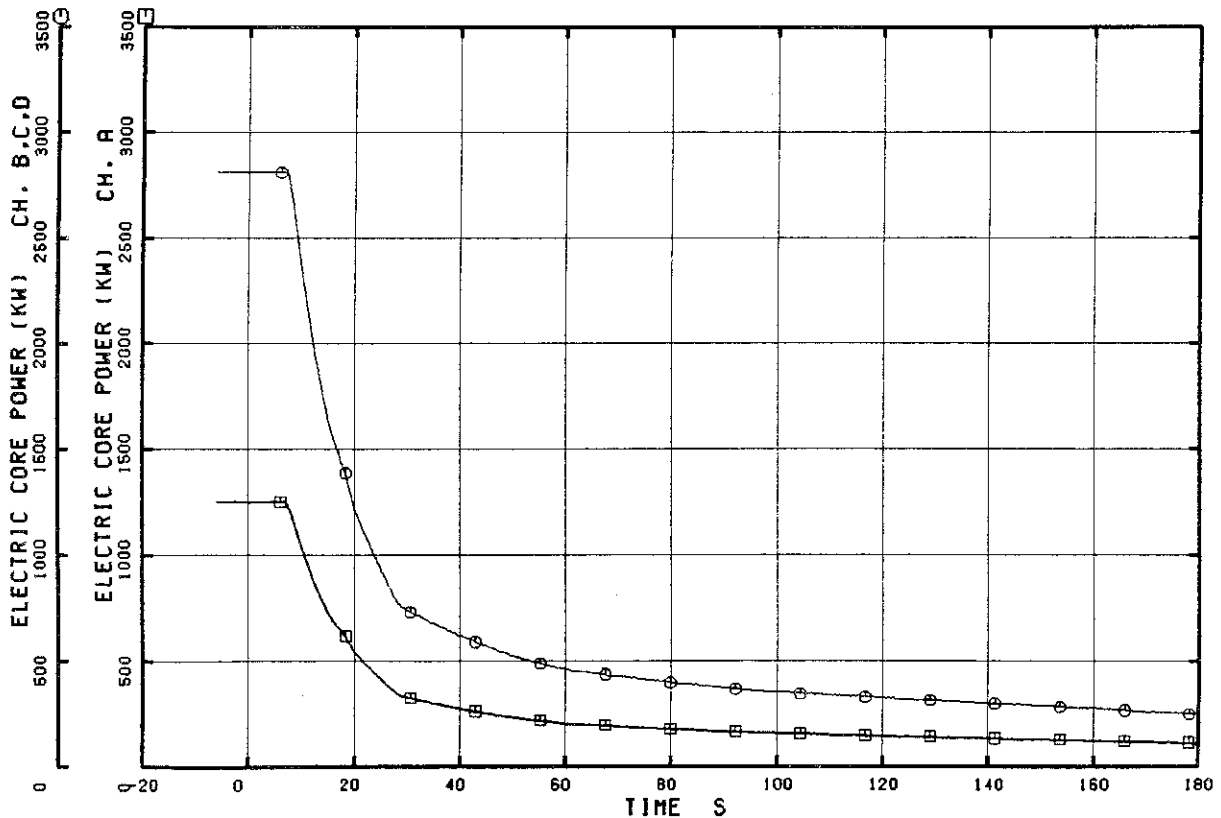


Fig. 2.29 Electric Core Power

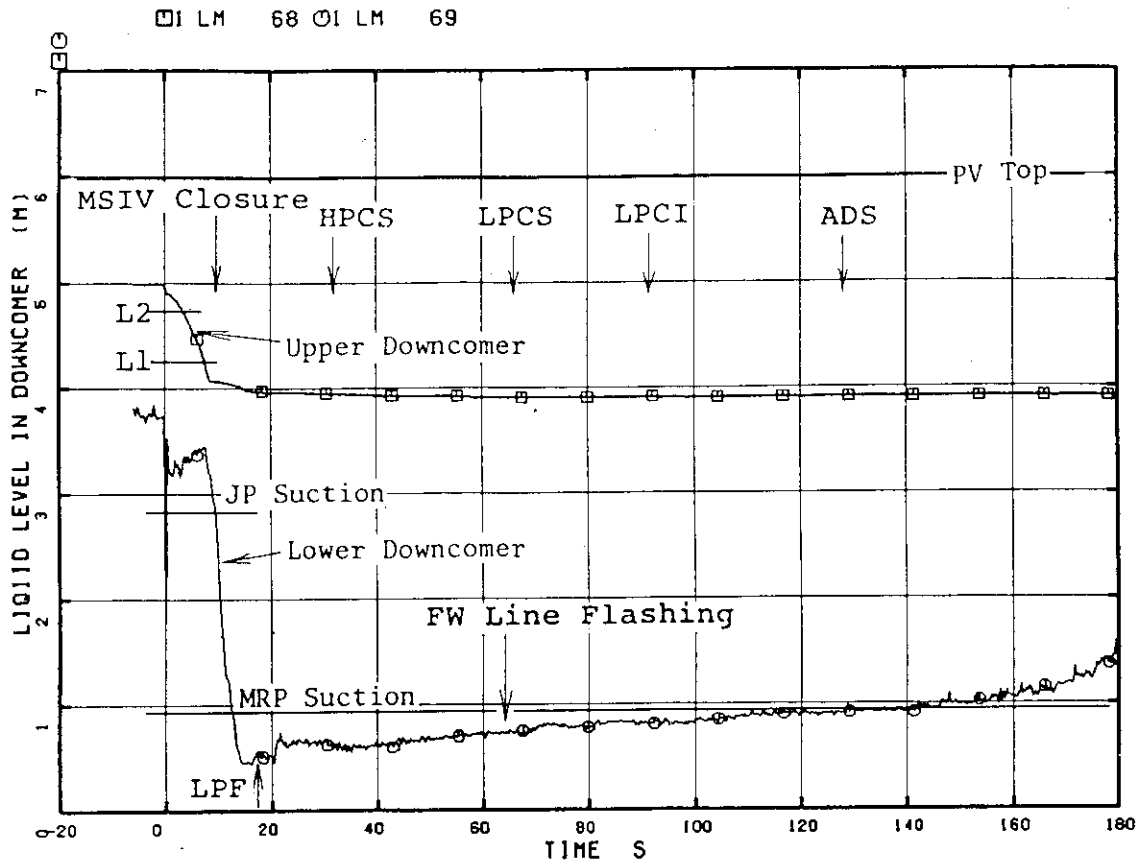


Fig. 2.30 Liquid Level in Downcomer

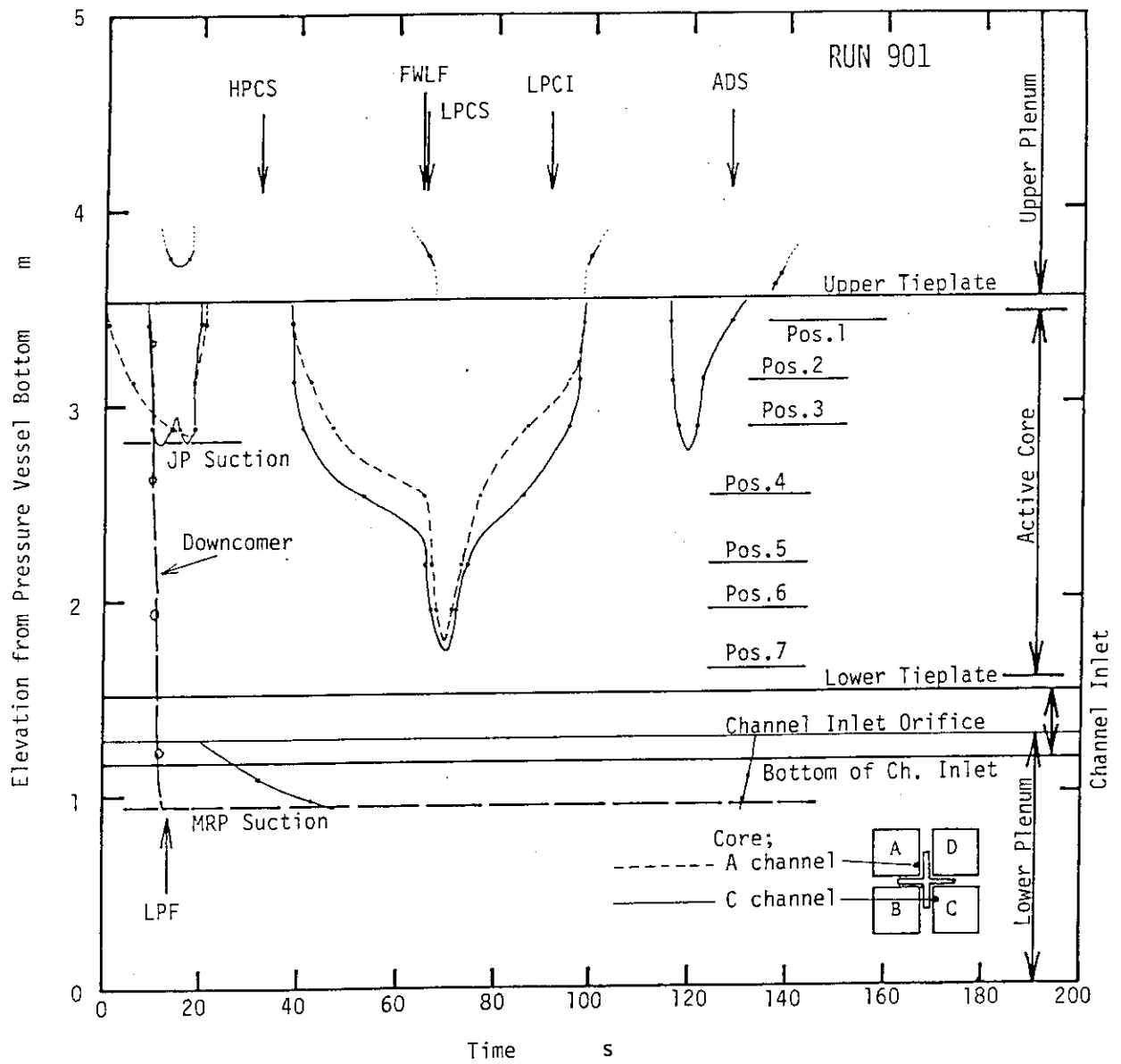


Fig. 2.31 Liquid Level Transients in Pressure Vessel

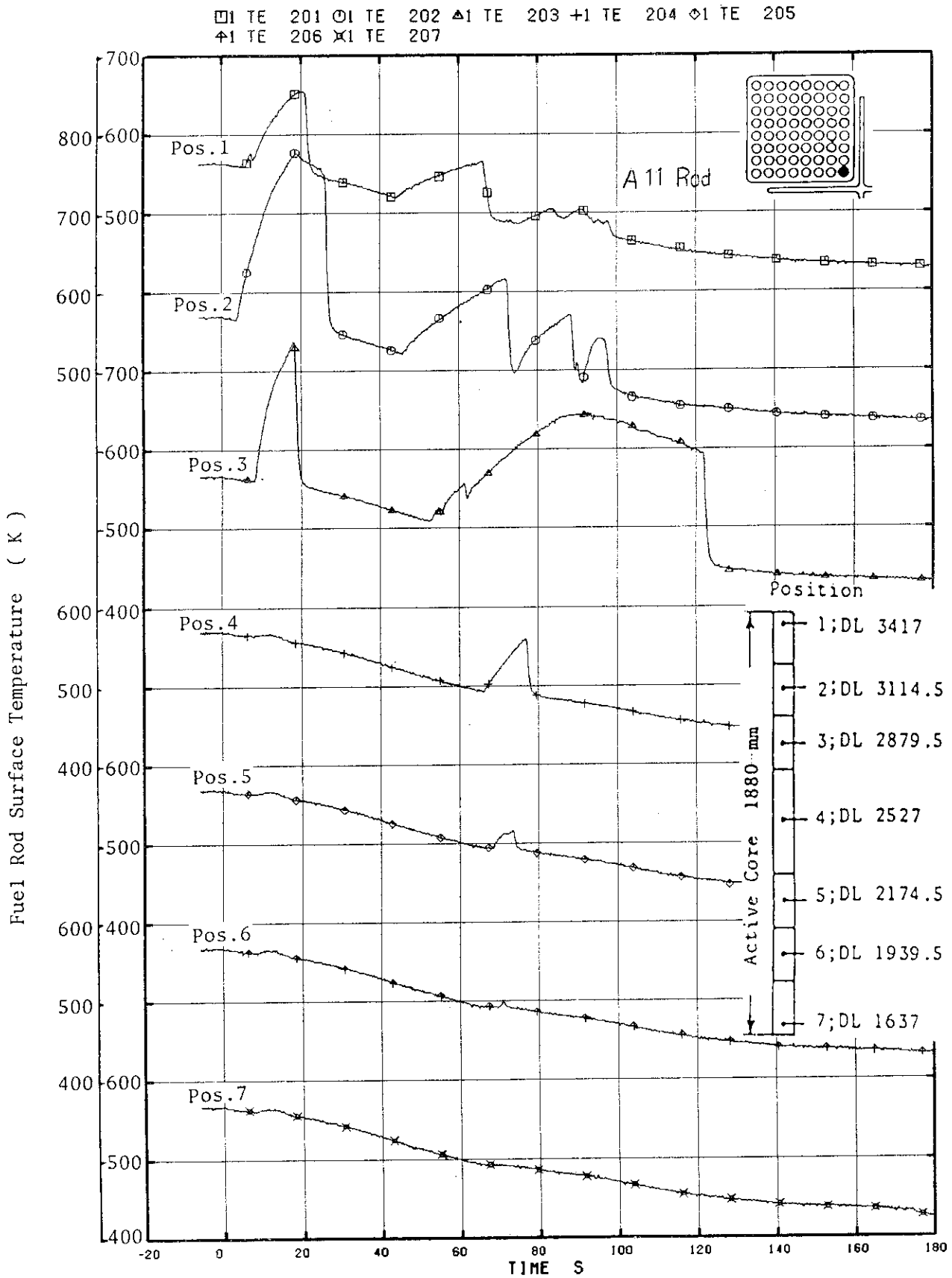


Fig. 2.32 Fuel Rod Surface Temperature All

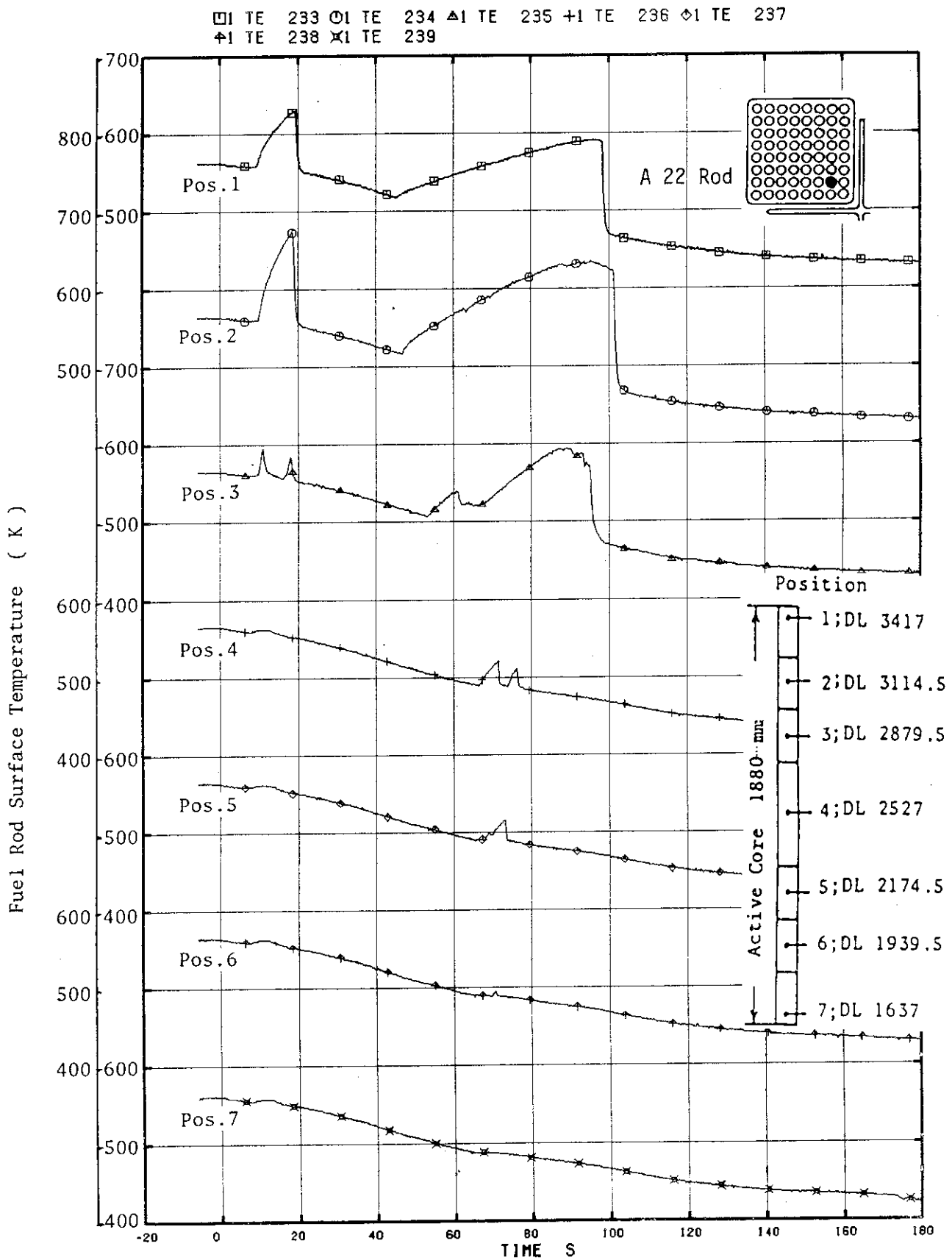


Fig. 2.33 Fuel Rod Surface Temperature A22

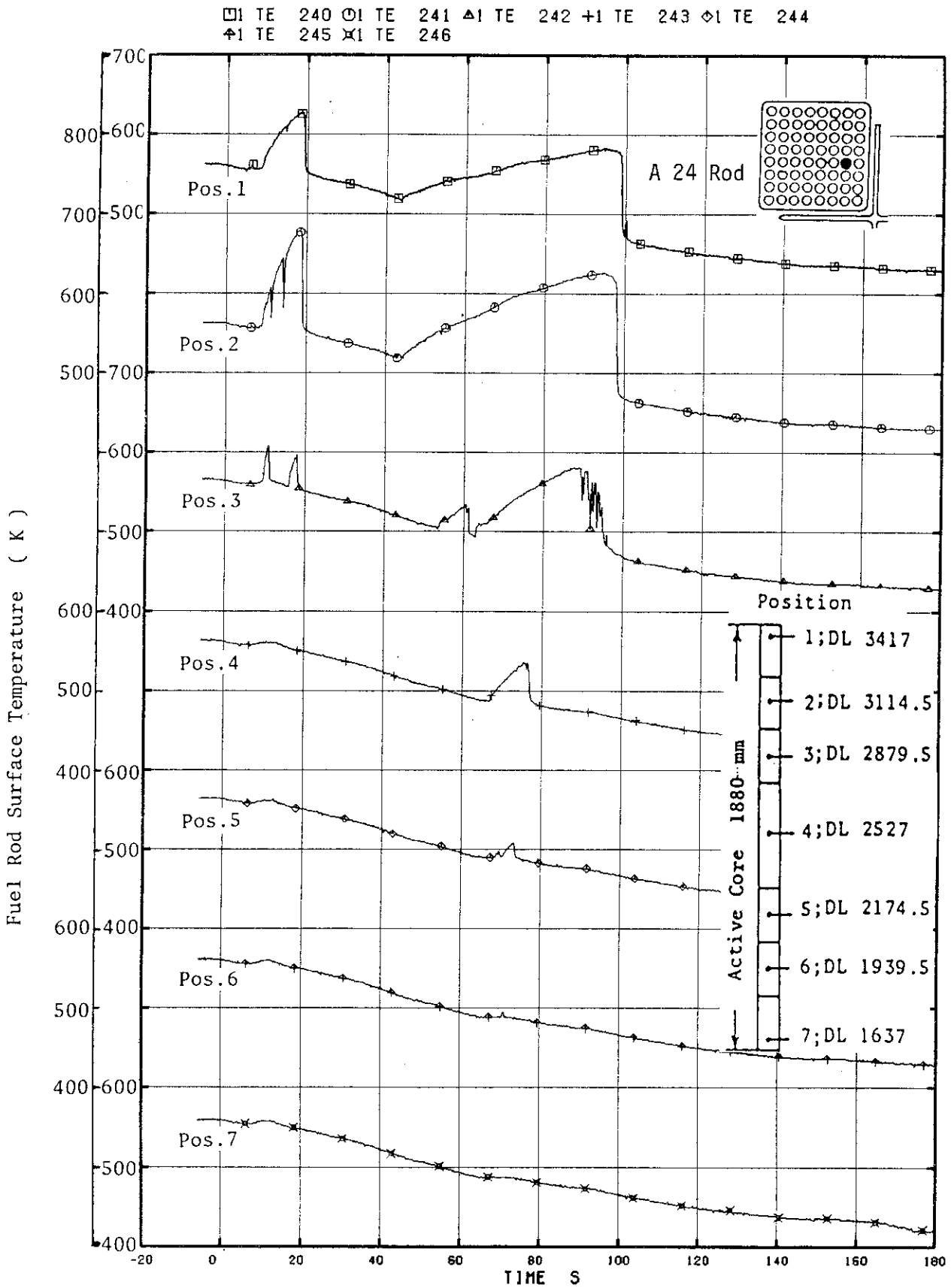


Fig. 2.34 Fuel Rod Surface Temperature A24

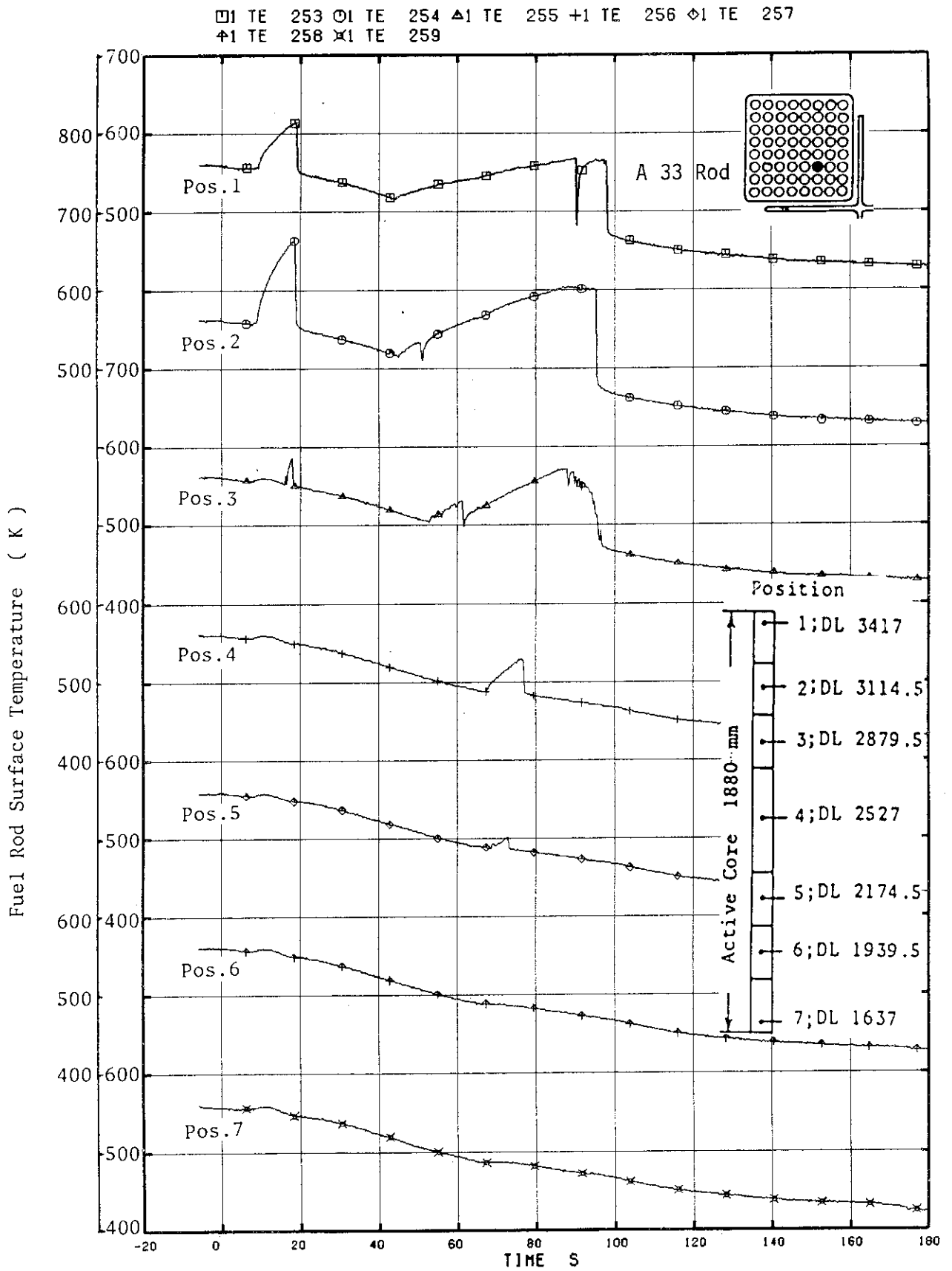


Fig. 2.35 Fuel Rod Surface Temperature A33

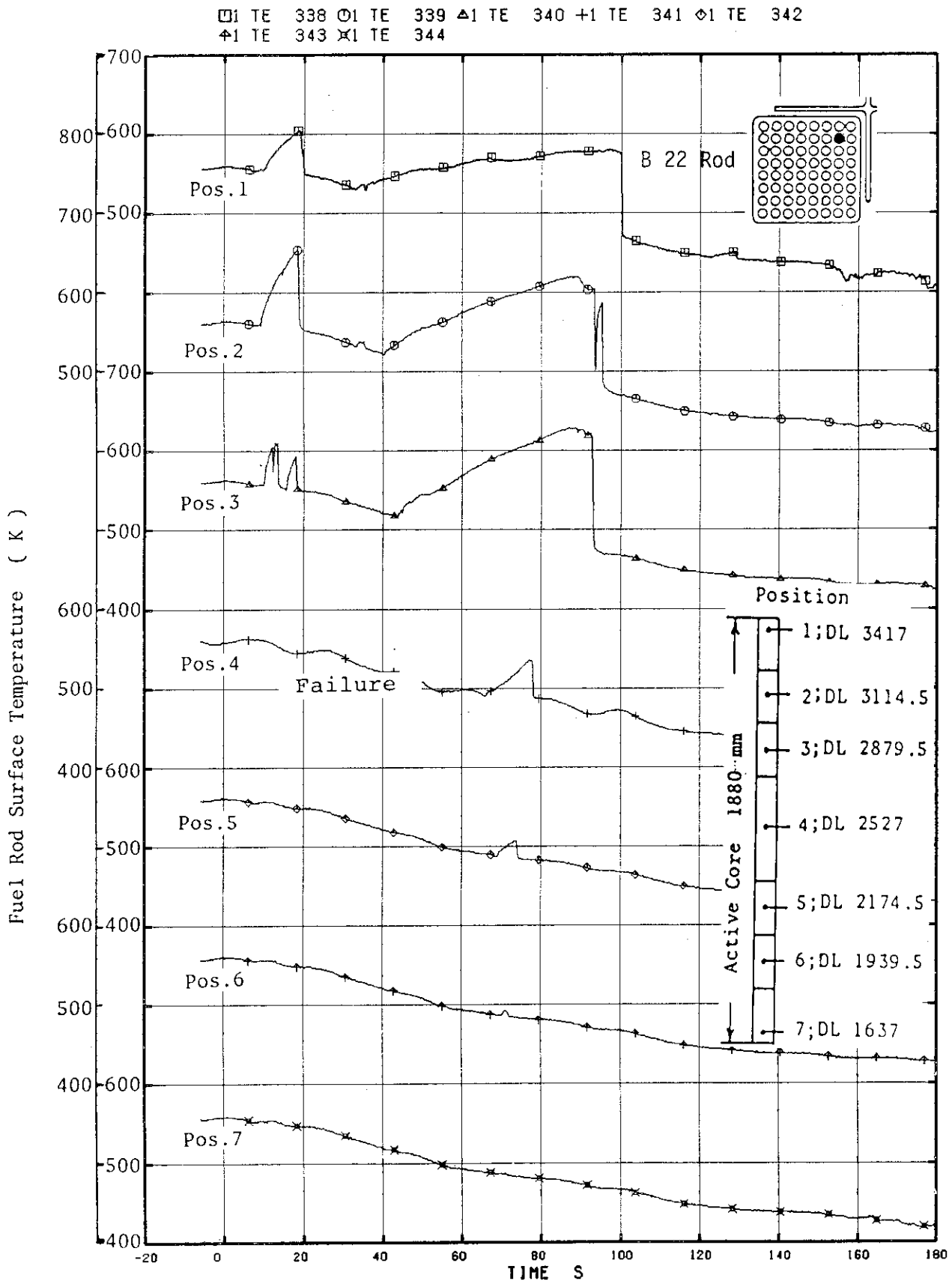


Fig. 2.36 Fuel Rod Surface Temperature B22

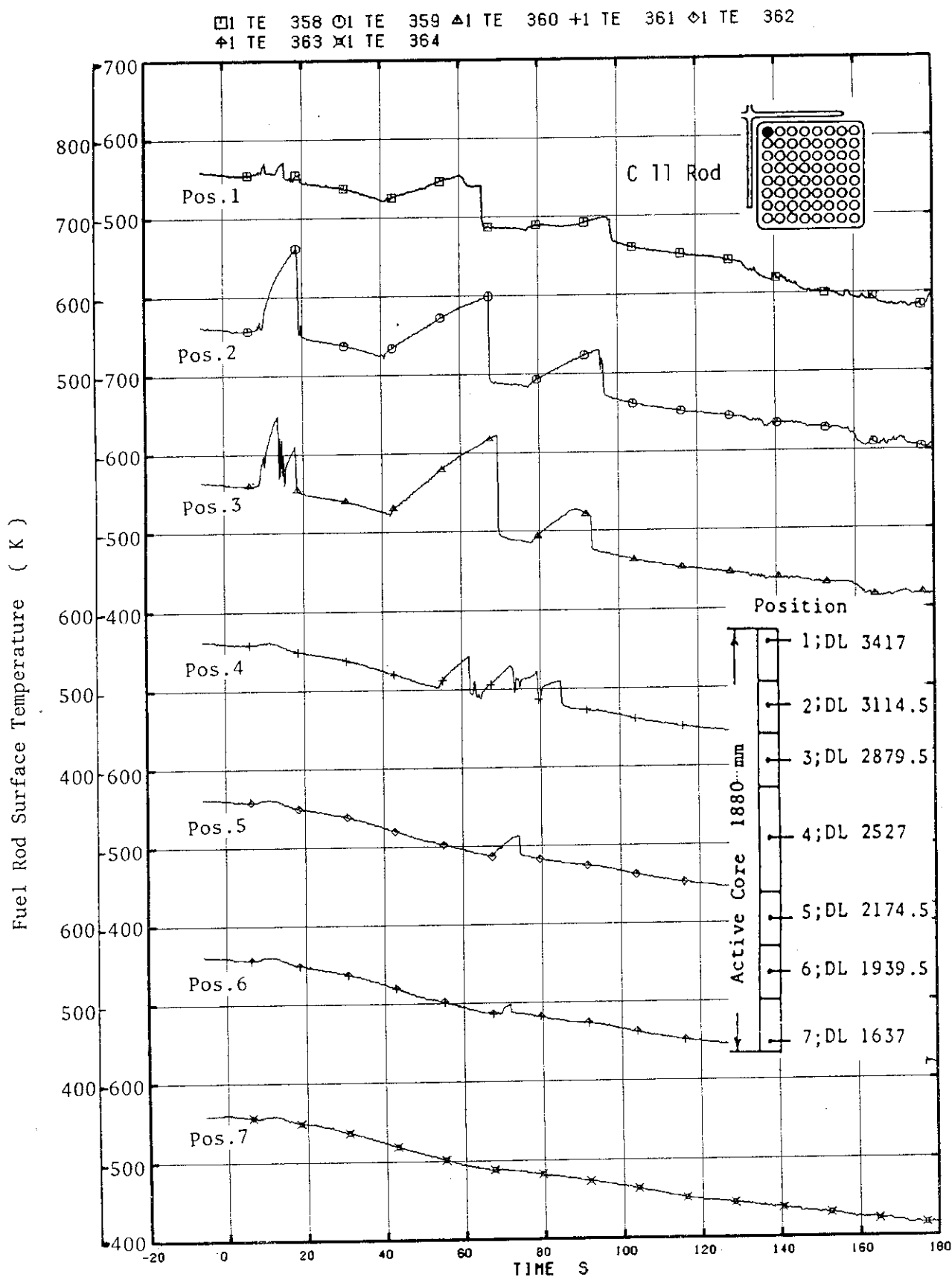


Fig. 2.37 Fuel Rod Surface Temperature C11

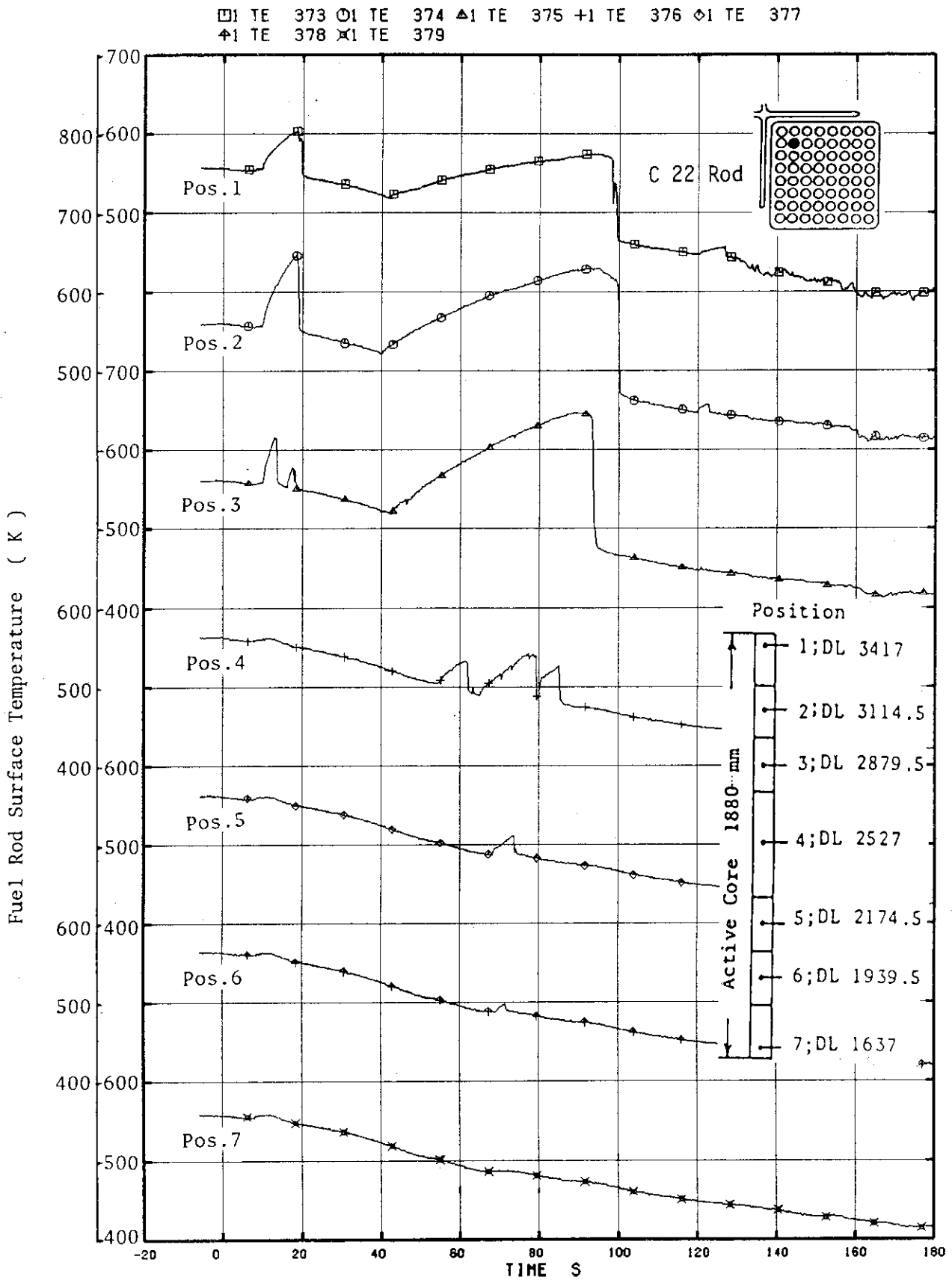


Fig. 2.38 Fuel Rod Surface Temperature C22

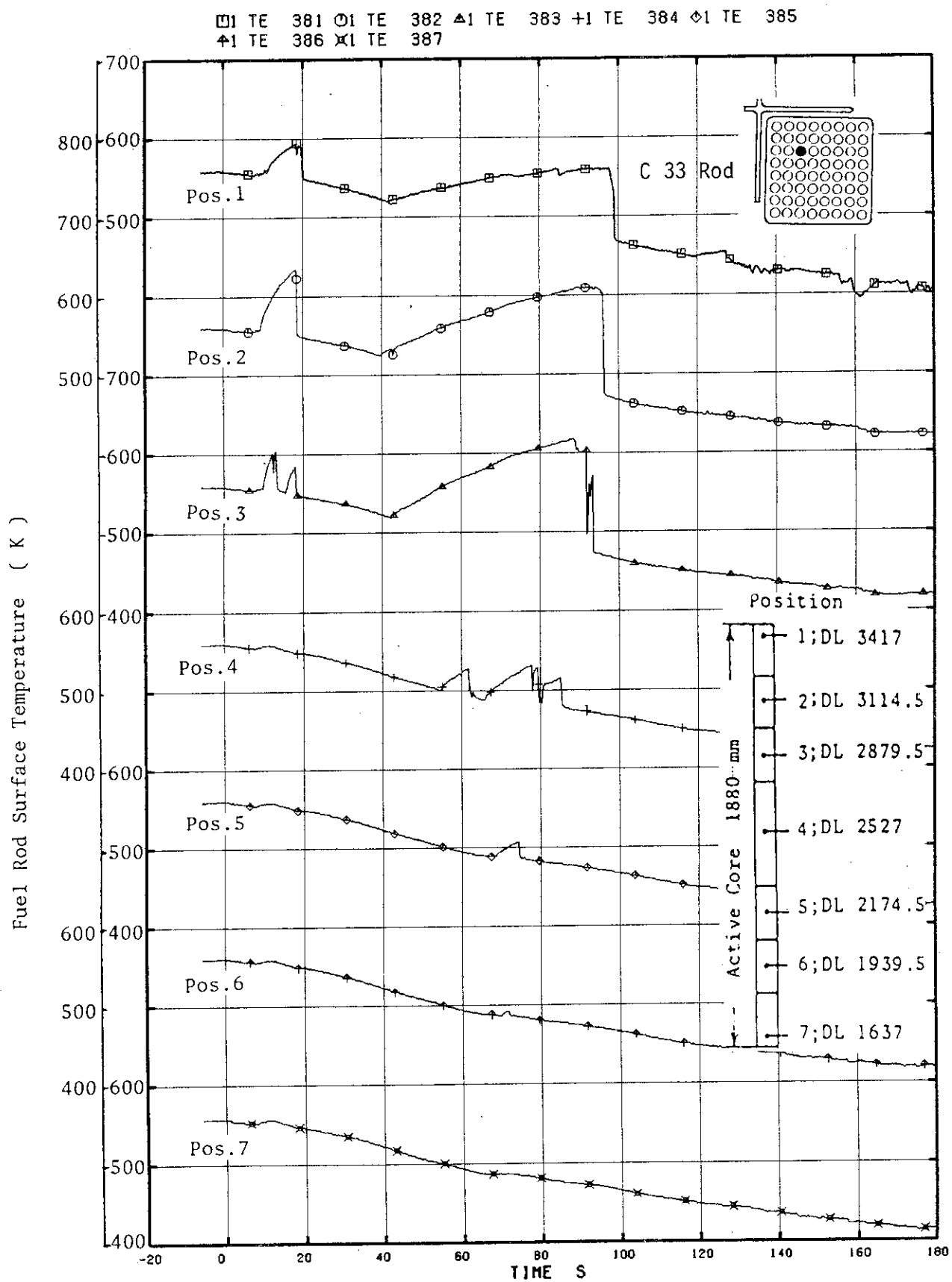


Fig. 2.39 Fuel Rod Surface Temperature C33

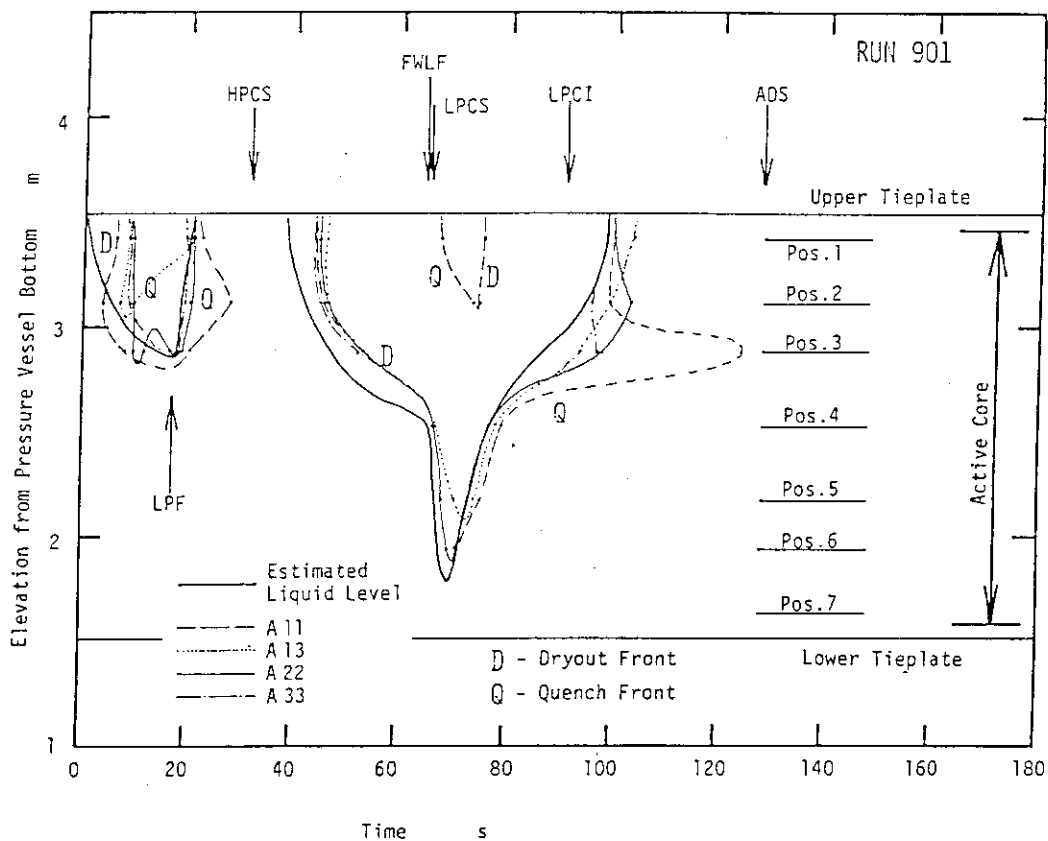


Fig. 2.40 Dryout and Quench Fronts in Channel A

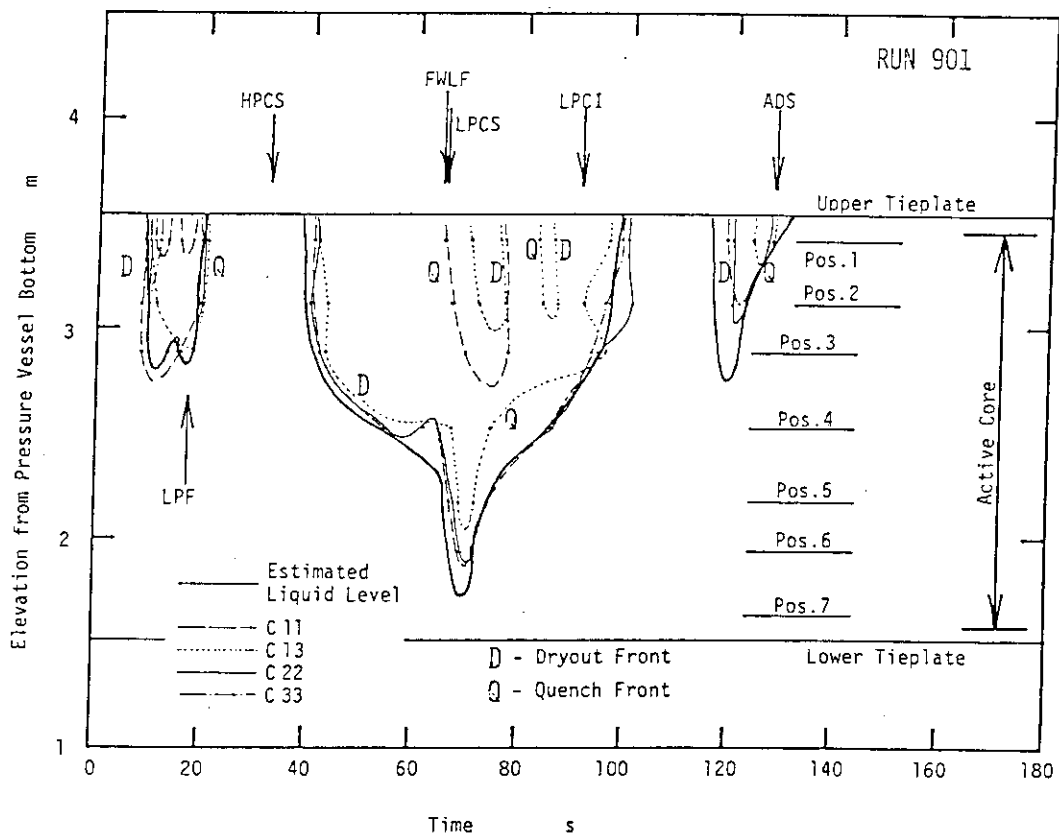


Fig. 2.41 Dryout and Quench Fronts in Channel C

01 DE 20 01 DE 21

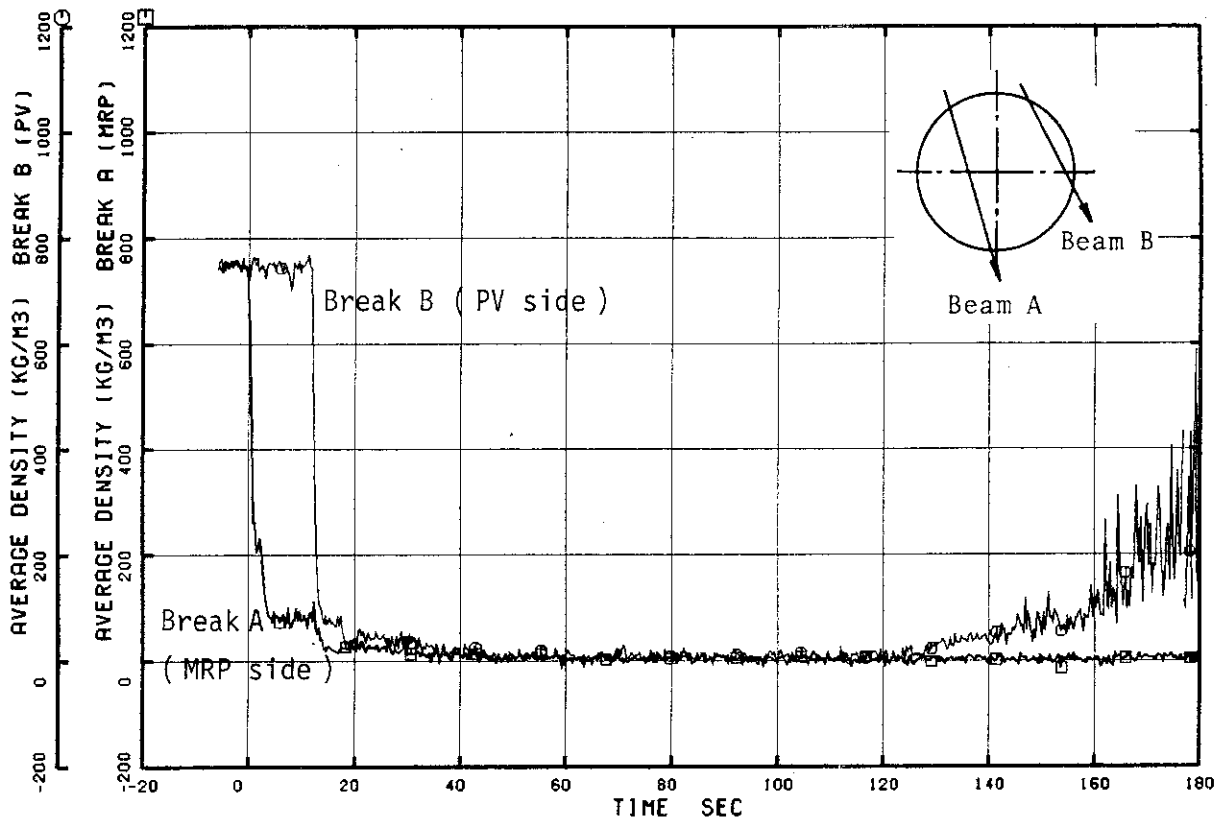


Fig. 2.42 Average Fluid Densities at Break

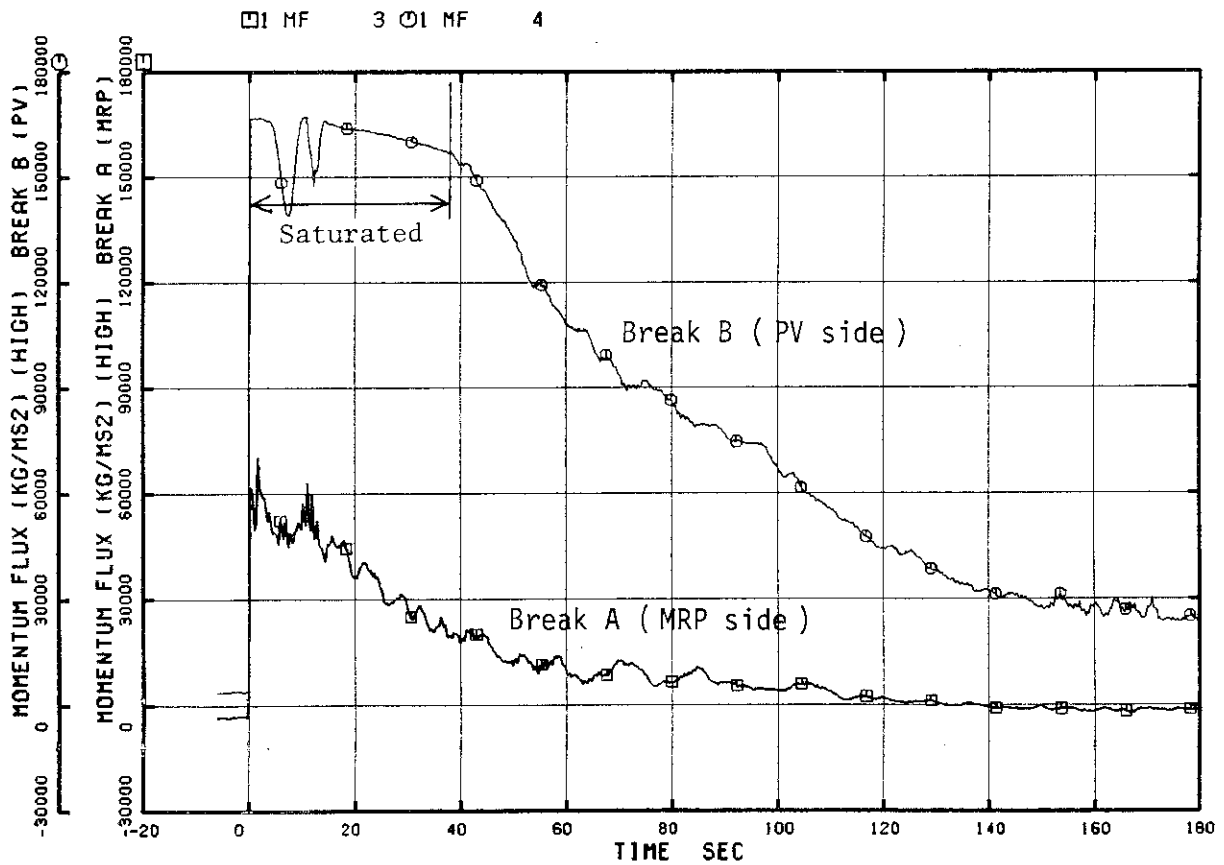


Fig. 2.43 Momentum Fluxes at Break

□1 FA 13

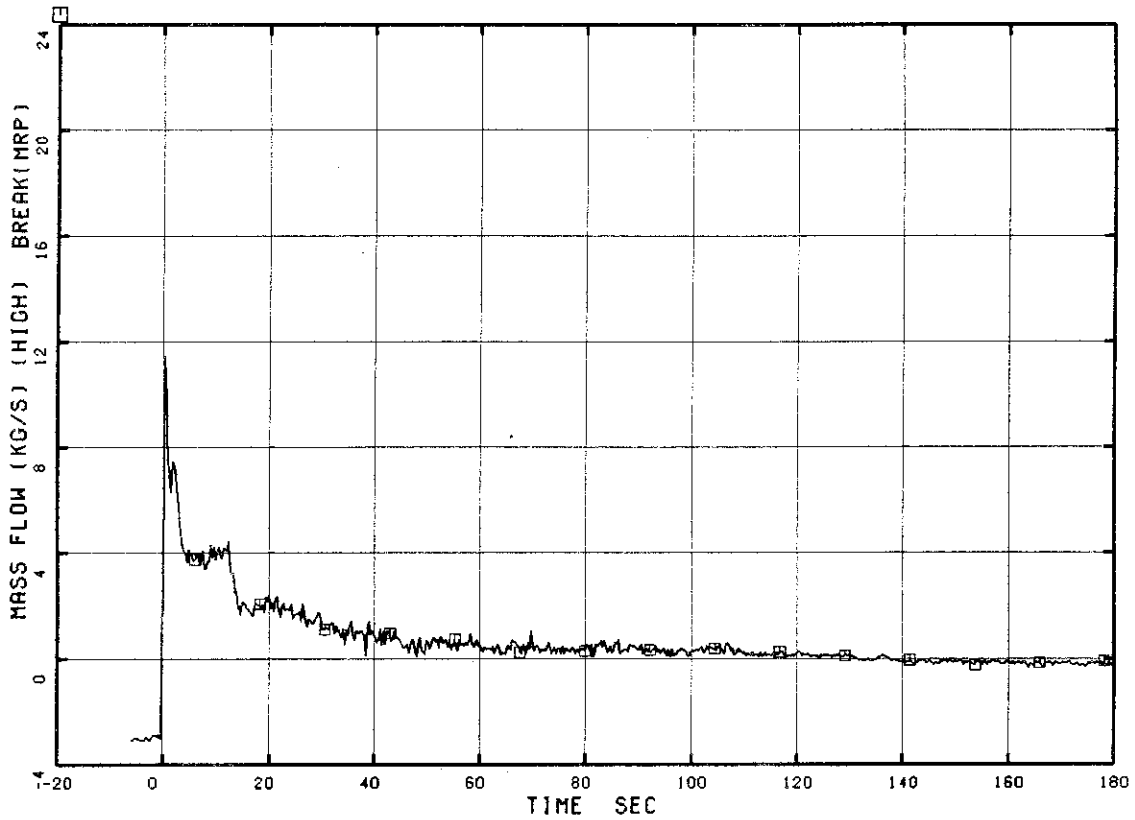


Fig. 2.44 Discharge Flow Rate at Break A (MRP side)

□1 FA 4

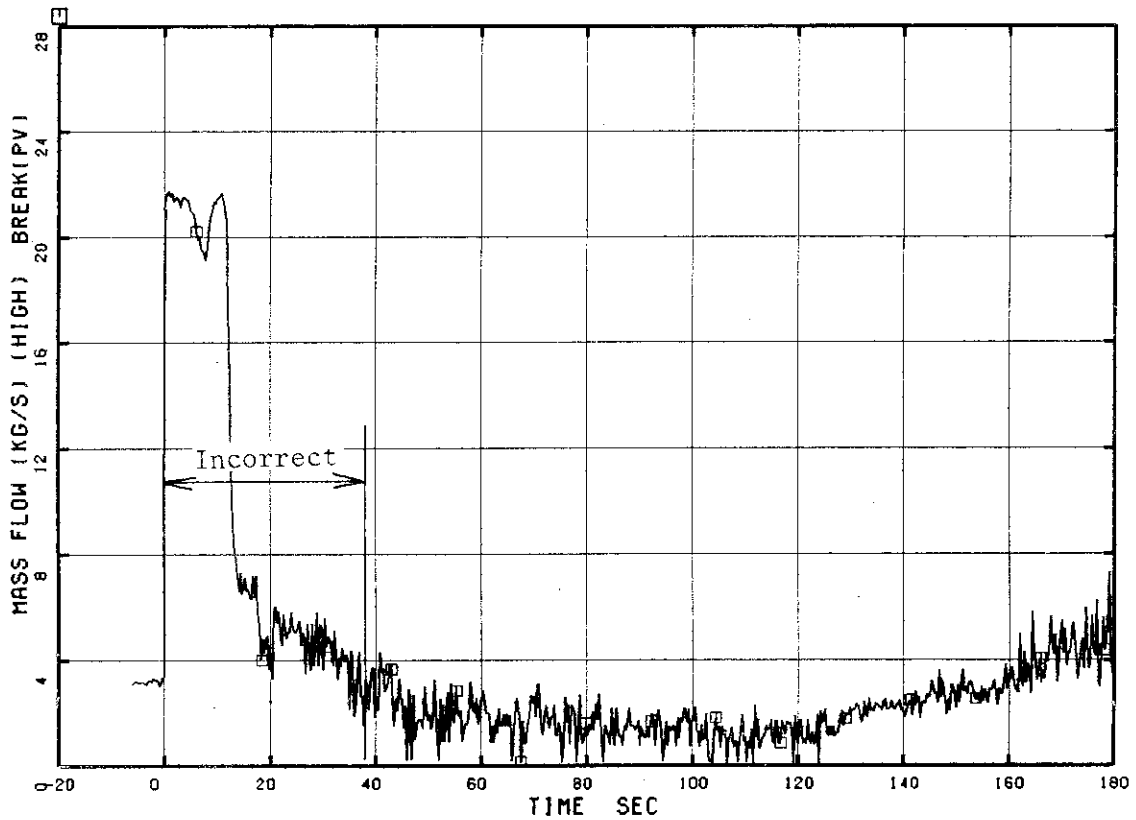


Fig. 2.45 Discharge Flow Rate at Break B (PV side)

3. ANALYSIS OF RUN901 TEST RESULTS BY RELAP4J

3.1 Computer Code

RELAP4J⁽⁵⁾ is an improved version of the RELAP4/MOD2 code. RELAP4J calculate the pressure, fluid and heat transport, cladding temperature, etc., during a transient of a light water nuclear reactor modeled with fluid volumes, junctions, heat slabs, pumps and valves, etc. The principal approximations in the RELAP4J calculation include the use of (a) homogenous fluid equations with the phases in thermodynamic equilibrium and (b) one-dimensional fluid and heat conduction transport equations.

Improvements of RELAP4J from RELAP4/MOD2 are as follows;

1) Discharge coefficient C_D for the Moody's choking flow decided from the experimental results is used. The discharge coefficient is given as

$$C_D = 0.57 + 0.002/X,$$

where, X is the quality at the junction.

2) The modified Zaloudeck's correlation is used to calculate the subcooled choking flow. When the quality at the junction becomes greater than 0.0 the correlation is smoothly changed to the above Moody's correlation at the input-specific transition quality 0.05.

3) The choked flow in the high quality region is stipulated to be the greater of the Moody's choking flow or sonic choking flow. The transition quality 0.8 to be high quality region is given as the input data for the junction.

4) The bubble rise model options include the Wilson's correlation⁽⁶⁾ for the bubble rise velocity.

5) The liquid condition in the fluid volume is automatically selected between the mixture level formation with the bubble rise model and the homogeneous liquid-vapor mixture by the flow condition in the volume.

RELAP4J is a fast running code but it can not calculate the unequal steam and water velocities (slip) and unequal temperatures of the two-phase flow. The mixture level calculation model is incomplete, therefore, the mixture levels may be formed independently in the piled up fluid

volumes.

3.2 Calculation Model

The RELAP4J nodalization of ROSA-III are shown in Tables 3.1, 3.2 and 3.3 and Figs. 3.1 and 3.2. The core model has two core channels (peak- and average-power channels). Each core channel of one core model shown in Fig. 3.1 is divided vertically into seven volumes and that of another core model shown in Fig. 3.2 has one volume in order to prevent the nonexistent mixture level being calculated in the stacking volumes of the core. Nodalization shown in Fig. 3.1 was used for the base case A and Fig. 3.2 for the simplified case B. The nodalization of case A includes 33 volumes, 47 junctions and 19 heat slabs. The simplified nodalization of case B includes 21 volumes, 35 junctions and 19 heat slabs. The calculation with the simplified nodalization was performed as the sensitivity study.

Initial thermal-hydraulic conditions for the calculations were obtained from the experiments as shown in Table 2.3. The steam dome pressure was 7.35 MPa, the lower plenum temperature 551.8 K and the total core power 4.045 MW. Consistency of the input data were certified by a steady state calculation. Figure 3.3 shows the initial flow distribution.

Input data for axial power distributions of the peak and the average power channels are the same as that of ROSA-III for the average power rods. Therefore, the PCT was not properly calculated.

The experimental data of the steam discharge flow, the feedwater flow and the ECCS flows, which are shown in Fig. 3.4 through 3.6, were used as the input data in the analysis as a function of time.

Optional choking models 1) through 3) presented in the previous section 3.1 were applied to the junctions at the jet pump drive nozzles and the breaks.

The bubble rise model was applied to all volumes in the pressure vessel to calculate the mixture levels. The bubble-gradient parameter (ALPH) was 0.8 in the core and bypass volumes and 0.0 in the other volumes.

The recirculation pump was modeled by the rated values and the homologous curves. As for the torque homologous curves the LOFT bingham pump torque data were used because the torque curves of the ROSA-III recirculation pump were not yet obtained completely.

Form loss coefficient at the junction was calculated in the code from geometrical form change at the junction. Measured reverse flow form loss coefficients were used at the junctions in the jet pump suction line.

The input data list of the RELAP4J calculation having 14 core volumes is presented in Appendix A.

3.3 Comparison with the Experimental Data

Major results of the RELAP4J calculation are compared with the experimental data in this section. Both of two calculations with the base case model having the core model vertically divided into seven volumes per channel and with the simplified model having the core without vertical divide are compared with the experimental data. The case A and case B calculations took 4 and 2 hours of CPU time, respectively, by FACOM M-200 computer at JAERI.

3.3.1 Pressure Transient

Comparison of lower plenum pressure transients between the calculated results and the data is shown in Fig. 3.7. Overall agreement was good between the calculated pressure transient and the data. The results by two RELAP4J models were similar to each other. The pressure recovery after MSIV closure at 9.2s after break calculated in case B was larger than that calculated in case A because the upper core did not dryout in case B to be mentioned in Section 3.3.5.

Temporary hold of the pressure after 64.8s caused by the FWLF was not calculated because the feedwater line of ROSA-III was not modeled in this analysis.

The calculated pressure transients at the upstream side of the breaks B and A in both cases shown in Figs. 3.8 and 3.9 agreed well with the

data. Rapid decrease of the calculated pressure at the break B upstream immediately after the break resulted in flashing in the MRP suction volume as shown in Fig. 3.14.

3.3.2 Differential Pressure

Differential pressure between RELAP4J volumes was calculated using a computer plot program, but the volumes which consist of RELAP4J models are so large that the calculated differential pressure may include error by the head term in comparison with the experimental data.

Differential pressure (DP) between the lower and upper plena shown in Fig. 3.10 presented very good agreement with the data. After the LPCI injection at 90.9 s, the calculated DP decreased temporarily whereas the data did not.

Figure 3.11 presents the calculated DP between the channel inlet chamber and the upper plenum. The DP calculated in case A was lower than that in case B throughout the test, which means that the core flow rate was lower in case A than in case B.

3.3.3 Break Flow

Measured break flow shown in Figs. 2.45 and 2.46 using drag disks and gamma densitometers involved an error of at least $\pm 20\%$, and the break flow of the PV side break B was incorrect till 38 s after the break because of the saturation in the drag disk data. Therefore, emphasis was placed on the calculation of the incipient time of the break flow decrease due to uncovering of the recirculation line inlet, which agreed very well with the data as shown in Figs. 3.12 and 3.13.

The calculated density transient at the break upstream agreed well with that of the data except for the temporary decrease in the calculated density at the break B upstream before the rapid decrease at 12.5 s after the break.

The calculation results mentioned above show that the break flow was calculated well using the modified Zaloudeck's correlation and the Moody's

choking in spite that the RELAP4J nodalization did not simulate the break nozzle of ROSA-III. The pressure decrease in the upstream volume of the break might have been compensated with the discharge coefficient C_D for Moody's choking recommended for the thin edge orifice giving good agreement of the calculated break flow with the data.

The nearly equal break flow rates were calculated in cases A and B.

3.3.4 Core Flow and Jet Pump Flow

The calculated total flow rate through the SEO shown in Fig. 3.16 shows that they agree well with the data till LPF initiation. After the LPF initiation the initial temporary increase in the core inlet flow was calculated well by RELAP4J but the calculated flow became very little compared with the data after the LPF mitigation. The discontinuity of the liquid phase at the SEO after the LPF lowered the calculated flow rate through the SEO. The data had also large uncertainties after the initiation of the LPF.

When the whole core was uncovered about 55 s after the break the calculated flow through the SEO began to flow downward. The temporarily downward flow after 64.8 s in the data was caused by the feedwater line flashing and was not calculated because the feedwater piping was not modeled.

The calculated guide tube inlet flow rates are compared in Fig. 3.17 with the data. The flow reversal observed in the data was calculated, but the flow rate was less than a half of the data until the LPCI actuation at 91 s. When the core bypass was filled with LPCI liquid the flow through the guide tube inlet turned upward temporarily and reversed again because the liquid in the upper plenum began to fall through the core bypass to the lower plenum.

Calculated total flow through the Upper Tie Plate (UTP) and the Lower Tie Plate (LTP) of the core in cases A and B are compared in Figs. 3.18 through 3.21. The flow through the UTP was calculated larger than that

through the LTP until the LPF initiation in two cases. The flow through the LTP shown in Fig. 3.19 was larger in case B than in case A till the initiation of the LPF. The peak flow rate at the LPF was larger in case A than in case B, but the total upward flow through the LTP between the initiation and the mitigation of the LPF was calculated larger in case B than in case A. The flow through the LTP turned downward temporarily during the liquid level in the core decreased to the LTP in two cases. The flow through the LTP began to flow upward after the LPCI actuation at 90.9s.

Figures 3.22 through 3.25 show the calculated flow through the Jet Pump (JP) suction, drive nozzle and discharge, which are compared with the measured JP discharge flow. The calculated results in two cases agreed well each other and the JP discharge flow in the broken loop agreed well with the data. But the JP discharge flow in the intact loop was calculated reversely after the LPF initiation compared with the data.

3.3.5 Liquid Levels in the Pressure Vessel

Liquid level transients in the pressure vessel calculated in cases A and B are shown in Figs. 3.26 and 3.27, respectively. Core volume was represented by a vertical train of seven volumes in case A while it was represented by a single volume in case B. Liquid level transients calculated in the two cases showed almost the same behavior except for the mixture levels in the core.

Calculated liquid level decrease after break in the downcomer agreed very well with the data. The difference of the recirculation line (RL) nozzle level between the calculation model and the data was caused by the incomplete modeling of the downcomer shape adjusting the total height and the fluid volume by just one node in the RELAP4J calculation. Calculated liquid level in the downcomer decreased to the RL nozzle level at 12.6 s after the break and did not recover till 120 s in both cases as was in the data.

Calculated liquid level in the upper plenum began to decrease at 8.4

s after the break and started to recover at 15.7 s due to LPF and the upper plenum level existed throughout the calculation. RELAP4J can not calculate the slip between liquid and steam nor it can calculate the flows of liquid and steam separately through the junctions. Therefore, the liquid in the upper plenum could not drop to the core and the bypass after the liquid levels were formed in the core and the bypass.

The liquid levels were formed in every core volumes before LPF in case A but were not formed in the core volumes before LPF in case B with the same bubble rise model.

After LPF initiation liquid levels were formed in the bypass and lower plenum volumes in both calculation as well as in the data and they began to decrease thereafter. However, the calculated liquid level in the lower plenum decreased faster than the data because RELAP4J could not calculate the steam flow independently through the junction. The steam generated in the lower plenum was accumulated in the lower plenum until the liquid level in the lower plenum decreased to the jet pump discharge.

Liquid levels in peak and average-power core channels of the data began to decrease at the same time as shown in Fig. 2.31. However, the calculated liquid level in the peak-power channel began to decrease about 15 s later than in the average-power channel in both cases. The liquid levels in the core decreased rapidly to the bottom of the core especially in the peak-power channel. The liquid levels in the core decreased finally to the bottom of the channel inlet chamber in both cases while the bottom part of the core was not uncovered in the data even after the FWLF. This was because the accumulated liquid in the upper plenum did not flow down into the core in the calculation but fall back liquid was enough in the data. Therefore, the ECCS water accumulated in the upper plenum finally overflowed to the downcomer from the top of the steam separator in both cases before the actuation of LPCI. The bypass was filled up with the ECC water 5 s after the LPCI actuation at 90.9 s, and, then, the core began to be reflooded from the bottom and also the liquid level in the

upper plenum dropped because the bypass and the upper plenum were connected. The liquid level in the lower plenum stayed at the jet pump discharge level because the steam did not go out from the lower plenum through the SEO even after the LPCI actuation.

Calculated liquid levels in the core show some difference between two cases A and B. In case B the liquid levels did not decrease before LPF and they started to decrease 5 s after initiation of level falls in the base case A. After the bypass was filled up with liquid the levels in the core recovered very fast in case B while recovered more slowly in case A. These differences came only from the vertical division of the core volumes since the same bubble rise model was used in every core volumes in both cases.

The calculated liquid levels oscillated hard in the reflooding stage in both cases. These liquid level oscillations were also observed in every core volumes when the volume became almost empty even before the LPCI actuation because of higher void fraction in each volume.

3.3.6 Fuel Rod Surface Temperature

Calculated fuel rod surface temperatures are compared with the data in Figs. 3.28 through 3.31 for the average-and peak-power rods in cases A and B.

The dryout and quench front behaviors are closely related with the liquid level transients in the core as mentioned in Section 2.3. By the RELAP4J the fuel rod surface temperature is calculated with reference to the average thermal-hydraulic conditions in the adjacent volume to the heat slab. Therefore, the dryout and quench fronts are calculated to move vertically in accordance with the calculated liquid level transients through the vertically separated core volumes in the base case A, but in case B the dryout and quench occurred at the same time at every heat slab in the core. This difference between two calculation resulted in the different pressure response.

As mentioned in the previous section the steam accumulated in the core formed the liquid levels in the vertically stacked core volumes in the base case A. In the peak-power channel the fuel surface above the midplane of the core dried out before LPF initiation whereas no dryout was observed at Position 4 in the data. The accumulated steam in the core prevented the heater rod surface from quenching till the end of the calculation.

Figures 3.32 through 3.39 show the heat transfer coefficients used to obtain the heater rod surface temperature. At about 15 s after the break, the heat transfer mode at the upper part of the core changed from the nucleate boiling to the pool film boiling because the decrease in the core flow brought the DNB. When the whole core was covered with the steam after 95 s after the break the heat transfer mode changed from the superheated vapor to the pool film boiling or the nucleate boiling from the bottom of the core due to the bottom-up reflooding. The top-down quench was not observed in the RELAP4J calculation.

3.4 Conclusions for the RELAP4J Calculations

The post test calculation of the ROSA-III large break test RUN 901 was performed with the RELAP4J code and the following conclusions were obtained.

- (1) The overall trends of the system pressure and differential pressure between the top and bottom of the pressure vessel calculated by RELAP4J agreed well with the data.
- (2) The time of incipient decrease in the break flow agreed well with the data which indicates the Zaloudeck's and the Moody's choking flow model with the RELAP4J discharge coefficient correlation can predict the break flow accurately.
- (3) The homogenous two-phase flow model in RELAP4J was not able to calculate the counter current flow at the upper tie plate. This resulted in the accumulation of the spray water in the upper plenum contrary to the experiment. The core inlet flow rate calculated until the beginning of the

lower plenum flashing agreed well with the data. Therefore, the slip model is necessary for the code to calculate the mixture level more accurately.

(4) The bubble rise model in RELAP4J calculated the mixture level in each volume independently resulting in discontinuous liquid levels in the vertically stacked core volumes. However, the overall trend of the mixture level transient in the core agreed with the data.

(5) The quench behavior of the fuel rod surface was not calculated well by the code.

(6) Simplification of the core nodalization from the seven vertically stacked volumes to one volume eliminated the discontinuity in the liquid level in the core and made the calculation speed faster by a factor of two. However, the same heat transfer coefficient was applied to the seven heat slabs in the core volume, and the dryout or quench behavior of the heater rod was the same in the whole core.

Table 3.1 Description of Volumes for RELAP4J Model

Description	Case A	Case B
Steam Dome	4	4
Upper Plenum and Steam Separator	3	3
Average Power Channel Pos.1	24	
2	23	
3	22	
4	21	2
5	20	
6	19	
7	2	
Peak Power Channel Pos.1	31	
2	30	
3	29	
4	28	19
5	27	
6	26	
7	25	
Channel Inlet Chamber	32	20
Lower Plenum	1	1
Core Bypass and Guide Tube	18	18
Downcomer	33	21
Intact Loop MRP Suction Line	12	12
MRP	13	13
MRP Discharge	14	14
Intact Loop JP	15	15
JP Discharge	16	16
JP Suction Line	17	17
Broken Loop MRP Suction Line	5 and 6	5 and 6
MRP	7	7
MRP Discharge Line	8	8
Broken Loop JP	9	9
JP Discharge	10	10
JP Suction Line	11	11

Table 3.3 Description of Heat Slabs for RELAP4J Model

Description	Case A and B
Average-Power Heater Rods Pos.1	7
2	6
3	5
4	4
5	3
6	2
7	1
Peak-Power Heater Rods Pos.1	17
2	16
3	15
4	14
5	13
6	12
7	11
Electrode in Channel Inlet	19
Electrode in Lower Plenum	8
Vessel Wall (Steam Dome)	18
(Downcomer)	9
(Lower Plenum)	10

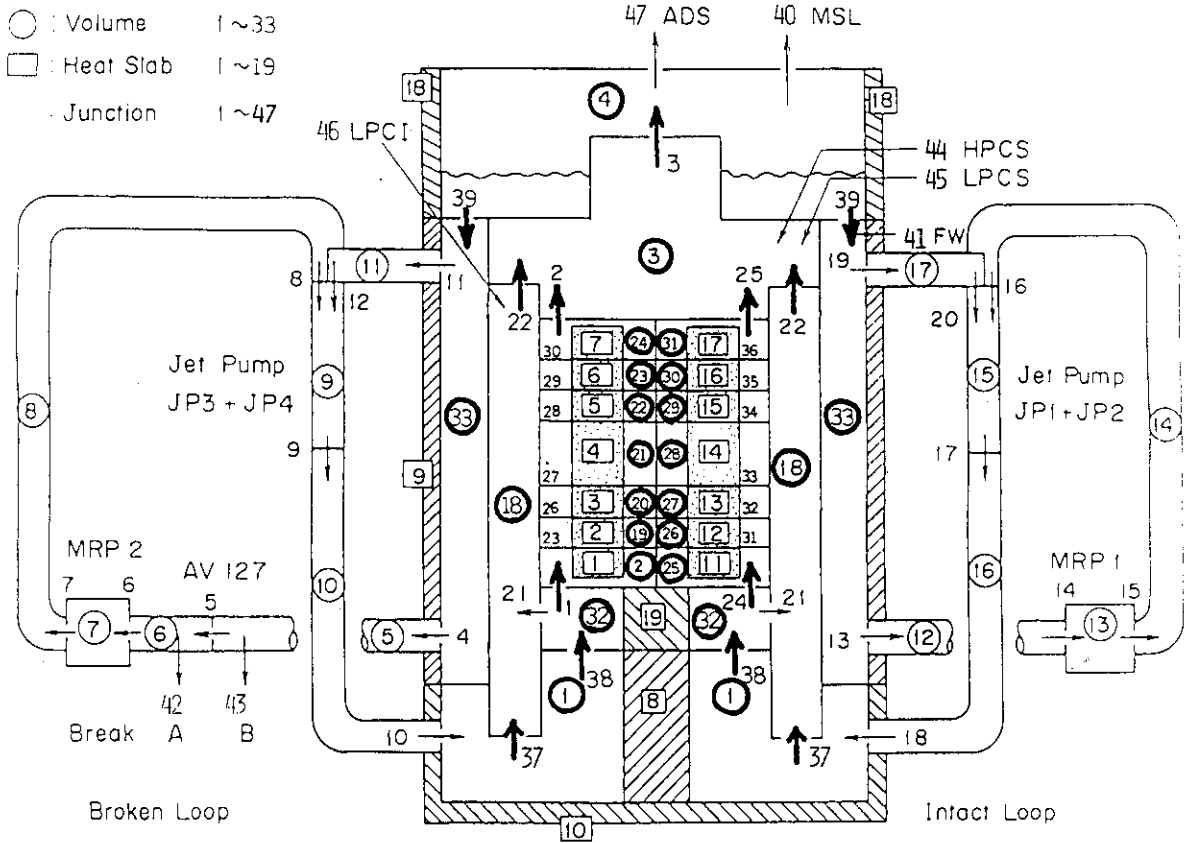


Fig. 3. 1 RELAP4J Nodalization of ROSA-III (Base Case A)

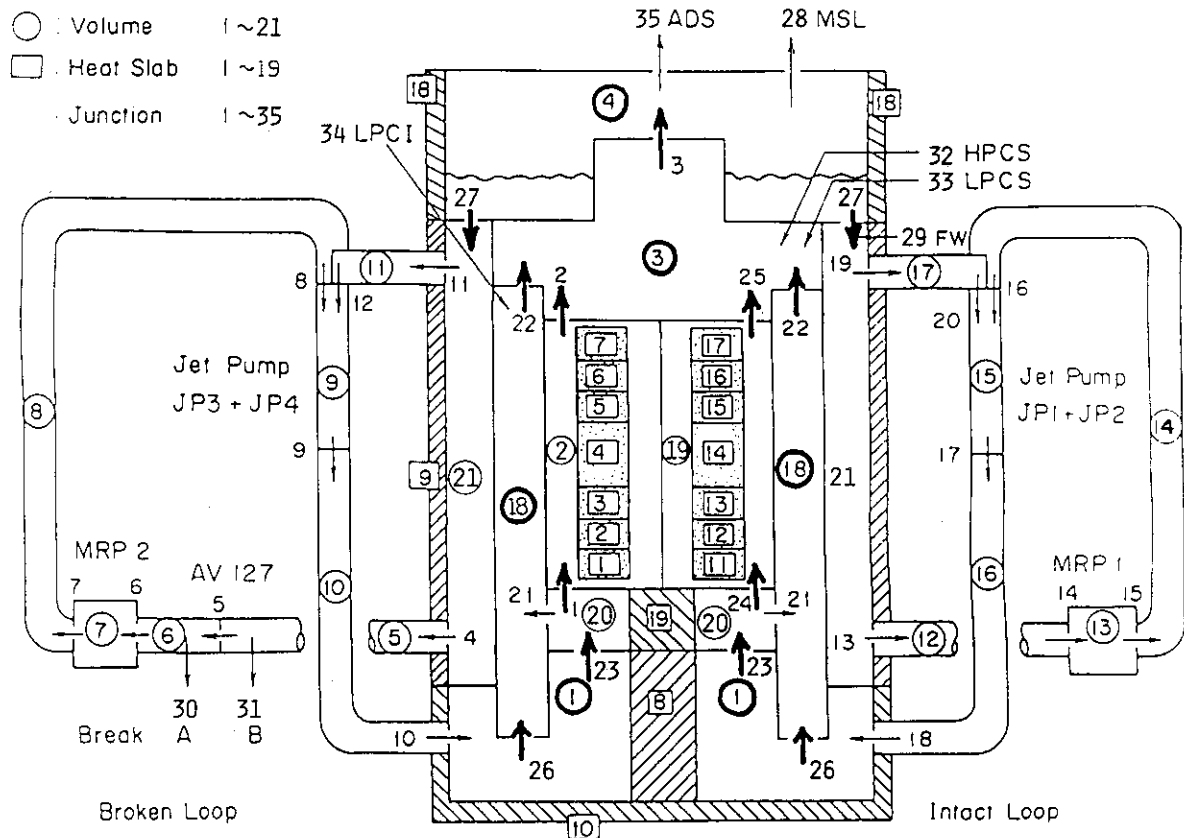
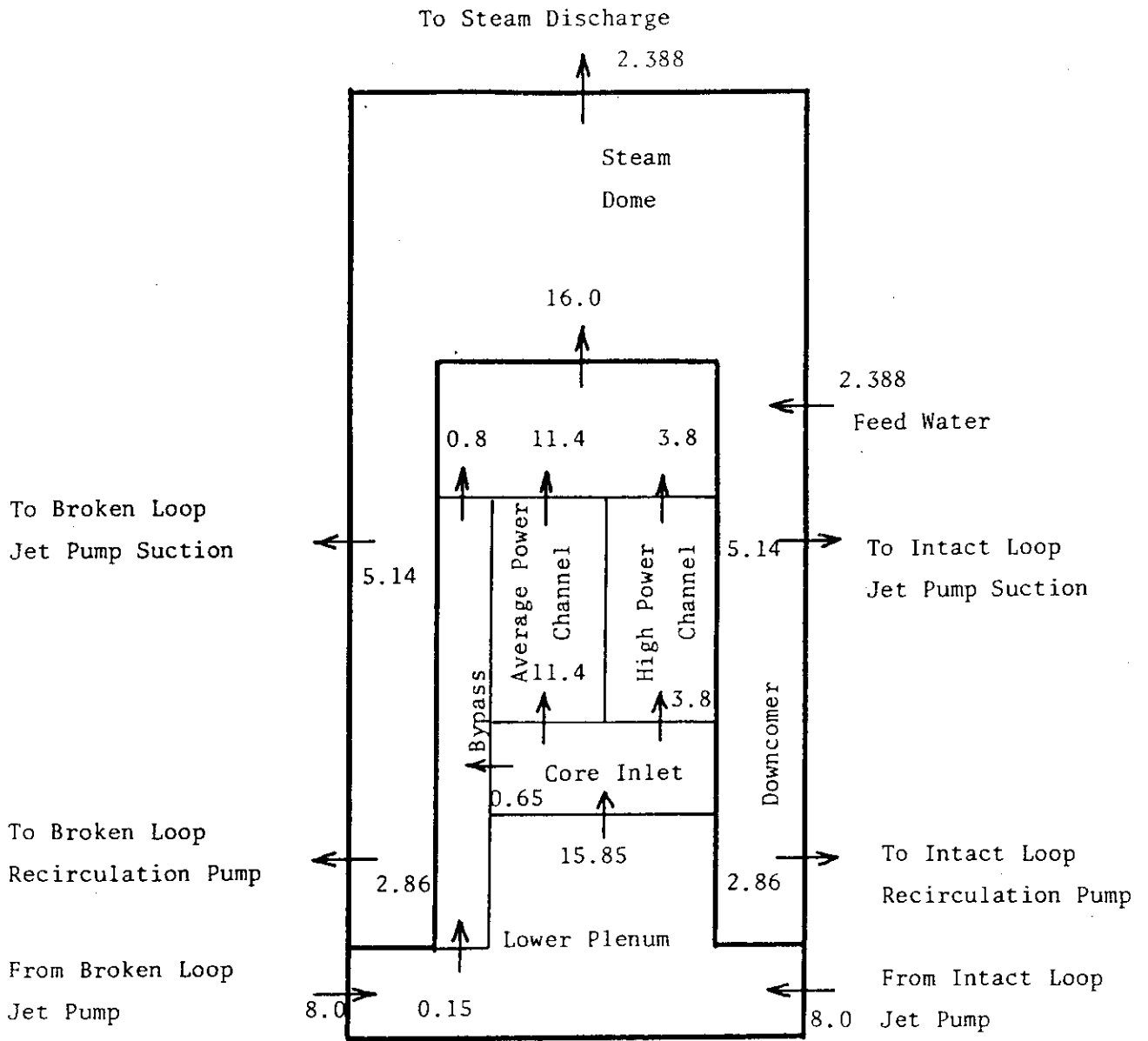


Fig. 3. 2 RELAP4J Nodalization of ROSA-III (Case B) (Reduced Case)



Note : Flow Rate in kg/s

Fig. 3. 3 Initial Flow Distribution of RUN 901

□ FM 71 ○ R JWJ40 △ R JWJ28

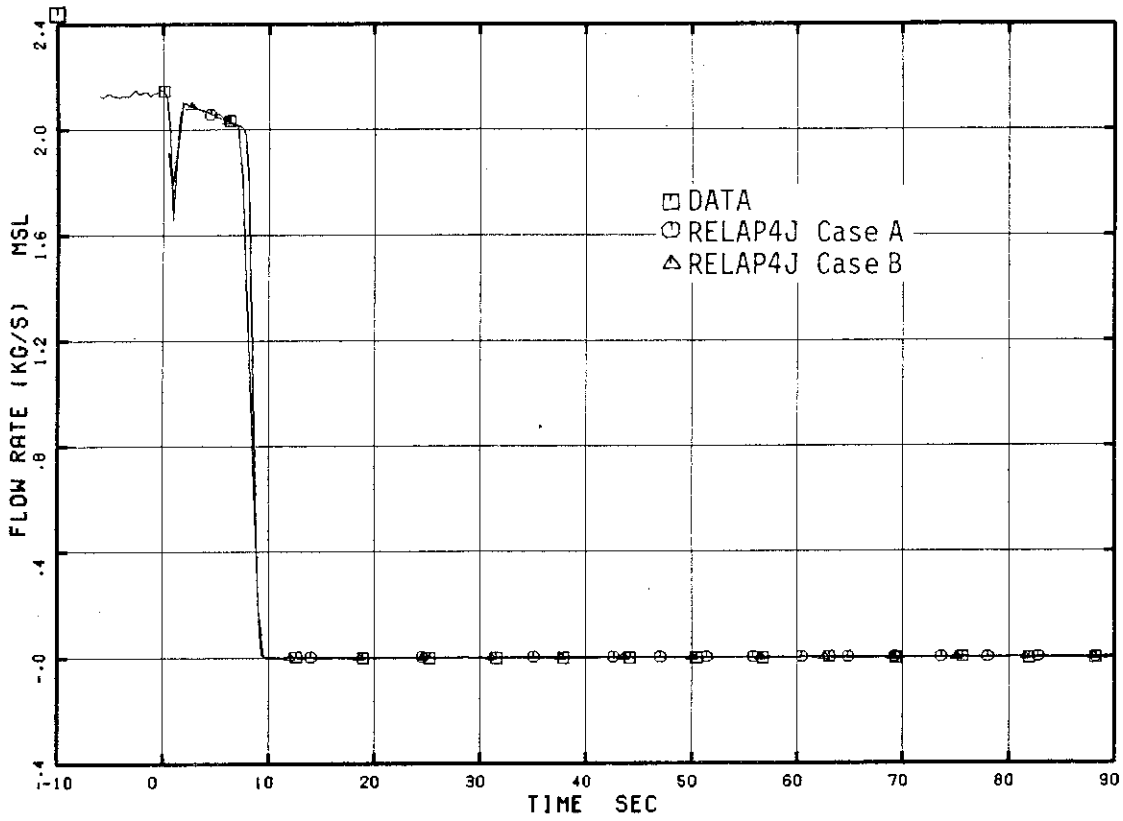


Fig. 3. 4 Main Steam Discharge Flow Rate

□ FV 76 ○ R JWJ41 △ R JWJ29

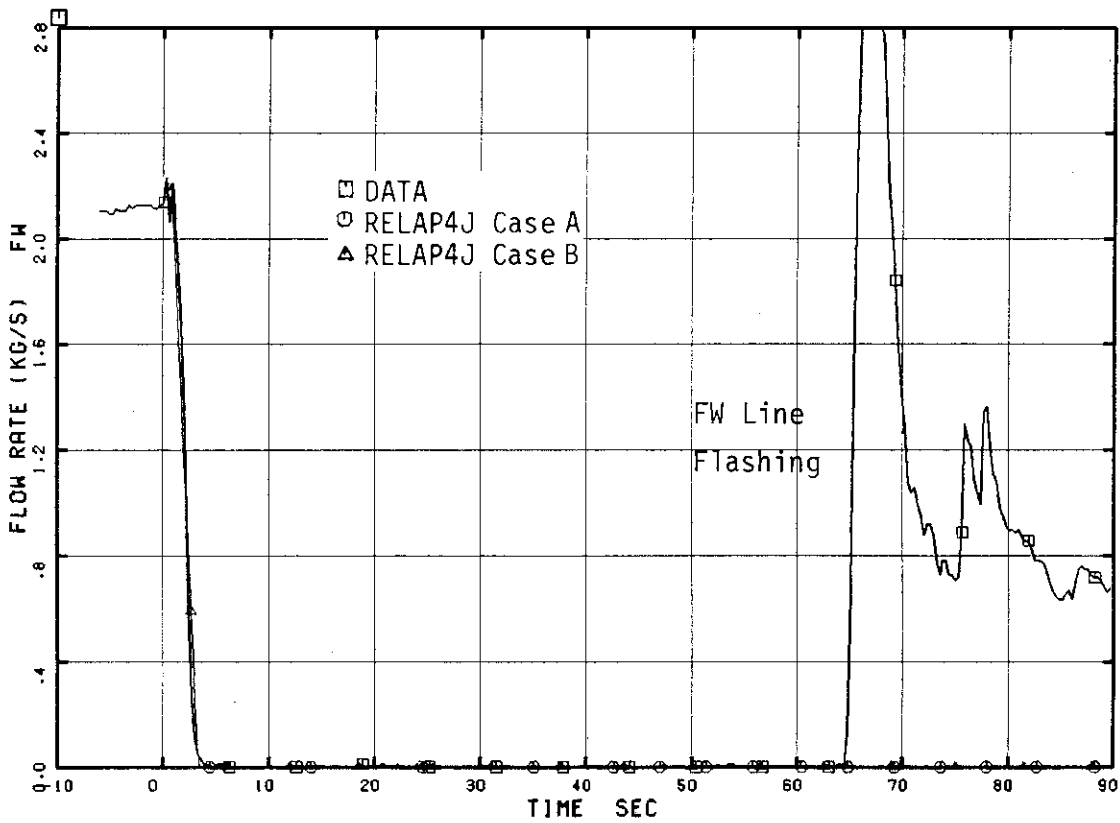


Fig. 3. 5 Feedwater Flow Rate

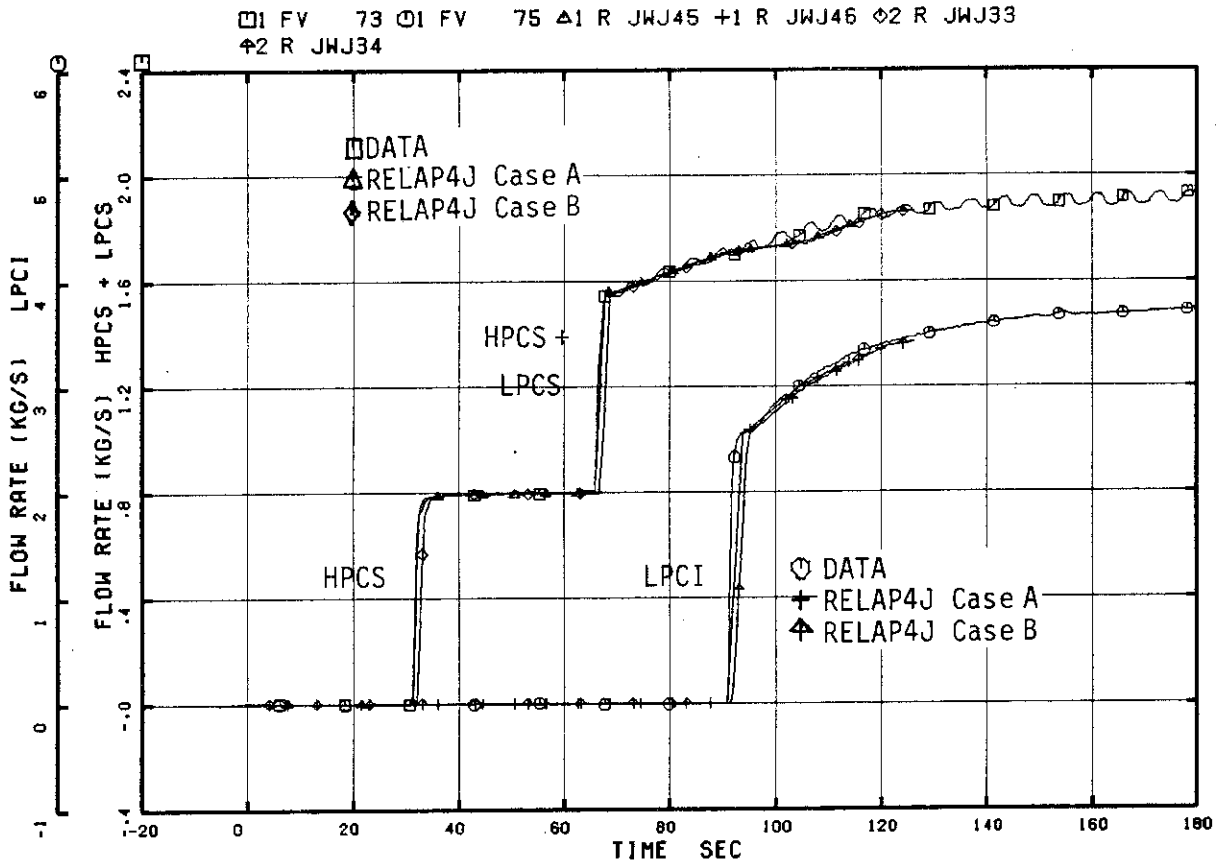


Fig. 3. 6 HPCS + LPCS and LPCI Flow Rate

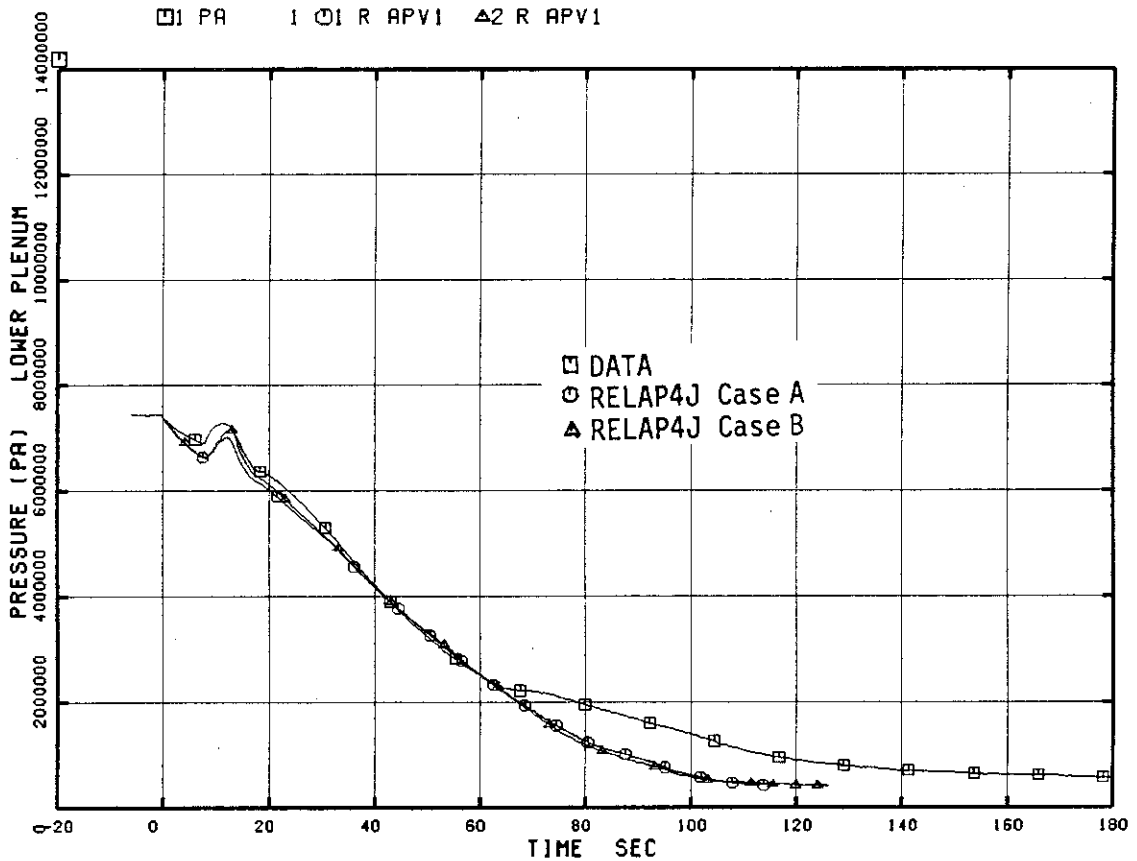


Fig. 3. 7 Lower Plenum Pressure

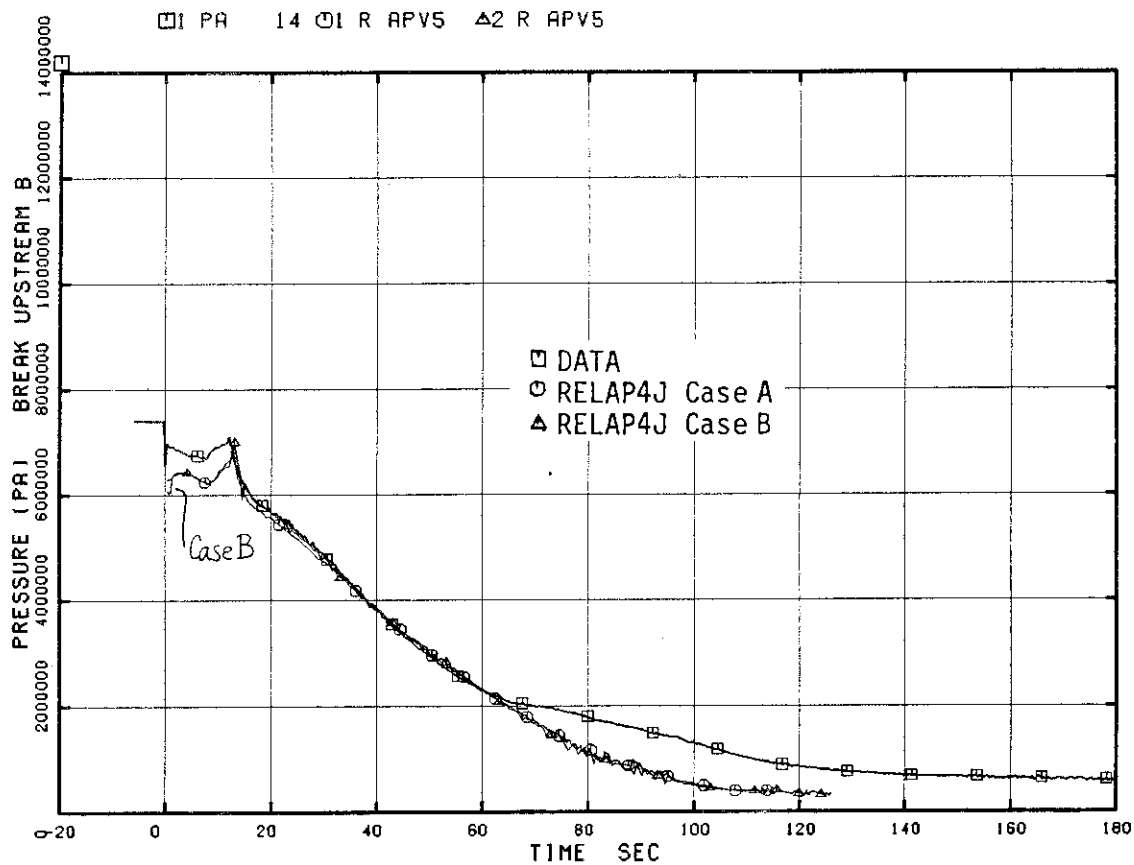


Fig. 3. 8 Pressure at Break B Upstream (PV Side)

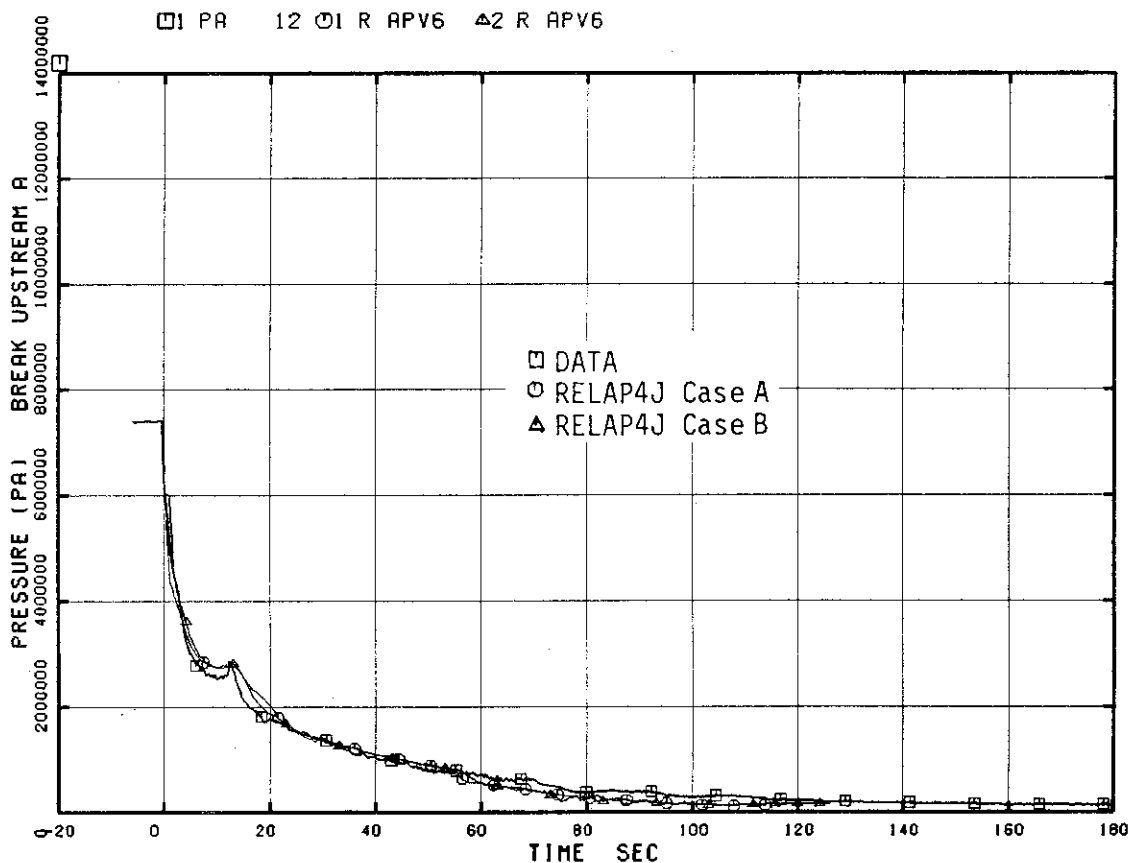


Fig. 3. 9 Pressure at Break A Upstream (MRP Side)

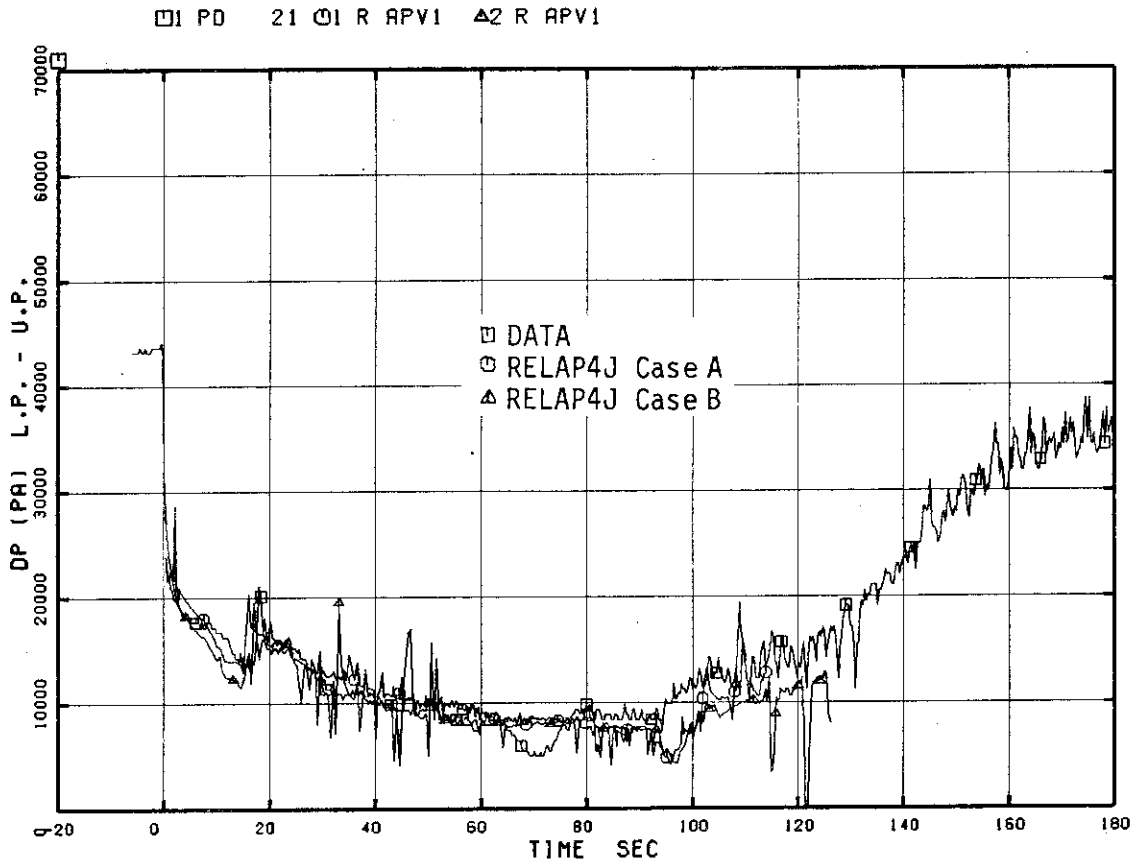


Fig. 3.10 Differential Pressure between Lower and Upper Plena

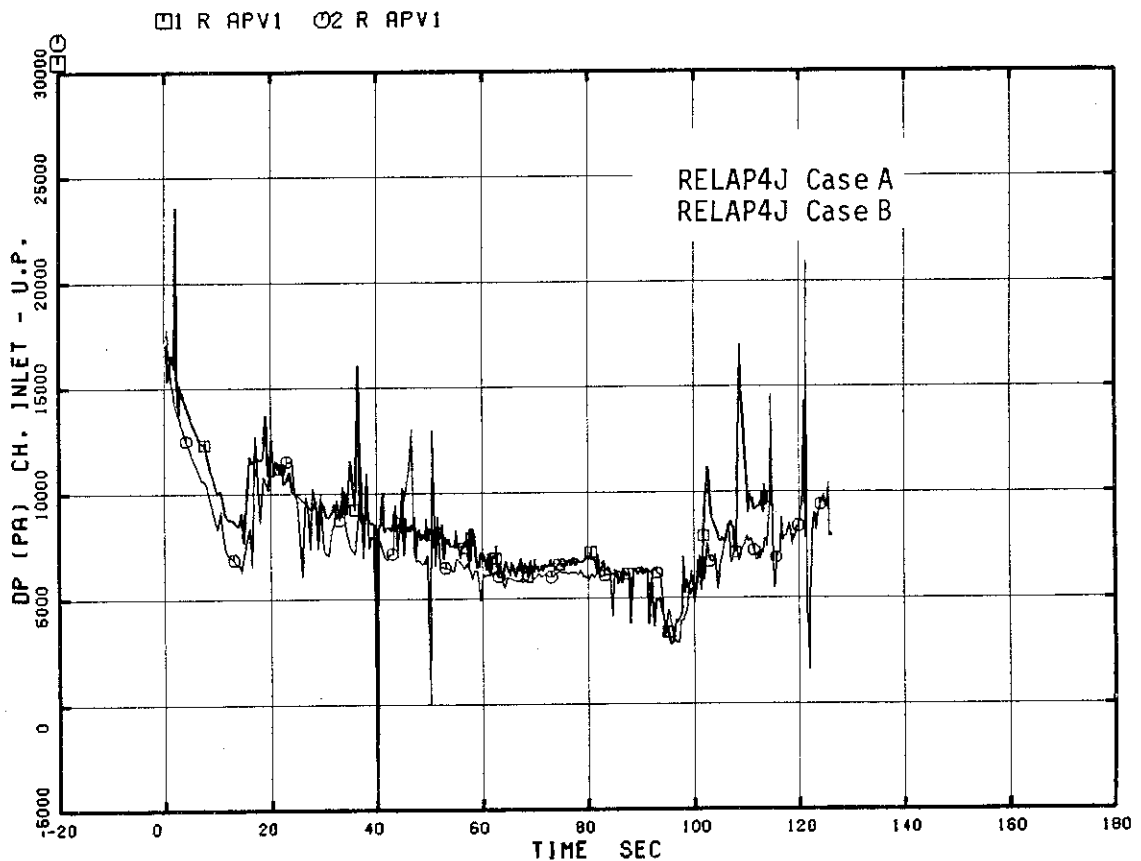


Fig. 3.11 Differential Pressure between Channel Inlet and Upper Plenum

□ 1 FA 4 ○ 1 R JWJ43 △ 2 R JWJ31

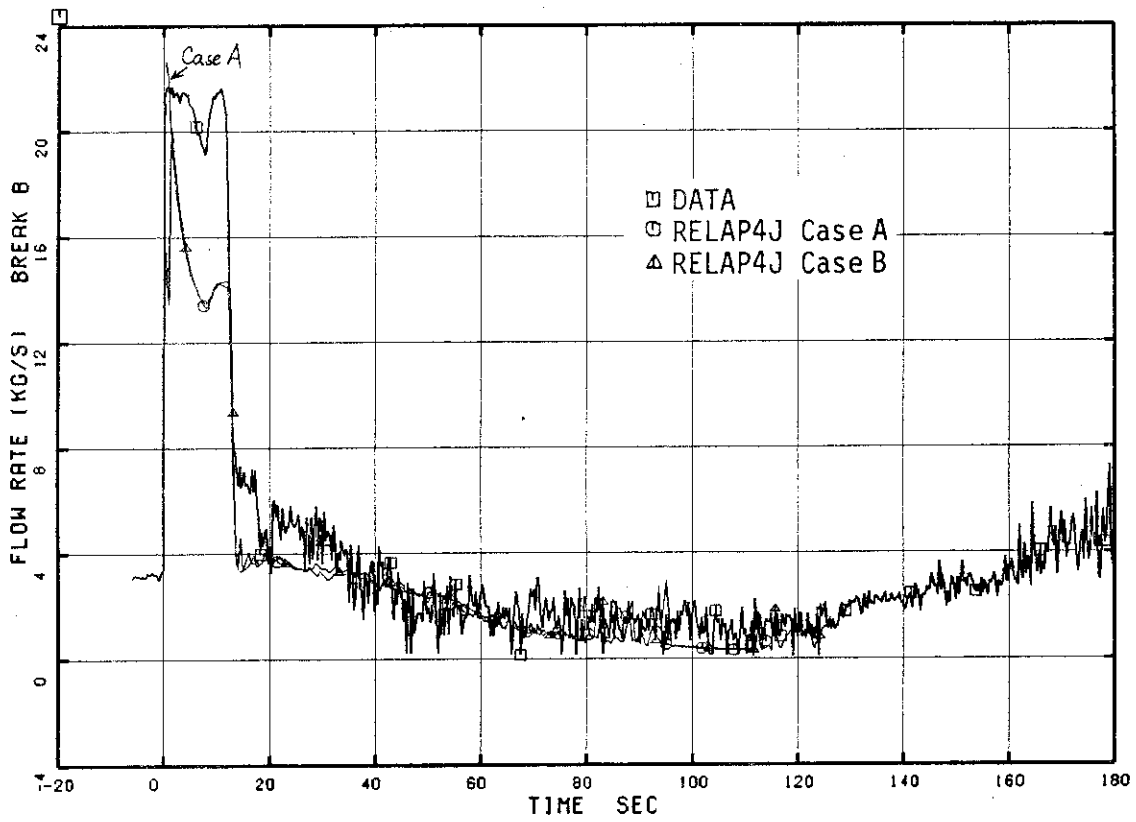


Fig. 3.12 Break Flow from Break B (PV side)

□ 1 FA 13 ○ 1 R JWJ42 △ 2 R JWJ30

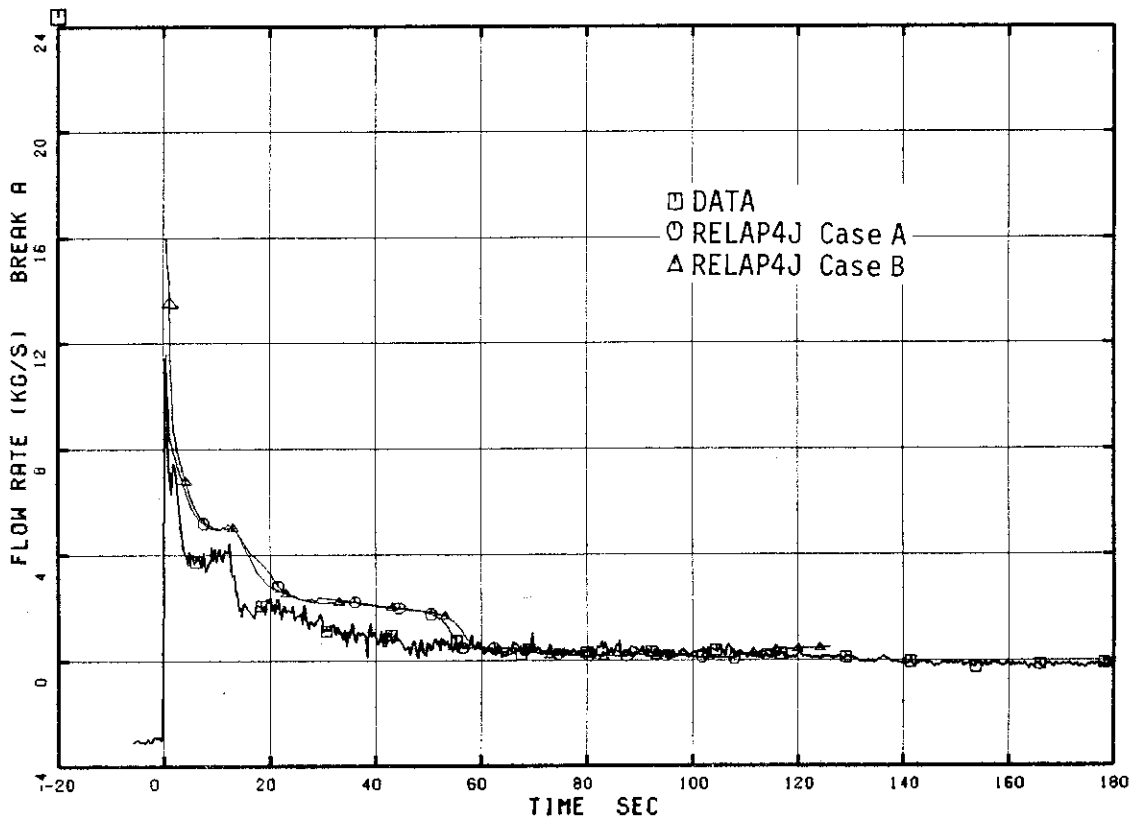


Fig. 3.13 Break Flow from Break A (MRP side)

□ DE 128 ○ R ARV5 ▲ 2 R ARV5

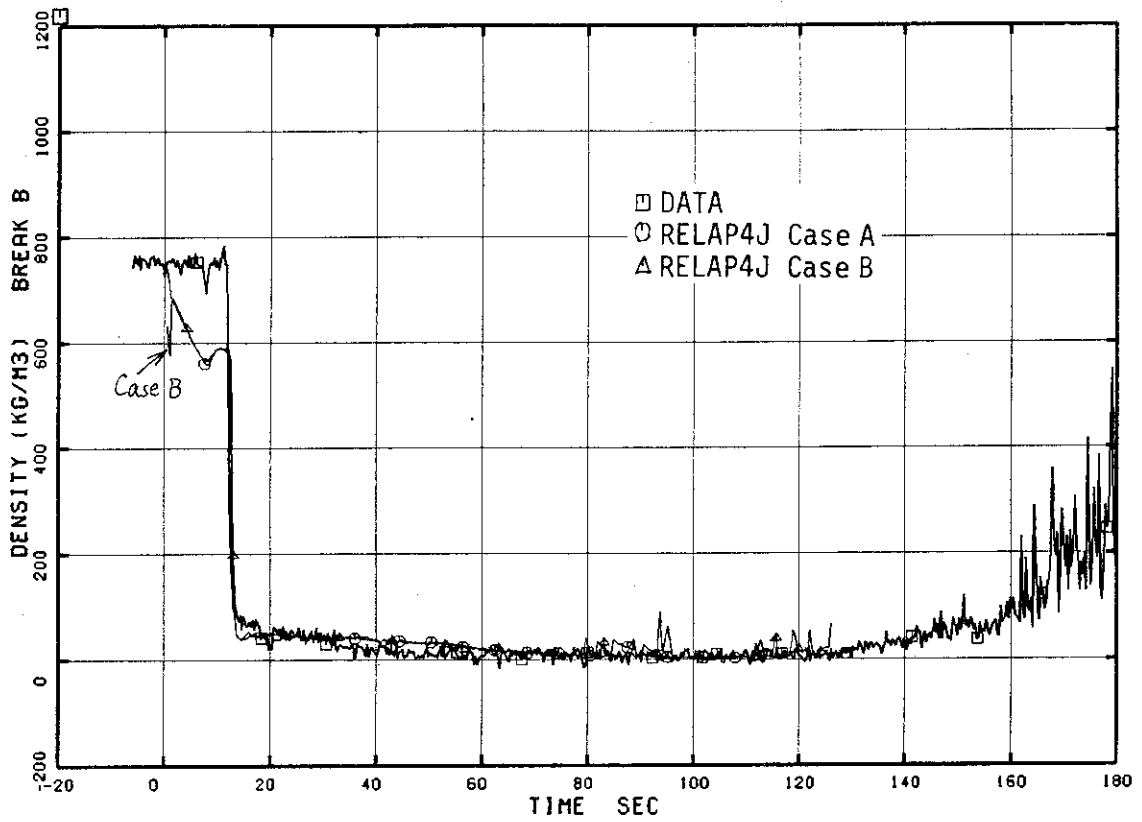


Fig. 3.14 Average Fluid Densities at the Break B Upstream

□ DE 126 ○ R ARV6 ▲ 2 R ARV6

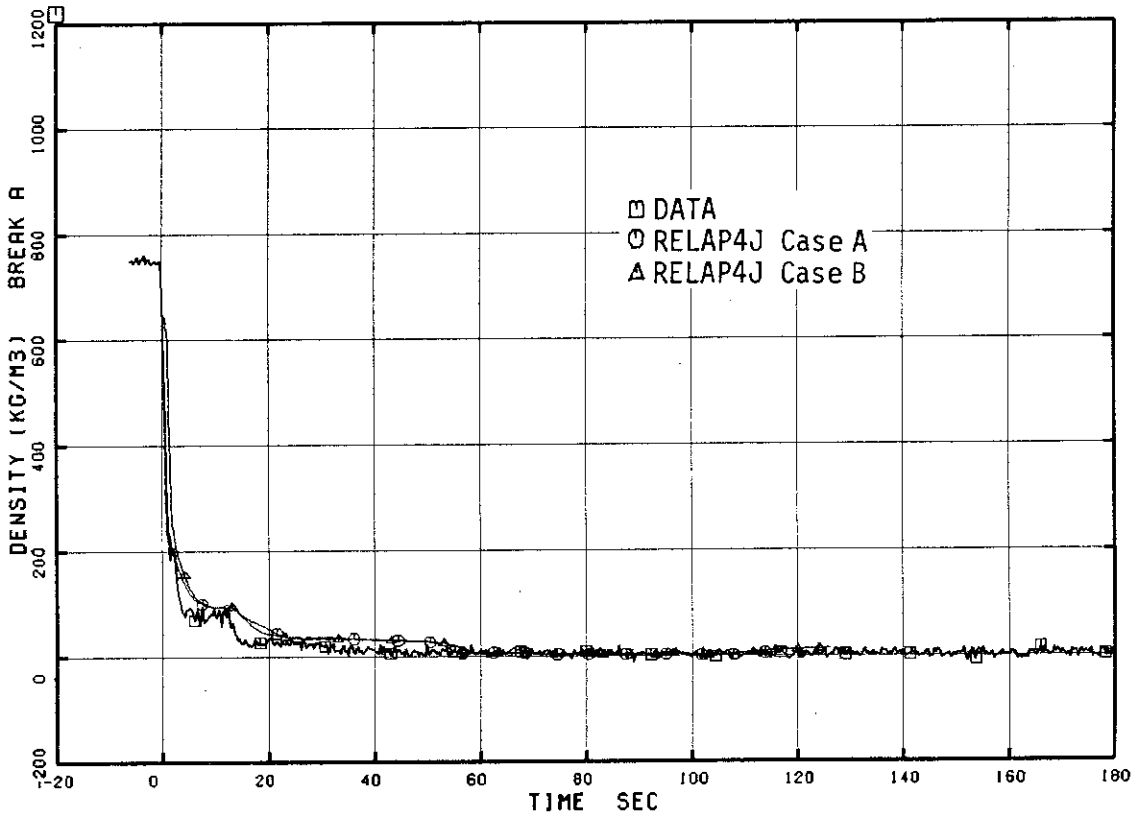


Fig. 3.15 Average Fluid Densities at the Break A Upstream

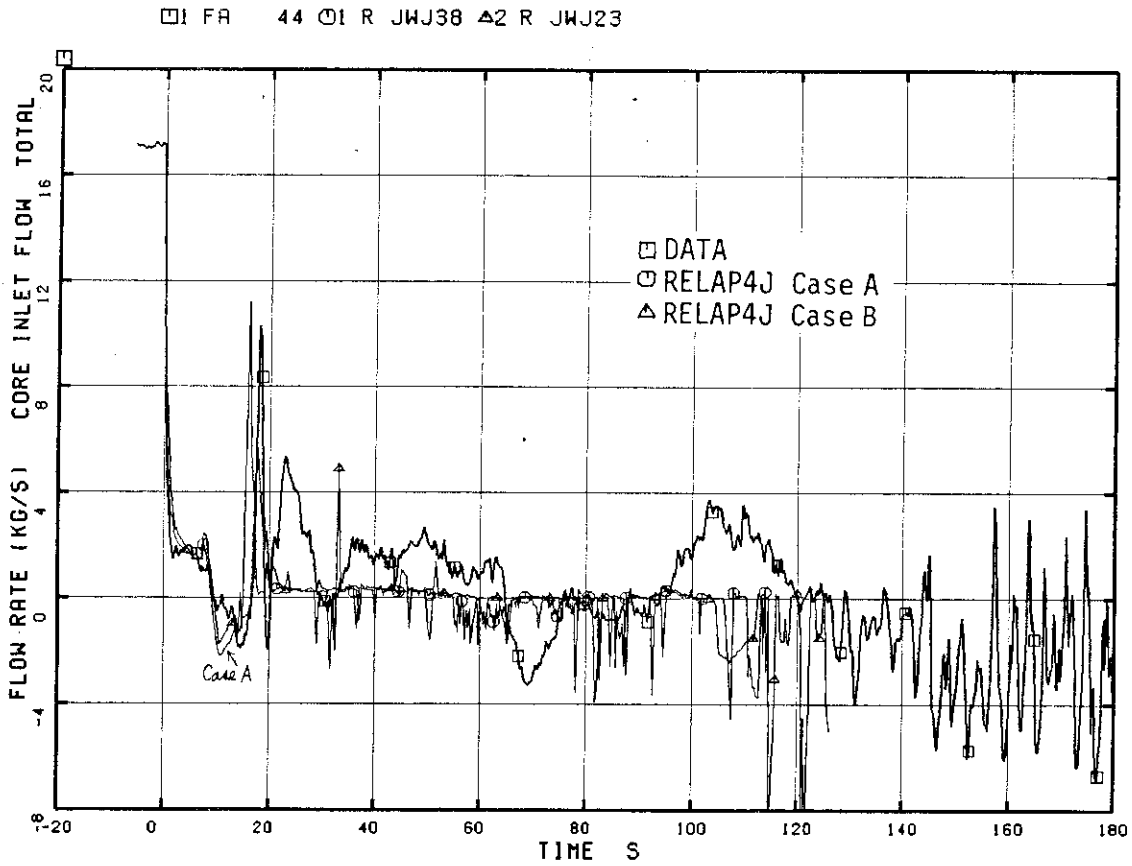


Fig. 3.16 Total Core Inlet Flow through SEO

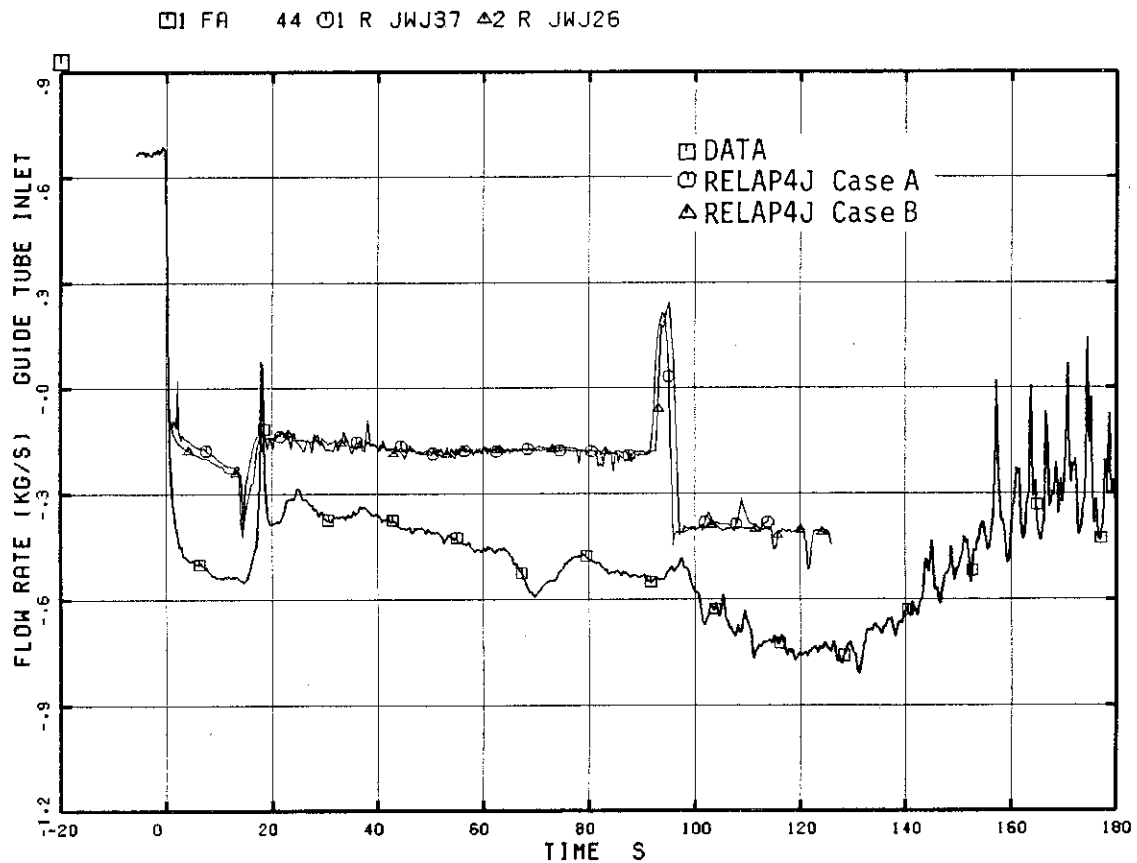


Fig. 3.17 Guide Tube Inlet Flow

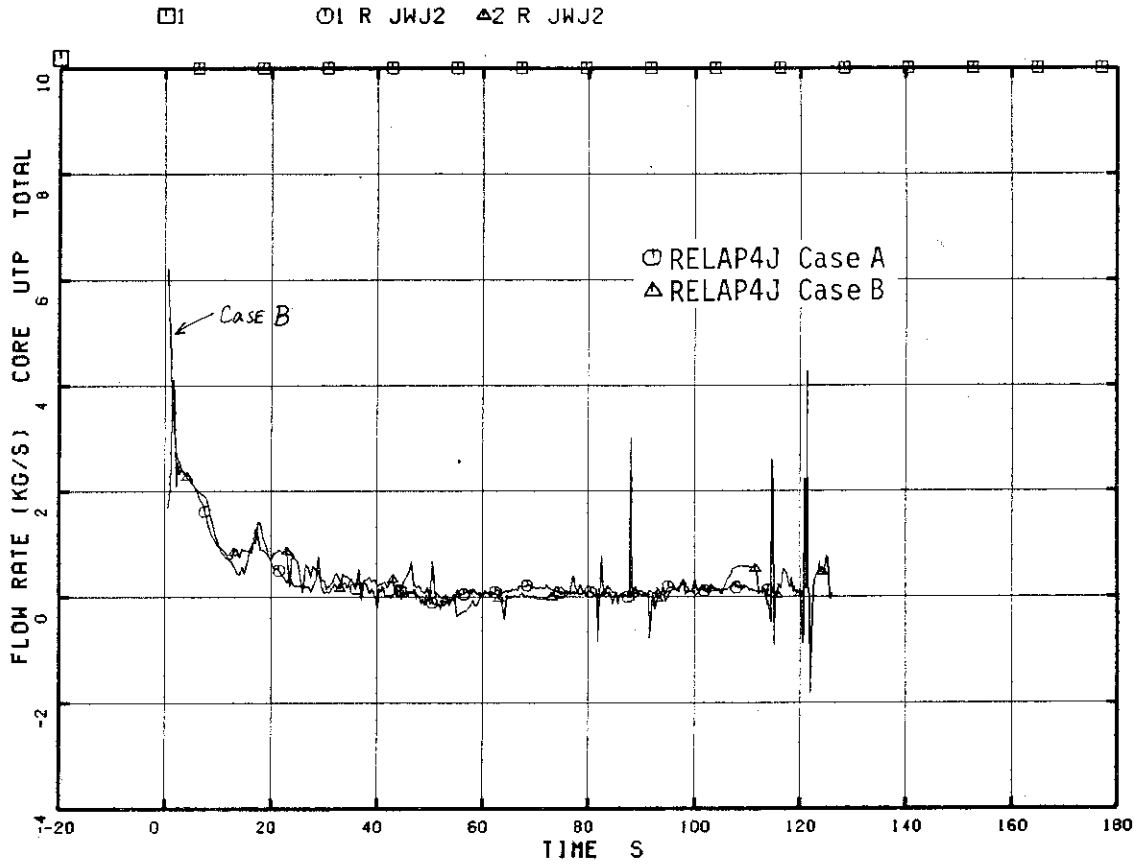


Fig. 3.18 Total Core Flow through UTP

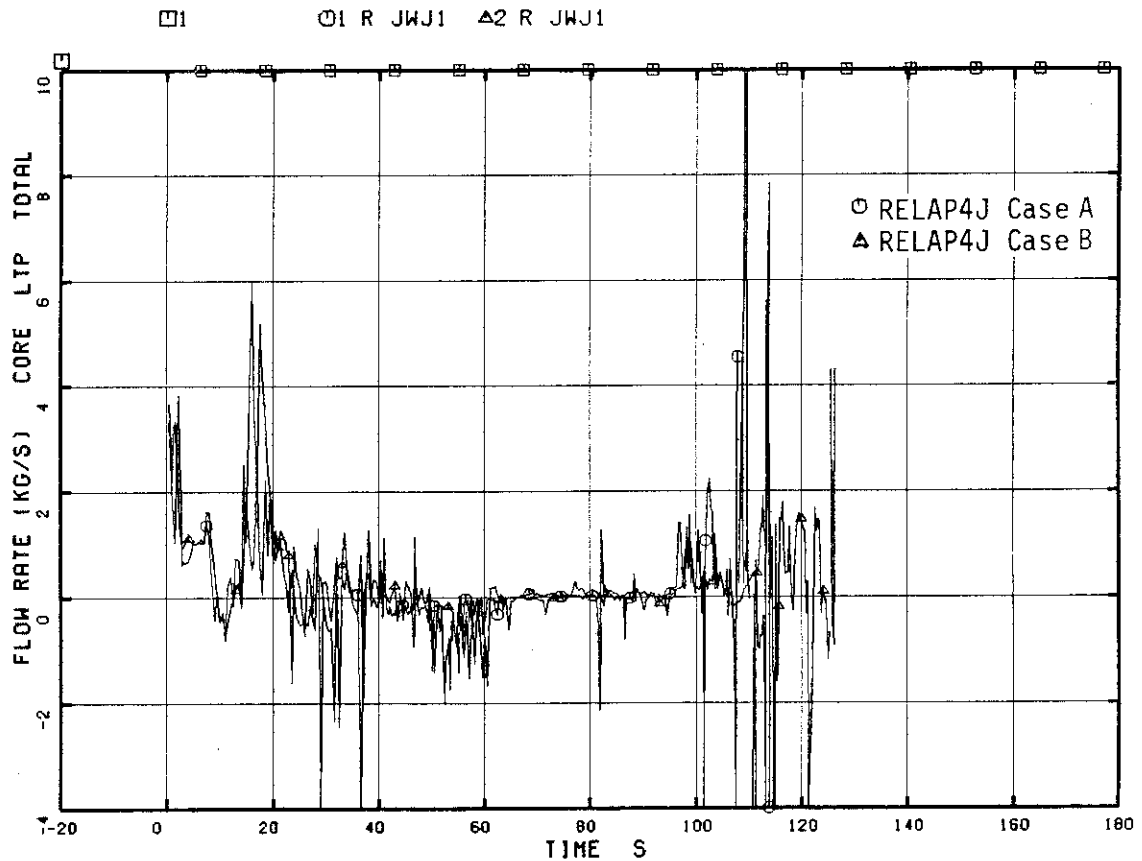


Fig. 3.19 Total Core Flow through LTP

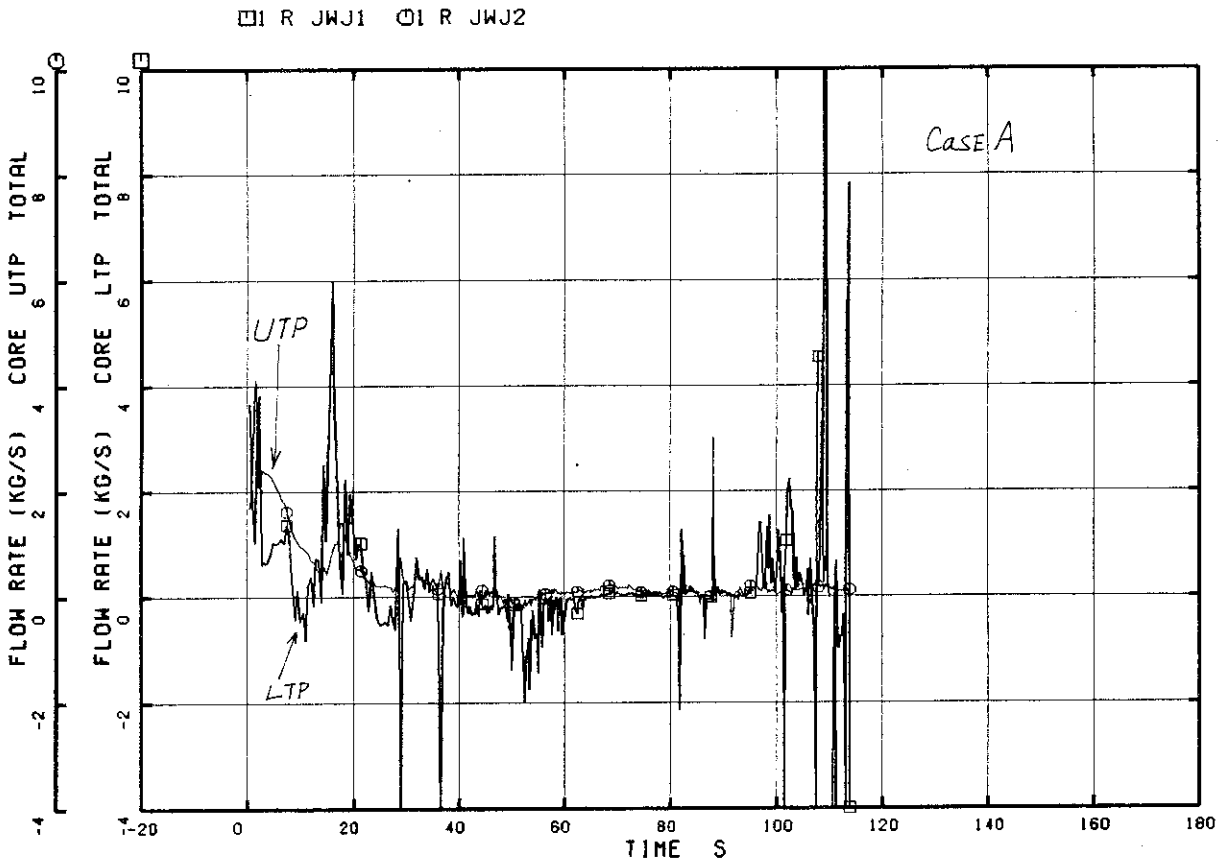


Fig. 3.20 Total Core Flows through UTP and LTP (Case A)

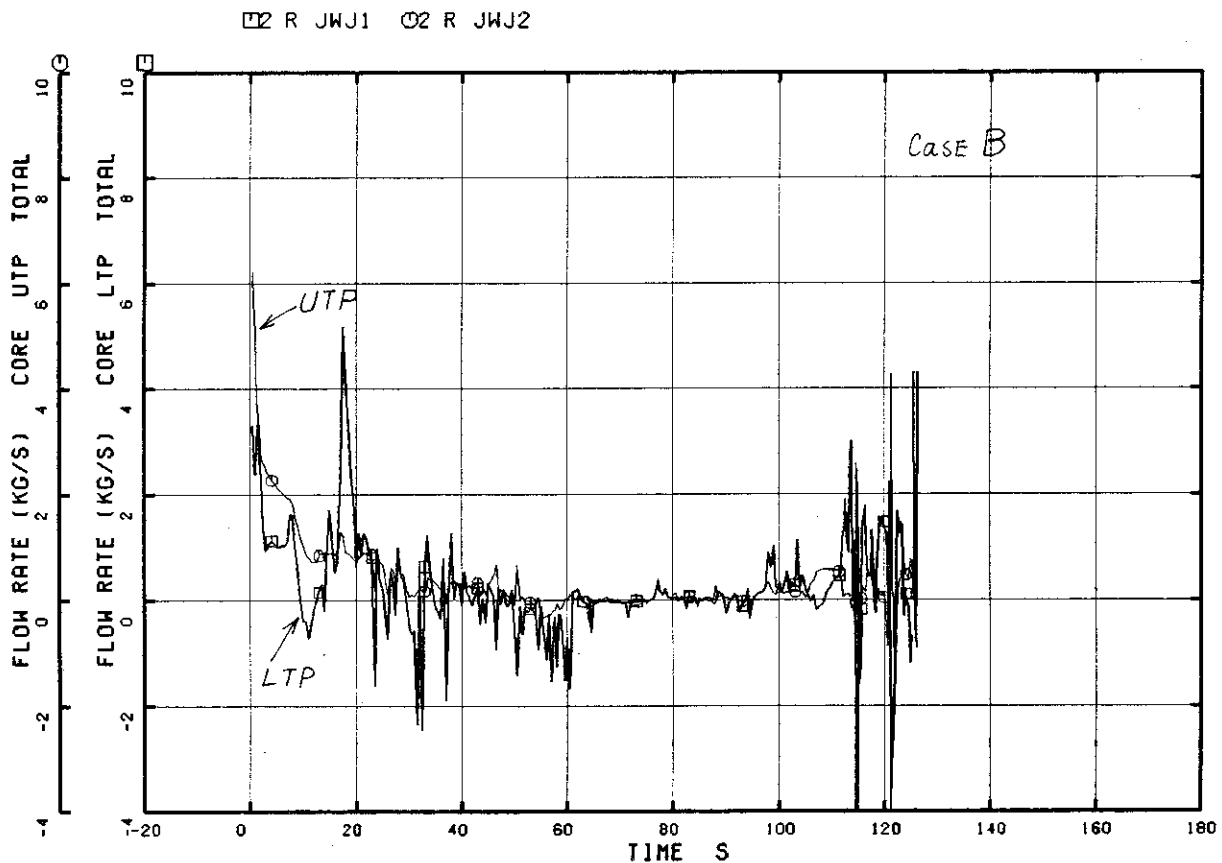


Fig. 3.21 Total Core Flows through UTP and LTP (Case B)

□ FM 720 ○ R JWJ16 △ R JWJ17 +1 R JWJ20

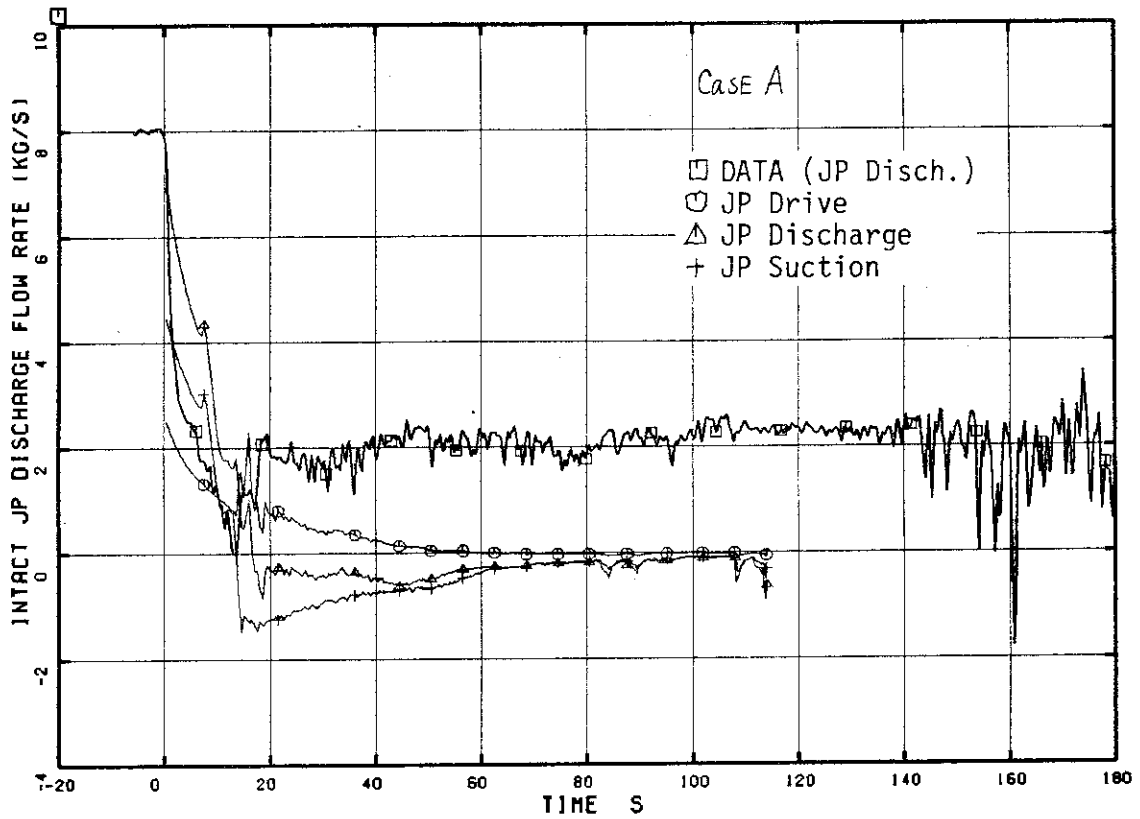


Fig. 3.22 Jet Pump Flow (Intact Loop Side ; Case A)

□ FM 722 ○ R JWJ8 △ R JWJ9 +1 R JWJ12

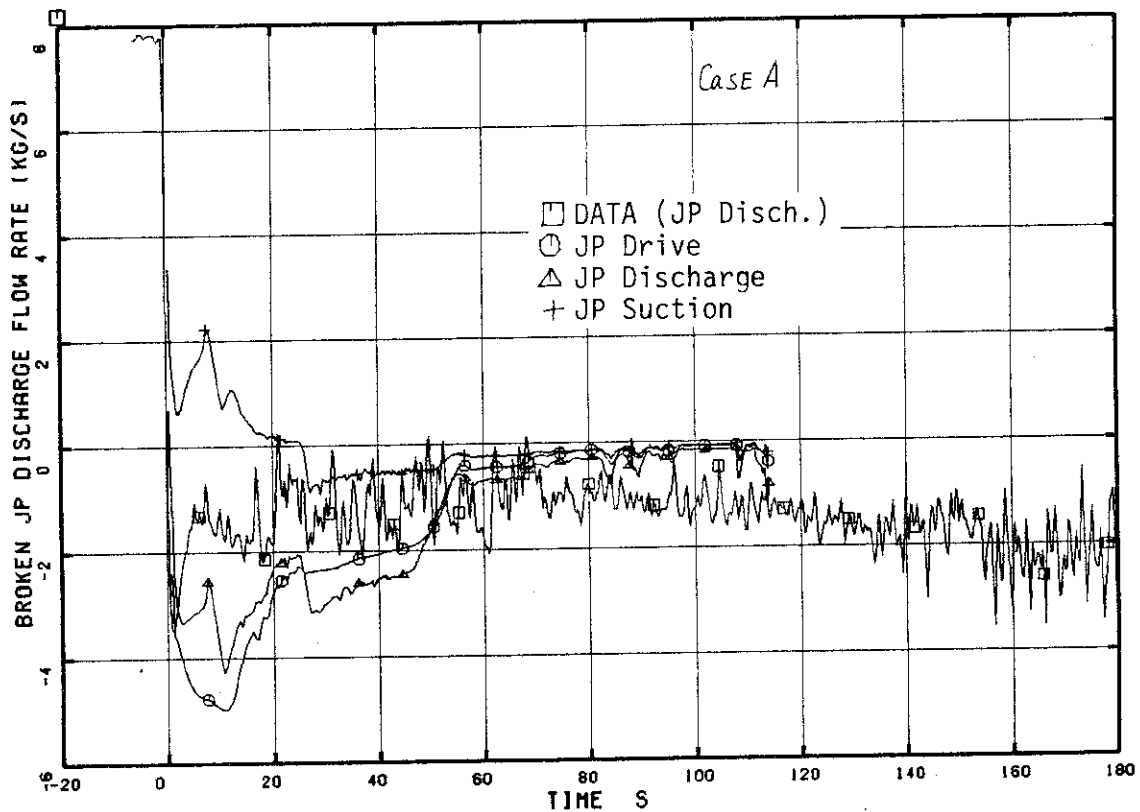


Fig. 3.23 Jet Pump Flow (Broken Loop Side ; Case A)

□ 1 FM 720 ○ 2 R JWJ16 △ 2 R JWJ17 + 2 R JWJ20

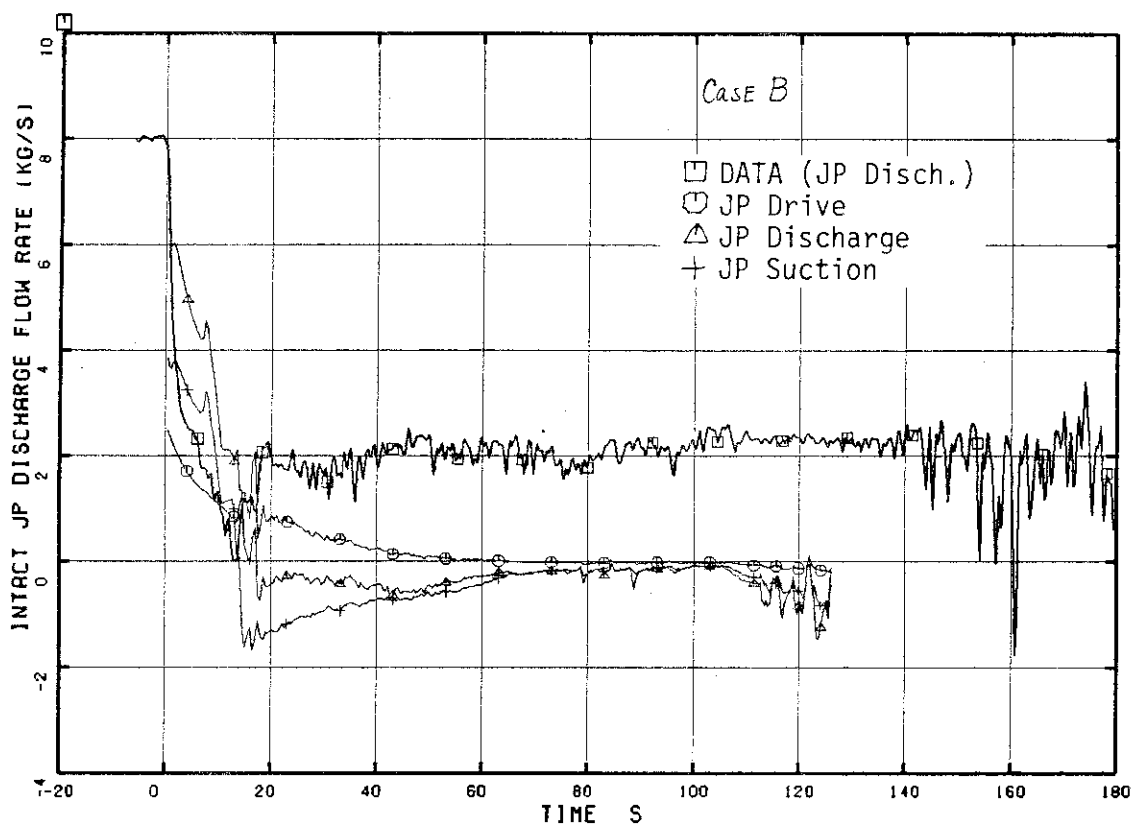


Fig. 3.24 Jet Pump Flow (Intact Loop Side ; Case B)

□ 1 FM 722 ○ 2 R JWJ8 △ 2 R JWJ9 + 2 R JWJ12

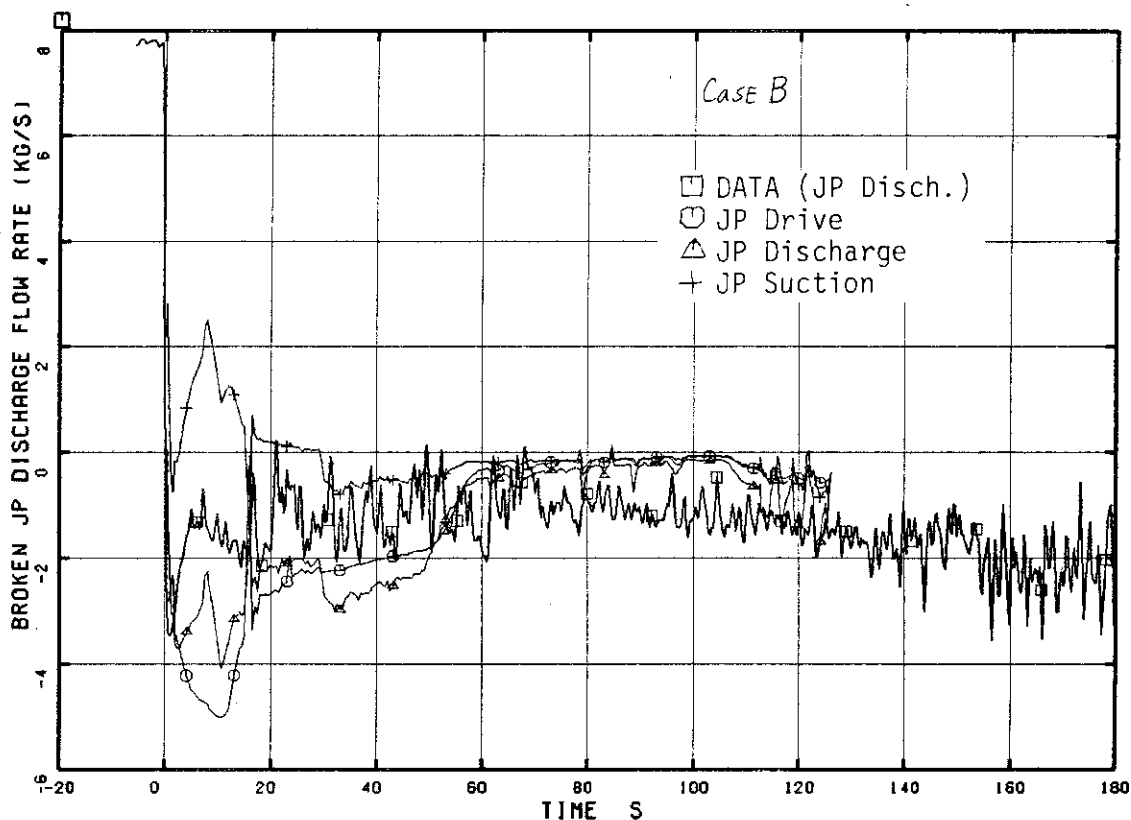


Fig. 3.25 Jet Pump Flow (Broken Loop Side ; Case B)

RUN 901

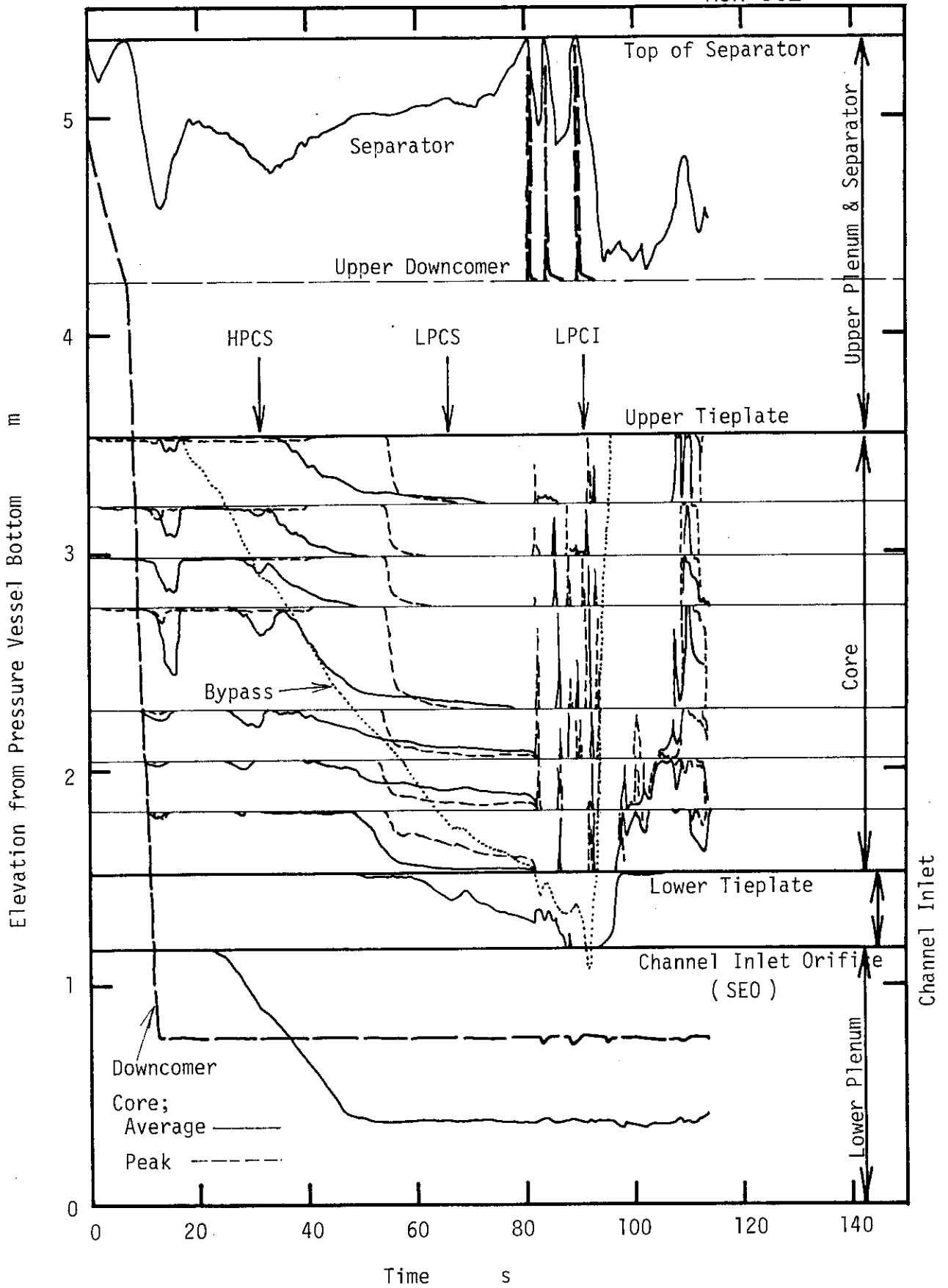


Fig. 3.26 Liquid Levels in the Pressure Vessel (Case A)

RUN 901

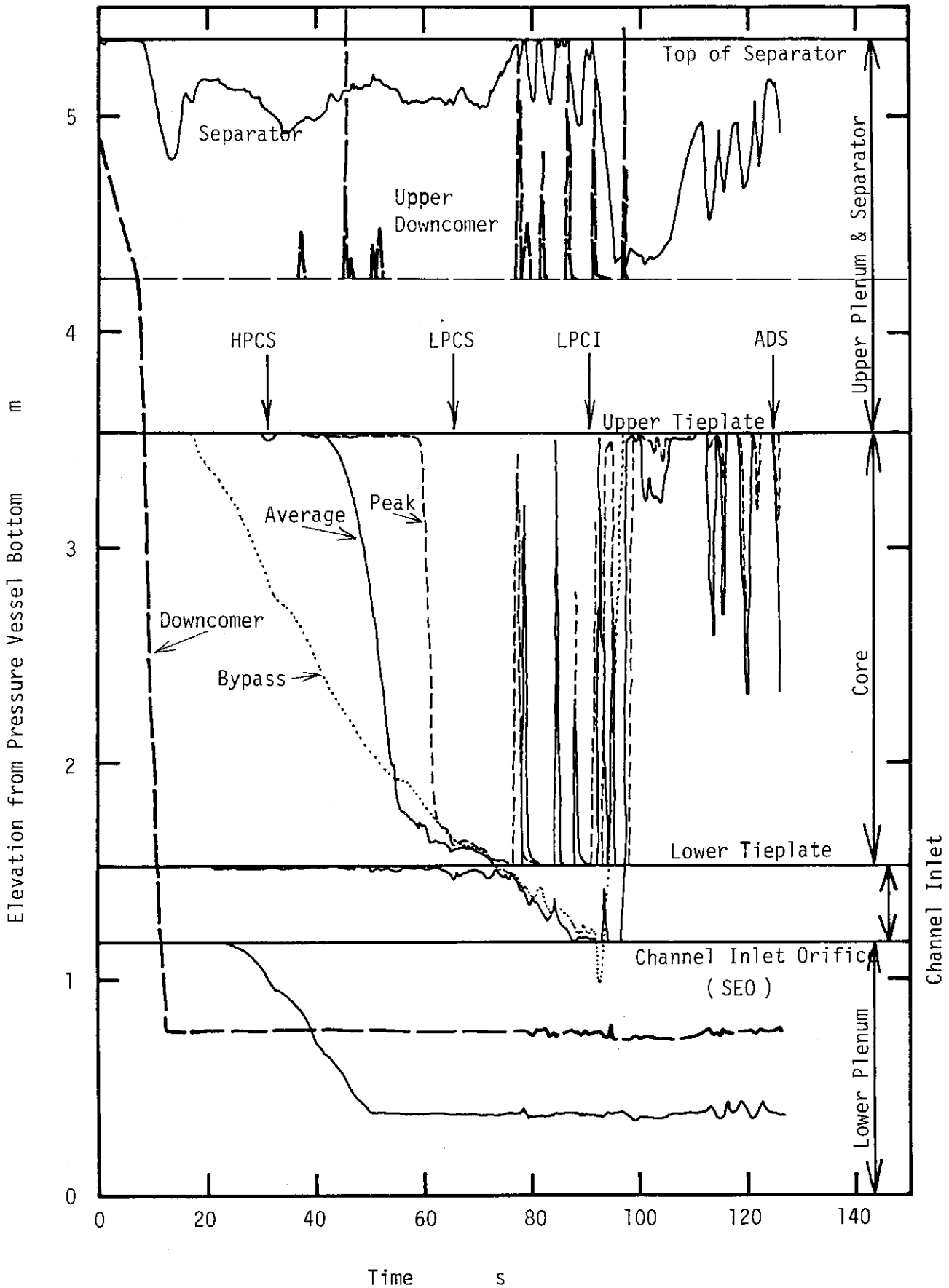


Fig. 3.27 Liquid Levels in the Pressure Vessel (Case B)

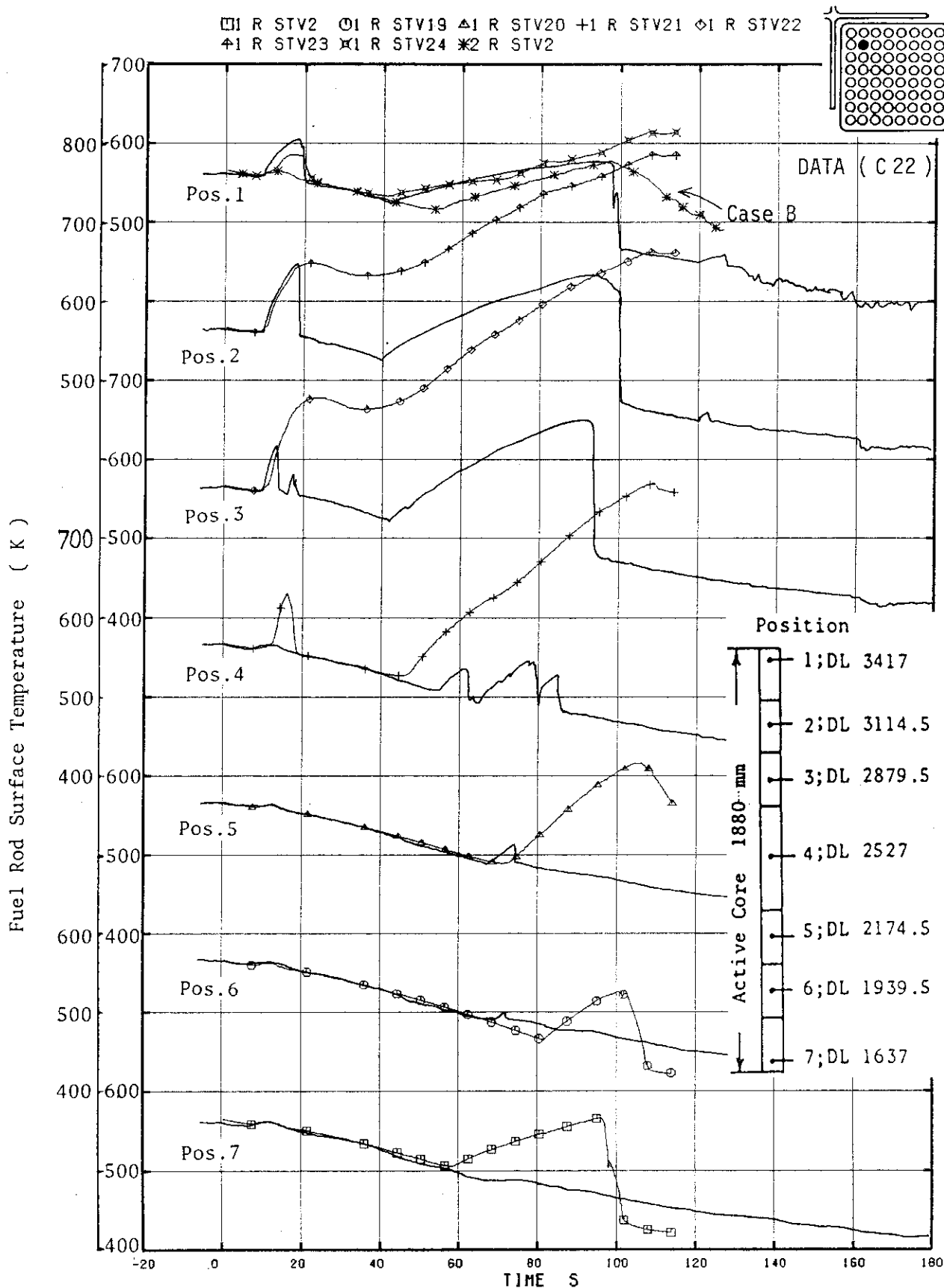


Fig. 3.28 Fuel Rod Surface Temperature in Case A
(Average Power Channel)

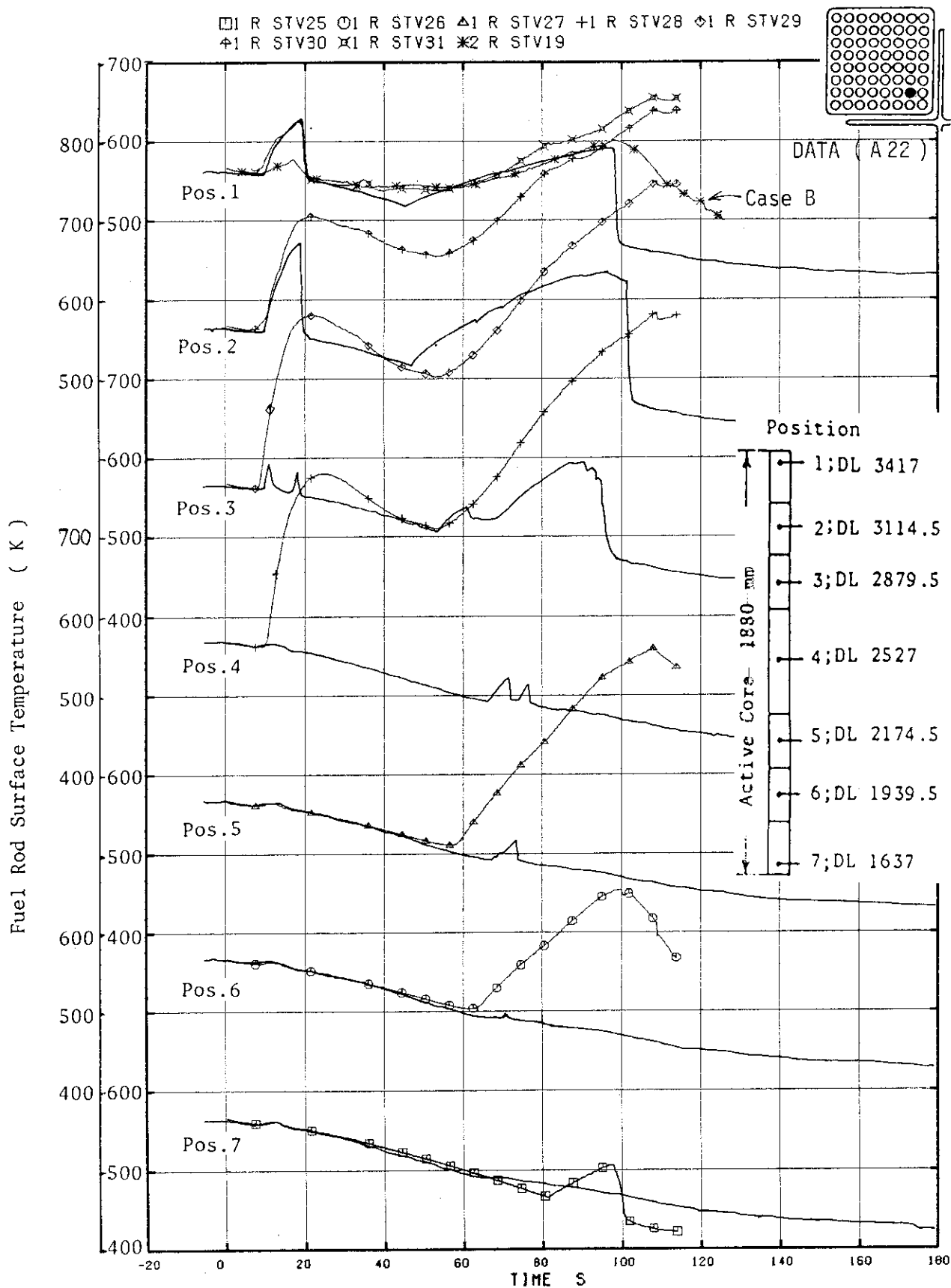


Fig. 3.29 Fuel Rod Surface Temperature in Case A
(Peak Power Channel)

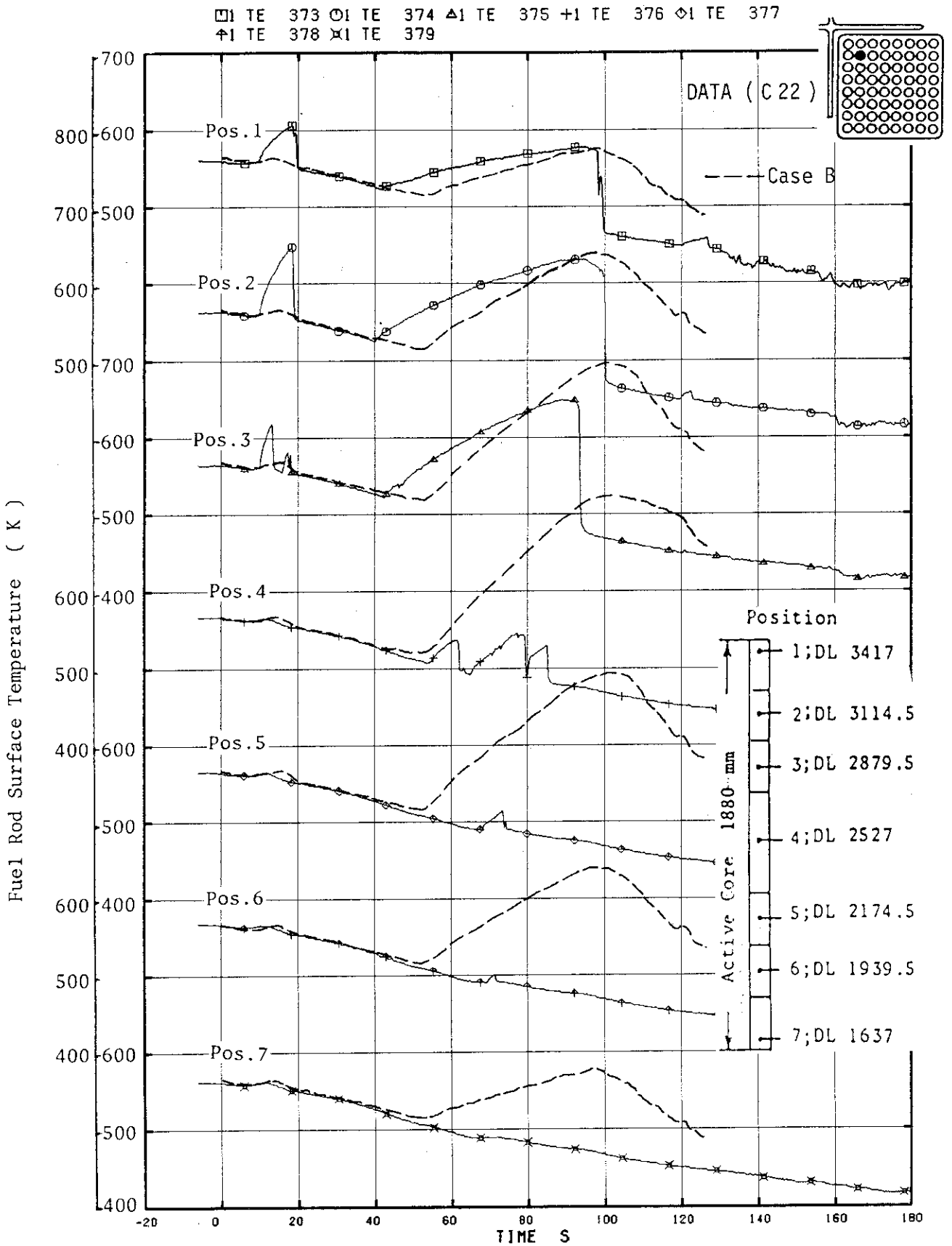


Fig. 3.30 Fuel Rod Surface Temperature in Case B
(Average Power Channel)

□ TE 233 ○ TE 234 △ TE 235 + TE 236 ◇ TE 237
 † TE 238 × TE 239

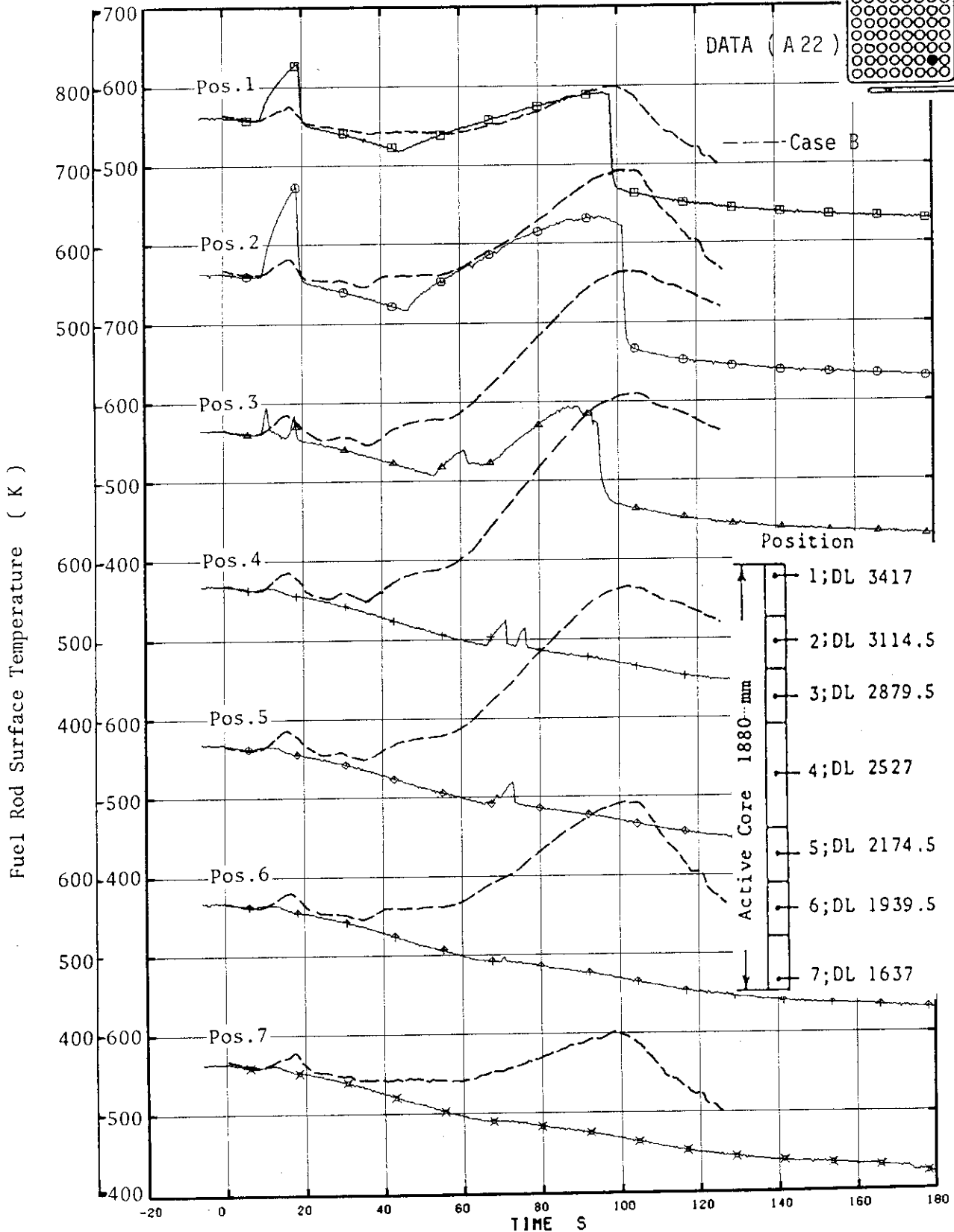
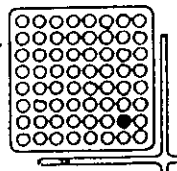


Fig. 3.31 Fuel Rod Surface Temperature in Case B
 (Peak Power Channel)

□ R HCV24 ○ R HCV31

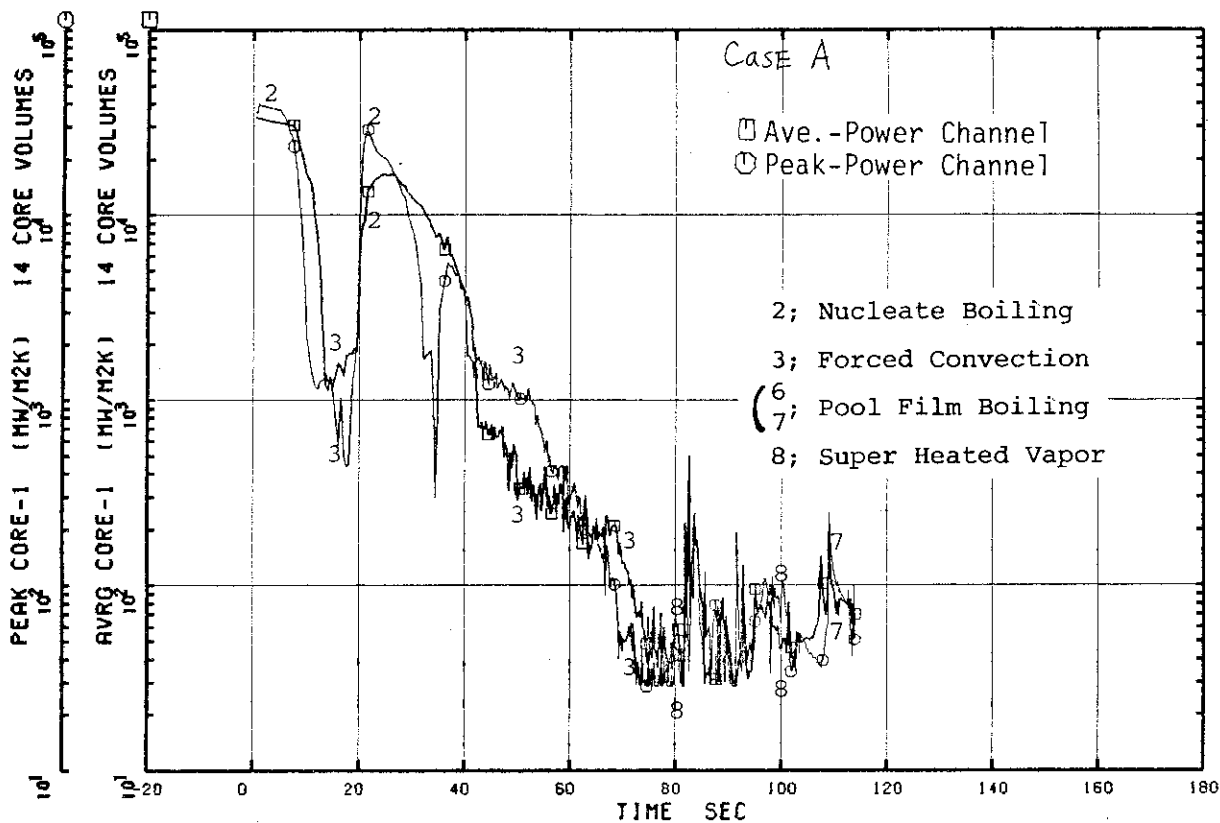


Fig. 3.32 Heat Transfer Coefficient at Position 1 (Case A)

□ R HCV23 ○ R HCV30

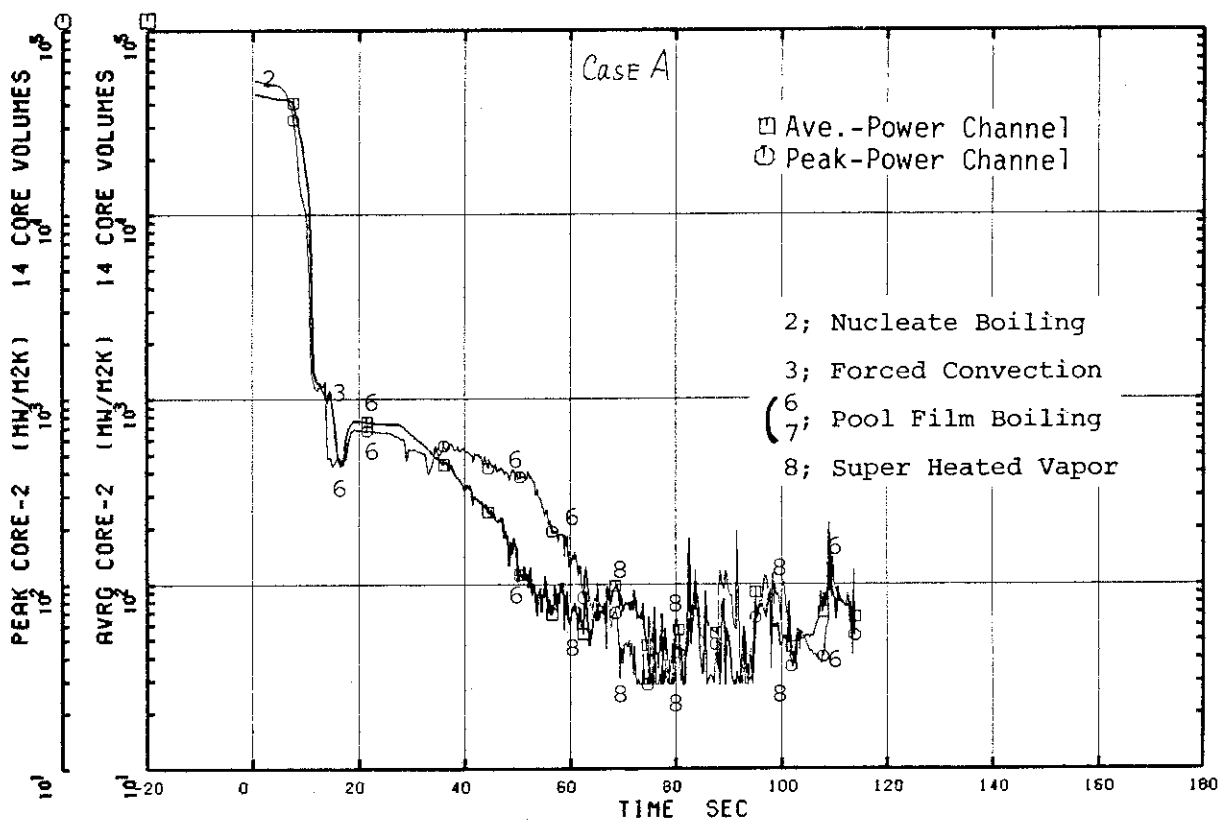


Fig. 3.33 Heat Transfer Coefficient at Position 2 (Case A)

□ R HCV22 ○ R HCV29

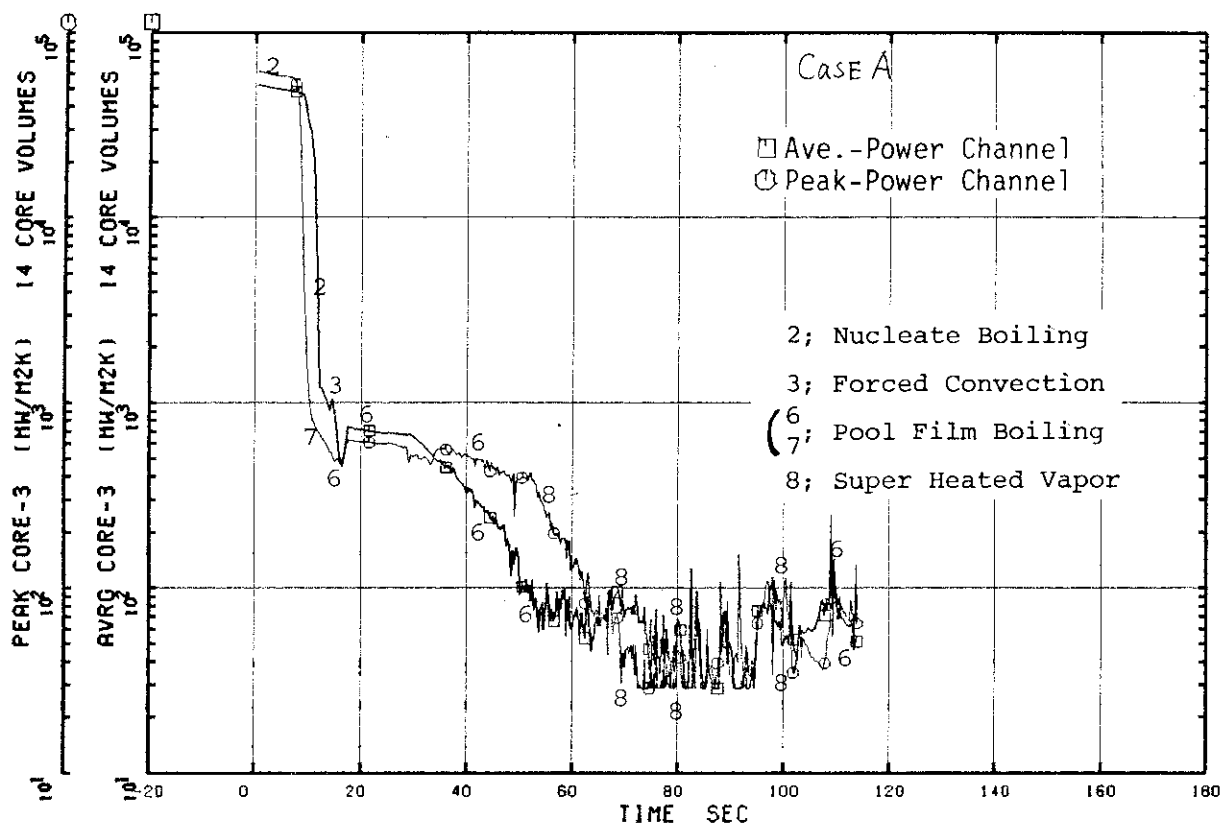


Fig. 3.34 Heat Transfer Coefficient at Position 3 (Case A)

□ R HCV21 ○ R HCV28

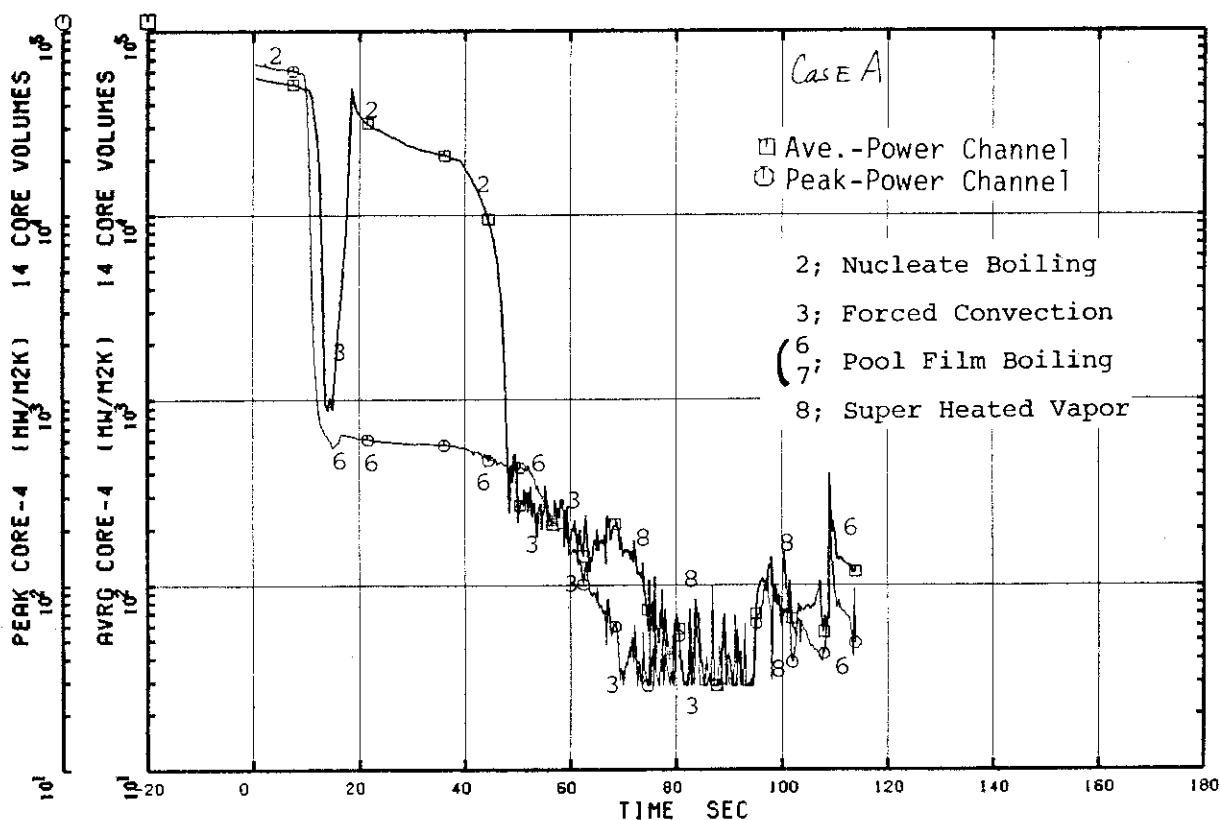


Fig. 3.35 Heat Transfer Coefficient at Position 4 (Case A)

□ R HCV20 ○ R HCV27

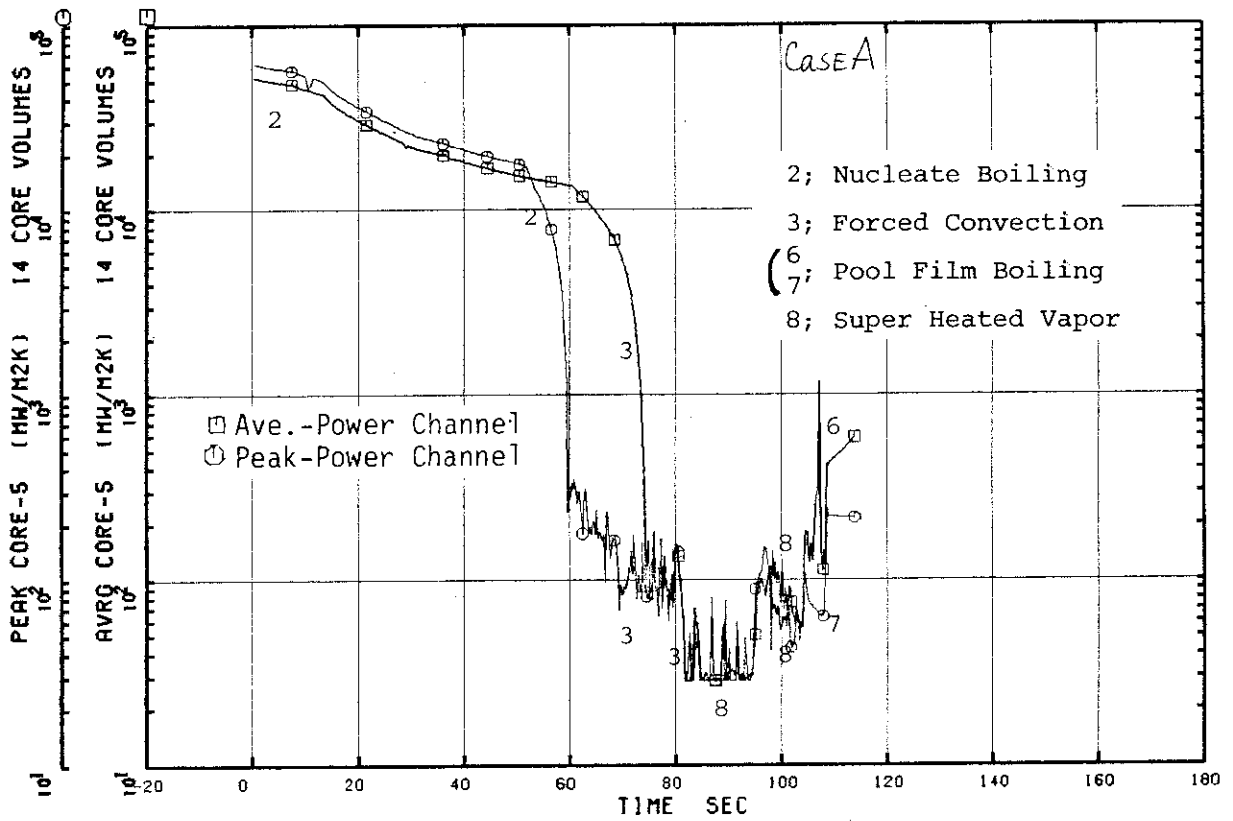


Fig. 3.36 Heat Transfer Coefficient at Position 5 (Case A)

□ R HCV19 ○ R HCV26

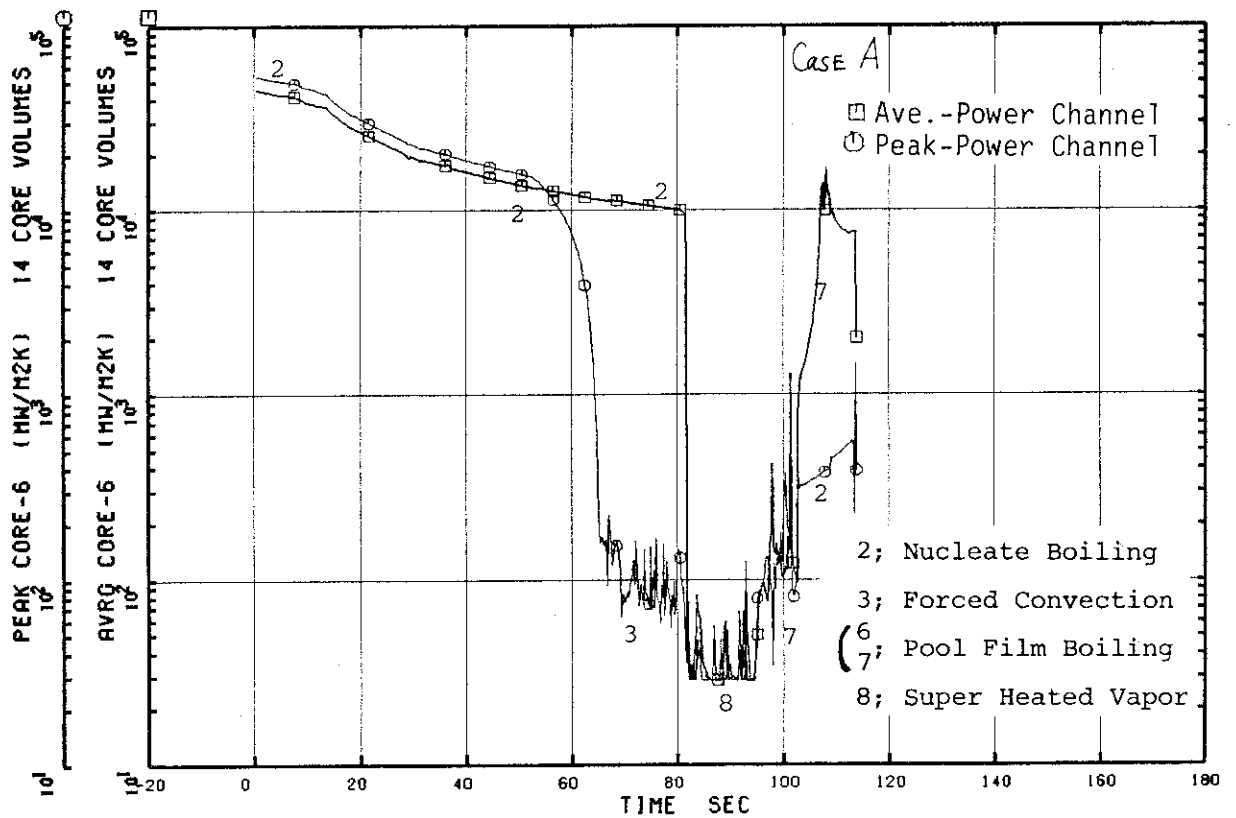


Fig. 3.37 Heat Transfer Coefficient at Position 6 (Case A)

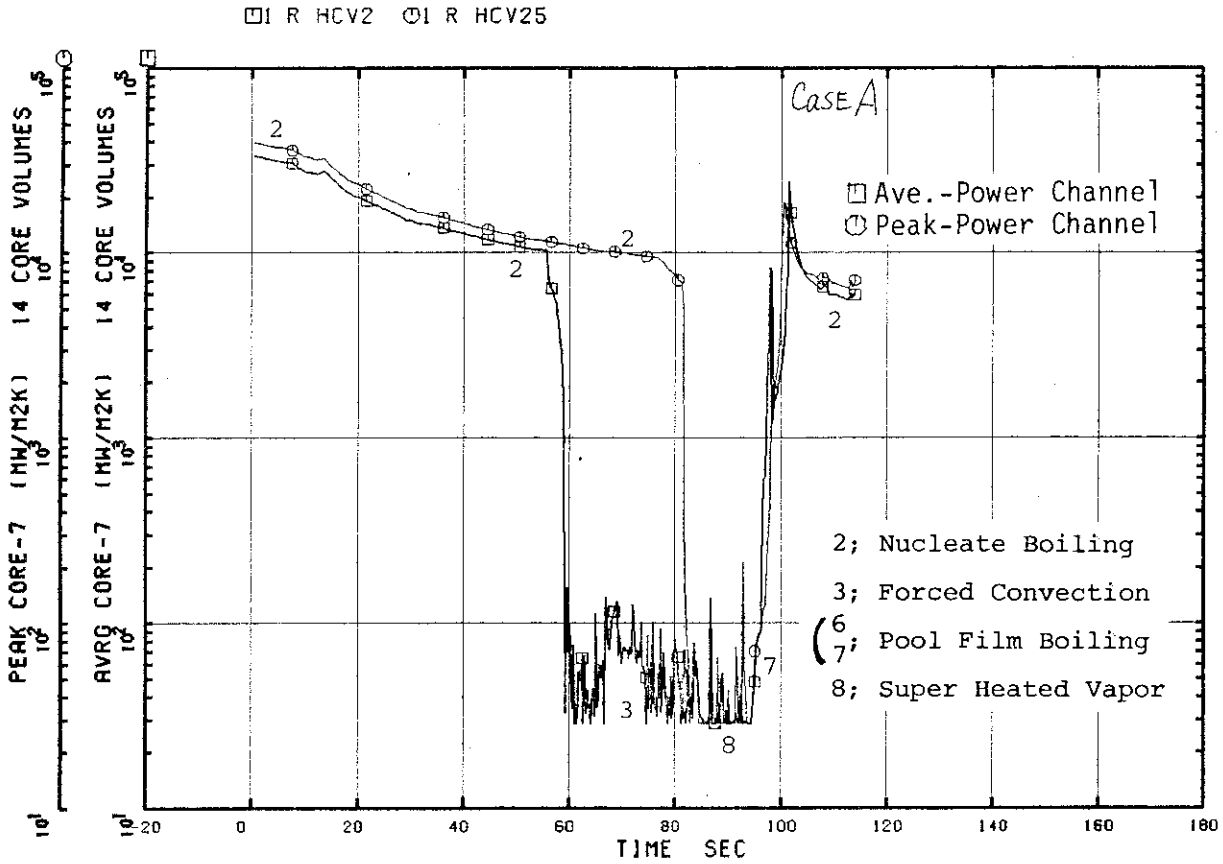


Fig. 3.38 Heat Transfer Coefficient at Position 7 (Case A)

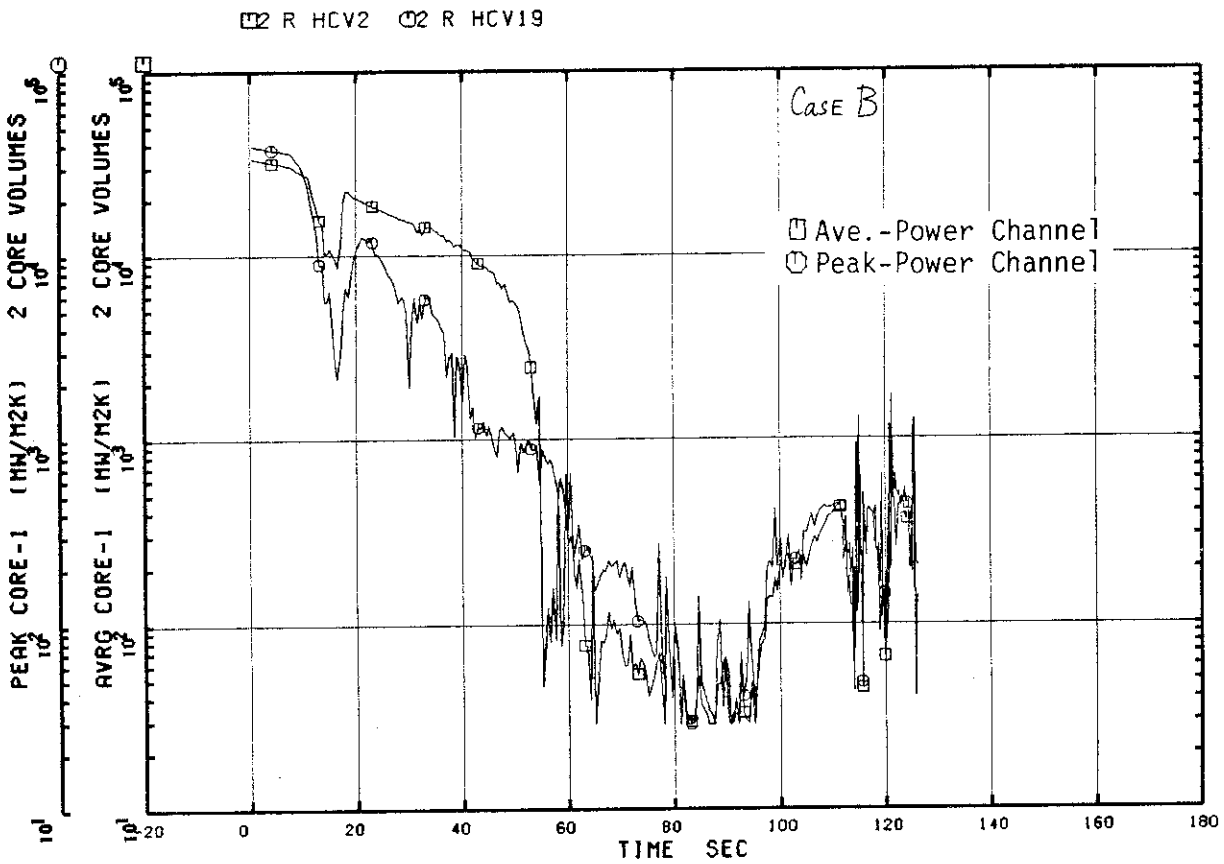


Fig. 3.39 Heat Transfer Coefficient at Position 1 (Case B)

4. ANALYSIS BY RELAP5/MOD1/001

4.1 Computer Code

The RELAP5/MOD1/001 code⁽⁷⁾ uses a two-fluid, five-equation model for two-phase flow analysis. The five equations consist of one mass conservation equation for each phase, one momentum conservation equation for each phase and one overall energy conservation equation that is supplemented by the assumption that one of the two phases is saturated.

RELAP5 considers four constitutive relations in its hydrodynamic model. They are constitutive relations for the interphase mass transfer (vaporization and condensation), the interphase drag, the wall friction and the wall heat transfer. The interphase drag consists of dynamic drag and steady drag which depends on the four flow regime maps employed in RELAP5. The wall friction model uses the modified Baroczy two-phase friction multiplier correlation with the Colebrook correlation for the single-phase friction factor including wall roughness effects. The wall heat transfer correlation employs the RELAP4/MOD6 heat transfer correlation.

The RELAP5 numerical scheme is based on a linear, semi-implicit, integration scheme. This numerical scheme contributes to fast execution.

RELAP5 simulates the Light Water Reactor (LWR) with the various components: single volumes, single junctions, pipes, branches, pumps, valves, heat structures, etc. RELAP5 is designed to be primarily a one-dimensional program and has only one-dimensional volumes. The finite difference approximations to the conservation equation assume that fluid enters or leaves a one-dimensional volume only at its ends. RELAP5 does not calculate the mixture level within a volume. Therefore, the mixture level in the volume is assumed to pass downward or upward through the bottom of the volume when the void fraction in the volume exceeds or becomes below 0.96, respectively, in the present analyses.

Other features and models used in RELAP5 are as follow;

- 1) The critical flow model employs the characteristic analysis.
- 2) The code has no jet pump (JP) model and even the branch component can not fully simulate the momentum exchange in the JP. Therefore, two methods to simulate a JP are used in the present analyses. One is to assume a circulation pumps with the same coastdown characteristics and homologous curves as those of the MRP at the JP suction. The other⁽⁸⁾ is to apply the calculation model used in JETP components of the TRAC-BD1 code⁽⁹⁾ to RELAP5. The steady state flow jet pump model is now under development at JAERI.⁽¹⁰⁾
- 3) The code has a separator model with 100% separation efficiency but it is not applied to the separator in the present analyses.
- 4) Fluid inflow or discharge is modeled by a pair of the time dependent junction and volume as the boundary condition. The fluid condition passing through the time dependent junction refers the fluid condition in the upstream volume. Therefore, the void fraction in the steam dome affects the steam discharge flow rate from the steam dome to the time dependent volume even if the data are given as the input.

4.2 Calculation Model

Five cases A through E were calculated with the RELAP5/MOD1/001 code. Features of these calculated cases are presented in Table 4.1. Case A had a JP model simulating the suction flow using supposed circulation pumps in the JP suction with the same coastdown characteristics and homologous curves as the MRP. Cases B, C, D and E had the same JP model as used in the JETP components of the TRAC-BD1 code. Cases A, B and C used an orifice for the break simulation and cases D and E simulated the break nozzles of the ROSA-III by a single volume and a valve. Case C was a sensitivity analysis for case B. The orifice area used in case C was 60% of case B so that the calculated differential pressure decrease in the lower downcomer should agree with that of the experimental data shown in Fig. 2.16.

Nodalization diagrams of ROSA-III for the RELAP5/MOD1/001 code are shown in Tables 4.2 and 4.3 and Figs. 4.1, 4.2 and 4.3. Each nodalization includes two core channels (peak- and average-power channels) vertically divided into seven volumes in a same manner as in the RELAP4J nodalization for the base calculation case A. The ROSA-III was modeled by 94 volumes, 101 junctions and 33 heat slabs for case A, 92 volumes, 99 junctions and 33 heat slabs for cases B and C and 96 volumes, 103 junctions and 33 heat slabs for cases D and E.

Initial thermal-hydraulic conditions for the calculations were obtained from the experimental data shown in Table 2.5. Consistency among the input data were confirmed by a steady state calculation. The initial flow distribution was almost the same as the flow distribution in the RELAP4J calculation. Core power distribution in the RELAP5 calculations was also the same as that in the RELAP4J calculations.

The Experimental flow data were used for the feedwater flow and the ECCS flow and the steam discharge flow through the steam line as a function of time. In the RELAP5 calculation the fluid condition in the upstream volume affects the input flow data for a time dependent junction. Then RELAP5 did not give, for example, the same steam discharge flow rate as the input data when the quality in the steam dome as the upstream volume for the steam line decreased below 1.0 as shown in Fig. 4.4.

In RELAP5 the characteristic analysis model is used as the critical flow model to calculate the break flow. Break flow was discharged from the pipe end to the time dependent volume in cases A through C. In cases D and E the break nozzle was simulated by the volume and valve as shown in Fig. 4.3.

Recirculation pump was modeled by the rated values given in a table and the homologous curves. Input values were almost the same as used in the RELAP4J calculation. In case E the moment of inertia and the rated density were changed because the input values used in cases A through D were proved to be in error.

Form loss coefficients at the junctions were primarily calculated from geometrical form change along the junction and supplementally by abrupt area change model of RELAP5.

Input data of the RELAP5/MOD1/001 calculation are presented in Appendices B, C and D for cases A, C and E, respectively.

4.3 Comparison with the Experimental Data

Major results of the RELAP5/MOD/001 calculation are compared with the experimental data in this section.

The calculations except for case C were not continued after about 35 s because the system pressure decreased too fast resulting in too early LPF initiation. Case C calculation was made for 133 s because the overall transient of the system pressure agreed well with the data.

Case A through E took CPU times of 4, 10, 30, 12 and 24 hours to calculate 35, 32, 132, 47 and 36 s after the break, respectively, with FACOM M-200 Computer in JAERI.

4.3.1 Pressure Transient

The calculated pressure transients in the lower plenum are compared with the data in Fig. 4.8. The calculated pressures decreased much faster than the data. The pressure transients calculated by the models having the same break models gave almost the same pressure transient after the break. The pressure decrease calculated in cases A and B were maximum among the calculated results, and after the MSIV closure the pressure recovered a little because the recirculation lines were uncovered a little after the MSIV closure. The pressure recovery calculated in cases D and E were a half of the measured pressure recovery. The lower pressure recovery calculated in case E than in case D was due to the early core uncover by the lower core inlet flow rate caused by the small moment of inertia of the MRP. The pressure recovery calculated in case C after the MSIV closure compared well with the data because the recirculation line uncover was later than in the other calculations to be shown in Figs.

4.57 and 4.58. The LPF initiated 6.3 s, 6.0 s, 0.7 s, 3.7 s and 3.3 s earlier than the data in cases A, B, C, D and E, respectively. The temporary halt in the pressure decrease after the LPF, initiated at 6.25 MPa, was not adequately calculated in all cases because of the inadequate RELAP5 interphase mass transfer (vaporization) model. The mixture inside shroud was spouted out to the downcomer through the separator top after the LPF resulting in the oscillations in the break flow and the pressure shown in Figs. 4.17 and 4.18.

Calculated initial heat loss was 18.0 kW in every case, which was much smaller than the rated ROSA-III heat loss of 140 kW. Therefore, the calculated low pressures were caused by the larger break flow than realistic one.

The temporary halt in the pressure decrease after the feedwater flashing at 64.8 s was not calculated in case C which had no volumes representing the feedwater line.

The pressure upstream of the PV-side break B shown in Fig. 4.9 indicated similar transient to that of the lower plenum except for a sudden decrease after the break in the data. The pressure calculated in case C agreed well with the data. The pressure transients at the upstream of the MRP-side break A are shown in Fig. 4.10. The calculated results presented good agreement with the data until the recirculation line uncover except for the result of case C calculation. The pressure decrease of case C until the recirculation line uncover was slower compared with the data. After the JP suction uncover the pressure decreased very fast in all cases showing that the steam break flow had little relation to the break form.

4.3.2 Differential Pressure

The calculated differential pressures, as mentioned in section 3.3.2, contain incorrect head. However, since the RELAP5 nodalization consists of the small sectioned volumes, the erroneous head in the differential pressure was smaller than the RELAP4 calculations.

Figures 4.11 and 4.12 show the differential pressures between the lower plenum and the upper plenum and between the upper plenum and the steam dome, respectively. The calculated differential pressures between the lower plenum and the upper plenum indicated a good agreement with the data until the calculated LPF initiation except for case A. The larger differential pressure calculated in case A was due to the large discharge flow of the JP. The pressure peaking observed after the LPF initiation in all case was much larger than the data, and it was followed by continuous large oscillations. In case C, after the LPF died away the differential pressure stayed larger than the data showing that the larger amount of liquid remained inside the shroud than the data since very little reverse flow occurred through the JP discharge after the LPF.

The calculated differential pressures between the upper plenum and the steam dome decreased steeply after the break because the flow loss through the steam separator was not estimated properly.

The lower downcomer heads are shown in Fig. 4.14. Calculated head in case C indicated good agreement with the data until the recirculation suction uncovering. While the results in cases A and B decreased fast compared with the data. In cases D and E, the downcomer head calculations were improved by use of the break nozzle simulated by the RELAP5 single volume and valve.

MRP-1 and MRP-2 heads are shown in Figs. 4.15 and 4.16. The MRP-1 head decreased after the break faster than the data in case E, but decreased slower than the data in the other cases. The MRP-2 head calculated in case E increased much more than in the other cases and the data. These were because the moment of inertia and the rated fluid density of the MRP had been changed in case E and the moment of inertia was underestimated.

4.3.3 Break Flow and Jet Pump Flow

The break flows from the PV-side break B and from the MRP-side break

A are shown in Figs. 4.17 and 4.18, respectively. The measured break flows involved an error of at least $\pm 20\%$, and the break flow from the break B was incorrect until 38 s after the break. Therefore, emphasis in comparisons was placed on the timing of the break flow decrease after the recirculation line uncovering.

Calculated break flow rates from the break B in cases A and B were larger than those in the other cases and decreased stepwise at 4 s after the break because of decrease in the fluid density upstream of the break as shown in Fig. 4.19 and decreased again due to the MRP suction line uncovering 4 s earlier than the data. Calculation in cases C, D and E presented similar break flow rates from the break B and also presented similar incipient time of the break flow decrease with the data. However, the steam break flow rates after the break flow decrease in cases D and E did not decrease much from those in cases A and B and were rather higher than that in case C. The fast pressure decrease in cases D and E as well as in cases A and B as shown in Fig. 4.8 was the result of this larger steam break flow rate. The simulated break nozzle by the single volume and valve in cases D and E did not work well in the steam break flow region.

Calculated break flow rates from the break A are shown in Fig. 4.18. In the MRP side break, the choking was calculated at the JP nozzle and the break. This two choking condition resulted in the decrease in the initial subcool break flow rate in case C but the similar steam break flow rates among every cases after 13 s. The break flow rate from the break A was smaller than that from B. Therefore, the difference in the break flow rate in each case did not seem to affect much the pressure behavior.

Calculated flow rates around the JP mixing region are compared with the measured JP discharge flow in Fig. 4.21 through 4.30. Flow around the JP connected to the broken loop calculated in case A, in which the model possessed the circulation pump in the JP suction lines, gave a sudden increase in the suction flow, the prolonged discharge flow in the forward

direction which was opposite to the data. The large suction flow in case A lowered the liquid level in the downcomer faster than the case B calculation and resulted in earlier decrease in the break flow through the break B. In case B the JP discharge flow reversed immediately after the break and agreed well with the data. The measured JP discharge flow presents only a trend in two-phase flow condition after the LPF initiation. Flows around the JP connected to the intact loop calculated in case E gave lower flow rates than those in cases B, C and D because of the smaller moment of inertia of the MRP in case E, which resulted in the later decrease of the mixture level in the downcomer and the later uncovering of the recirculation line.

Figure 4.31 through 4.40 show calculated velocity of liquid and steam through the break. The liquid and steam velocity were identical when the orifice break model was used. In cases D and E in which the nozzle break model was used the steam velocity was higher than liquid velocity when break flow was saturated. Oscillations were observed after the recirculation line uncovering in every results except for velocities at the break A in case A. This velocity oscillation was synchronized with the oscillation in the break upstream pressure shown in Figs. 4.9 and 4.10. as mentioned in Sec. 4.3.1.

4.3.4 Core Flow

Figures 4.41 through 4.45 show the total flow rate through the SEO, the LTP and the UTP compared with the data. Difference between the flows through the SEO and the LTP was the flow through the leak hole connecting between the core bypass and the channel inlet chamber.

As shown in Fig. 4.8, the system pressure decreased after the LPF initiation faster in every calculation than the data in spite of larger increase in the calculated core flow rates than the data. These were caused by the incorrect calculations of the vaporization model and the interphase drag. Large oscillations were observed in the core flow after the LPF in every calculation, which were synchronized with the

oscillations in the break flows and the pressure.

Figure 4.46 shows the comparison of the total core inlet flow rates through the SEO. In case A the calculated flow rate was much larger than the data, because the circulation pump assumed in the JP suction pushed water intensely into the lower plenum through the JP. The flow rates calculated in cases B, C and D with the same MRP and JP models were almost the same each other before the LPF initiation independent from the assumed break forms, but were by a factor of two larger than the data. In case E the flow rate agreed very well with the data until the LPF initiation because of the small moment of inertia of the MRP.

Figures 4.47 through 4.56 show the liquid and steam velocity through the UTP of the average and peak power channels in every case. Calculated steam velocity presented upward flow even when liquid velocity presented downward flow. After the HPCS actuation at 31.5 s steam velocity increased much in spite of the downward liquid flow presenting the counter current flow limiting (CCFL) which was observed especially in the peak power channel.

4.3.5 Liquid Levels in the Pressure Vessel

Figures 4.57 and 4.58 show the estimated mixture levels in the pressure vessel (PV). These mixture levels were assumed from the void fraction in the volume as mentioned in Sec. 4.1. The void fraction in the volumes in case C are shown in Figs. 4.59 through 4.66 as a reference. The initial decrease in the liquid level in the downcomer is compared with the data. In cases A and B the calculated downcomer level decreased to the recirculation line nozzle level 4s and 3s earlier than the data, respectively, because of the large calculated break flows. The circulation pump installed in the JP suction in case A pushed intensely the liquid in the downcomer to the JP after the break resulting in the faster level decrease in case A than in case B. In the other cases the liquid level decrease in the downcomer agreed well with the data.

The liquid level in the peak-power channel in the core was not always higher than that in the average-power channel while always in the data especially after the LPF. The temporary decrease in the liquid level in the peak-power channel was calculated after the LPF initiation in every case. In case A the core flow decreased slower after the break and stayed higher than that in the other cases and the data, therefore, the liquid level in the upper plenum stayed higher. But after the JP suction uncovering the JP discharge flow was quickly reversed in case A as shown in Fig. 4.22, while the flow through the UTP stayed upward resulting in that more of core was uncovered than in case B before the LPF initiation.

The large core uncovering before the LPF in case E compared with that in case D was the results of the small moment of inertia of the MRP. However, the trend of the large core uncovering only in case E agreed well with the data as shown in Fig. 2.31.

After the LPF initiation the liquid level was not formed in the lower plenum in any case because the vapor generated in the lower plenum was too small to form the liquid level. In case C the beginning of the core uncovering after the LPF was delayed more than 20 s compared with the data. Whole core was uncovered at 80s, and then the top-down reflooding occurred in the peak-power channel in case C. After LPCI actuation at 90.9s the injected liquid in the core bypass flowed into the lower core through the leak hole, while the lower plenum liquid level began to decrease. The core was almost reflooded at the LPCI initiation of 90.0 s by HPCS and the LPCS water in the data, whereas in case C the CCFL at the UTP prevented the spray water from flowing down into the core and bypass from the upper plenum and the core reflooding was much later than the data.

4.3.6 Fuel Rod Surface Temperature

Calculated fuel surface temperatures are compared with the data in Figs. 4.67 through 4.70. Figures 4.69 and 4.70 compares the data with the calculated results in case C. The behavior of the heater rod surface

temperatures was closely related to that of the liquid levels in the core. In the RELAP5 calculation dryout of the fuel rod surface is judged to occur when the void fraction in the adjacent volume to the heat slab is greater than 0.96. Figures 4.71 through 4.90 show the critical heat flux (CHF) and the heat transfer rate compared with the criteria of the void fraction 0.96. The criteria indicate 0.1 when the void fraction increases above 0.96, otherwise indicate 1.0. The boiling transition occurred in cases A, C, D and E during the low core flow period after break before the LPF initiation in the upper part of the peak-power channel and the temperature behavior agreed well with the data except for those in case E. In case E the surface temperature above position 4 rose after the boiling transition about 100 K higher than the measured temperature. The LPF terminated the temperature rise but the quench occurred much later.

The dryout after the LPF mitigation was calculated only in case C but was later than the data because the liquid level decrease and the initiation of dryout were calculated to occur comparatively late. However, the calculated temperature behavior agreed well with the data in Pos. 1 through Pos. 3. The top-down quench was calculated in the peak-power channel in case C.

4.4 Conclusions for the RELAP5/MOD1/001 Calculations

The post test calculations of the ROSA-III large break test, RUN 901, were performed with the RELAP5/MOD1/001 code and the following conclusions have been derived.

(1) The pressure calculated by RELAP5 agreed well with the data when the break area was multiplied by a factor of 0.6. With the RELAP5 characteristic analysis model without any adjustment the rate of system pressure decrease was overpredicted because the break flow rate was calculated to be much larger than the data. The liquid break flow before the recirculation line uncover was calculated well with the break nozzles simulated by the RELAP5 single volume and single valve. However, the steam

break flow rate and the rate of decrease in the system pressure were still larger than the data after the recirculation line uncovering.

(2) The RELAP5 code calculates the liquid and the steam flow rates of the two-phase flow through the junctions rigorously by an advanced two-phase flow model. The top-down quench in the core was calculated because of the counter current flow calculation at the upper tie plate (UTP). However, the ability to calculate the counter current flow at the UTP was still limited so that the spray water was predicted to accumulate in the upper plenum (UP) leading to a delay in reflooding of the core. Therefore, an appropriate counter current flow limiting (CCFL) model is necessary to improve the predictions.

(3) The mixture level behavior which was obtained from the calculated void fractions in volumes agreed well with the data prior to the lower plenum flashing (LPF). However, the drop in the core mixture level after the LPF and the core reflooding were both delayed compared to the data. An improvement in the RELAP5 interphase drag correlations is recommended.

(4) The flow reversal in the jet pump (JP) discharge line in the broken loop was not calculated by the model assuming a circulation pump at the JP suction, and the core inlet flow was predicted to be higher than the data. The JP characteristics calculated by the JETP component model of the TRAC-BD1 code agreed well with the data.

(5) The moment of inertia and the rated liquid density of the main recirculation pump (MRP) are found to be important for accurate calculation of the core inlet flow and the mixture level in the core before the LPF.

Table 4.1 Calculation Condition of RELAP5 Analysis

Case	Jet Pump Type (JP)	Break Form	MRP Data
A	Circulation Pump in JP Suction	Orifices 100% + 100%	
B	JP Model from TRAC-BDI Code	//	
C	//	Orifices 60% + 60%	
D	//	nozzles 100% + 100%	
E	//	//	Correction of Inertia and Rated Density

Table 4.2 Description of Components for RELAP5/MOD1/001

Component Number	Component Type	Number of Volume	Description
010	B		Lower Plenum
011	SV		Lower Plenum Bottom
020	P	2	Lower Plenum
030	B		Channel Inlet Chamber (Ave. Ch.)
031	B		Channel Inlet Chamber (Peak Ch.)
040	P	7	Average Power Channel
045	P	7	Peak Power Channel
050	B		Upper Plenum
051	P	2	Upper Plenum
052	SJ		051 → 060
060	P	4	Separator
070	SV		Upper Downcomer
071	6		Upper Downcomer
072	SJ		070 → 080
080	SV		Steam Dome
090	P	3	Guide Tube
095	SJ		090 → 100
100	P	3	Core Bypass
110	SV		Upper Downcomer
111	B		Upper Downcomer
112	P	3	Middle Downcomer
120	B		Middle Downcomer
130	P	4	Lower Downcomer
131	B		Lower Downcomer
132	SV		Downcomer Bottom
140	P	3	Intact Loop MRP Suction
150	Pu		Intact Loop MRP
160	P	6	Intact Loop MRP Discharge
170	SV		Intact Loop JP Suction
171	Pu*,SV**		Intact Loop JP Suction (Pump)
180	B		Intact Loop JP

Table 4.2 Description of Components for RELAP5/MOD1/001 (Continued)

Component Number	Component Type	Number of Volume	Description
185	P	5*,4**	Intact Loop JP Discharge
190	P	3	Broken Loop MRP Suction
200	P	3	Broken Loop MRP Suction
210	Pu		Broken Loop MRP
220	P	5	Broken Loop MRP Discharge
230	SV		Broken Loop JP Suction
231	Pu*,SV**		Broken Loop Jp Suction (Pump)
240	B		Broken Loop JP
245	P	5*,4**	Broken Loop JP Discharge
250	V		QSV 190→200
260	V		Break B 190→280 (PV Side)
270	V		Break A 270→281 (MRP Side)
280	TDV		Break B Containment (PV Side)
281	TDV		Break A Containment (MRP Side)
290	TDV		Main Steam Reservoir
292	TDV		HPCS Reservoir
300	TDJ		Main Steam 080→290
302	TDJ		HPCS 292→051
310	TDV		Feedwater Reservoir
320	TDJ		Feedwater 310→111
331	TDV		LPCI Reservoir
332	TDV		LPCS Reservoir
401	TDJ		LPCI 331→100
402	TDJ		LPCS 332→051
530**	SJ		230→231
532**	SJ		231→240
533**	SJ		170→171
534**	SJ		171→180
550***	SV		Break Pipe B (PV Side)
551***	SV		Break Pipe A (MRP Side)
555***	V		550→560

Table 4.2 Description of Components for RELAP5/MOD1/001 (Continued)

Component Number	Component Type	Number of Volume	Description
556***	V		551→561
560***	SV		Break Nozzle B (PV Side)
561***	SV		Break Nozzle A (MRP Side)
565***	V		560→280
566***	V		561→281
900	TDV		Heat Sink
910	V		080→900

* Case A


** Case B, C, D and E

*** Case E

Table 4.3 Description of RELAP5 Components (Heat Structure)

STRUCTURE NUMBER	SIDE	BDRY.VOL. NUMBER	HEAT TRF. SURF.AREA (M2)	
10001	LEFT	0	0.0	Average Power Channel Heater Rods Position 7 ↓ Position 6 Position 5 Position 4 Position 3 Position 2 Position 1
	RIGHT	40010000	1.6849	
10002	LEFT	0	0.0	
	RIGHT	40020000	1.6849	
10003	LEFT	0	0.0	
	RIGHT	40030000	1.6849	
10004	LEFT	0	0.0	
	RIGHT	40040000	3.3698	
10005	LEFT	0	0.0	
	RIGHT	40050000	1.6849	
10006	LEFT	0	0.0	
	RIGHT	40060000	1.6849	
10007	LEFT	0	0.0	
	RIGHT	40070000	1.6849	
20001	LEFT	0	0.0	Peak Power Channel Heater Rods Position 7 ↓ Position 6 Position 5 Position 4 Position 3 Position 2 Position 1
	RIGHT	45010000	0.56160	
20002	LEFT	0	0.0	
	RIGHT	45020000	0.56160	
20003	LEFT	0	0.0	
	RIGHT	45030000	0.56160	
20004	LEFT	0	0.0	
	RIGHT	45040000	1.1233	
20005	LEFT	0	0.0	
	RIGHT	45050000	0.56160	
20006	LEFT	0	0.0	
	RIGHT	45060000	0.56160	
20007	LEFT	0	0.0	
	RIGHT	45070000	0.56160	
1000001	LEFT	80010000	0.51530	Vessel Wall ↓
	RIGHT	900010000	0.51530	
1100001	LEFT	80010000	0.76529	
	RIGHT	900010000	0.88555	
1100002	LEFT	70010000	0.61949	
	RIGHT	900010000	0.71684	
1100003	LEFT	71010000	1.2102	
	RIGHT	900010000	1.4003	
1200001	LEFT	110010000	0.44692	
	RIGHT	900010000	0.51396	
1300001	LEFT	111010000	0.61827	
	RIGHT	900010000	0.70070	
1300002	LEFT	112030000	0.65973	
	RIGHT	900010000	0.74770	
1300003	LEFT	112020000	0.67104	
	RIGHT	900010000	0.76052	
1300004	LEFT	112010000	0.35626	
	RIGHT	900010000	0.40376	
1400001	LEFT	120010000	0.83620	
	RIGHT	900010000	0.97217	

Table 4.3 (Continued)

STRUCTURE NUMBER	SIDE	BDRY.VOL. NUMBER	HEAT TRF. SURF.AREA (M2)	
1400002	LEFT	130040000	0.56417	Vessel Wall 
	RIGHT	900010000	0.65590	
1400003	LEFT	130030000	0.56417	
	RIGHT	900010000	0.65590	
1400004	LEFT	130020000	0.56417	
	RIGHT	900010000	0.65590	
1400005	LEFT	130010000	0.56417	
	RIGHT	900010000	0.65590	
1400006	LEFT	131010000	0.64300	
	RIGHT	900010000	0.74755	
1400007	LEFT	132010000	0.68627	
	RIGHT	900010000	0.79786	
1500001	LEFT	10010000	0.26389	
	RIGHT	900010000	0.38076	
1500002	LEFT	11010000	0.29688	
	RIGHT	900010000	0.42836	
1600001	LEFT	900010000	0.80100	
	RIGHT	11010000	0.80100	

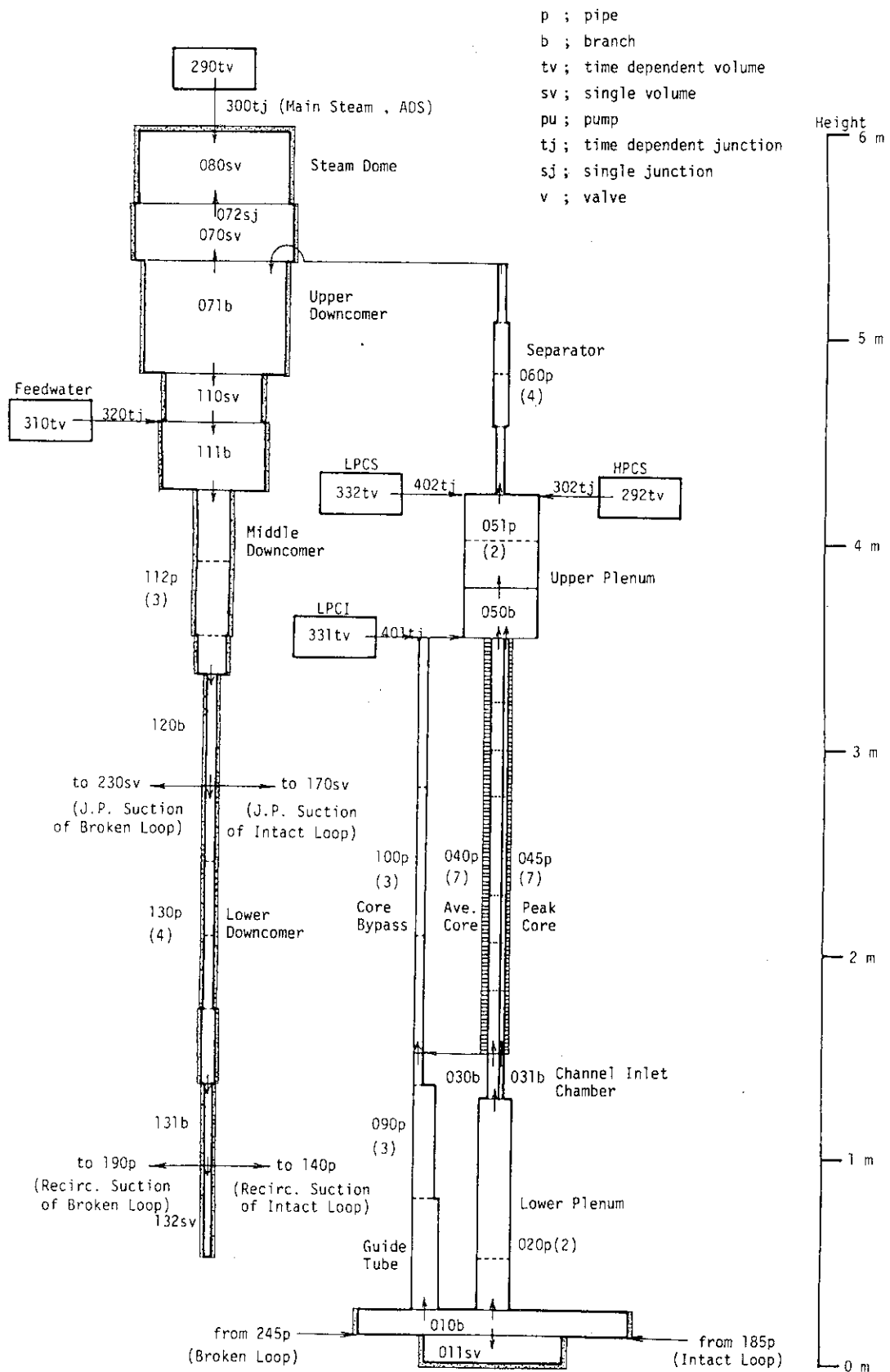


Fig. 4. 1 Nodalization Diagrams of ROSA-III Pressure Vessel for RELAP5/MOD1/001 Model

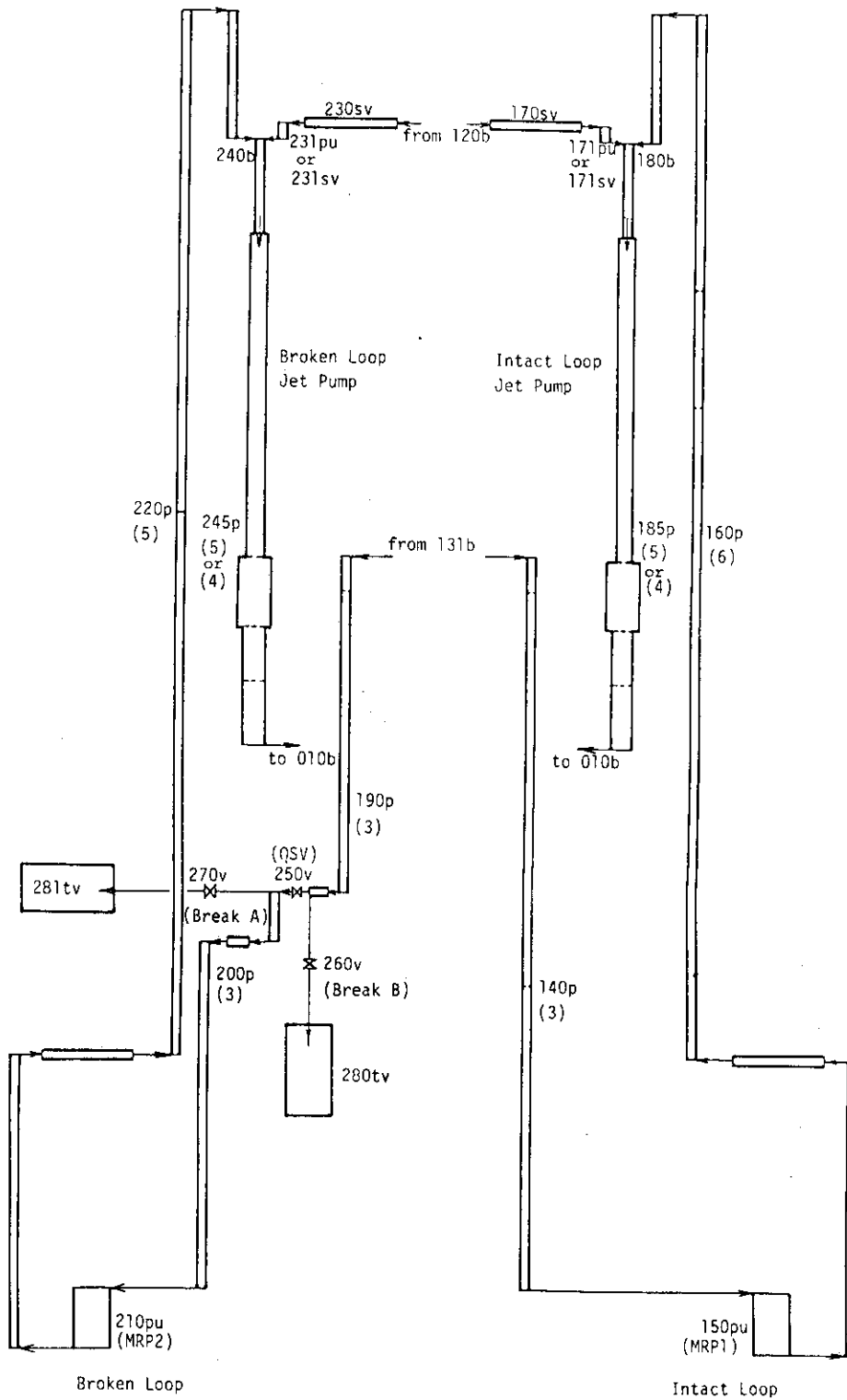


Fig. 4. 2 Nodalization Diagrams of ROSA-III Recirculation Loop

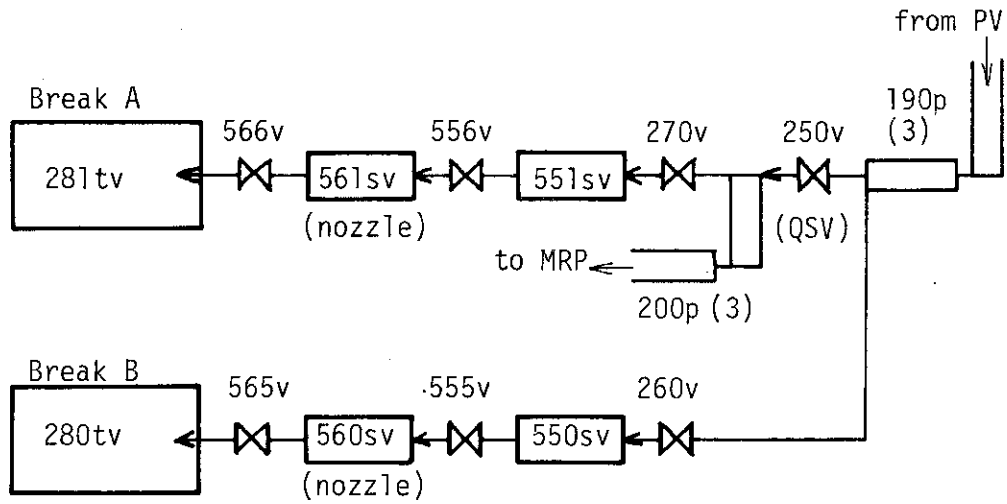


Fig. 4. 3 Nodalization Diagrams of Simulated Break Nozzles in Cases D and E

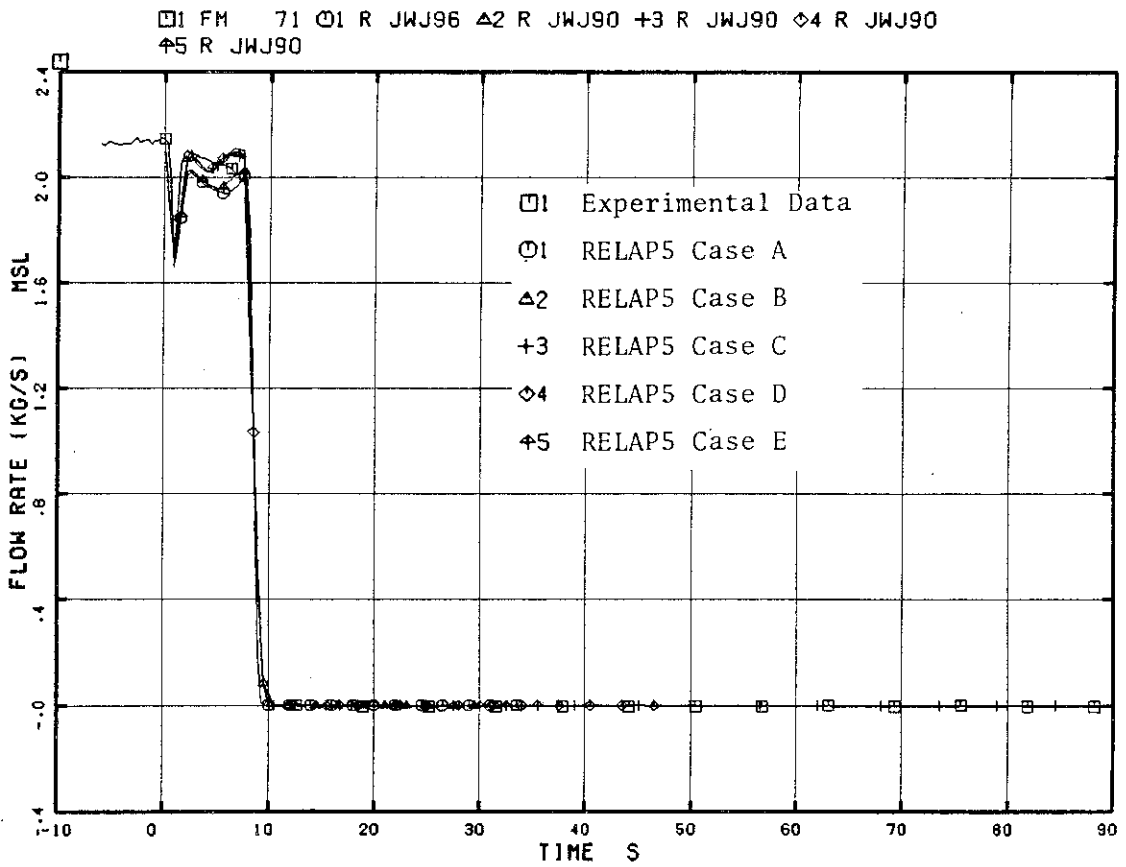


Fig. 4. 4 Main Steam Discharge Flow Rate

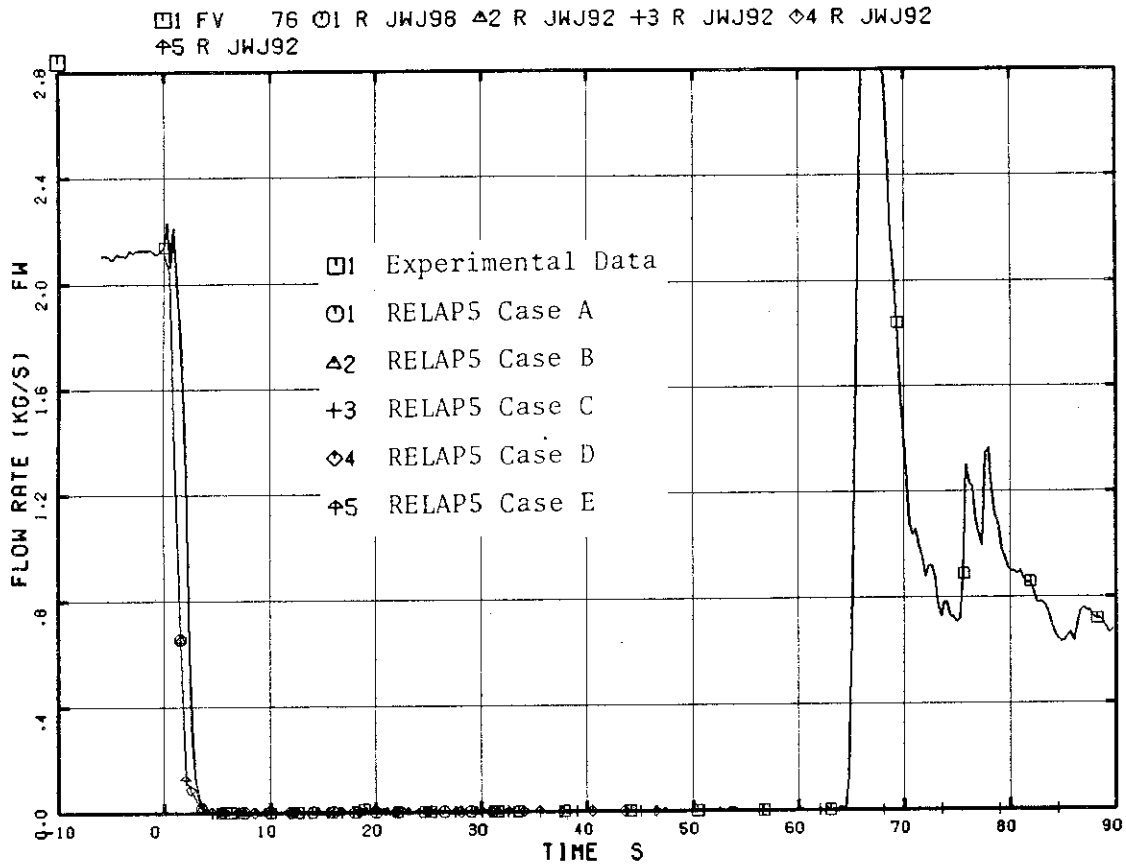


Fig. 4. 5 Feedwater Flow Rate

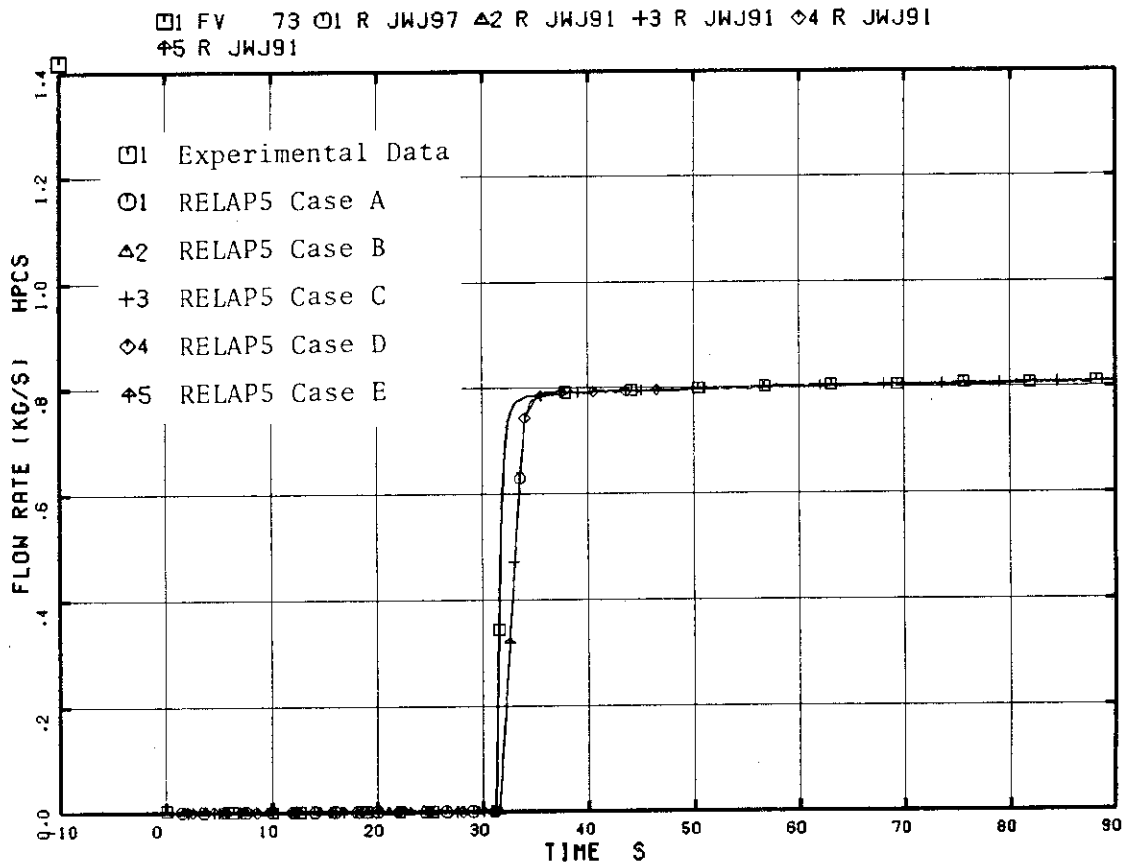


Fig. 4. 6 HPCS Flow Rate

□1 FV 75 ○1 FV 74 ▲3 R JWJ93 +3 R JWJ94

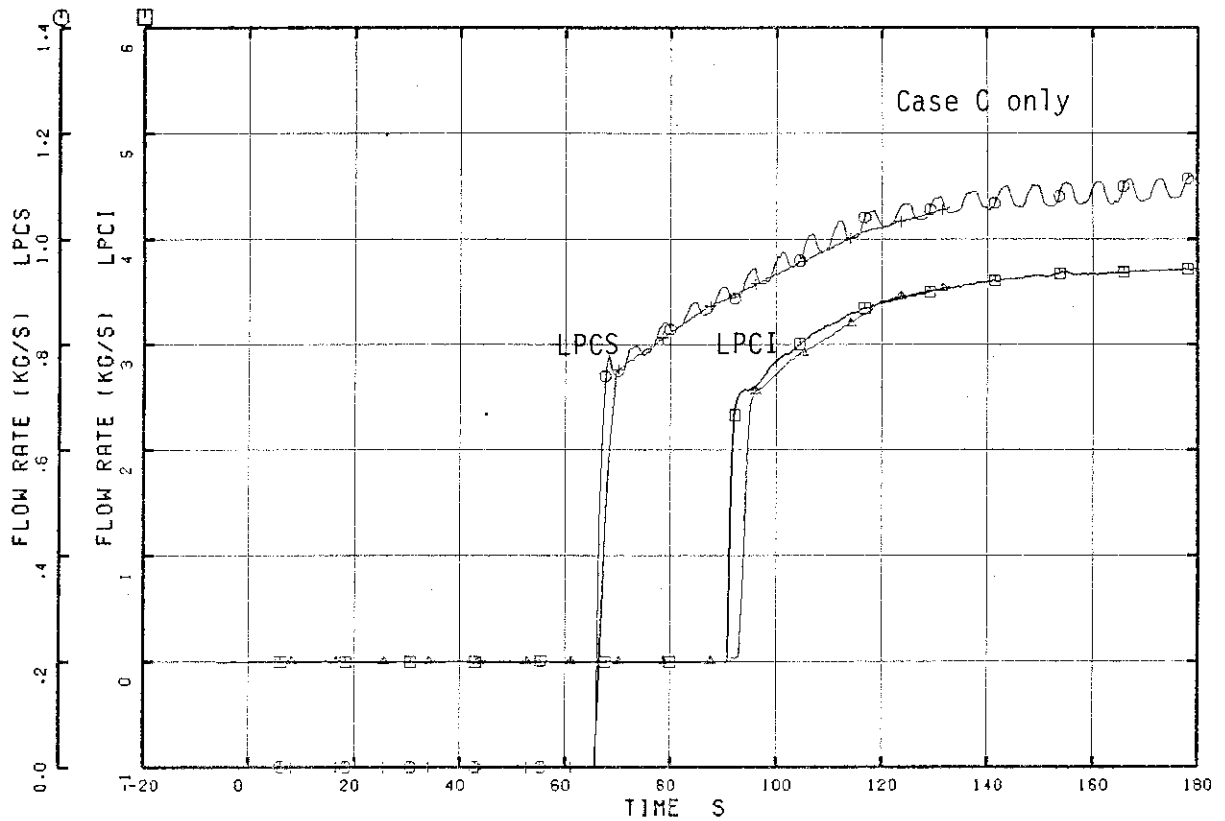


Fig. 4. 7 LPCS and LPCI Flow Rates (Case C)

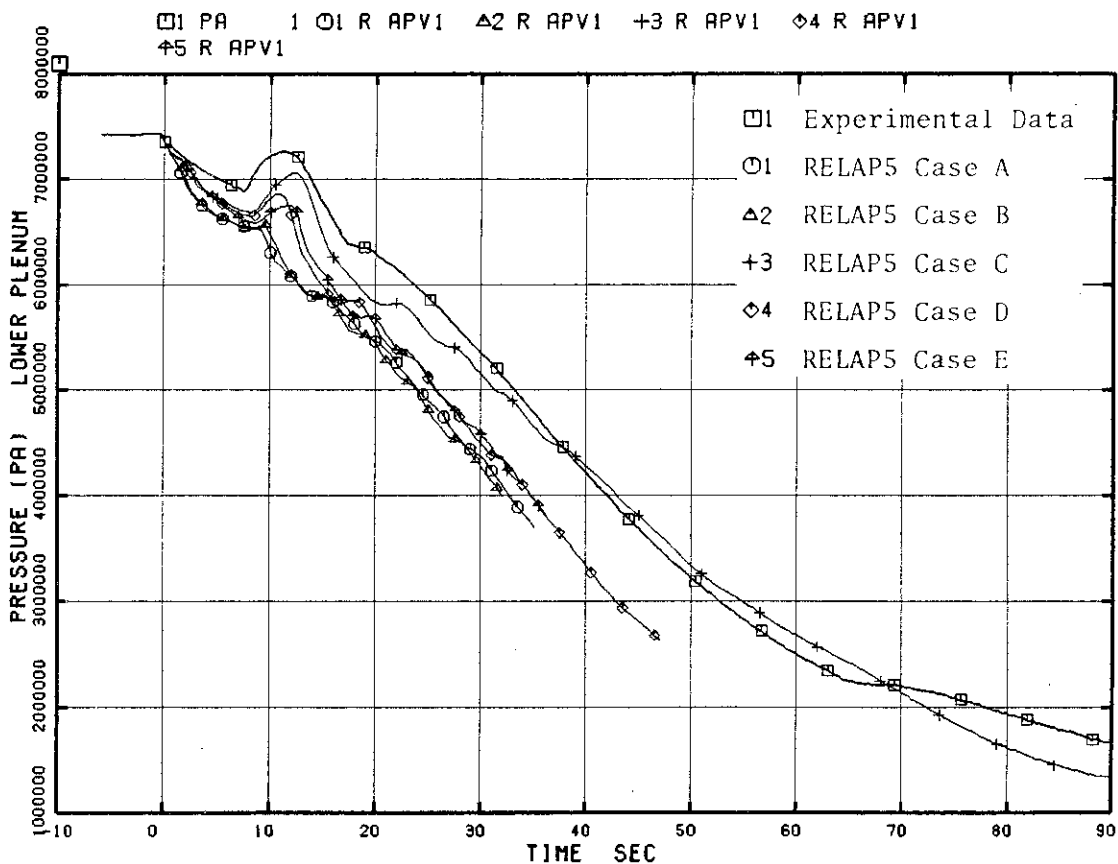


Fig. 4. 8 Lower Plenum Pressure

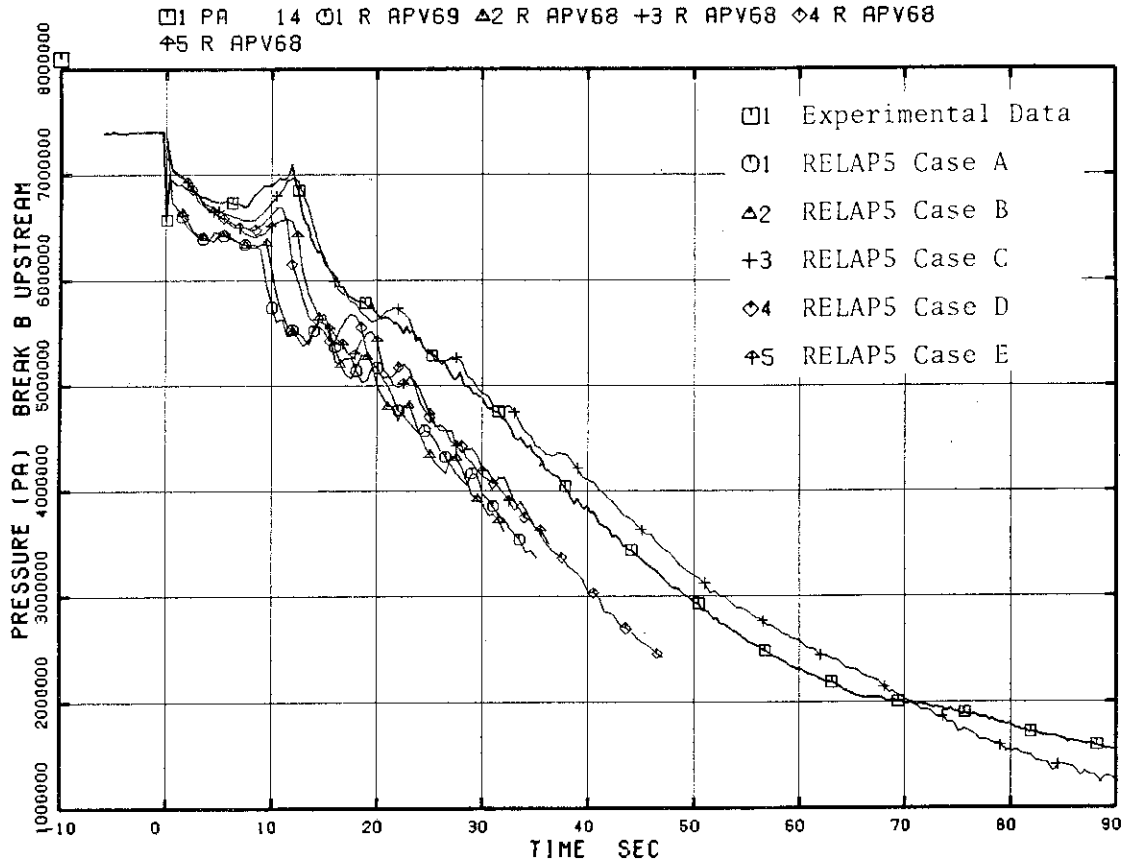


Fig. 4. 9 Pressure at Break B Upstream

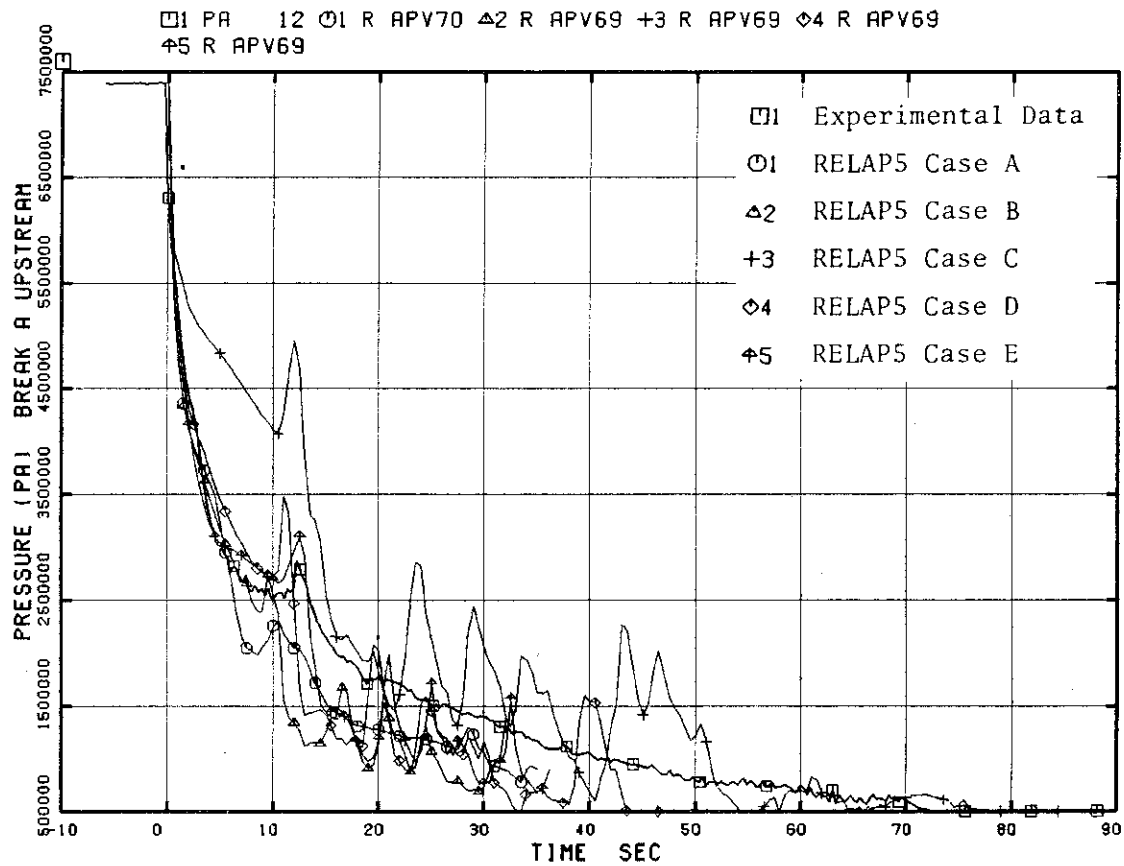


Fig. 4.10 Pressure at Break A Upstream

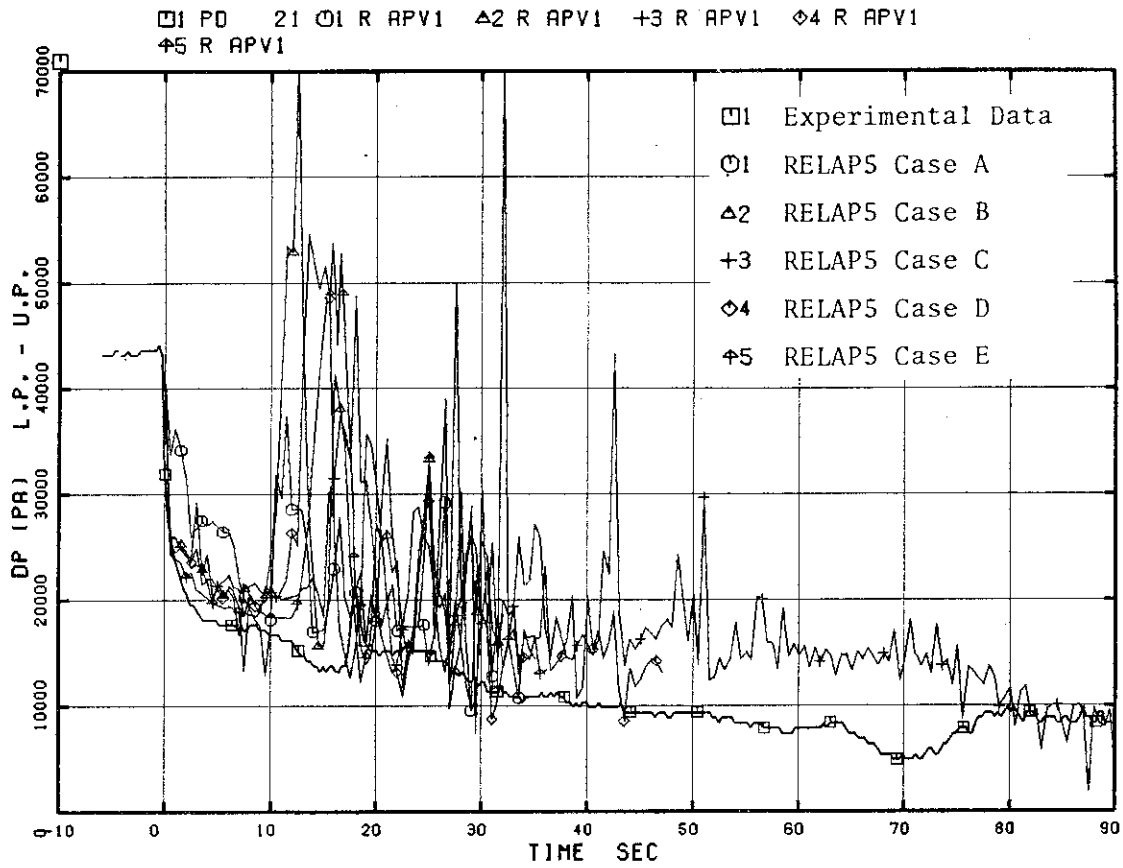


Fig. 4.11 Differential Pressure between Lower and Upper Plena

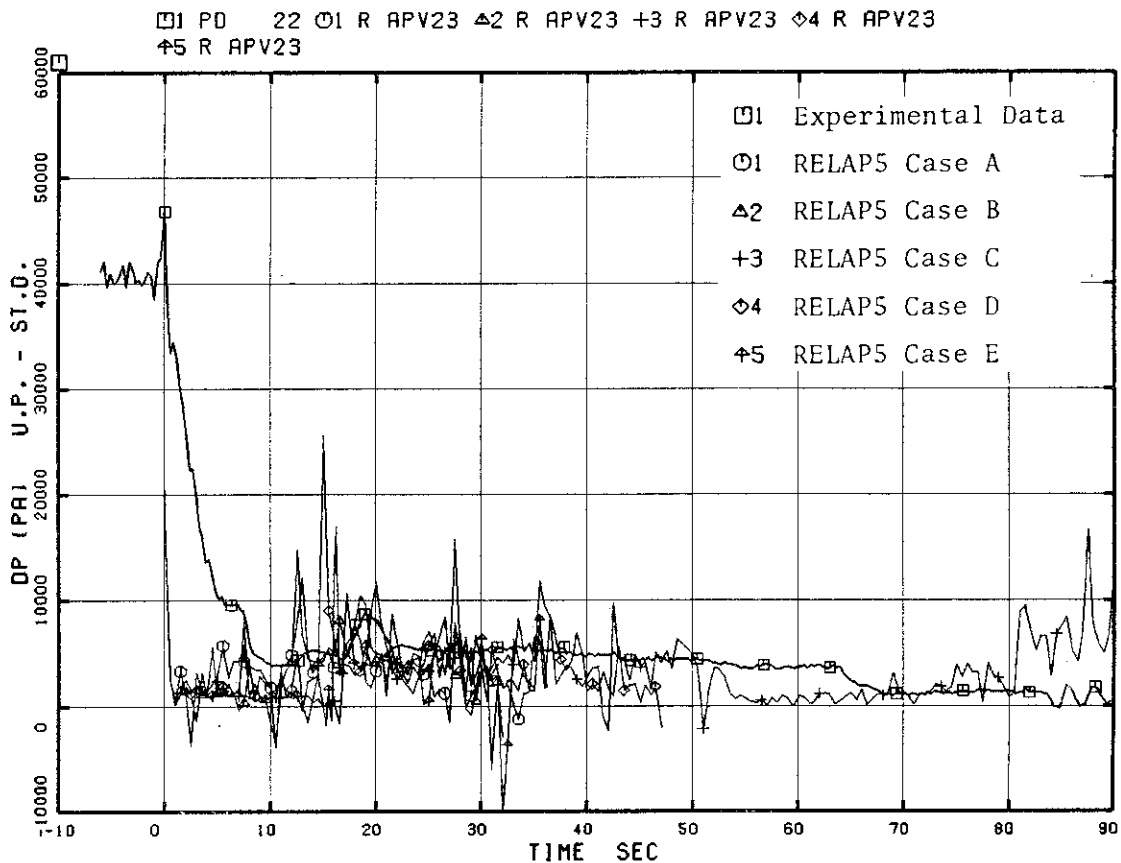


Fig. 4.12 Differential Pressure between Upper Plenum and Steam Dome

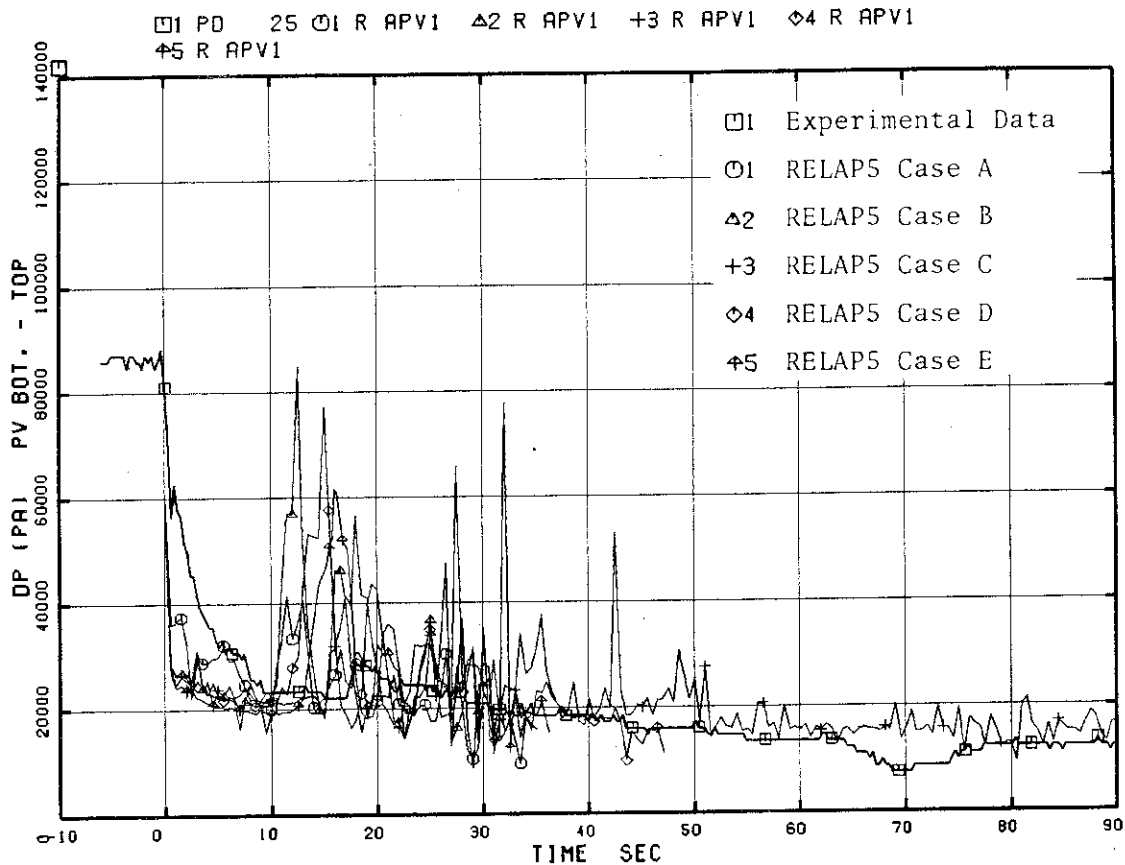


Fig. 4.13 Differential Pressure between Lower Plenum and Steam Dome

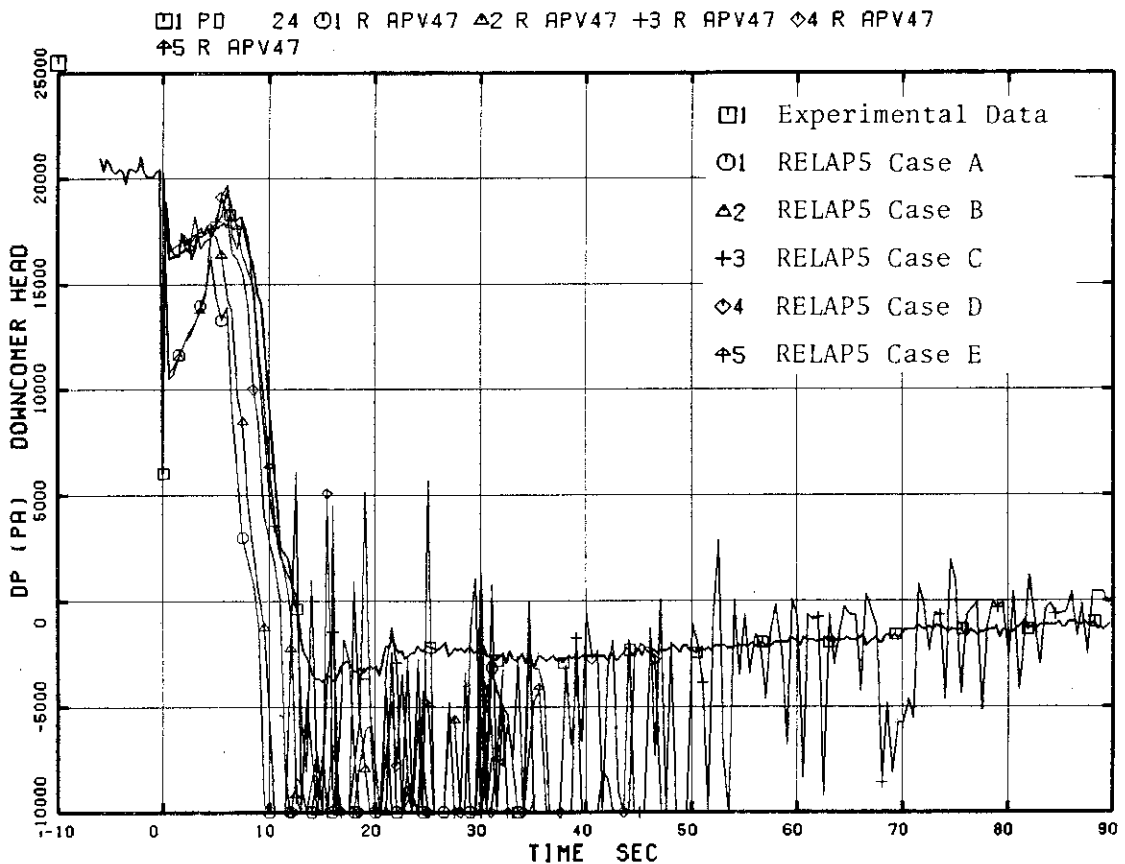


Fig. 4.14 Lower Downcomer Head

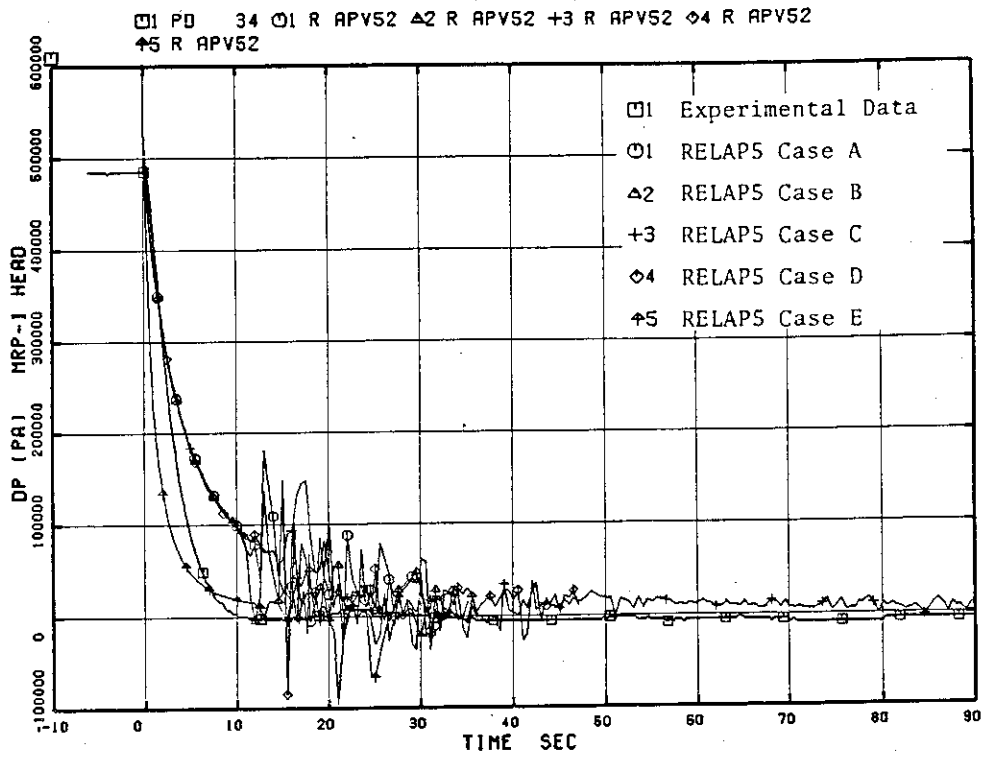


Fig. 4.15 Differential Pressure between MRP1 Delivery and Suction in Intact Loop

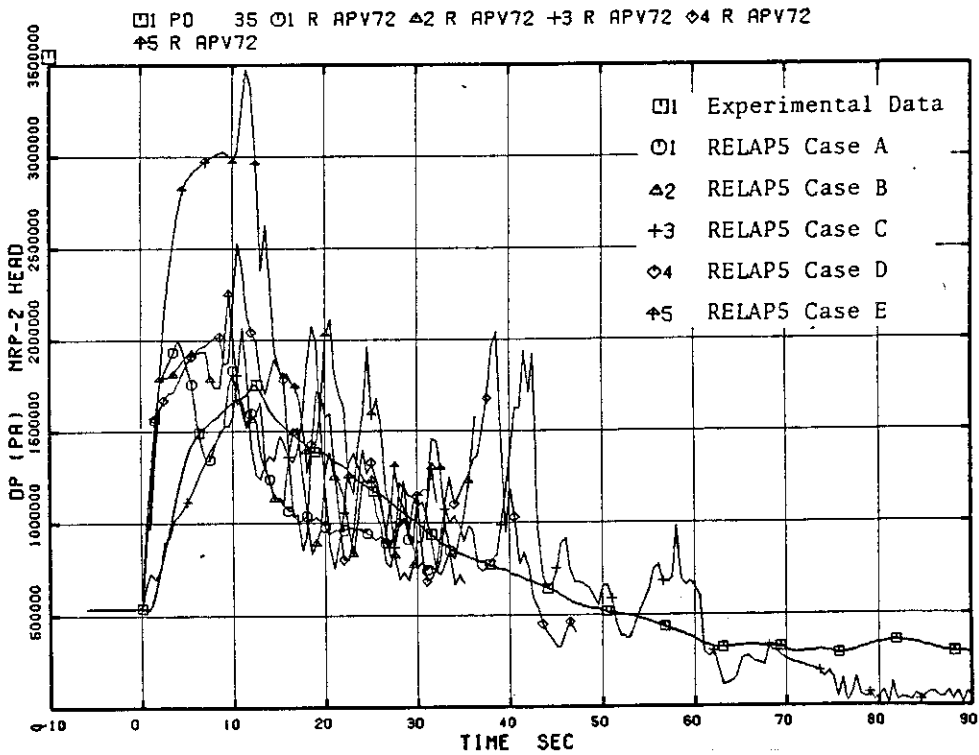


Fig. 4.16 Differential Pressure between MRP2 Delivery and Suction in Broken Loop

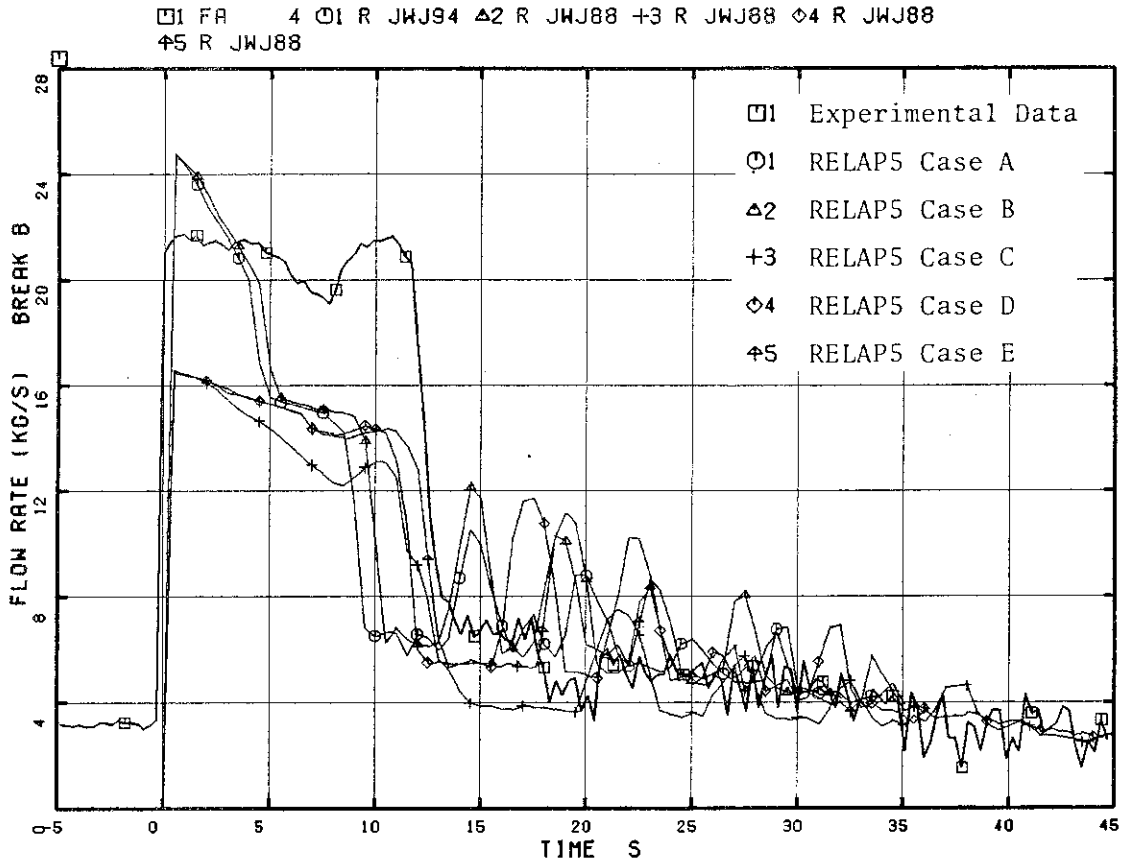


Fig. 4.17 Break Flow from Break B (PV side)

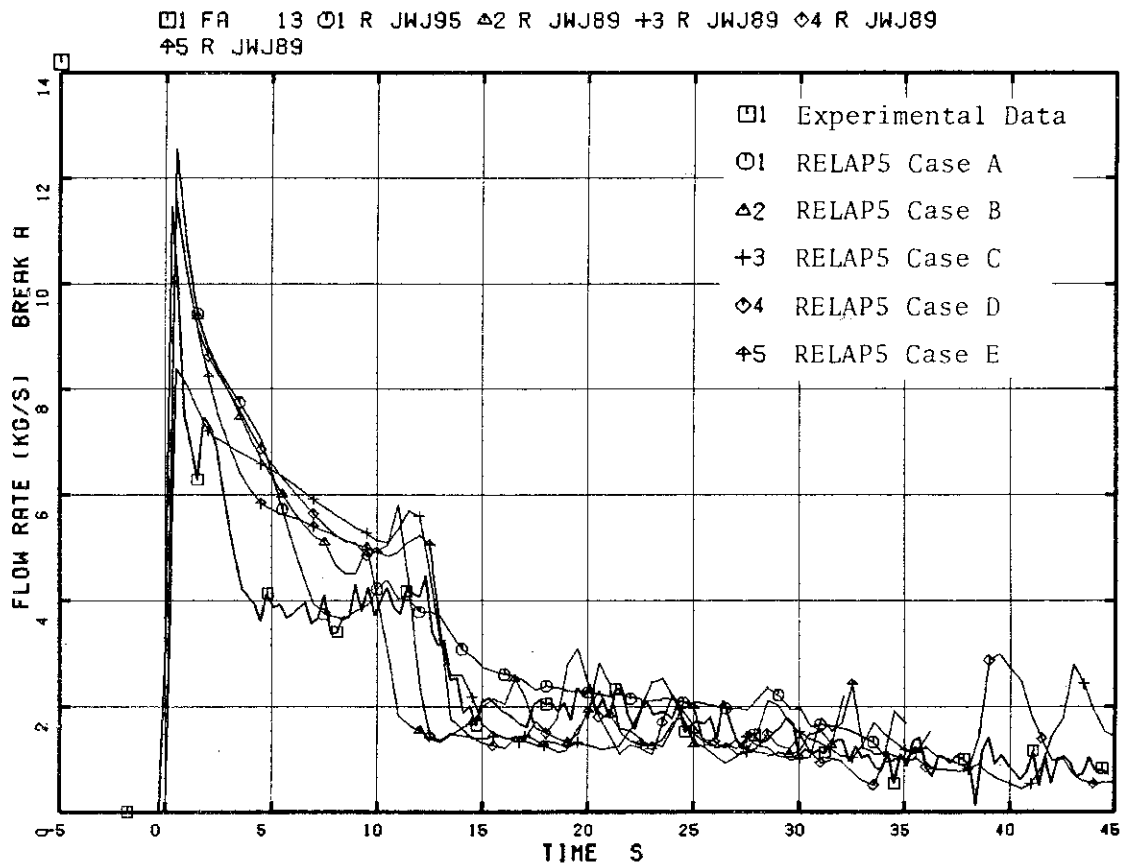


Fig. 4.18 Break Flow from Break A (MRP side)

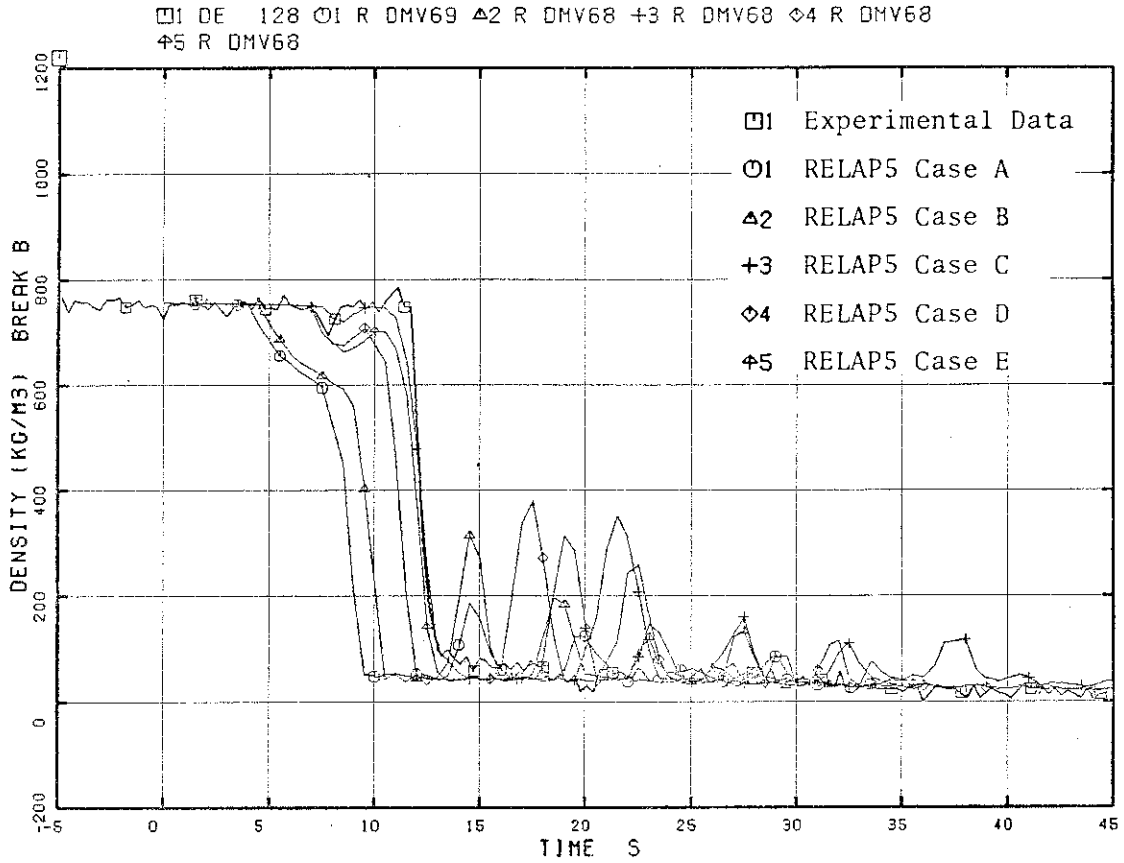


Fig. 4.19 Average Fluid Densities at Break B Upstream

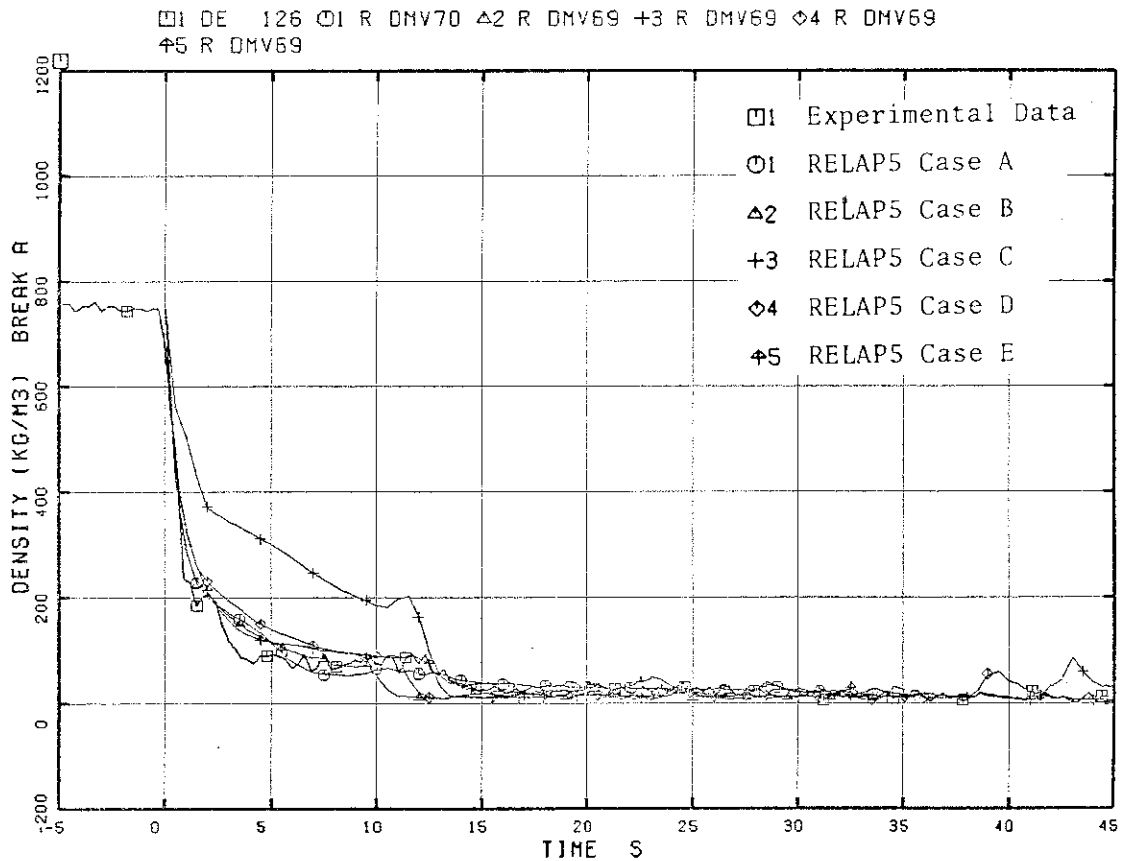


Fig. 4.20 Average Fluid Densities at Break A Upstream

□ I R JWJ68 ○ I R JWJ69 ▲ I R JWJ70

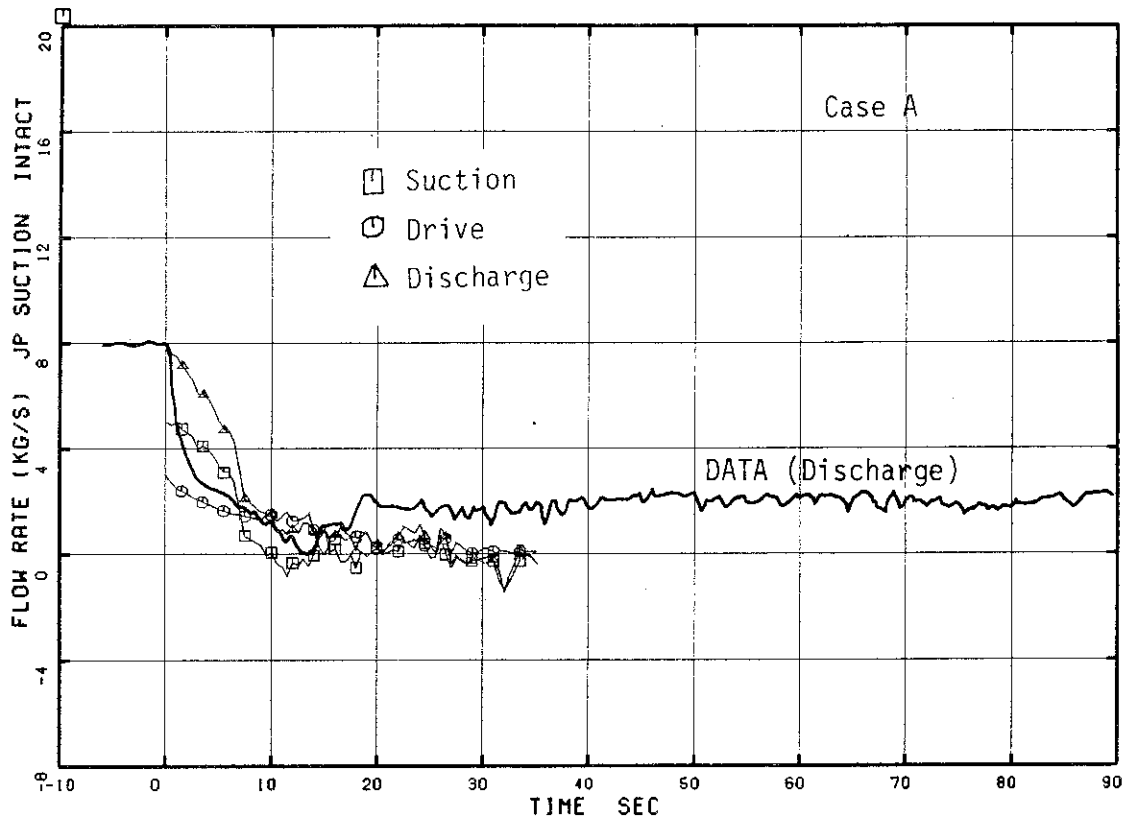


Fig. 4.21 Jet Pump Flow (Intact Loop ; Case A)

□ I R JWJ86 ○ I R JWJ87 ▲ I R JWJ88

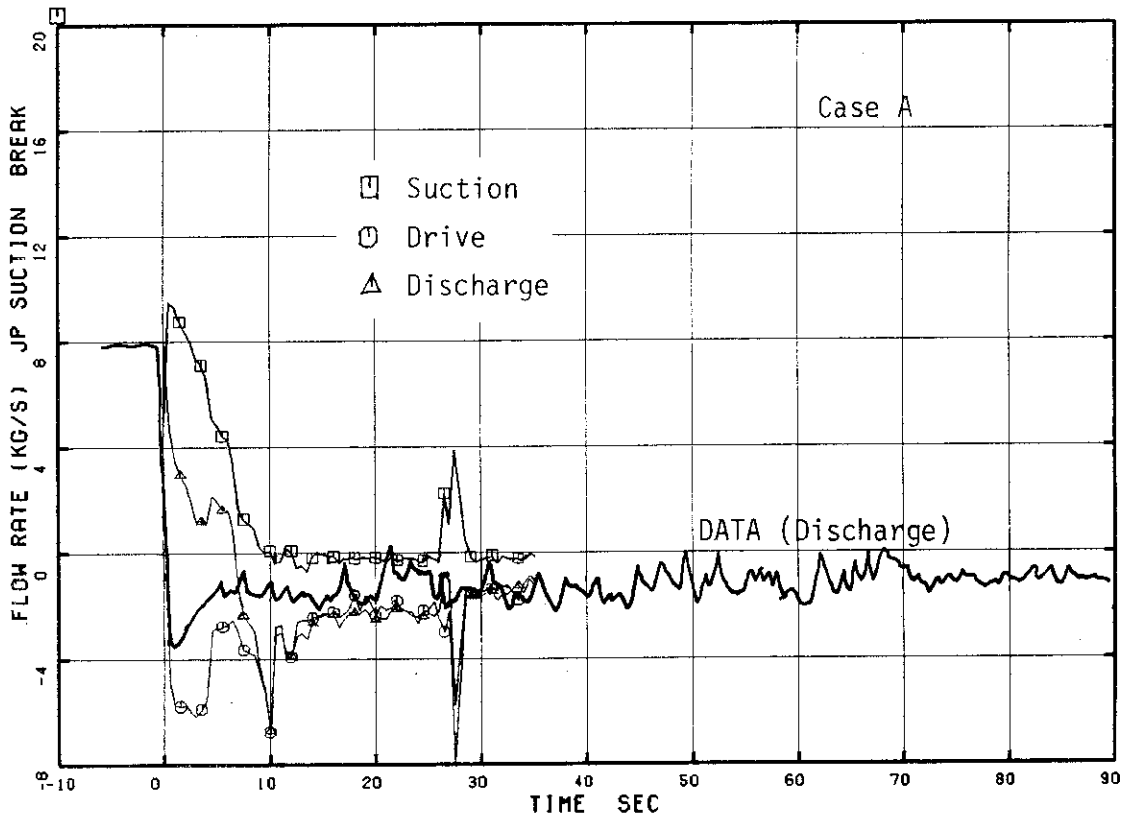


Fig. 4.22 Jet Pump Flow (Broken Loop ; Case A)

□ R JWJ98 ○ R JWJ67 ▲ R JWJ68

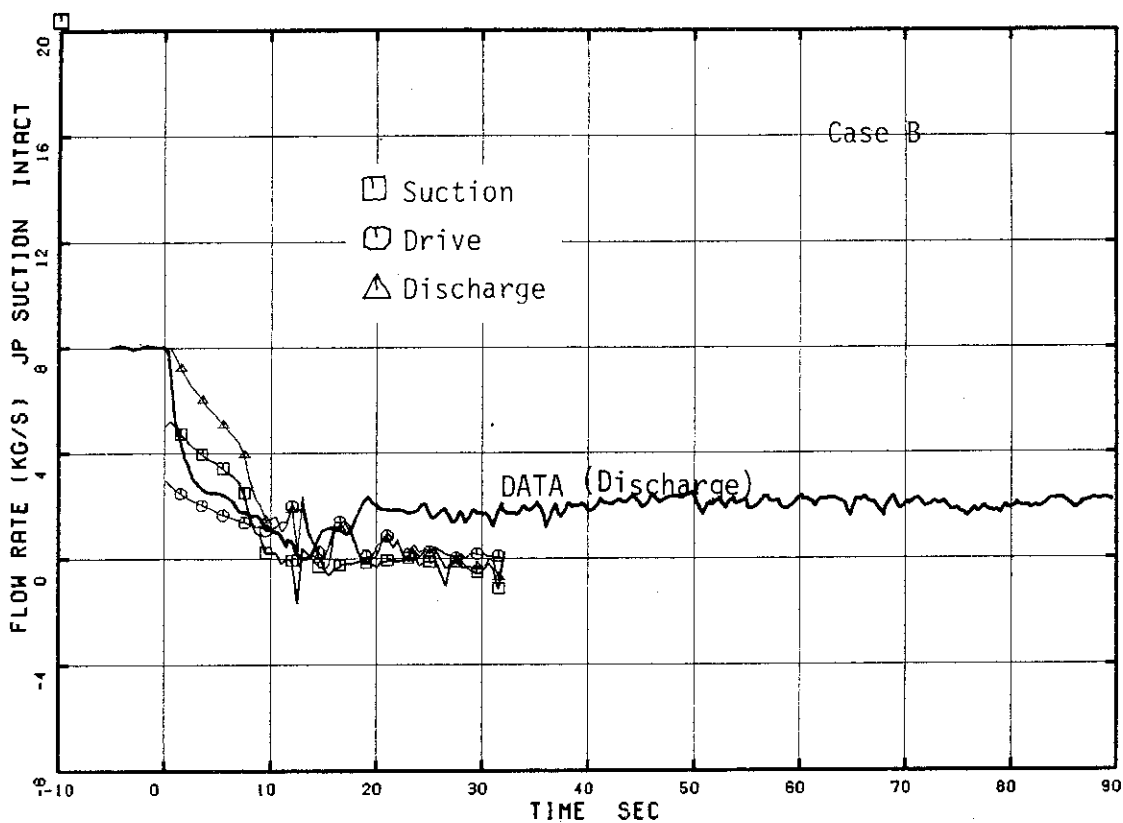


Fig. 4.23 Jet Pump Flow (Intact Loop ; Case B)

□ R JWJ96 ○ R JWJ82 ▲ R JWJ83

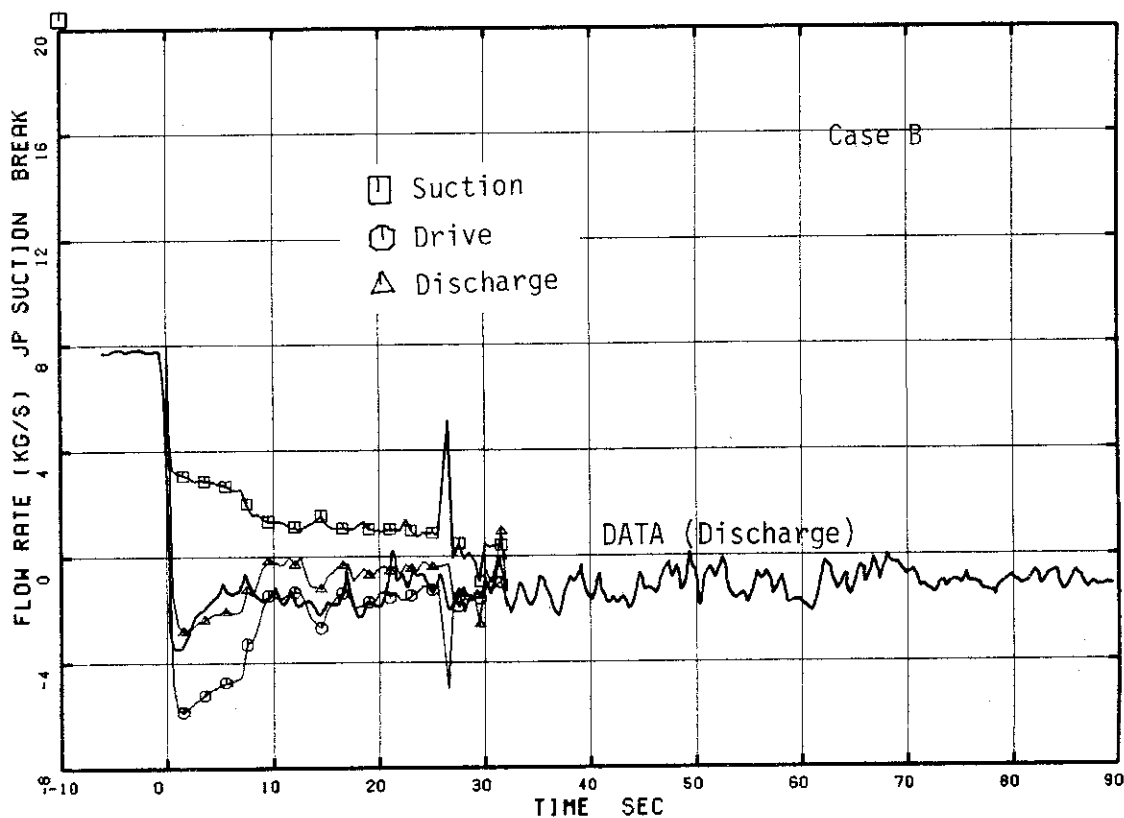


Fig. 4.24 Jet Pump Flow (Broken Loop ; Case B)

□ R JWJ98 ○ R JWJ67 ▲ R JWJ68

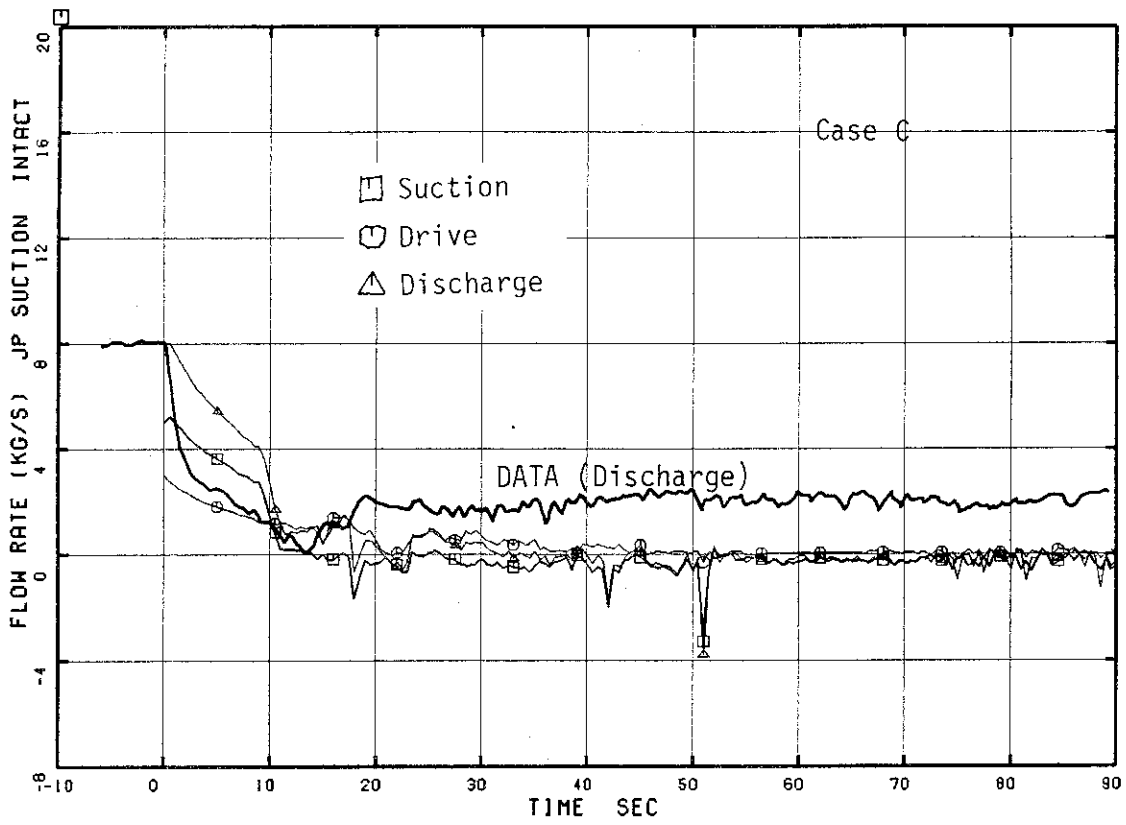


Fig. 4.25 Jet Pump Flow (Intact Loop ; Case C)

□ R JWJ96 ○ R JWJ82 ▲ R JWJ83

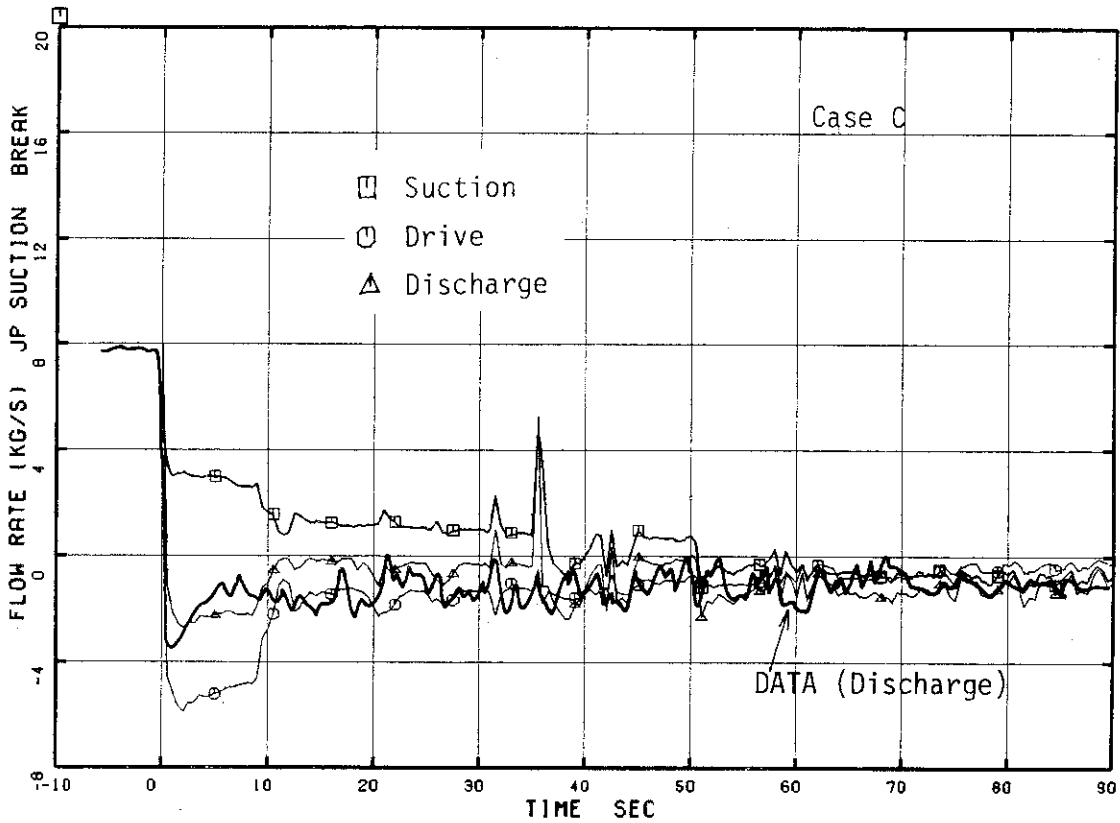


Fig. 4.26 Jet Pump Flow (Broken Loop ; Case C)

□ 4 R JWJ98 ○ 4 R JWJ67 ▲ 4 R JWJ68

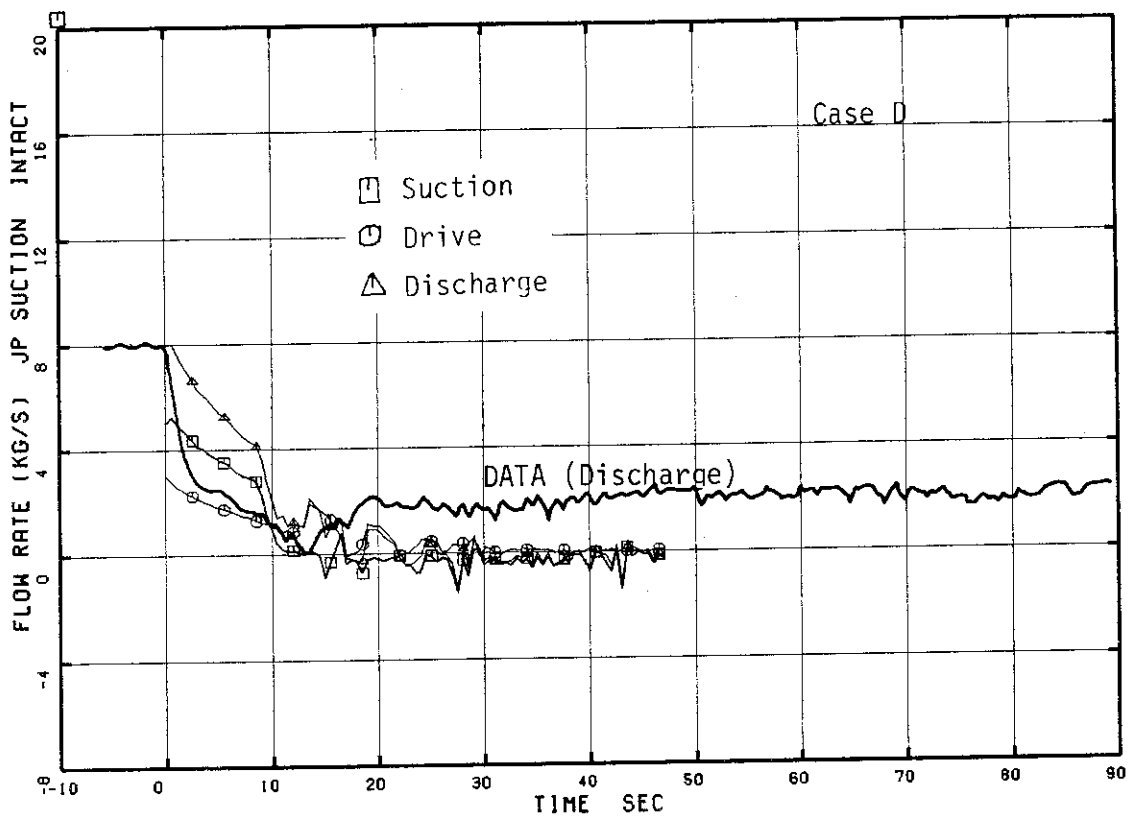


Fig. 4.27 Jet Pump Flow (Intace Loop ; Case D)

□ 4 R JWJ96 ○ 4 R JWJ82 ▲ 4 R JWJ83

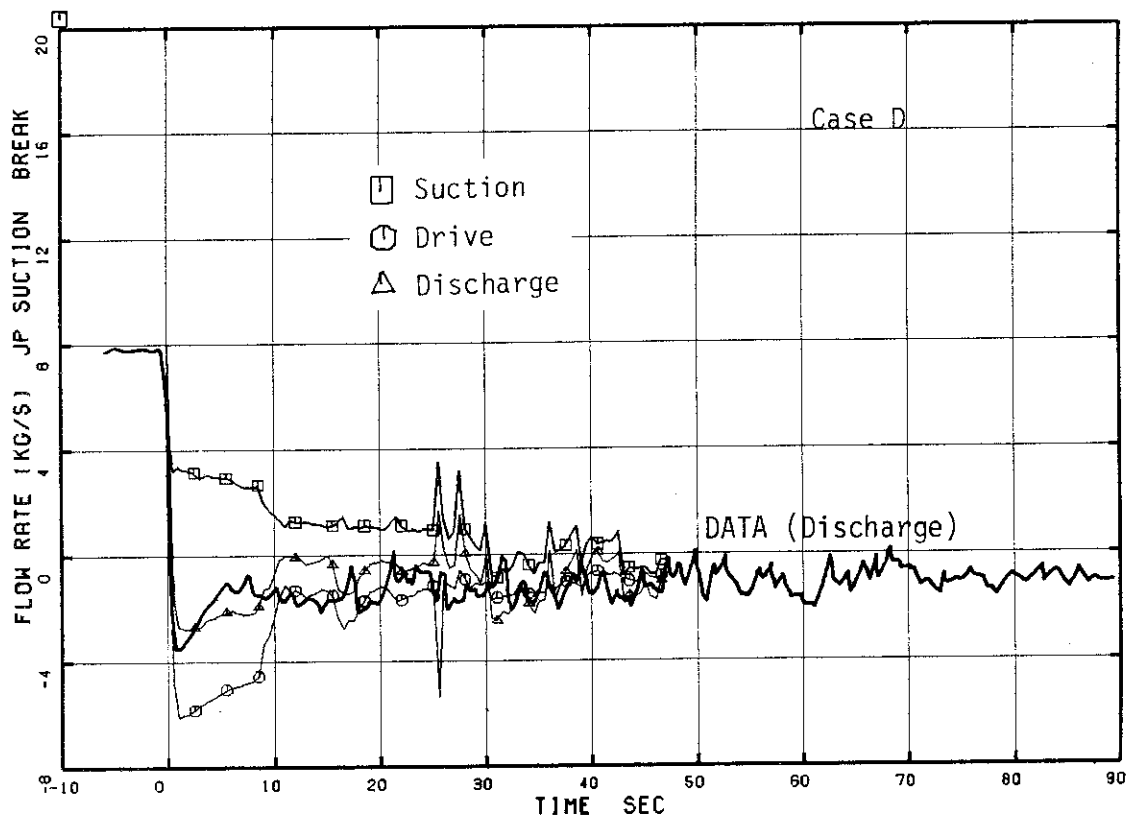


Fig. 4.28 Jet Pump Flow (Broken Loop ; Case D)

□ R JWJ98 ○ R JWJ67 △ R JWJ68

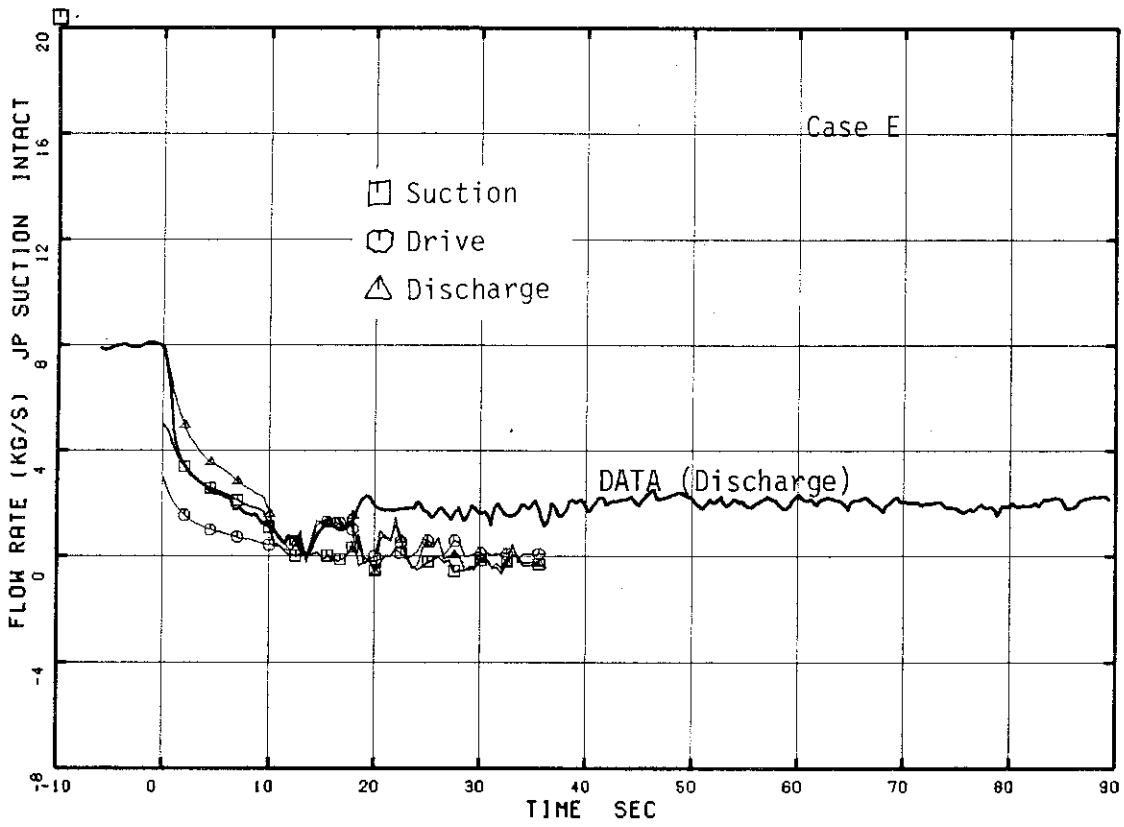


Fig. 4.29 Jet Pump Flow (Intact Loop ; Case E)

□ R JWJ96 ○ R JWJ82 △ R JWJ83

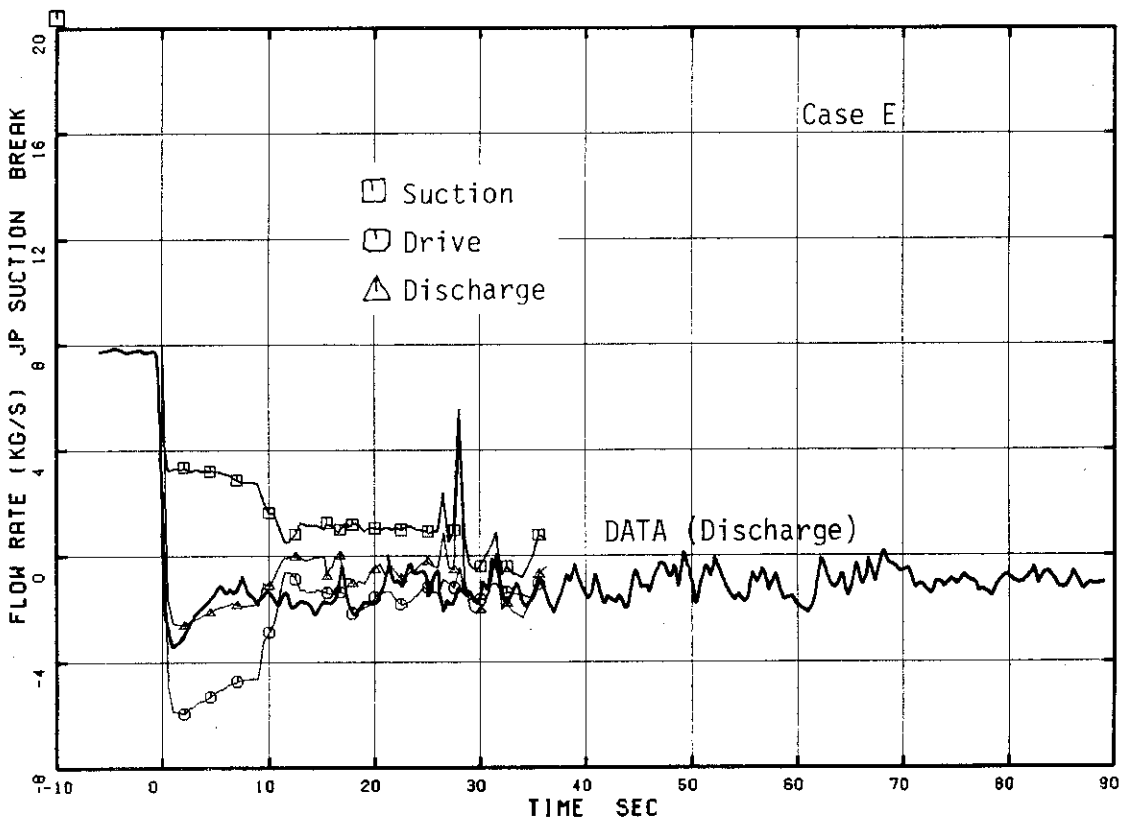


Fig. 4.30 Jet Pump Flow (Broken Loop ; Case E)

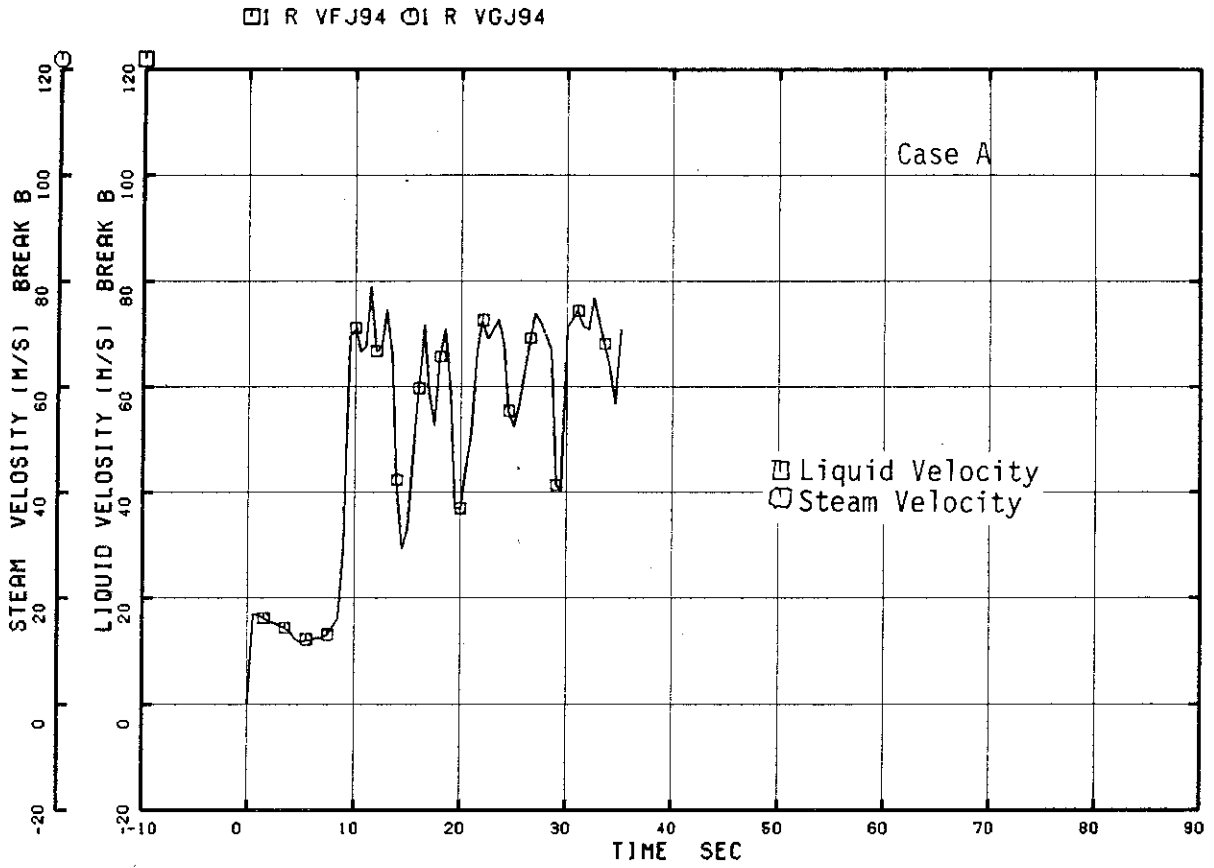


Fig. 4.31 Liquid and Steam Velocities through Break B (Case A)

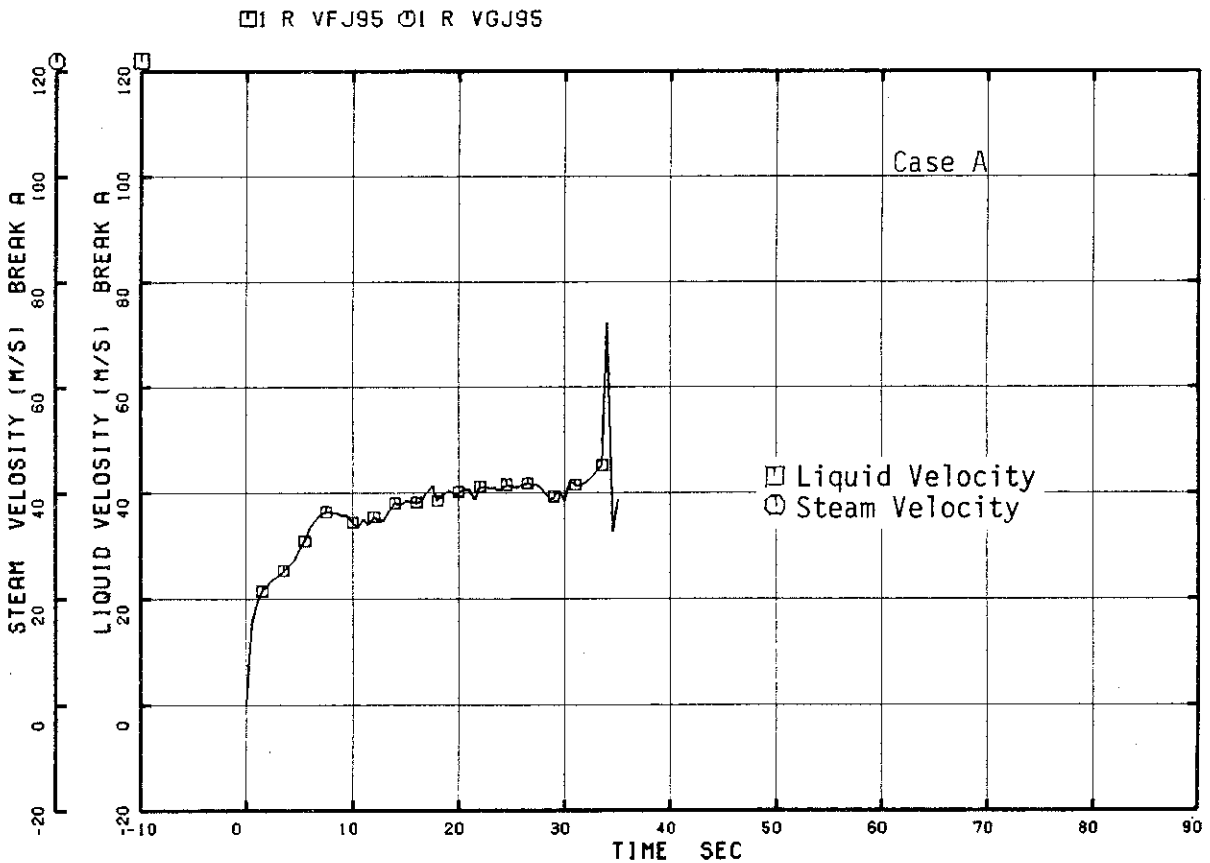


Fig. 4.32 Liquid and Steam Velocities through Break A (Case A)

□ R VFJ88 ○ R VGJ88

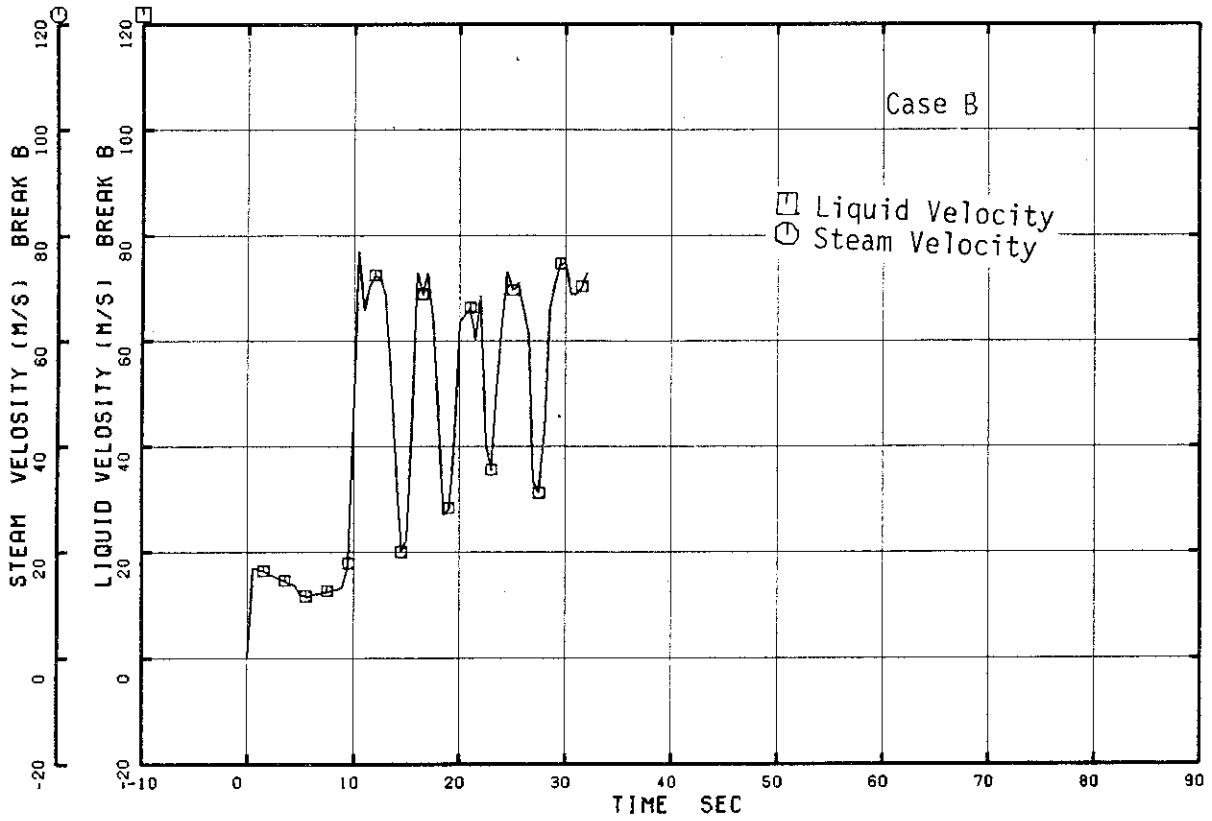


Fig. 4.33 Liquid and Steam Velocities through Break B (Case B)

□ R VFJ89 ○ R VGJ89

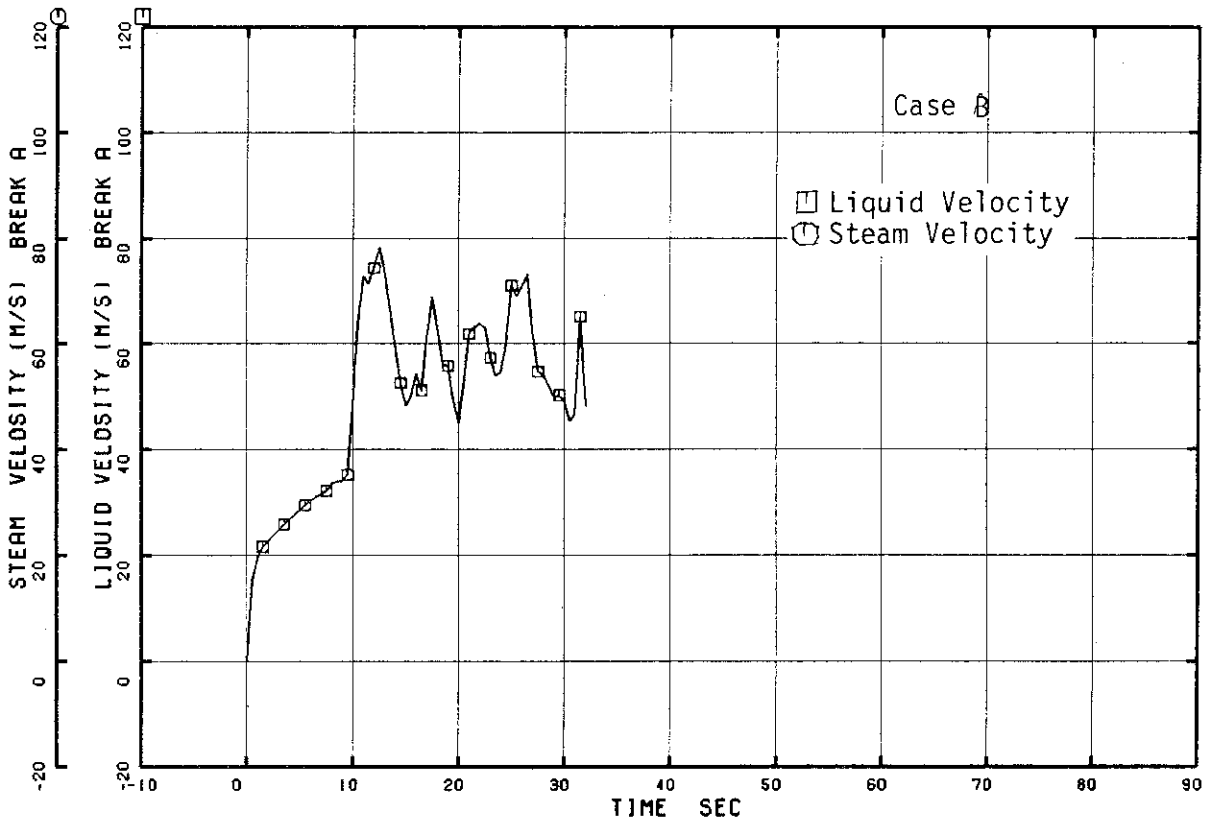


Fig. 4.34 Liquid and Steam Velocities through Break A (Case B)

□ R VFJ88 ○ R VGJ88

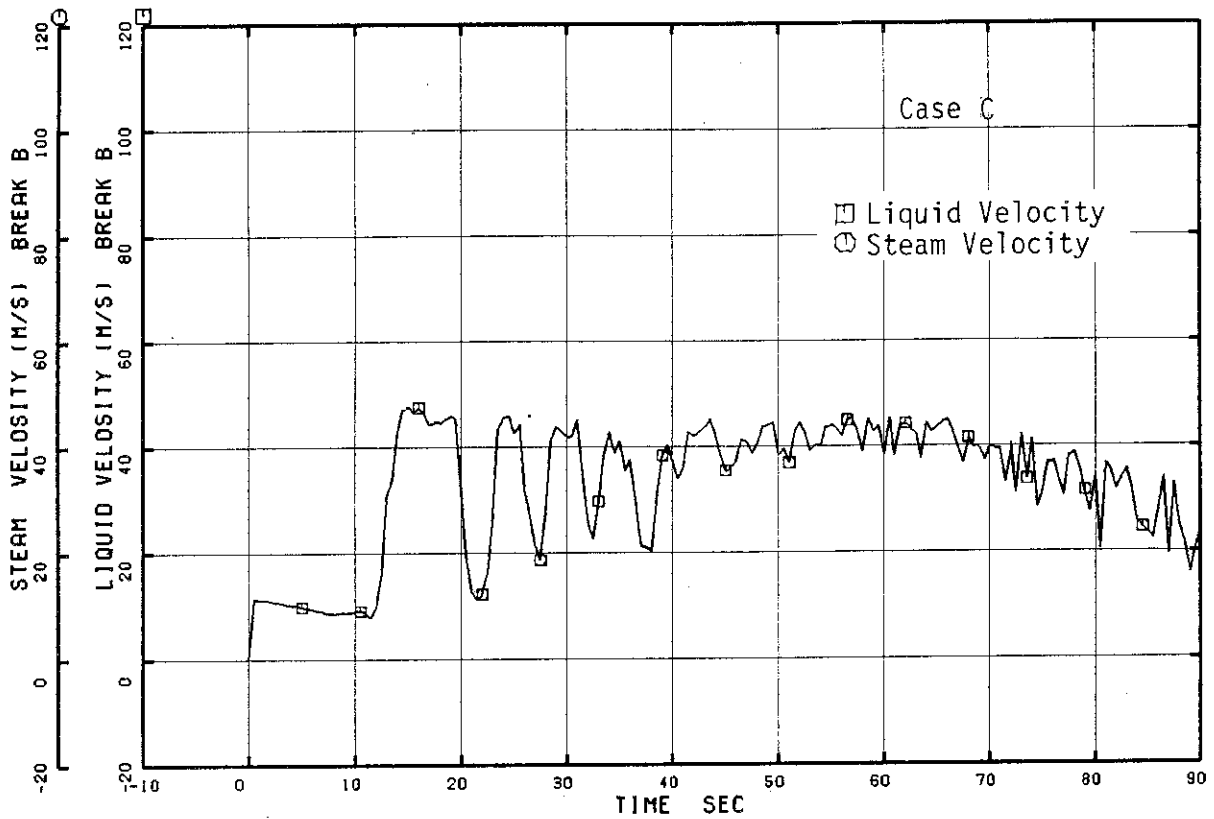


Fig. 4.35 Liquid and Steam Velocities through Break B (Case C)

□ R VFJ89 ○ R VGJ89

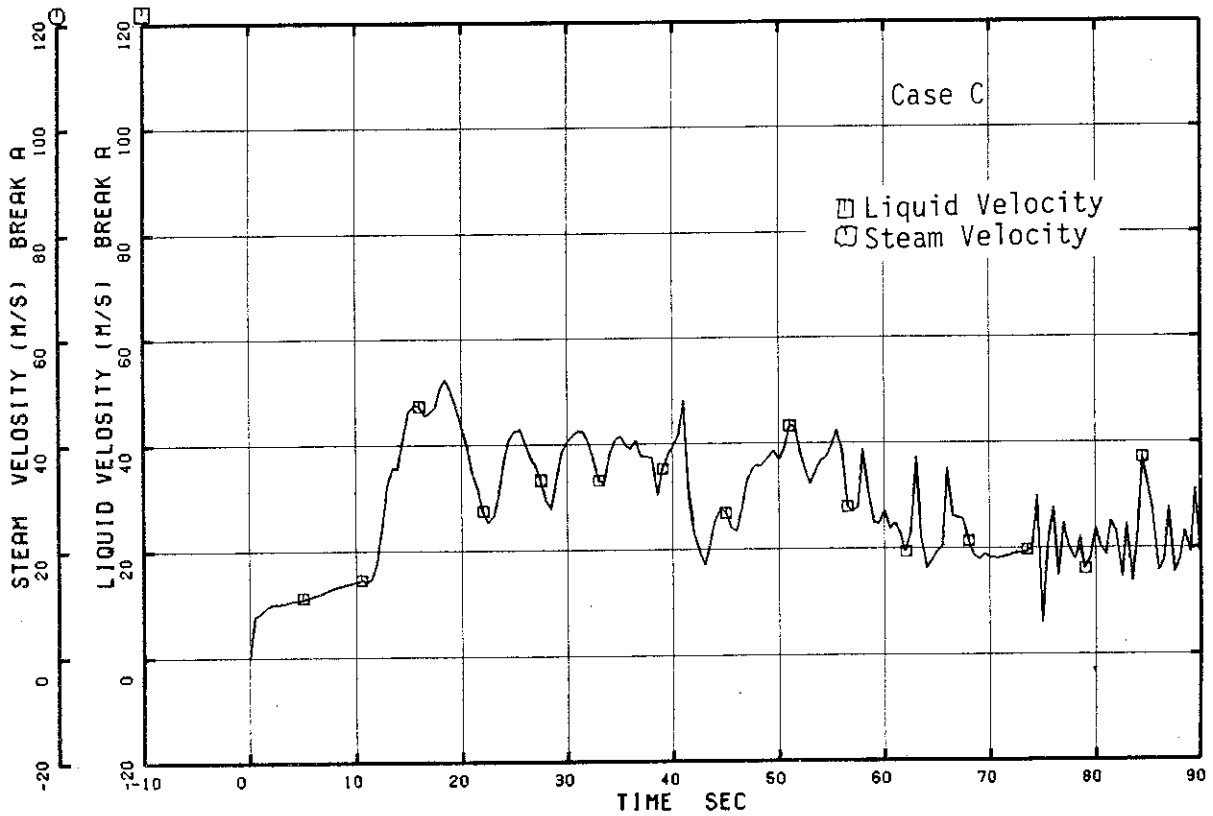


Fig. 4.36 Liquid and Steam Velocities through Break A (Case C)

□ 4 R VFJ88 ○ 4 R VGJ88

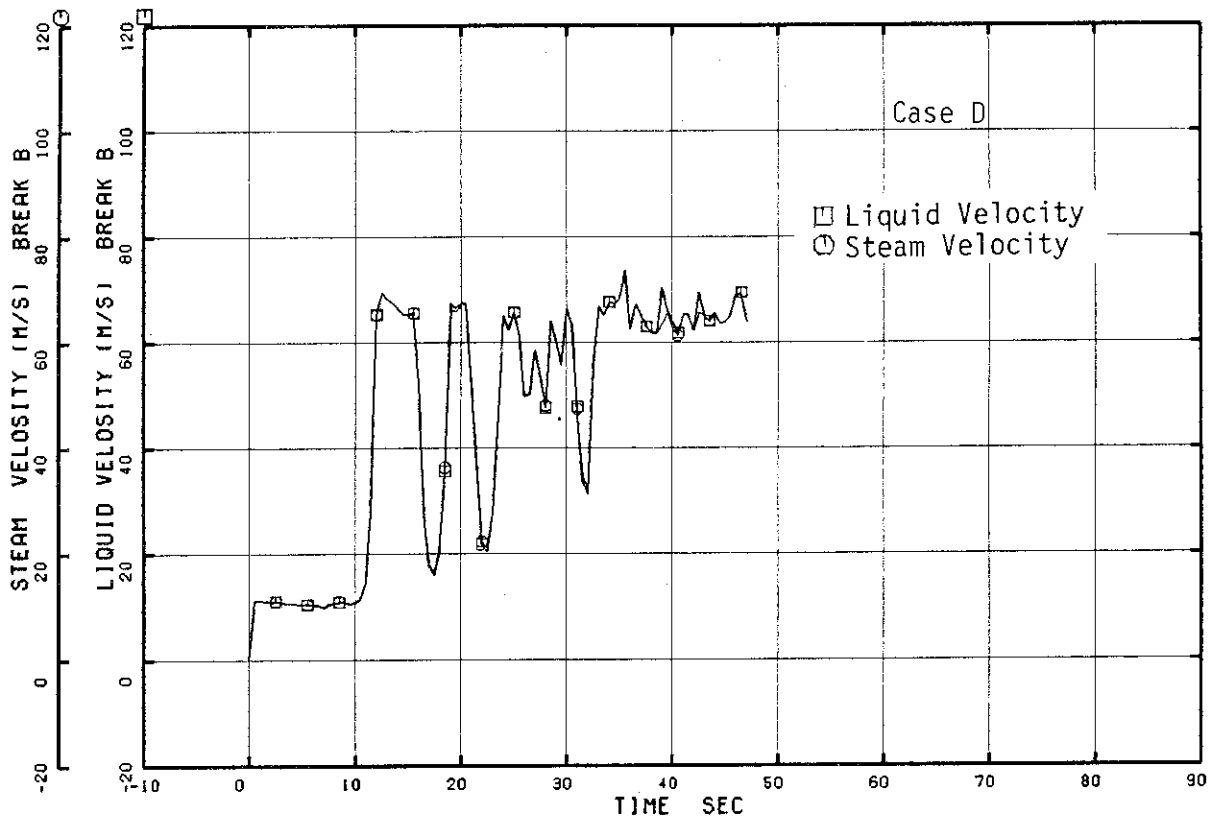


Fig. 4.37 Liquid and Steam Velocities through Break B (Case D)

□ 4 R VFJ89 ○ 4 R VGJ89

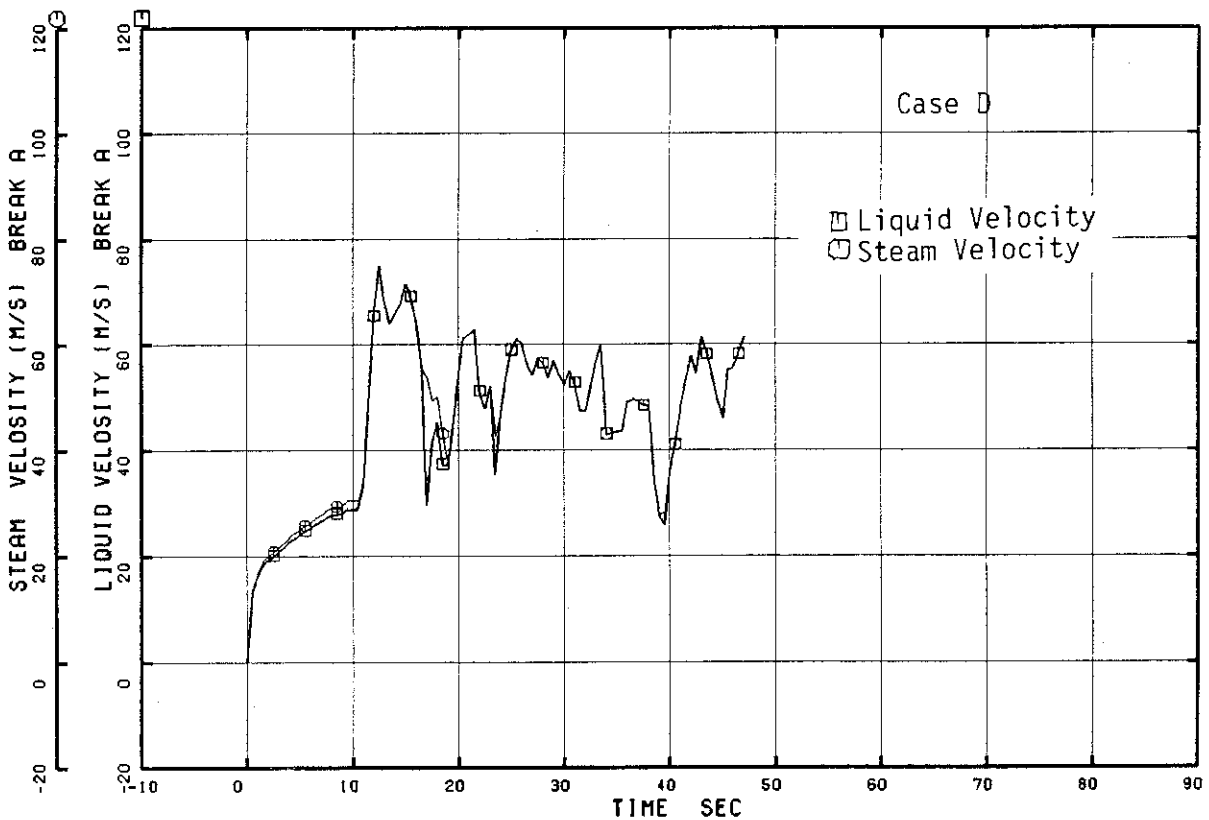


Fig. 4.38 Liquid and Steam Velocities through Break A (Case D)

□ R VFJ88 ○ R VGJ88

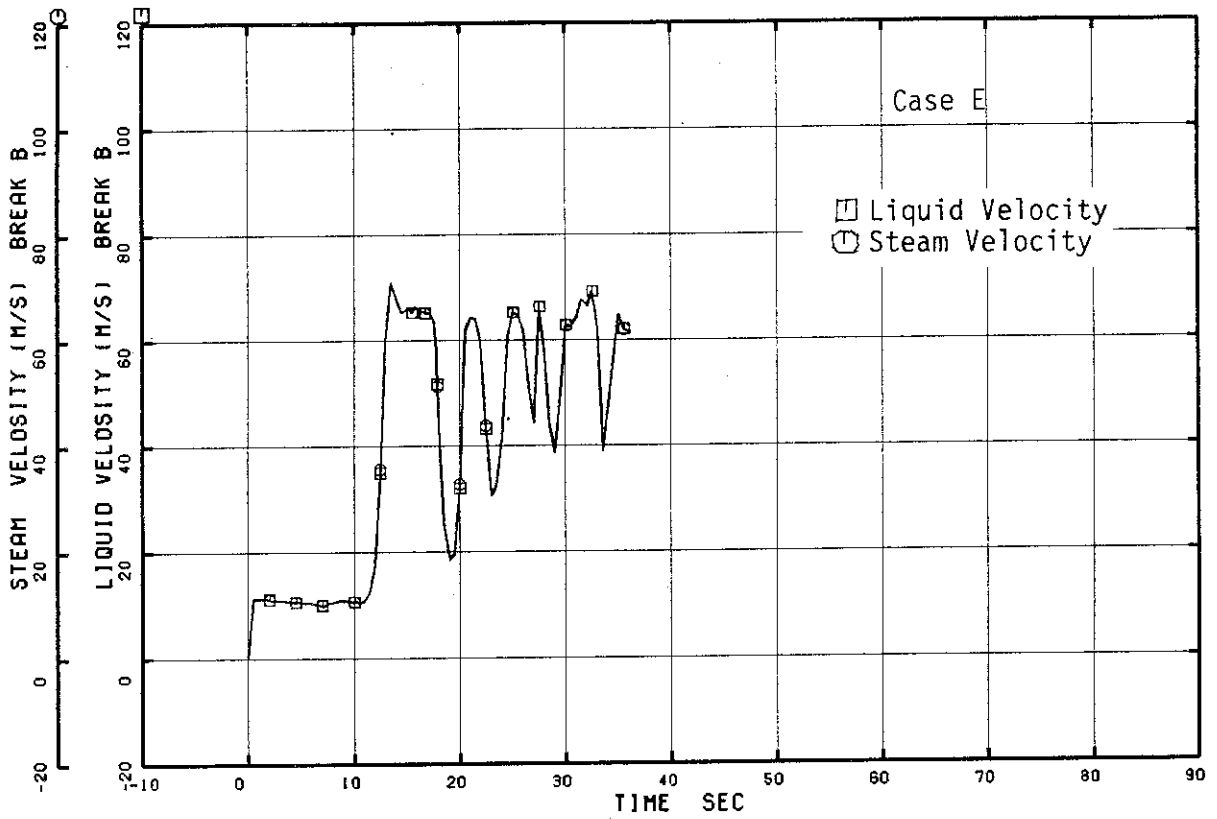


Fig. 4.39 Liquid and Steam Velocities through Break B (Case E)

□ R VFJ89 ○ R VGJ89

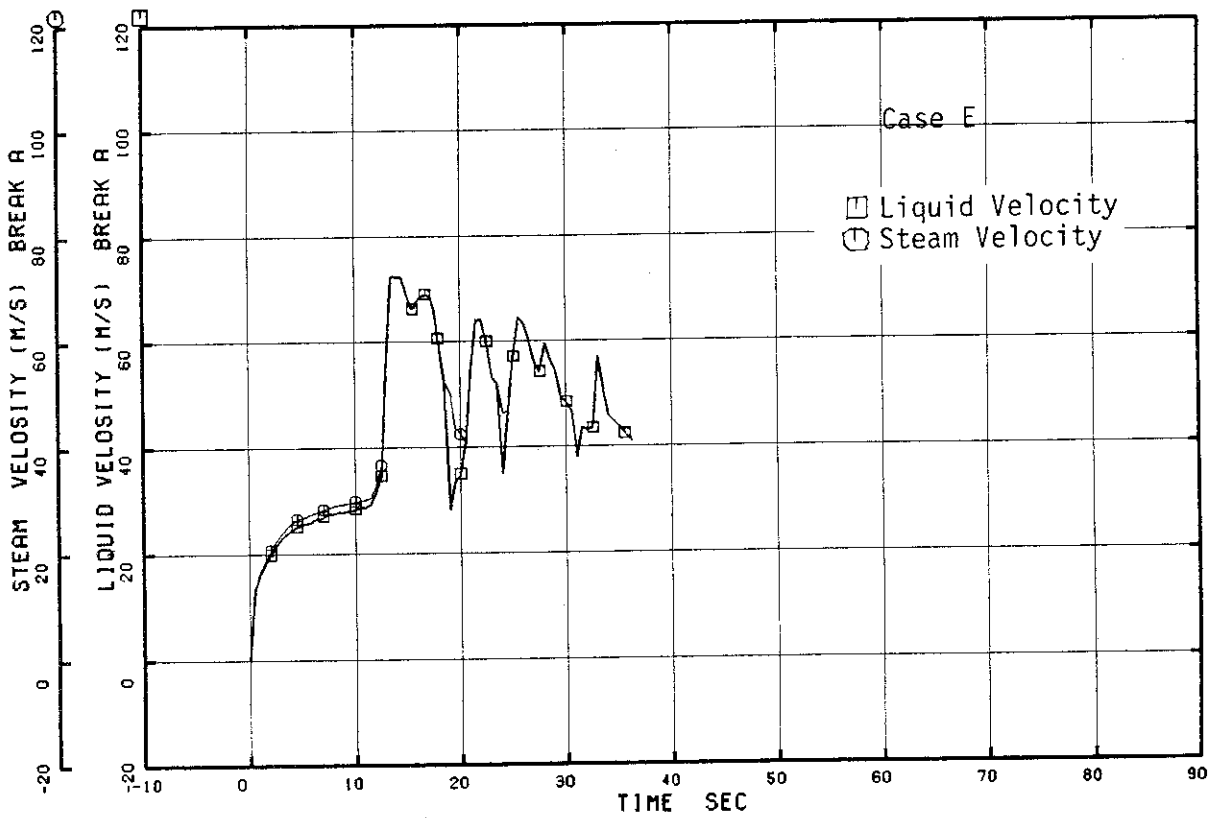


Fig. 4.40 Liquid and Steam Velocities through Break A (Case E)

□ 1 FA 43 ○ 1 R JWJ10 △ 1 R JWJ11 + 1 R JWJ26

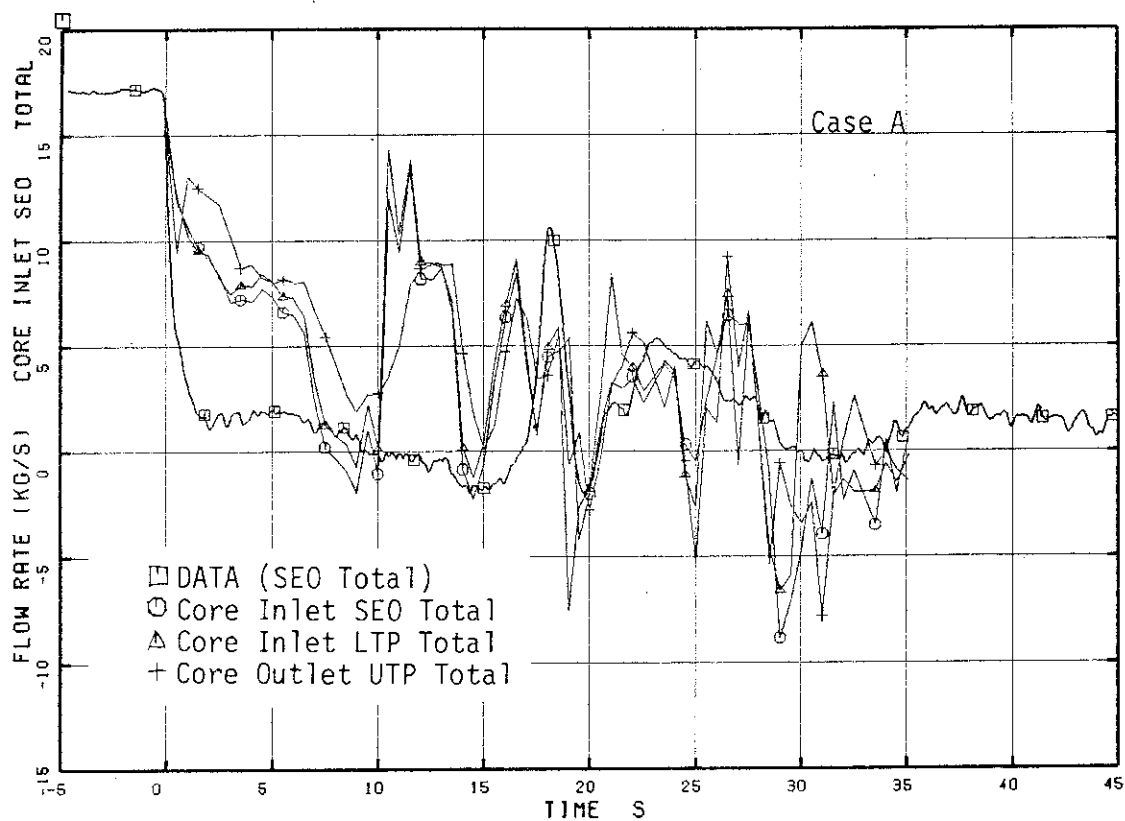


Fig. 4.41 Total Flow Rate through SEO, LTP and UTP (Case A)

□ 1 FA 43 ○ 2 R JWJ10 △ 2 R JWJ11 + 2 R JWJ26

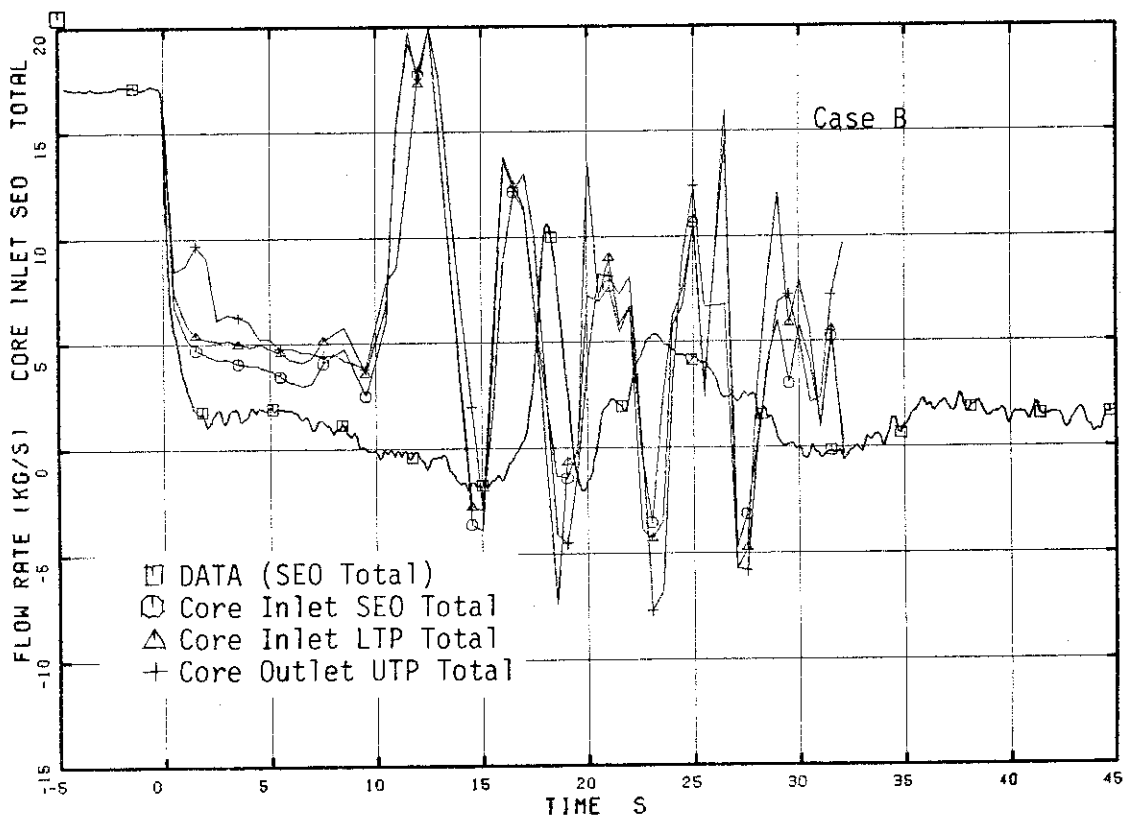


Fig. 4.42 Total Flow Rate through SEO, LTP and UTP (Case B)

□1 FR 43 ○3 R JWJ10 △3 R JWJ11 +3 R JWJ26

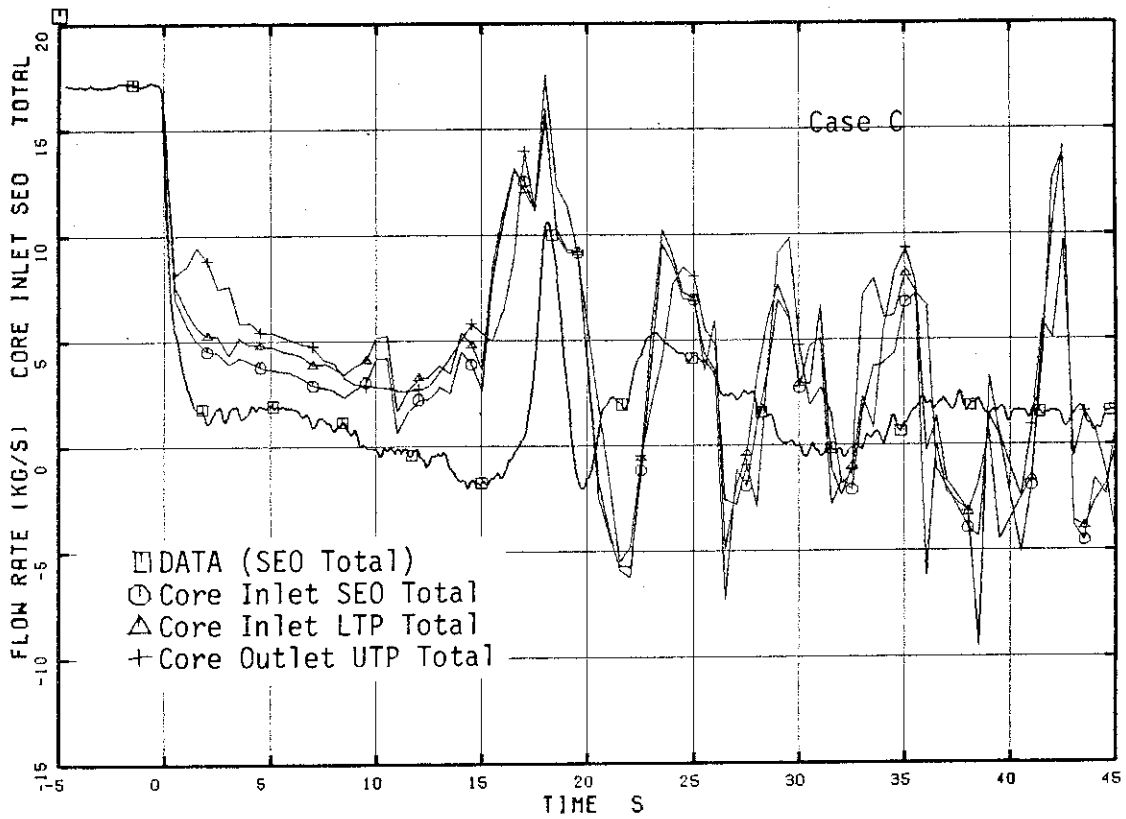


Fig. 4.43 Total Flow Rate through SEO, LTP and UTP (Case C)

□1 FR 43 ○4 R JWJ10 △4 R JWJ11 +4 R JWJ26

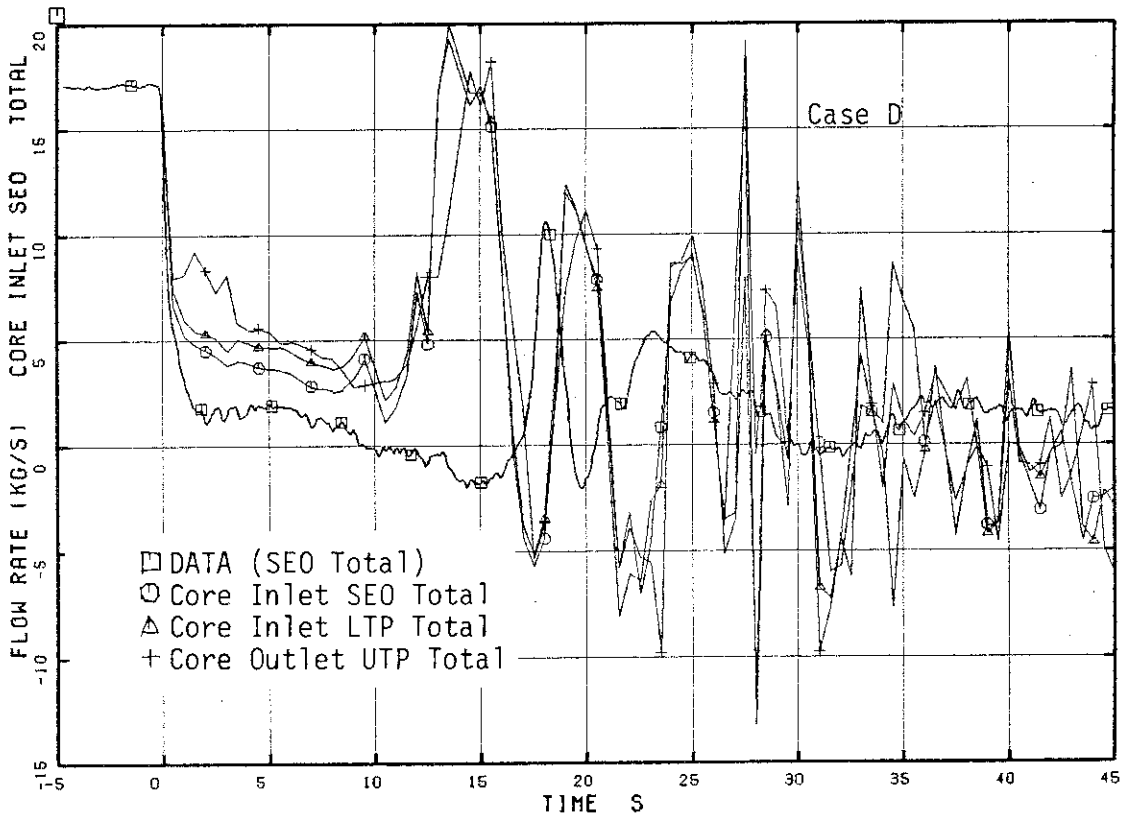


Fig. 4.44 Total Flow Rate through SEO, LTP and UTP (Case D)

□1 FA 43 ○5 R JWJ10 △5 R JWJ11 +5 R JWJ26

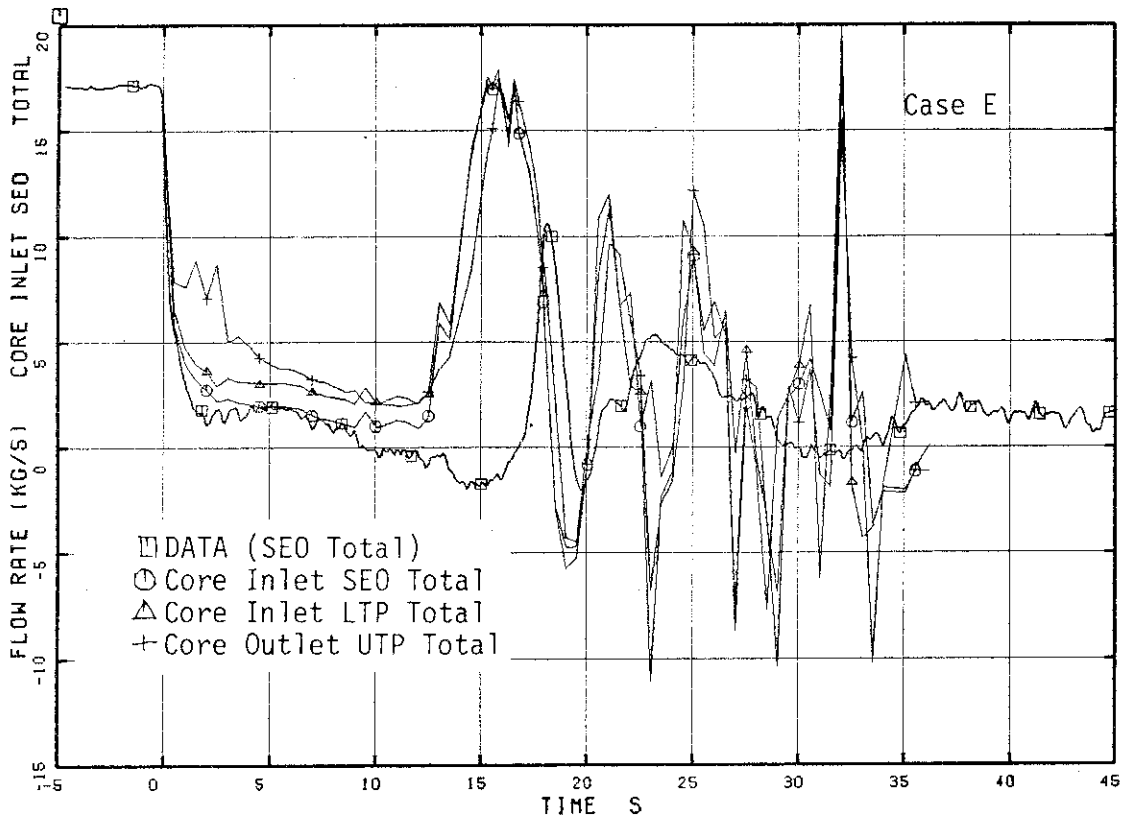


Fig. 4.45 Total Flow Rate through SEO, LTP and UTP (Case E)

□1 FA 43 ○1 R JWJ10 △2 R JWJ10 +3 R JWJ10 ◇4 R JWJ10
 †5 R JWJ10

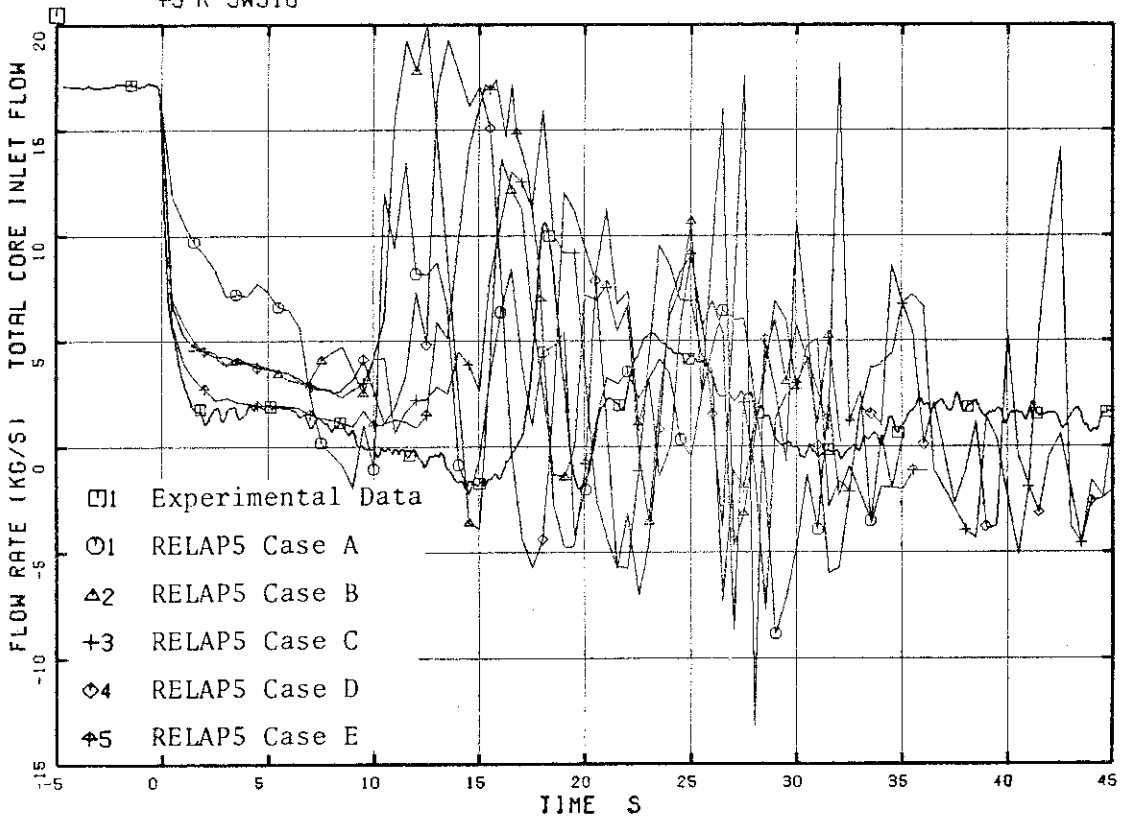


Fig. 4.46 Comparison of Total Flow Rates through SEO

□ I R VFJ26 ○ I R VGJ26

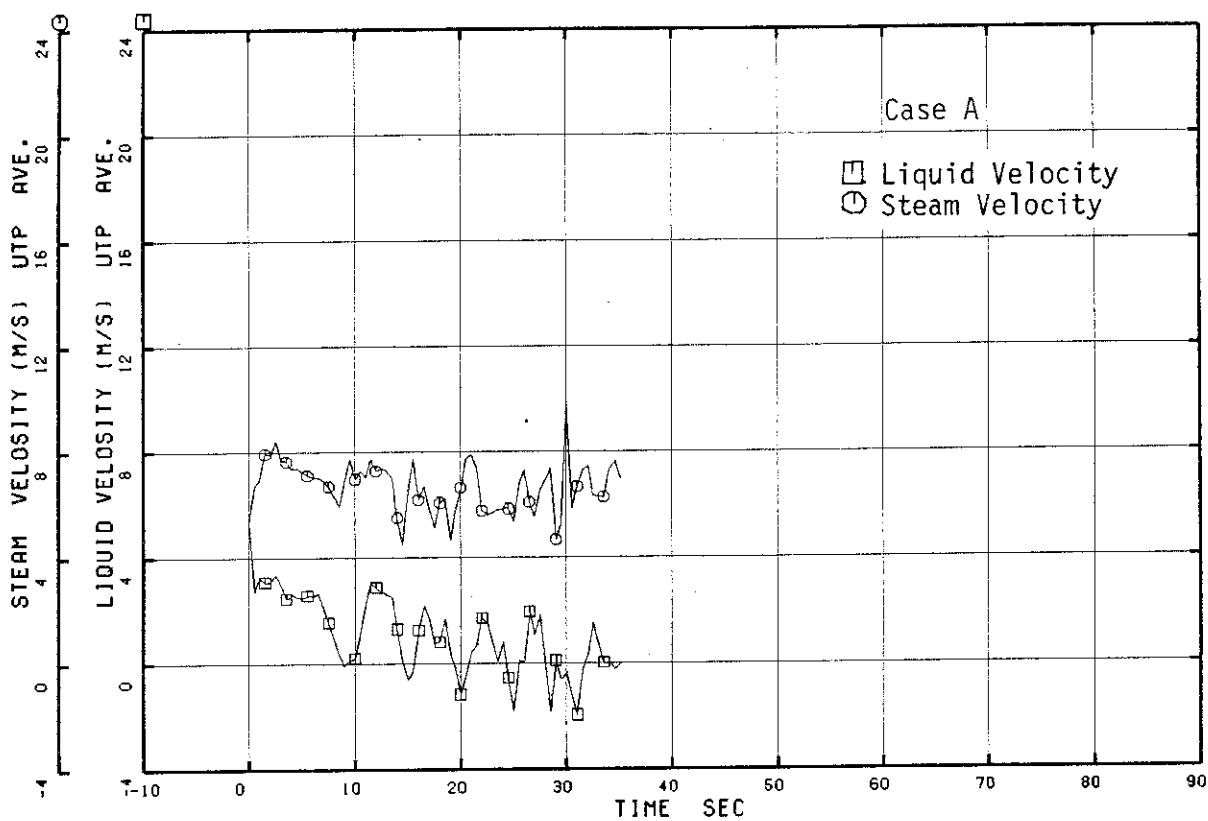


Fig. 4.47 Fluid Velocities through UTP of Average Power Channel (Case A)

□ I R VFJ25 ○ I R VGJ25

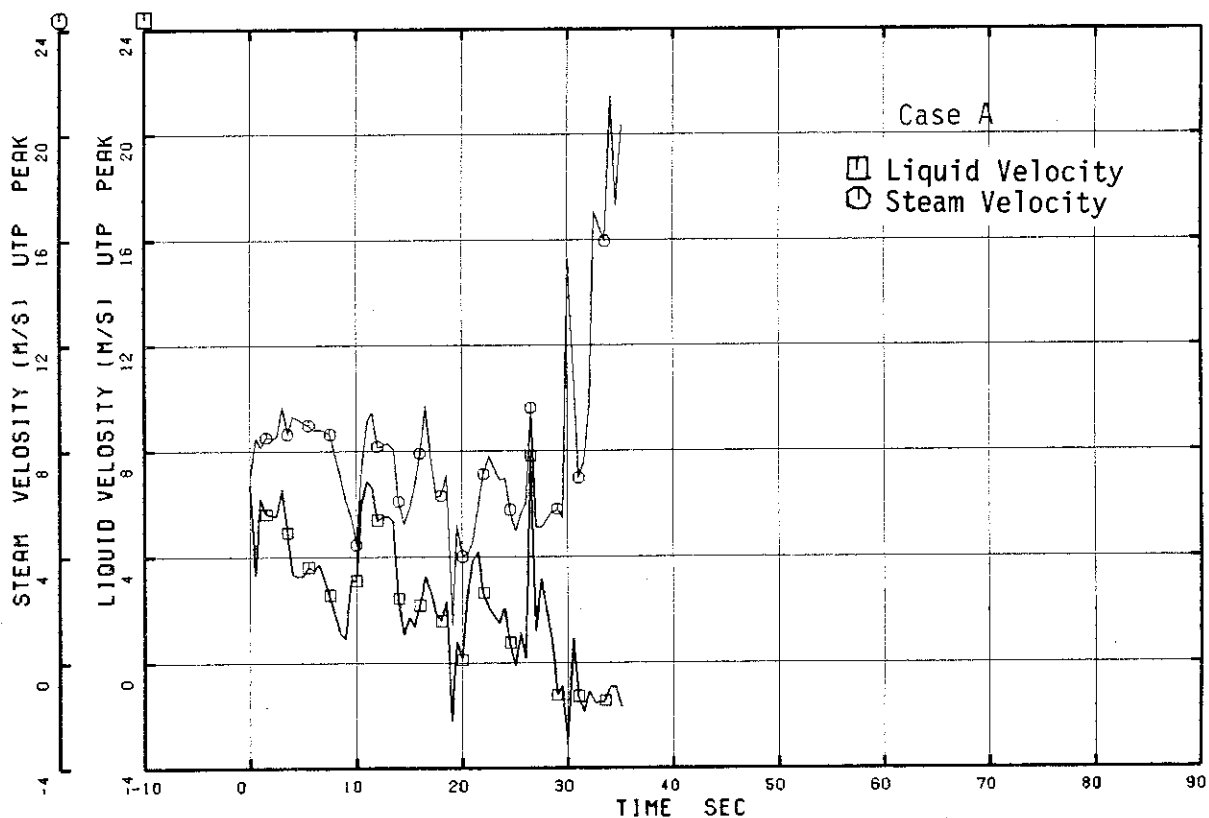


Fig. 4.48 Fluid Velocities through UTP of Peak Power Channel (Case A)

□ R VFJ26 ○ R VGJ26

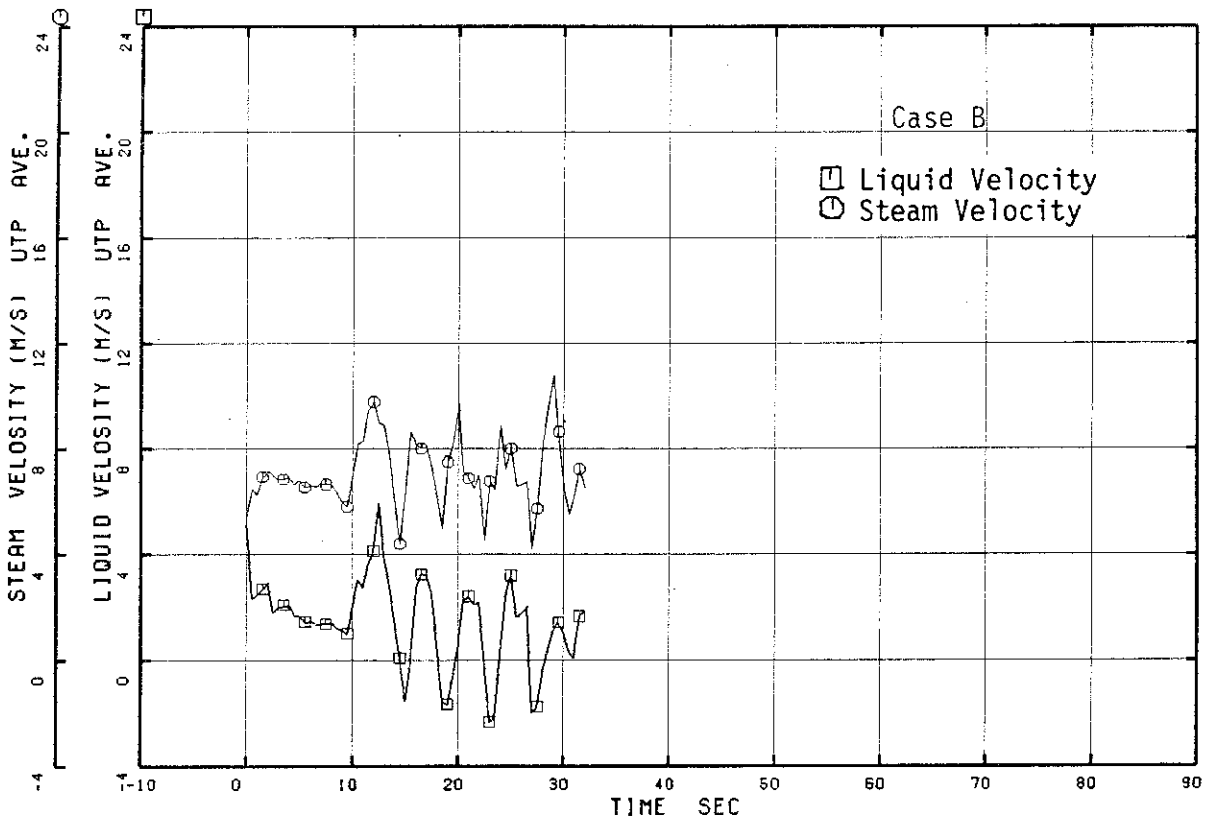


Fig. 4.49 Fluid Velocities through UTP of Average Power Channel (Case B)

□ R VFJ25 ○ R VGJ25

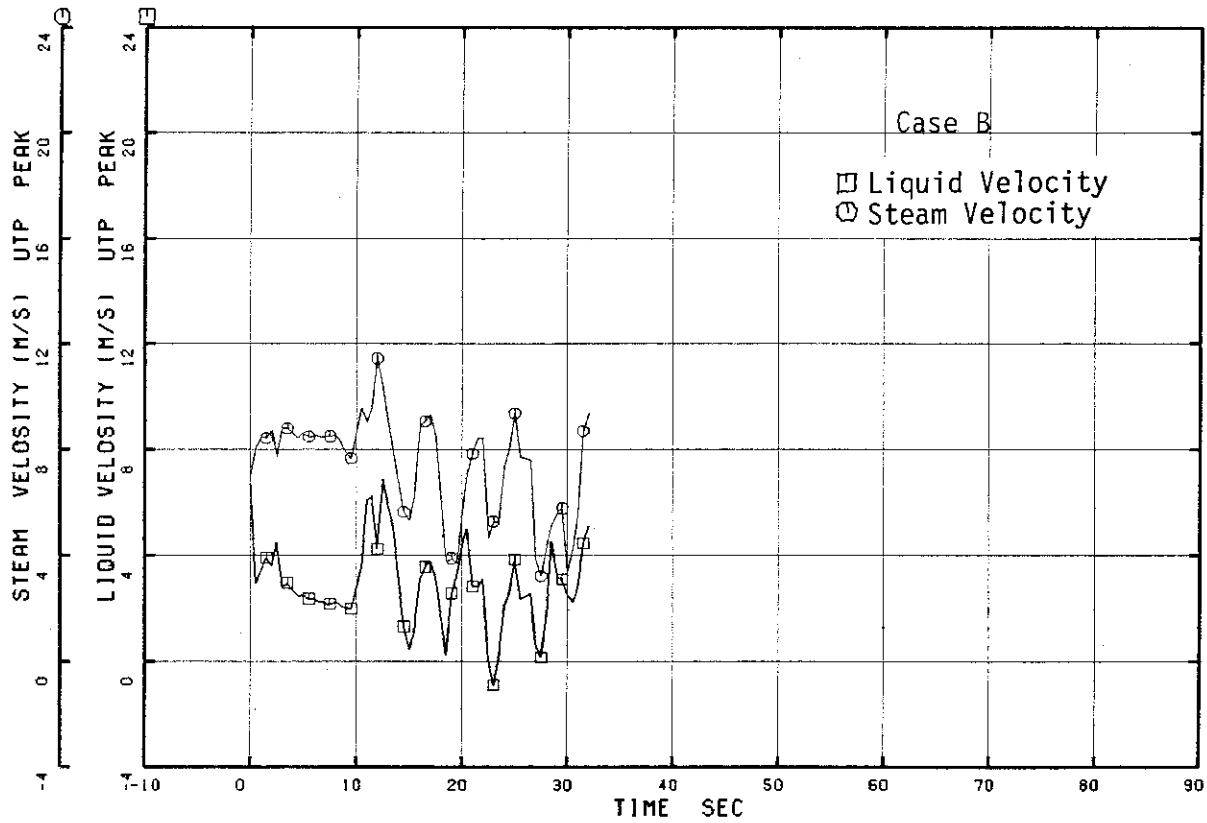


Fig. 4.50 Fluid Velocities through UTP of Peak Power Channel (Case B)

□ R VFJ26 ○ R VGJ26

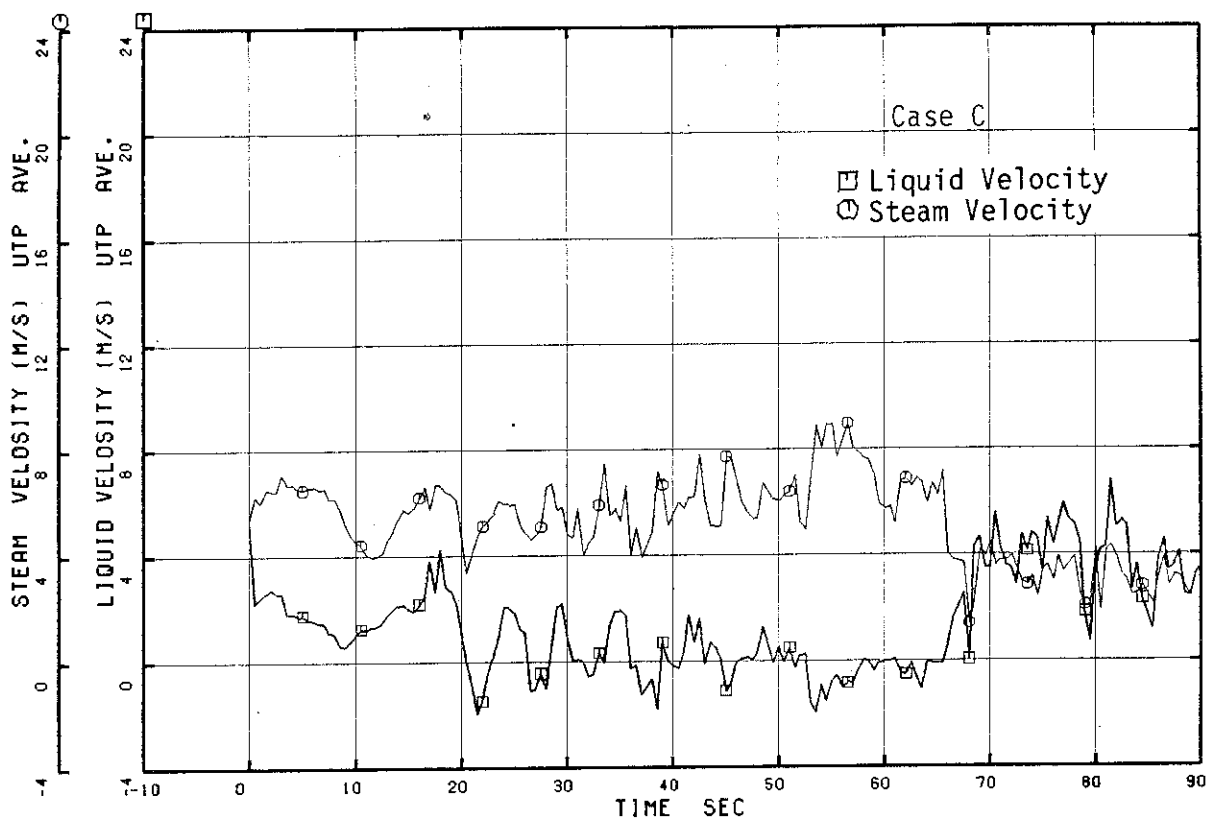


Fig. 4.51 Fluid Velocities through UTP of Average Power Channel (Case C)

□ R VFJ25 ○ R VGJ25

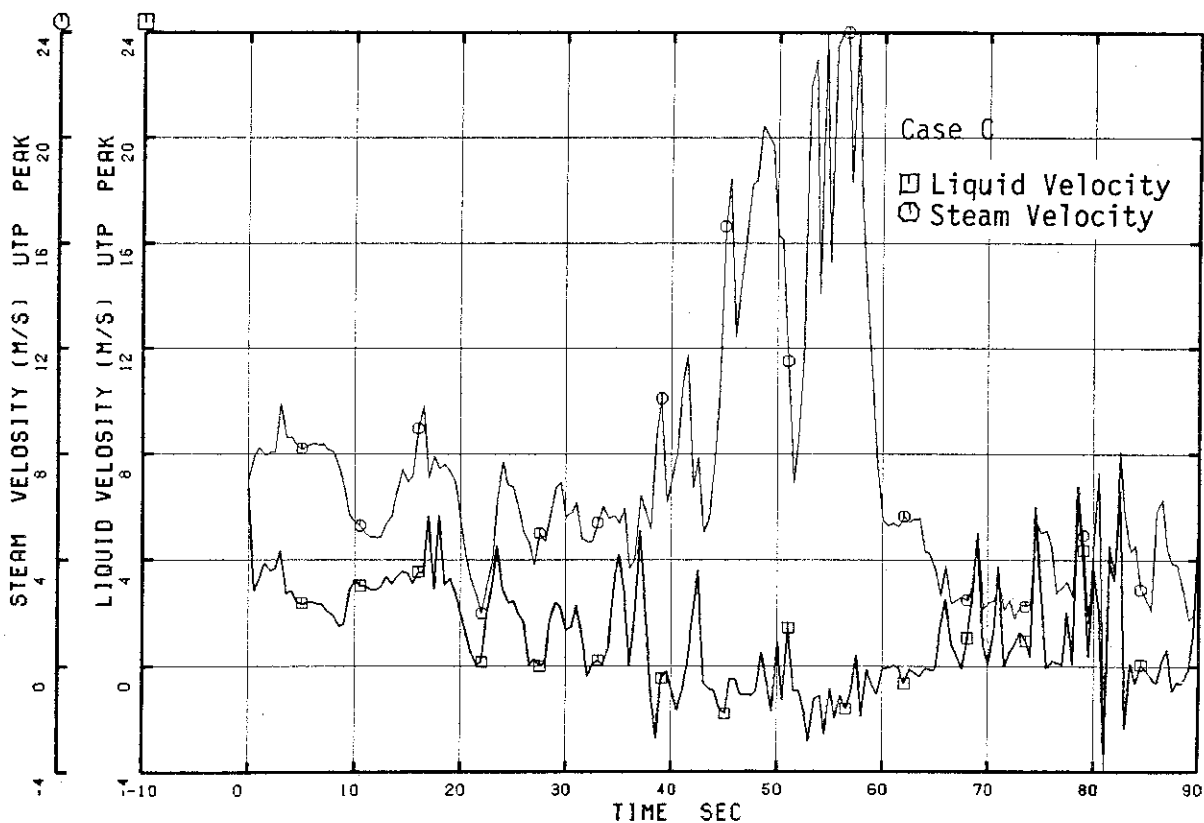


Fig. 4.52 Fluid Velocities through UTP of Peak Power Channel (Case C)

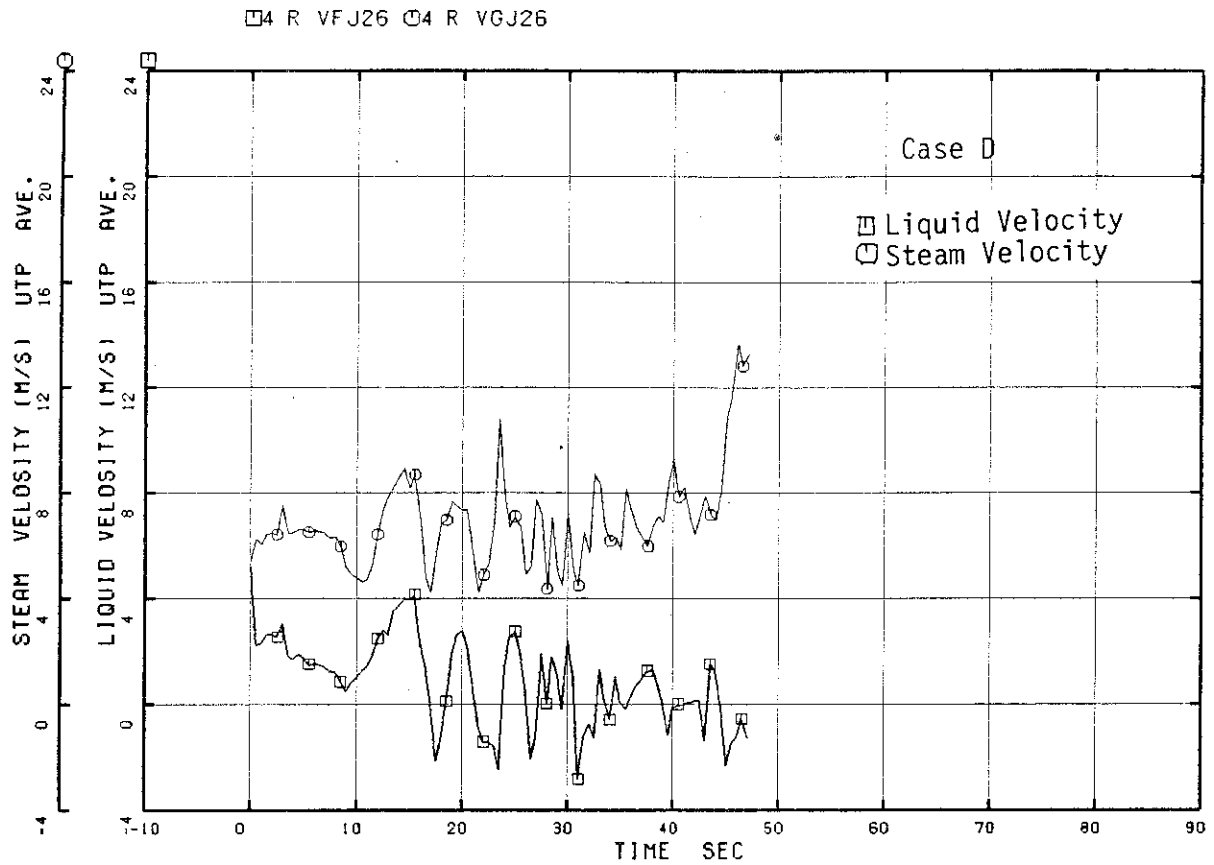


Fig. 4.53 Fluid Velocities through UTP of Average Power Channel (Case D)

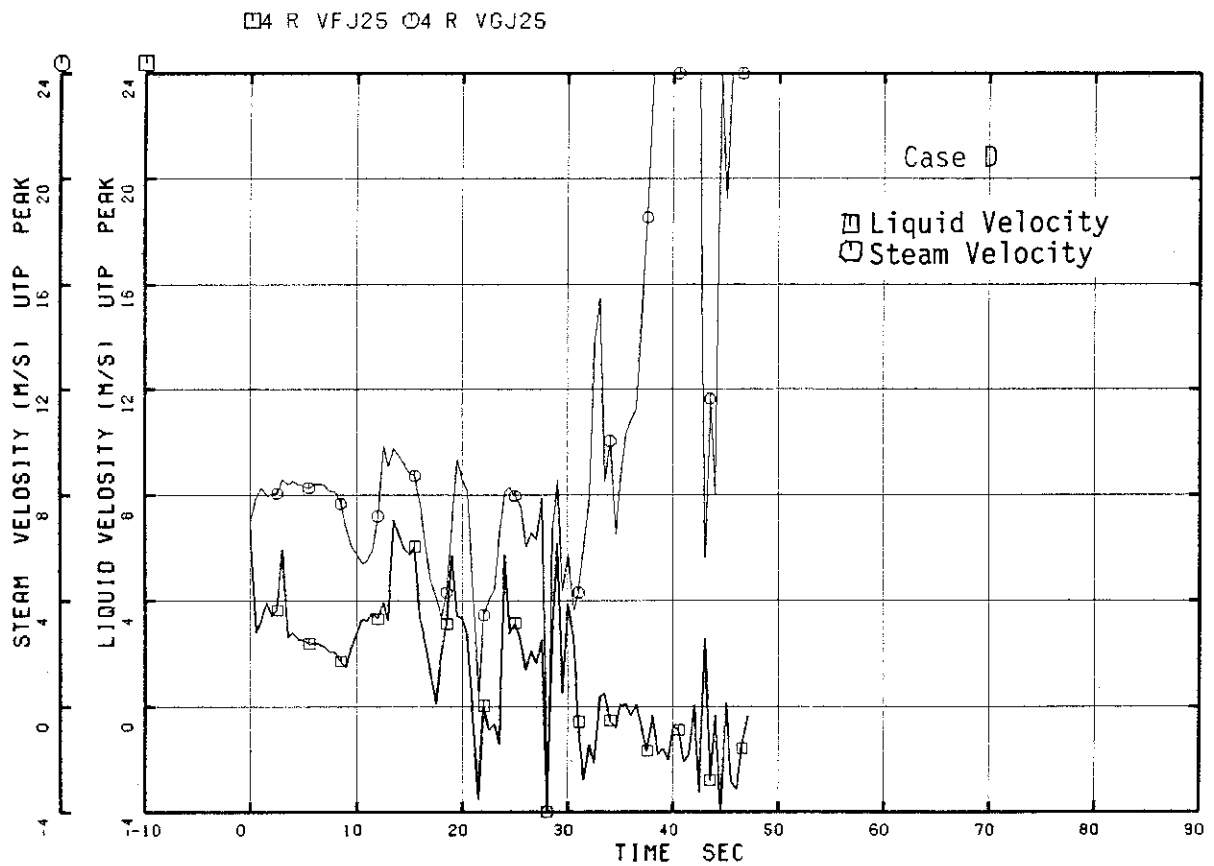


Fig. 4.54 Fluid Velocities through UTP of Peak Power Channel (Case D)

□ 5 R VFJ26 ○ 5 R VGJ26

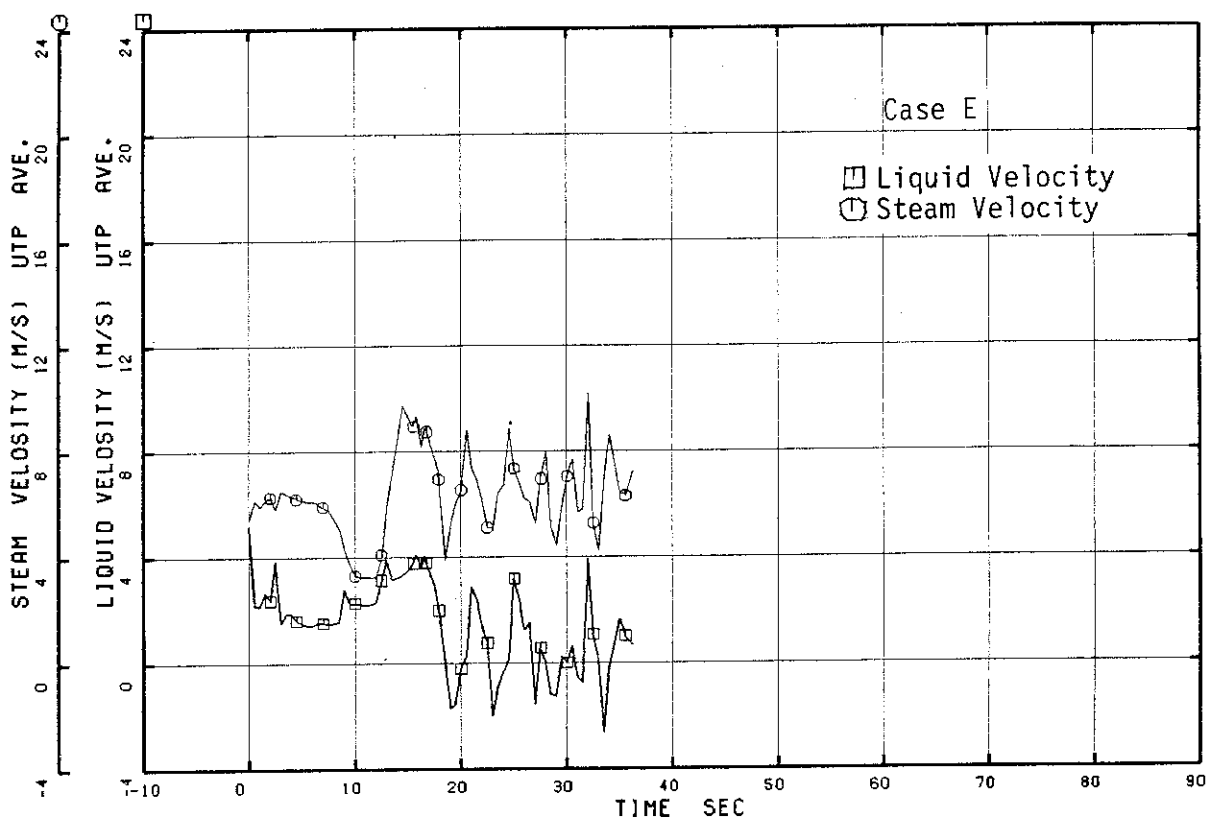


Fig. 4.55 Fluid Velocities through UTP of Average Power Channel (Case E)

□ 5 R VFJ25 ○ 5 R VGJ25

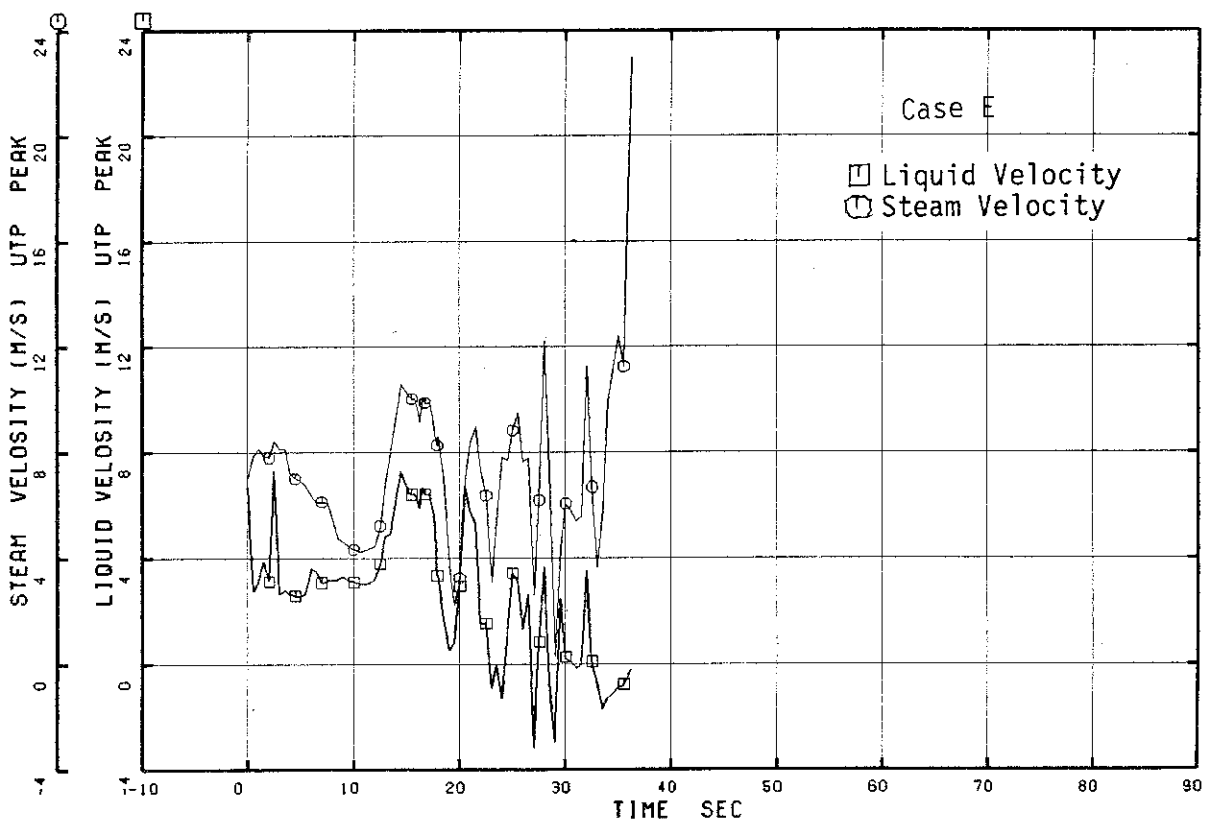


Fig. 4.56 Fluid Velocities through UTP of Peak Power Channel (Case E)

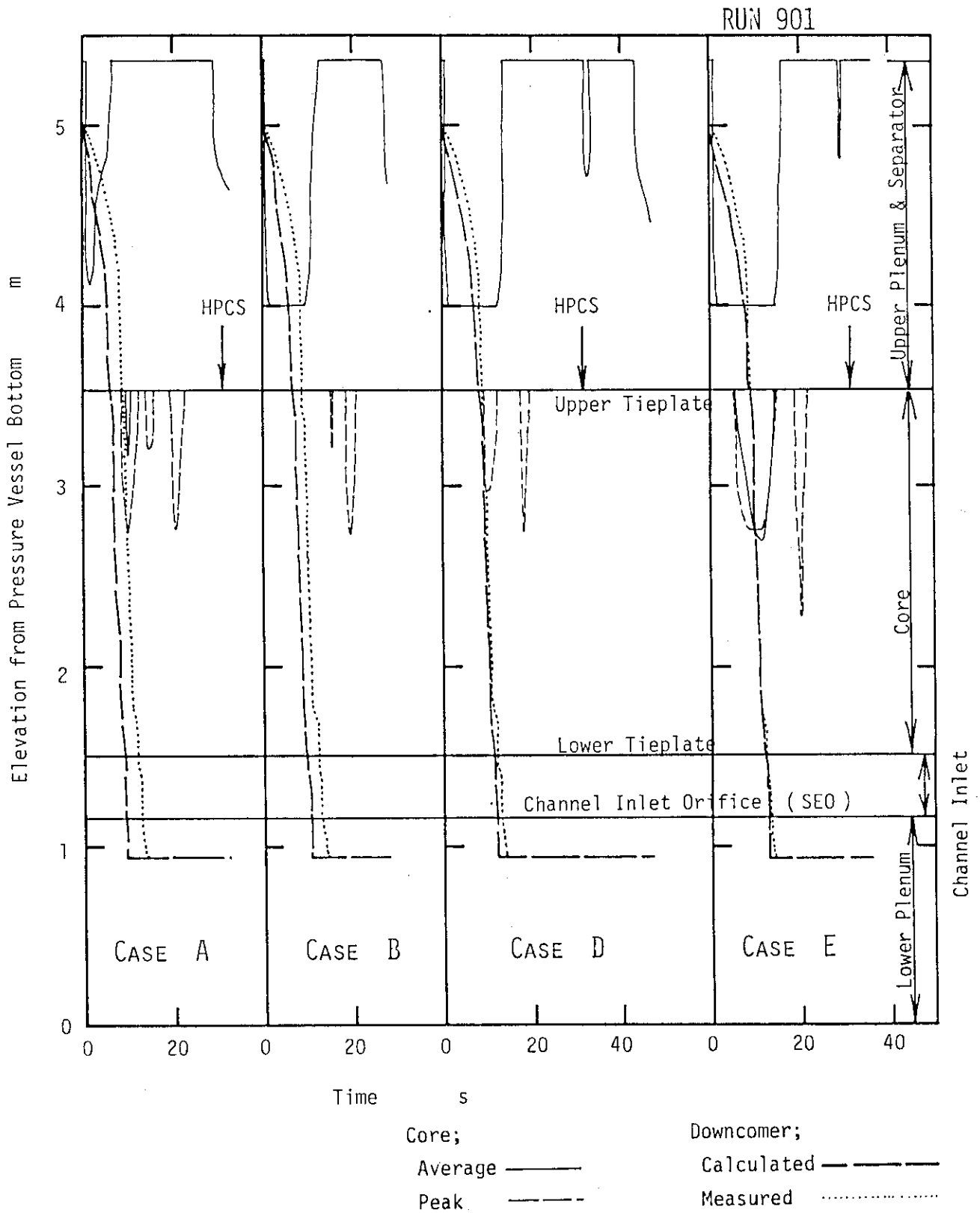


Fig. 4.57 Estimated Liquid Levels in PV (Cases A, B, D and E)

RUN 901

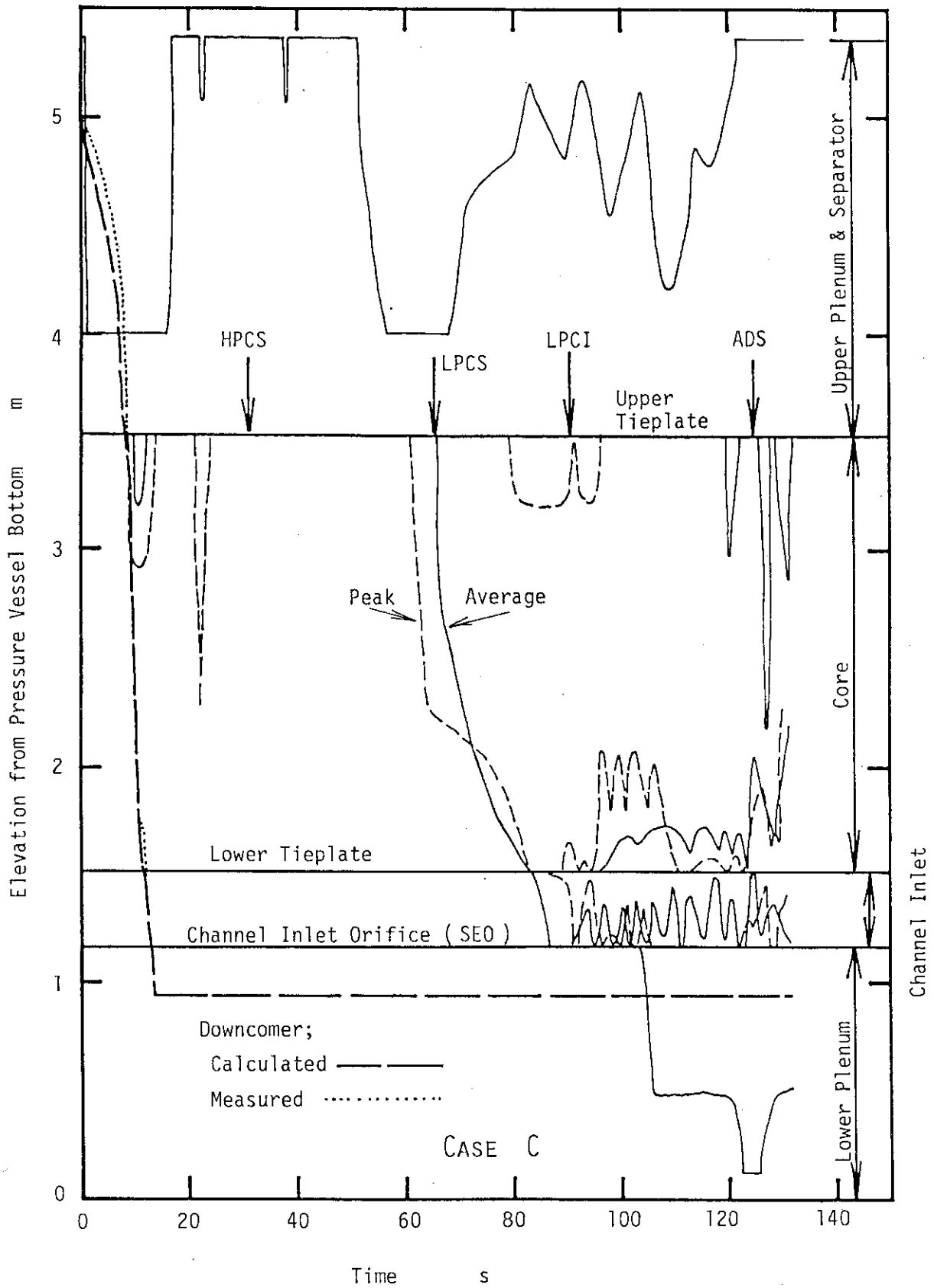


Fig. 4.58 Estimated Liquid Levels in PV (Case C)

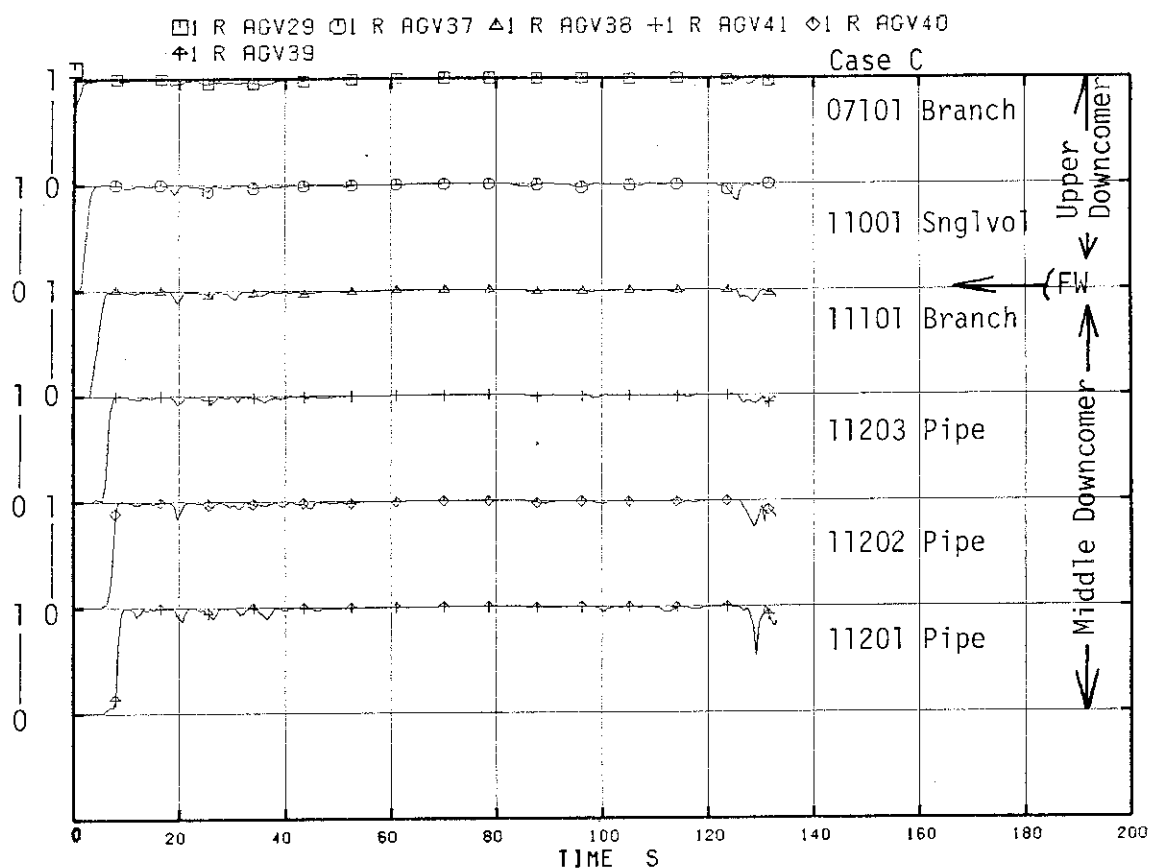


Fig. 4.59 Void Fractions in Upper Downcomer (Case C)

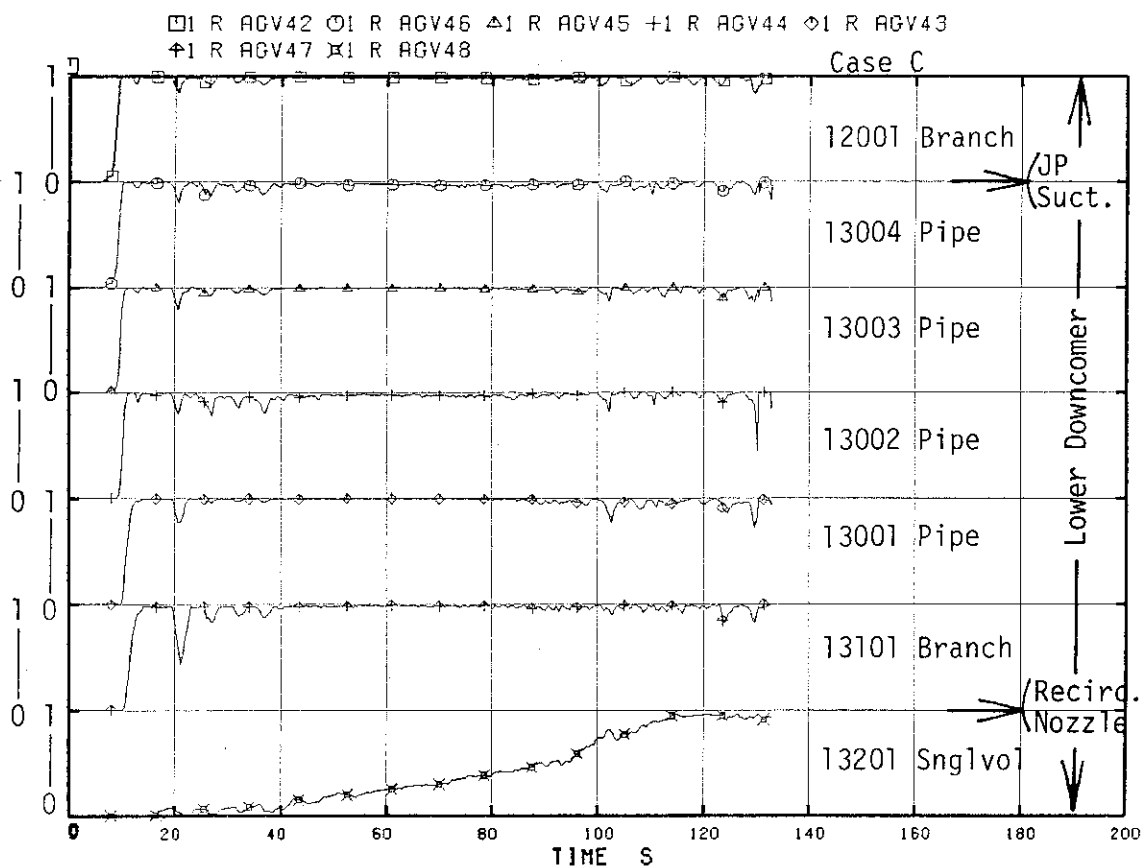


Fig. 4.60 Void Fractions in Lower Downcomer (Case C)

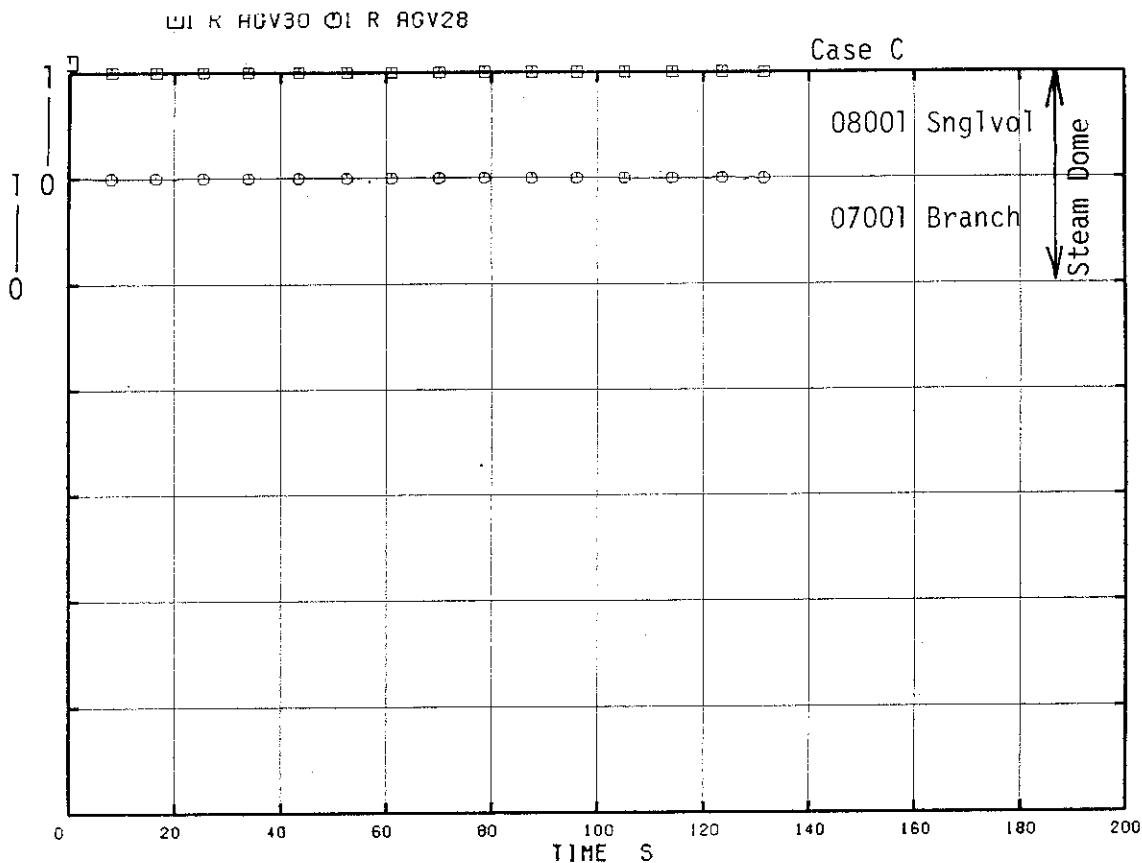


Fig. 4.61 Void Fractions in Steam Dome (Case C)

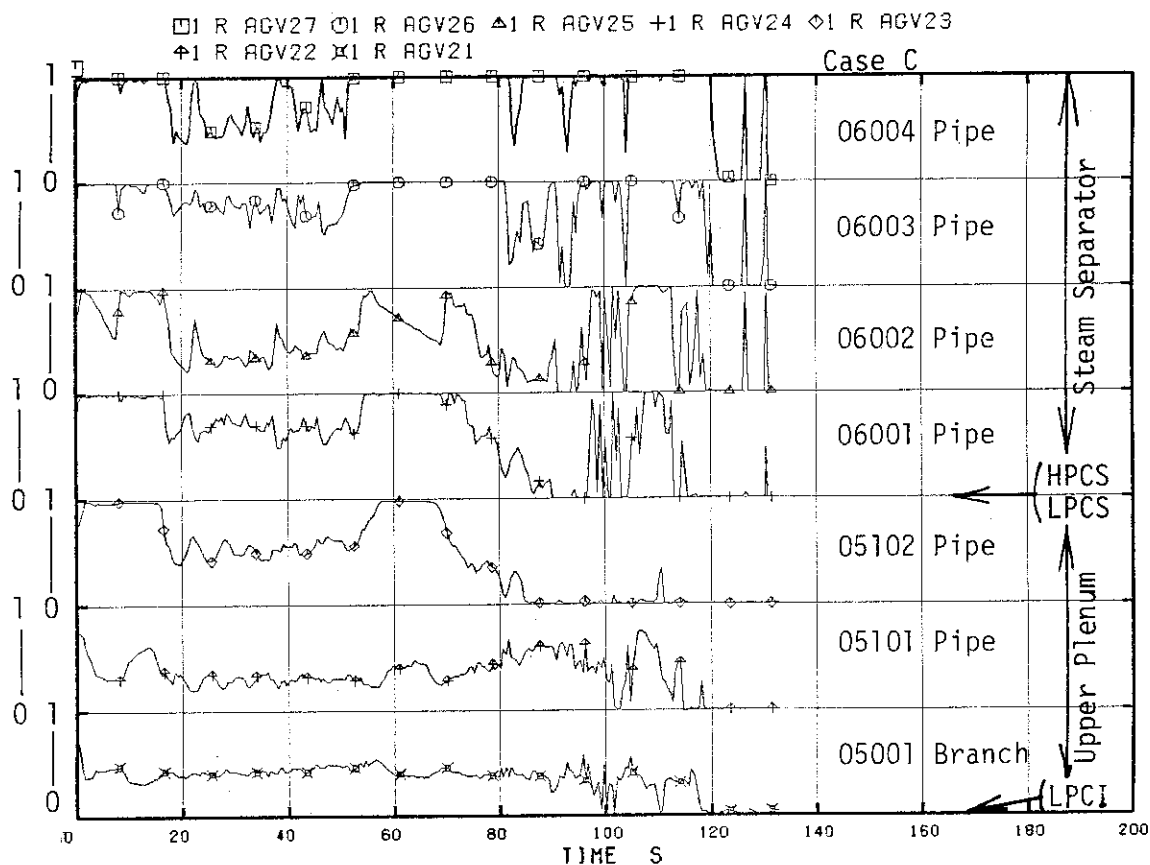


Fig. 4.62 Void Fractions in Upper Plenum and Separator (Case C)

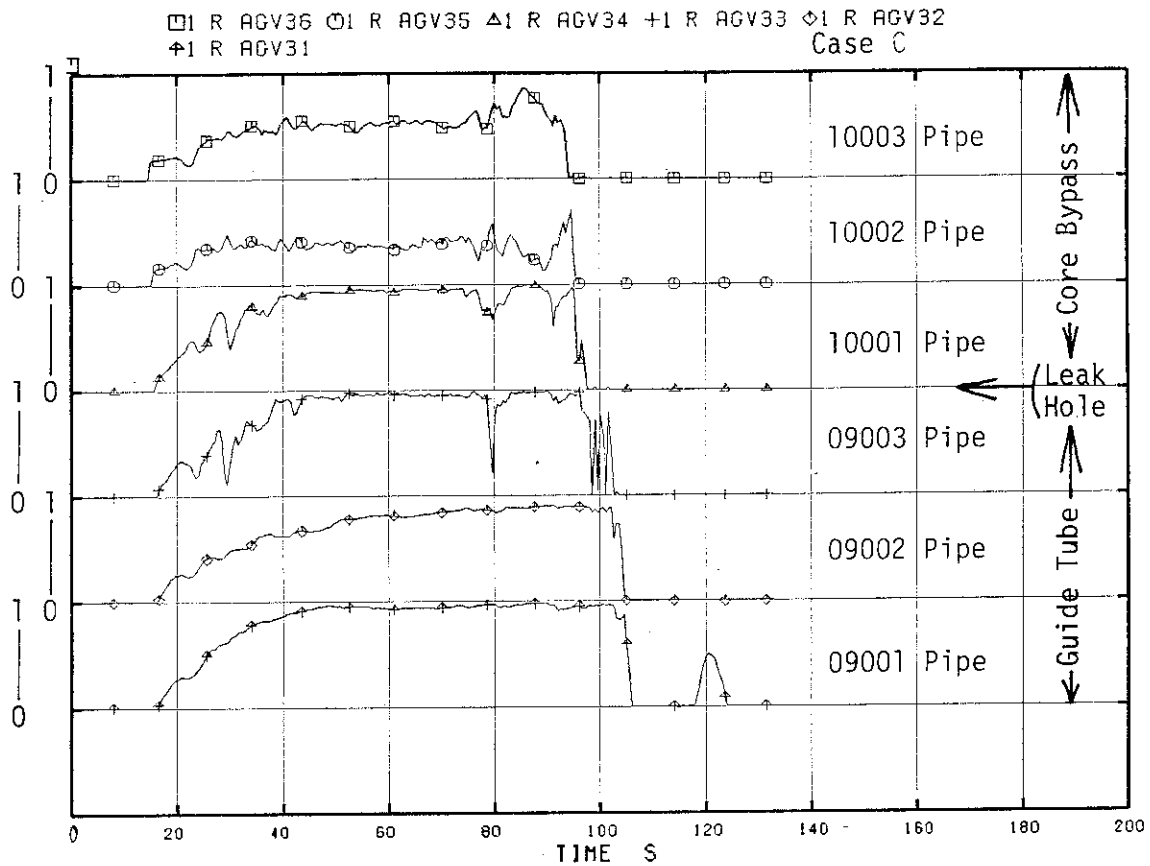


Fig. 4.63 Void Fractions in Bypass and Guide Tube (Case C)

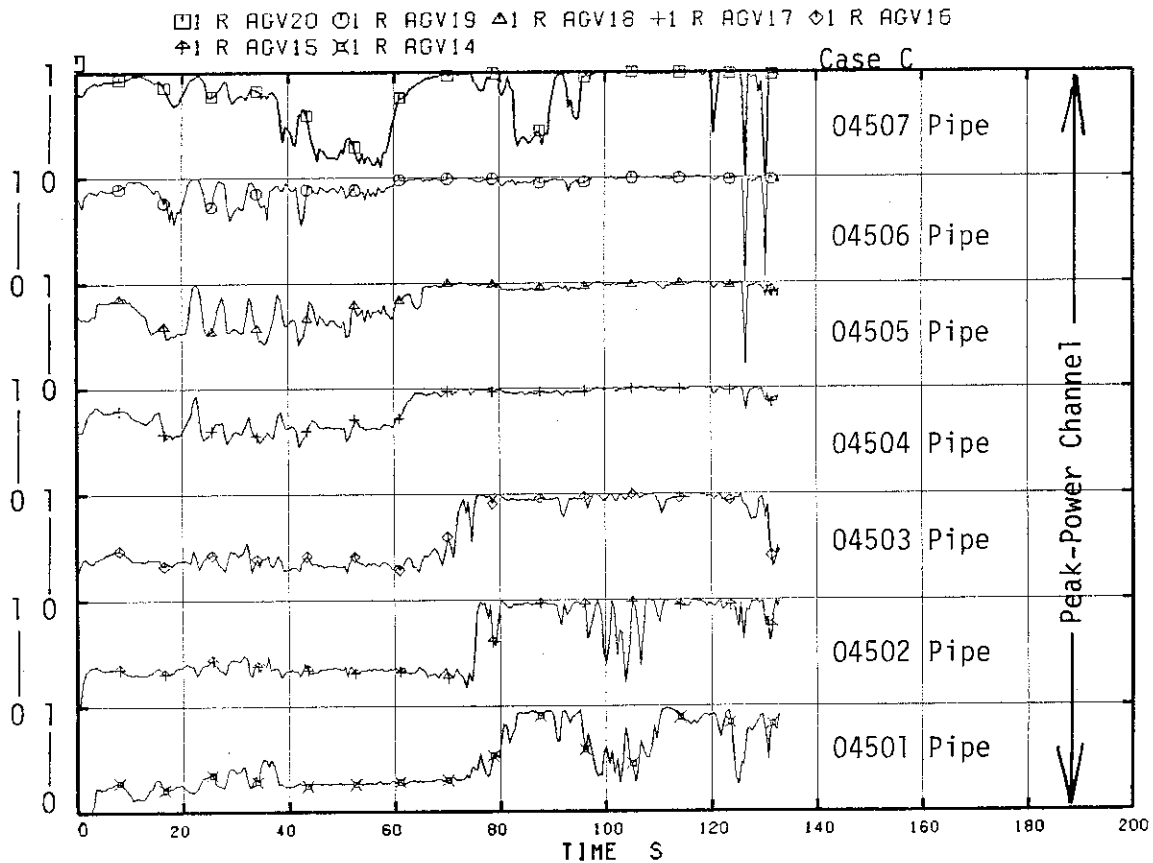


Fig. 4.64 Void Fractions in Peak-Power Channel (Case C)

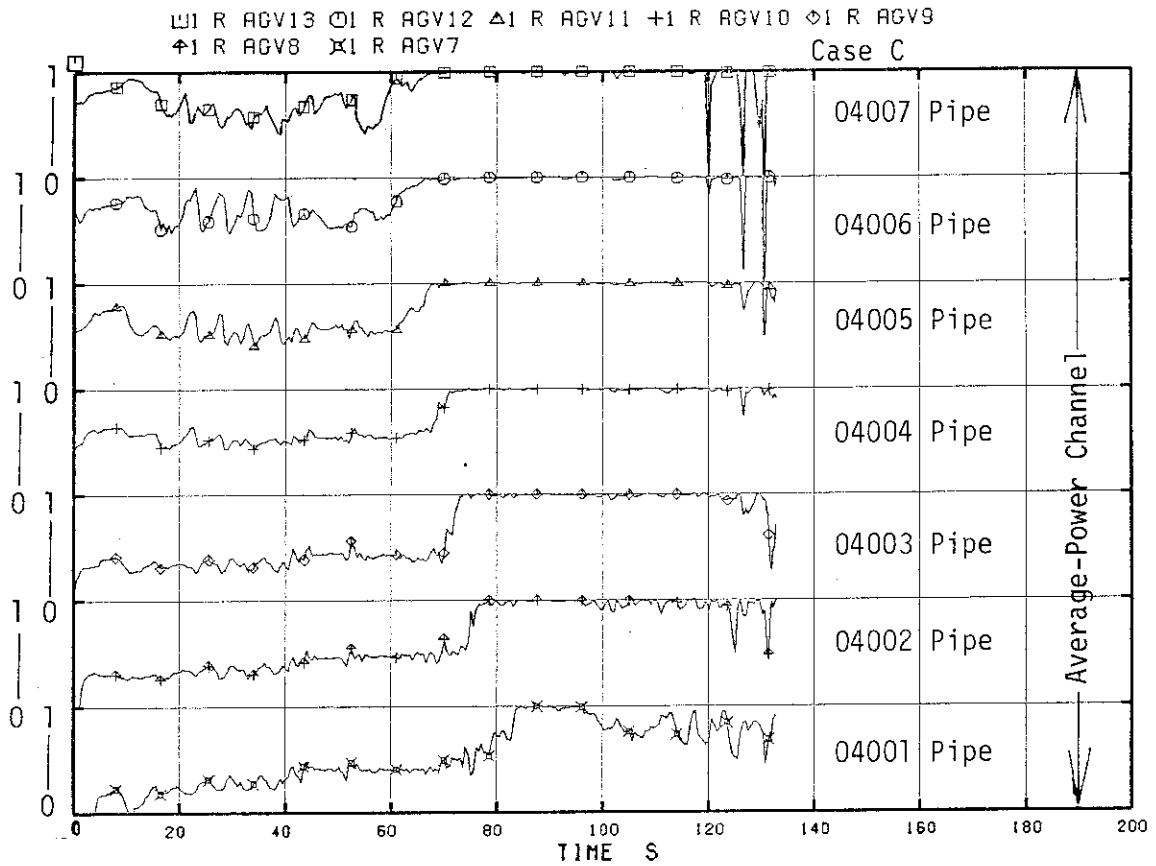


Fig. 4.65 Void Fractions in Average-Power Channel (Case C)

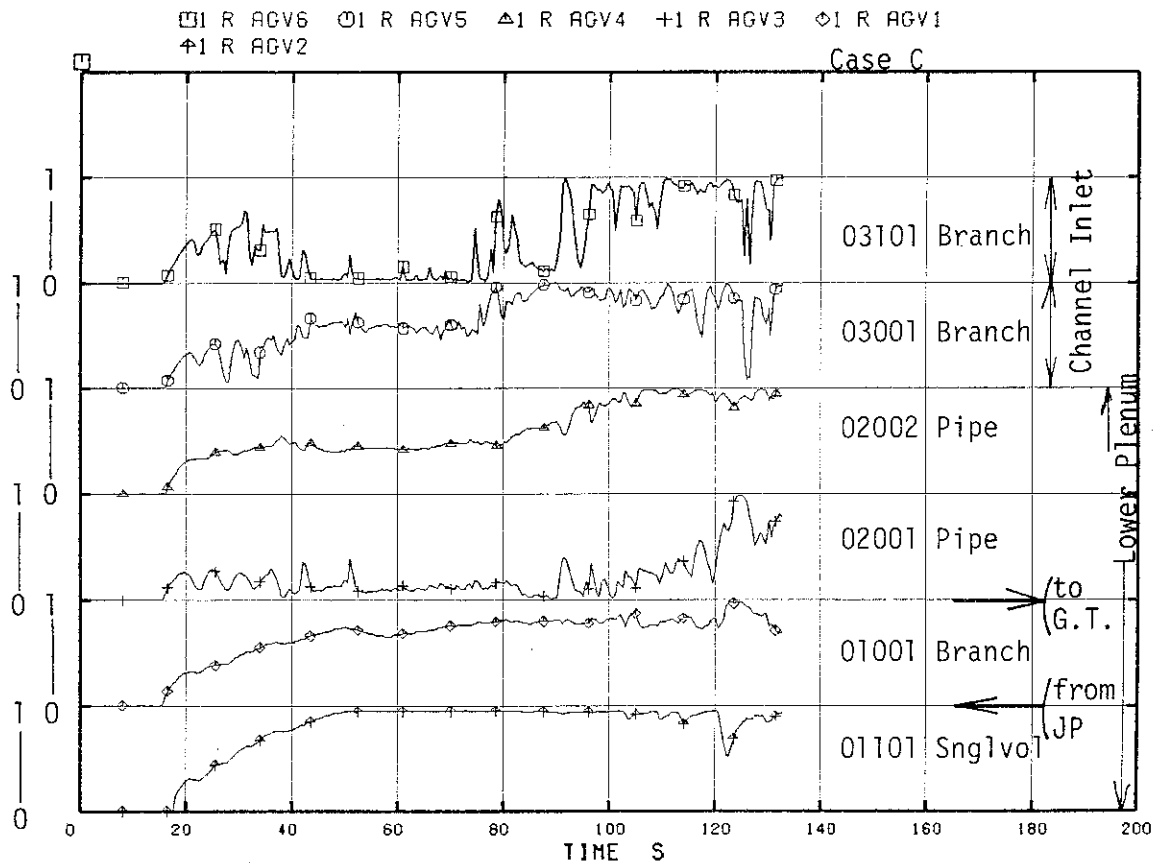


Fig. 4.66 Void Fractions in Lower Plenum (Case C)

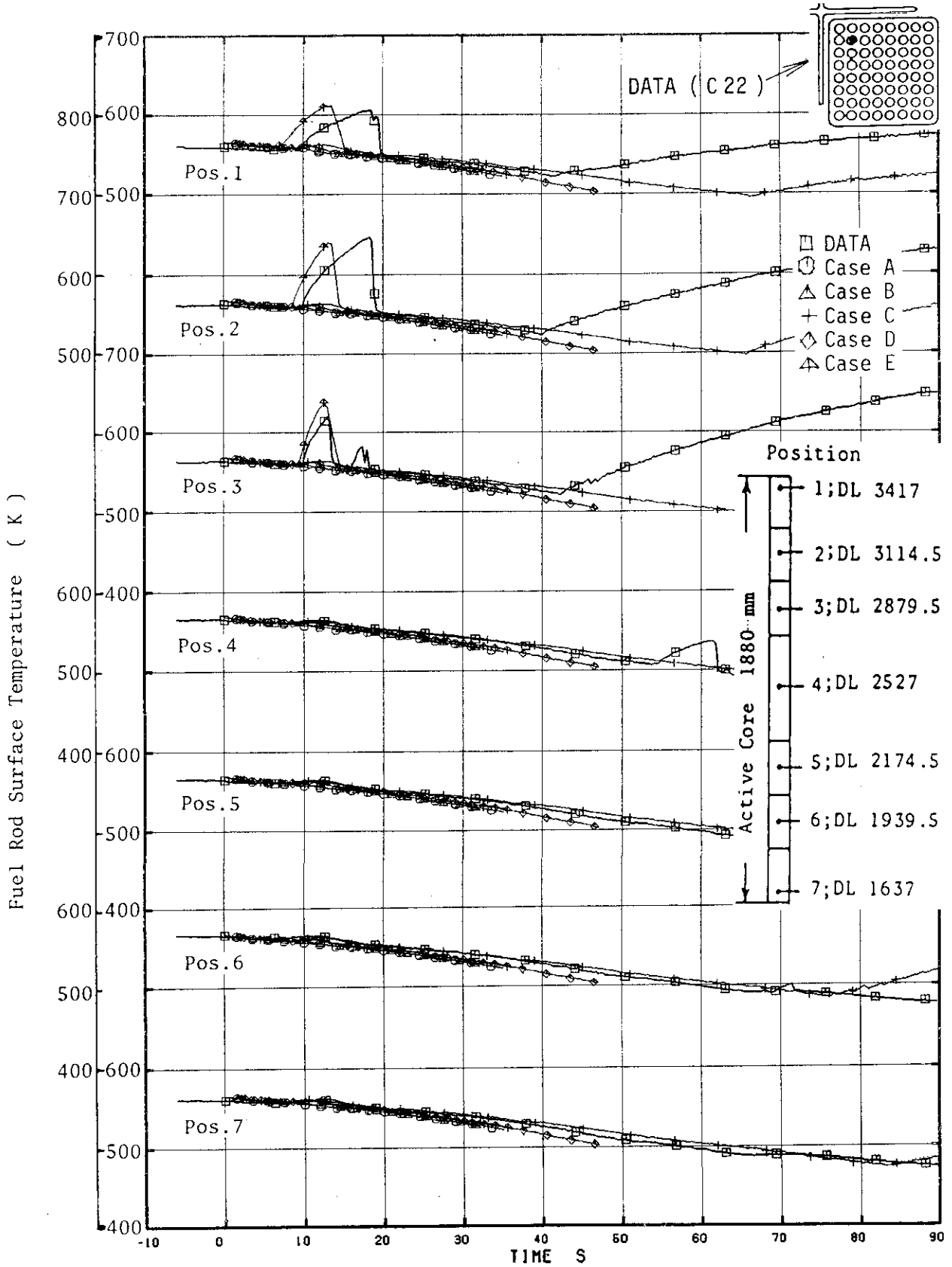


Fig. 4.67 Fuel Surface Temperatures (Average-Power Channel)

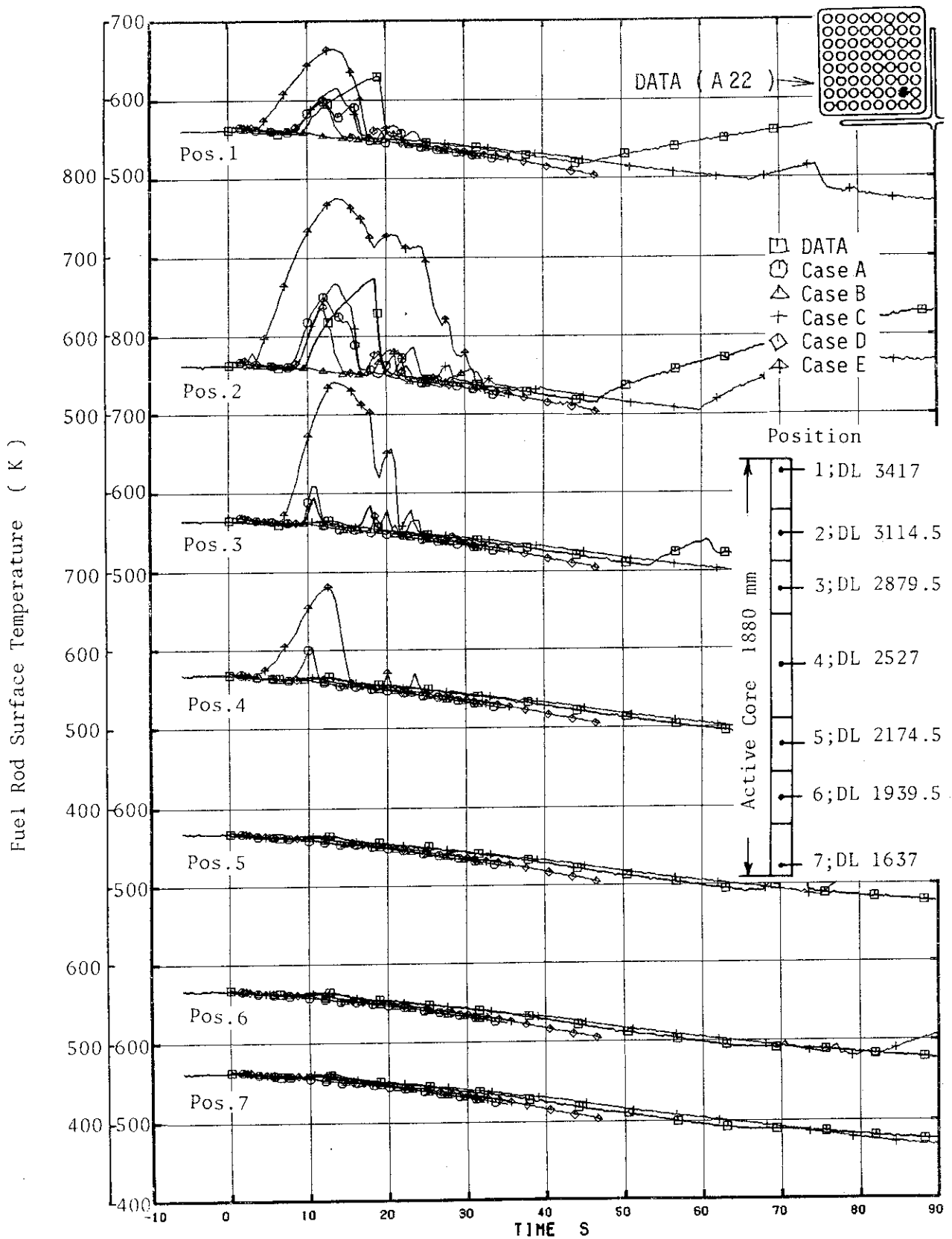


Fig. 4.68 Fuel Surface Temperatures (Peak-Power Channel)

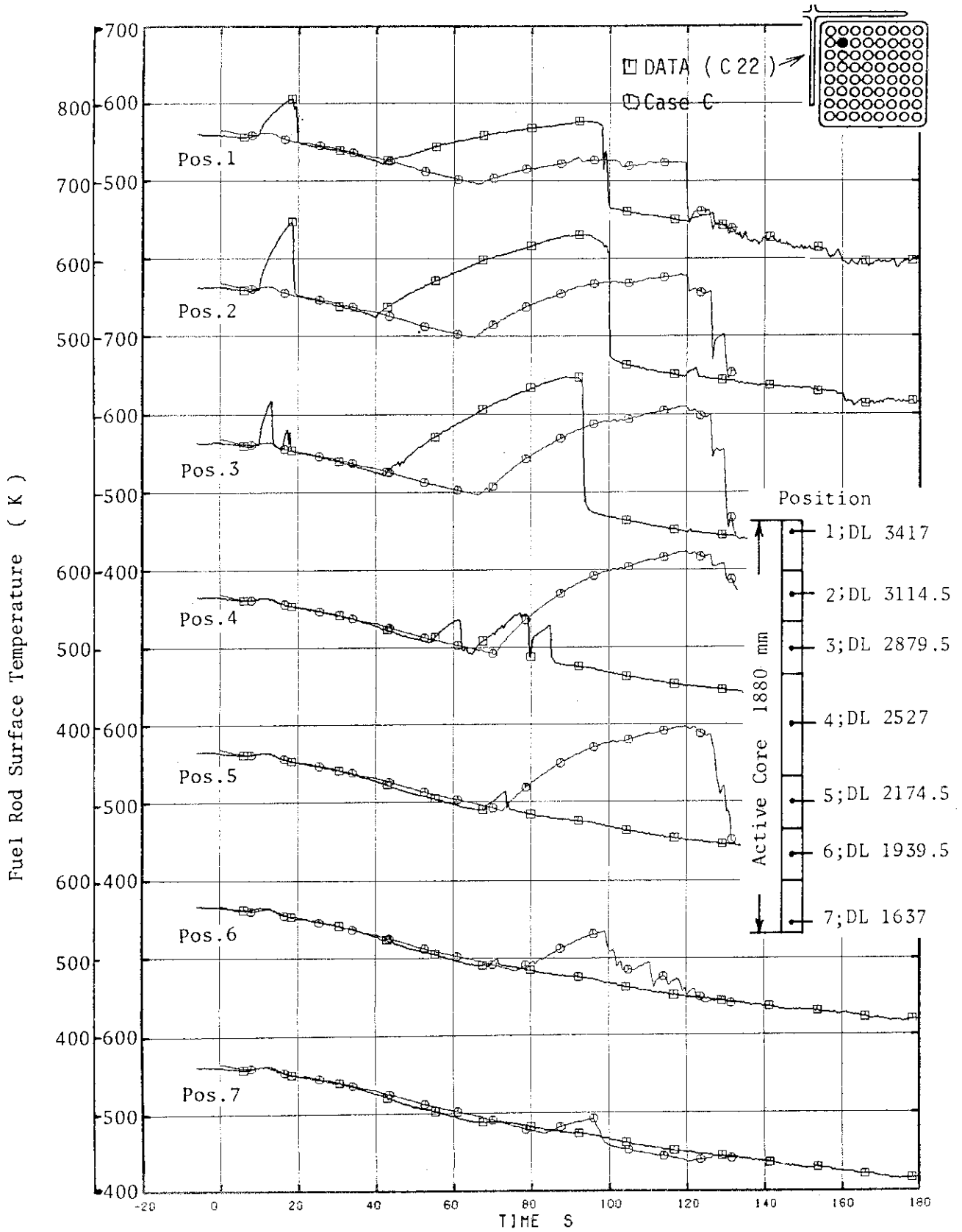


Fig. 4.69 Fuel Surface Temperatures (Average-Power Channel) (Case C)

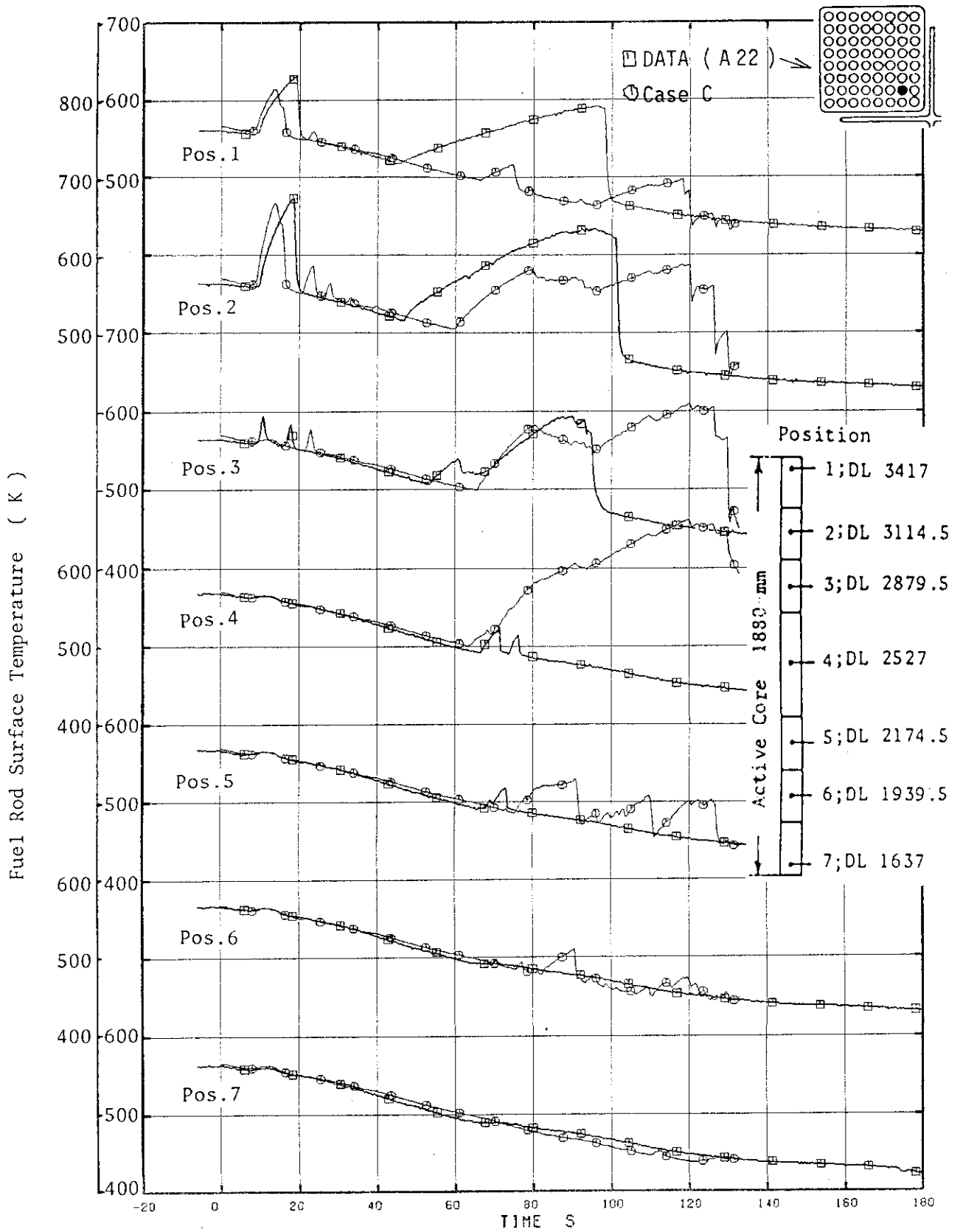


Fig. 4.70 Fuel Surface Temperatures (Peak-Power Channel) (Case C)

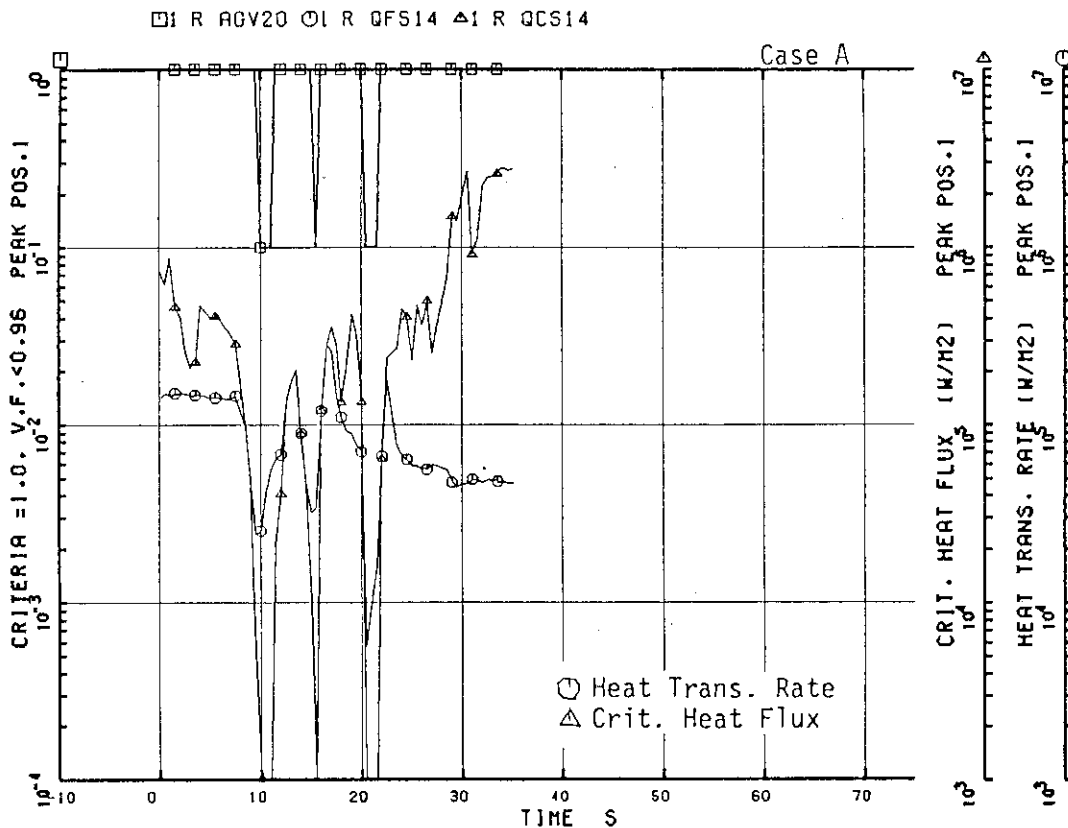


Fig. 4.71 CHF and Heat Transfer Rate at Position 1 in Peak-Power Channel (Case A)

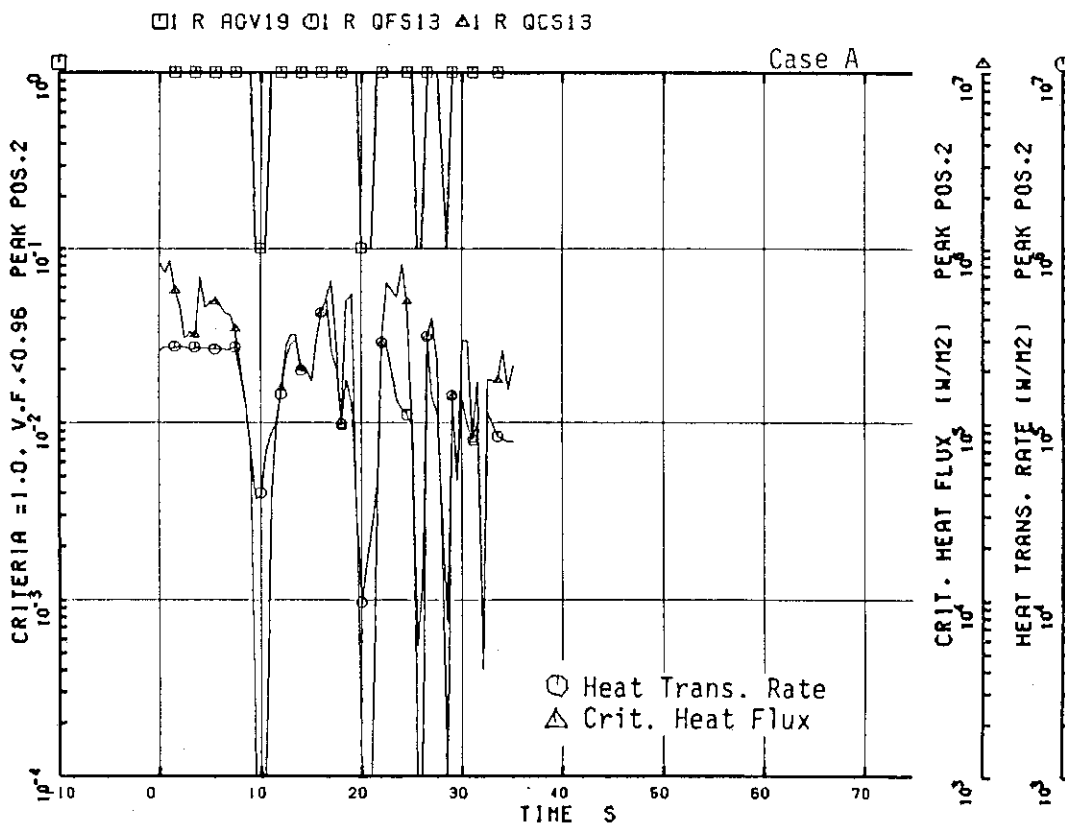


Fig. 4.72 CHF and Heat Transfer Rate at Position 2 in Peak-Power Channel (Case A)

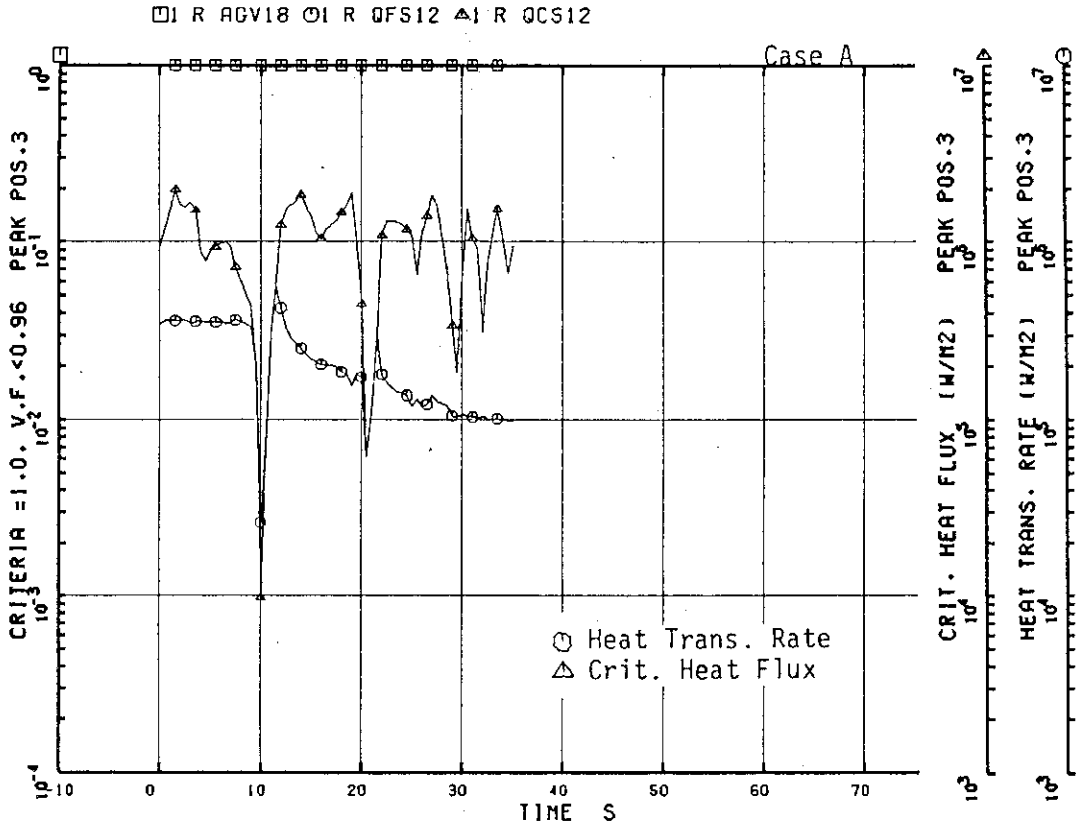


Fig. 4.73 CHF and Heat Transfer Rate at Position 3 in Peak-Power Channel (Case A)

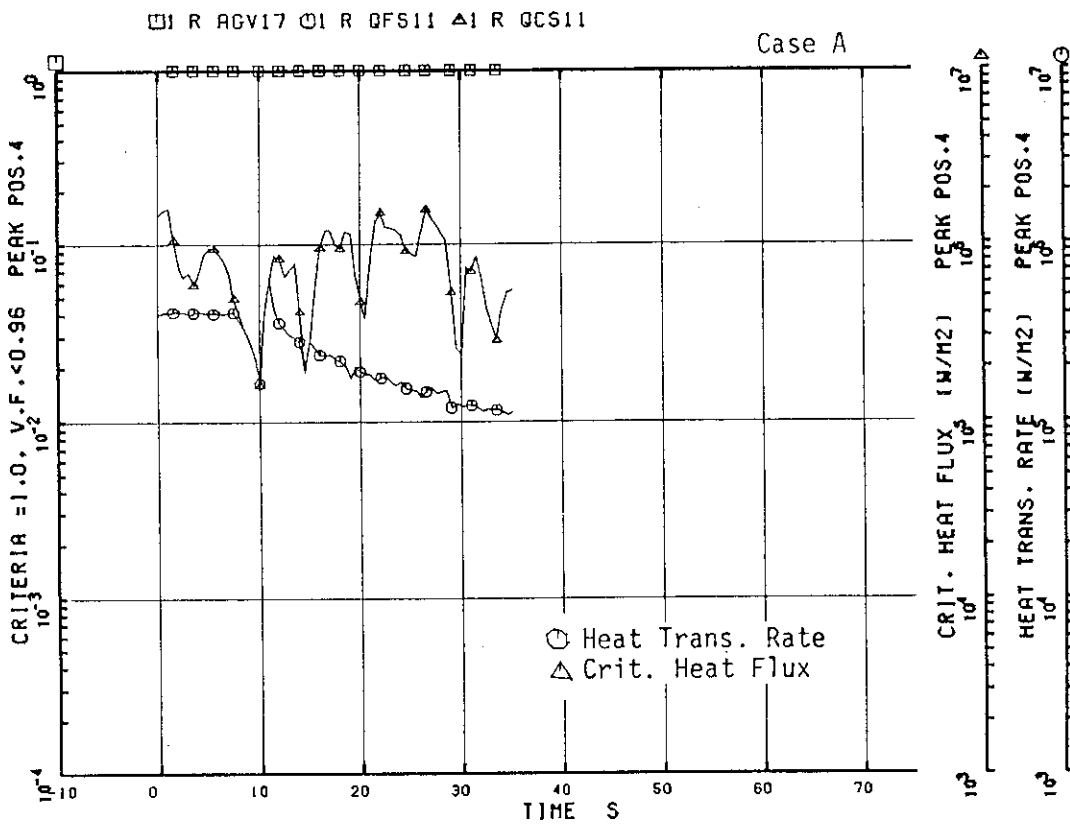


Fig. 4.74 CHF and Heat Transfer Rate at Position 4 in Peak-Power Channel (Case A)

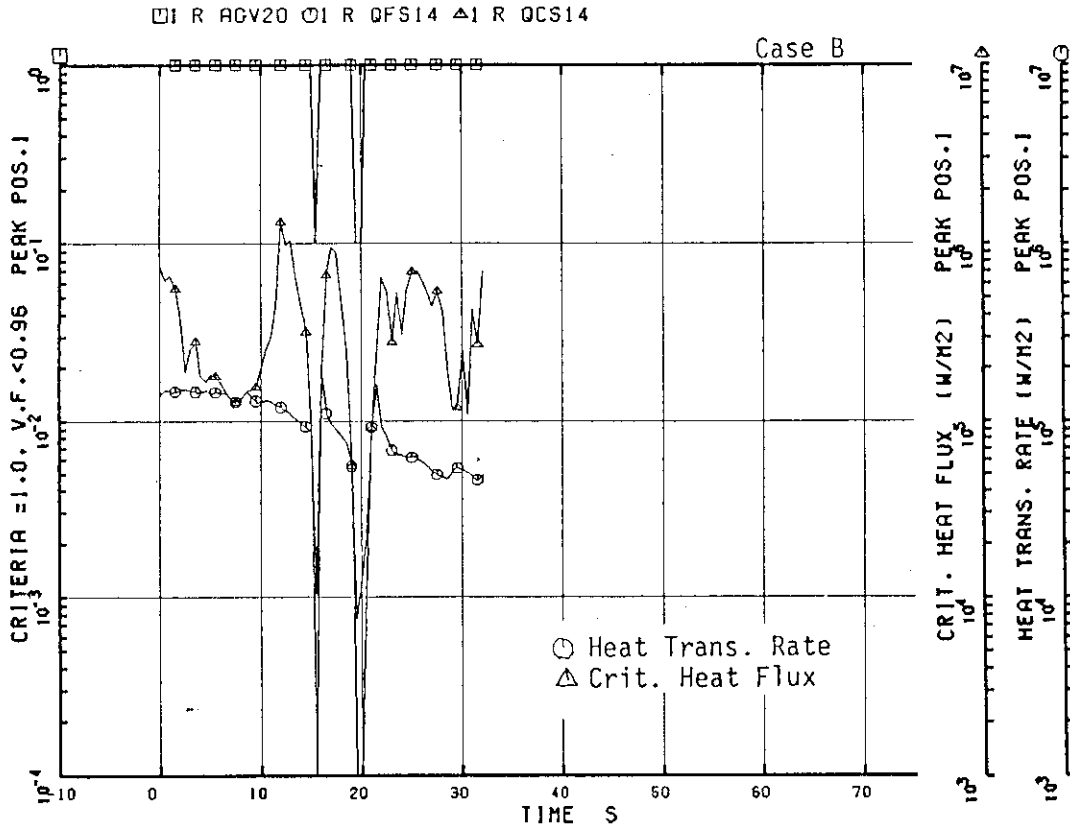


Fig. 4.75 CHF and Heat Transfer Rate at Position 1 in Peak-Power Channel (Case B)

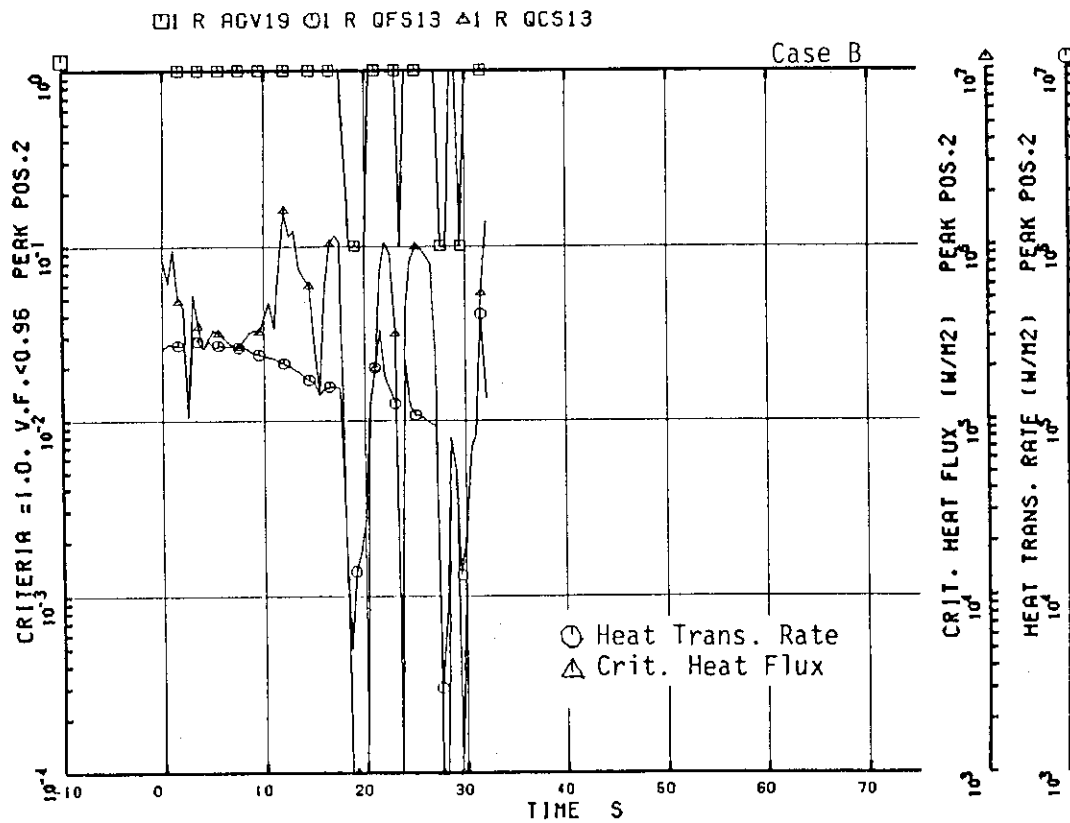


Fig. 4.76 CHF and Heat Transfer Rate at Position 2 in Peak-Power Channel (Case B)

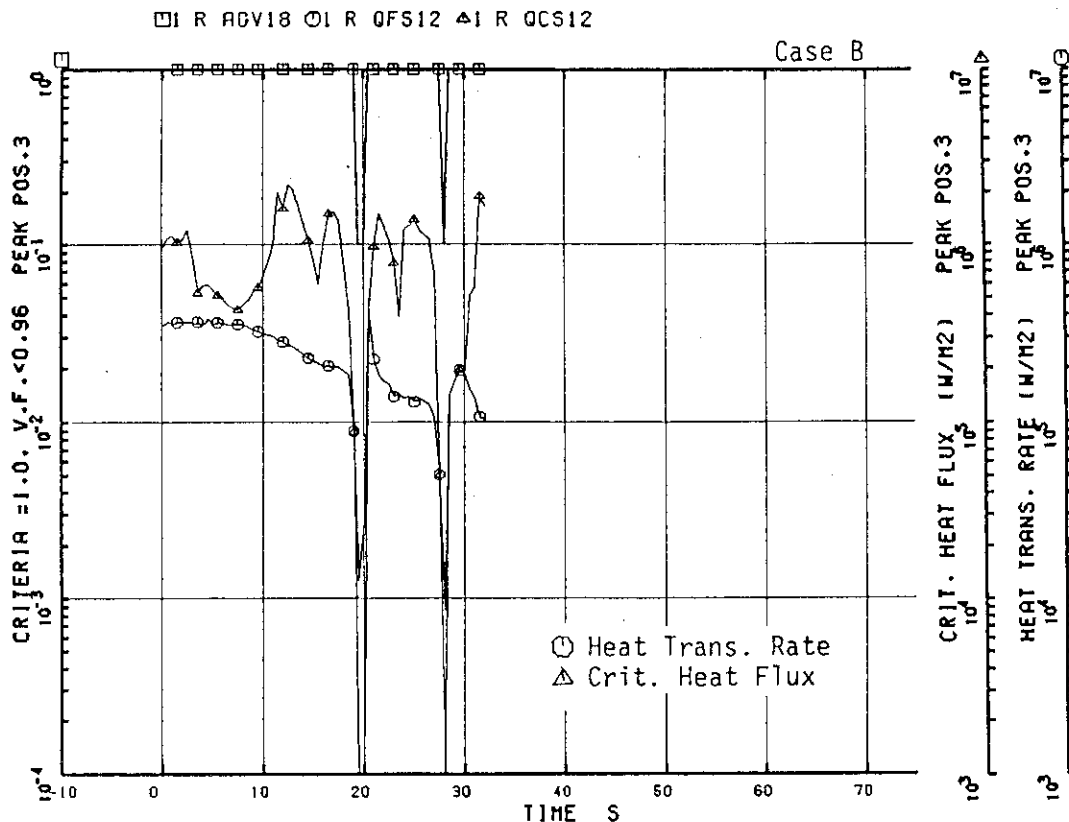


Fig. 4.77 CHF and Heat Transfer Rate at Position 3 in Peak-Power Channel (Case B)

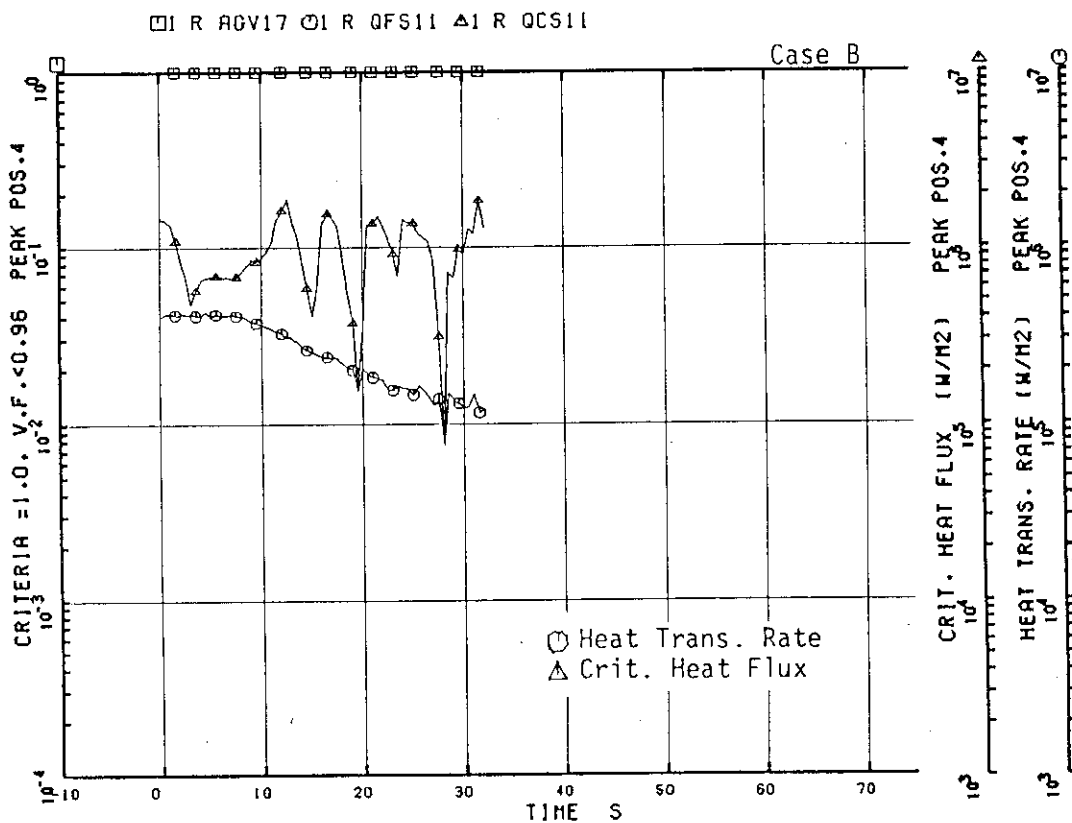


Fig. 4.78 CHF and Heat Transfer Rate at Position 4 in Peak-Power Channel (Case B)

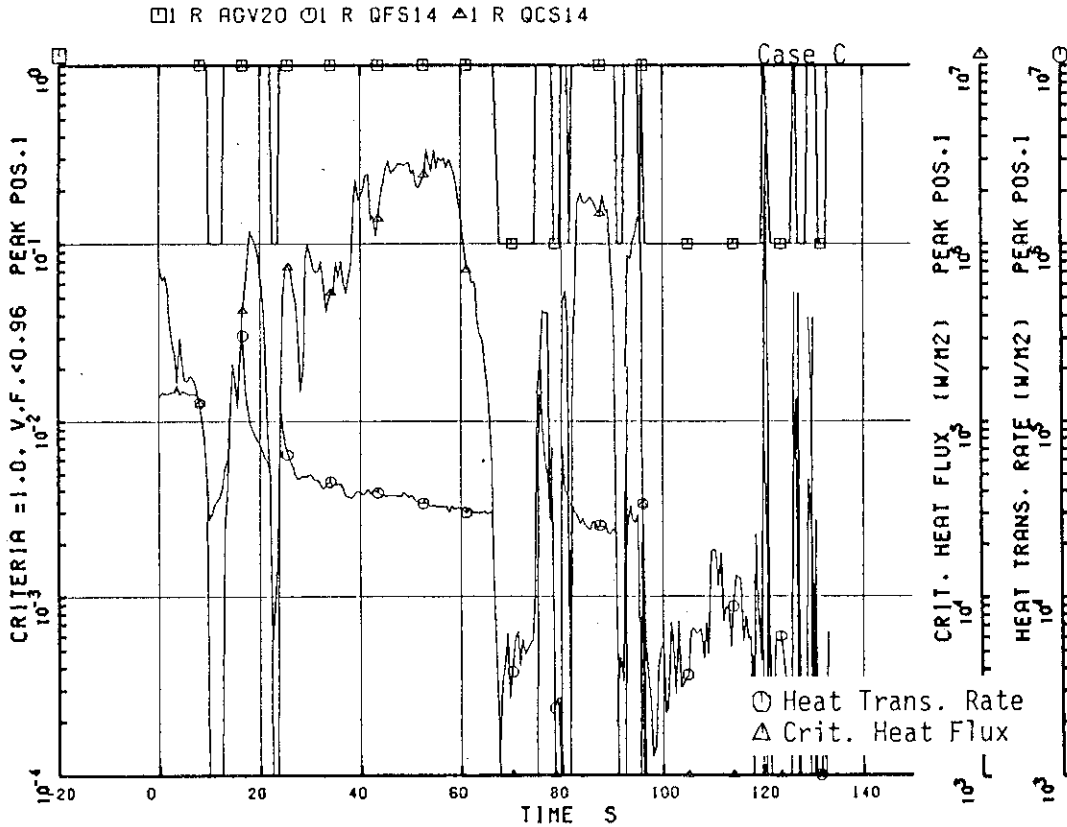


Fig. 4.79 CHF and Heat Transfer Rate at Position 1 in Peak-Power Channel (Case C)

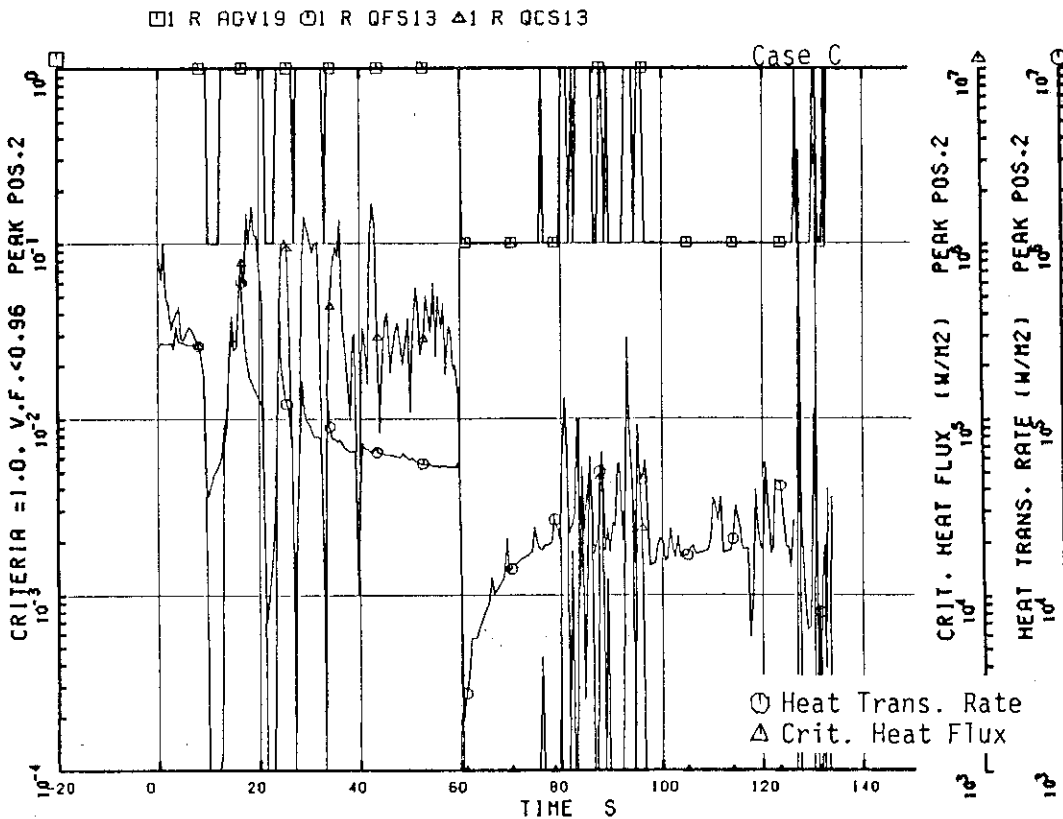


Fig. 4.80 CHF and Heat Transfer Rate at Position 2 in Peak-Power Channel (Case C)

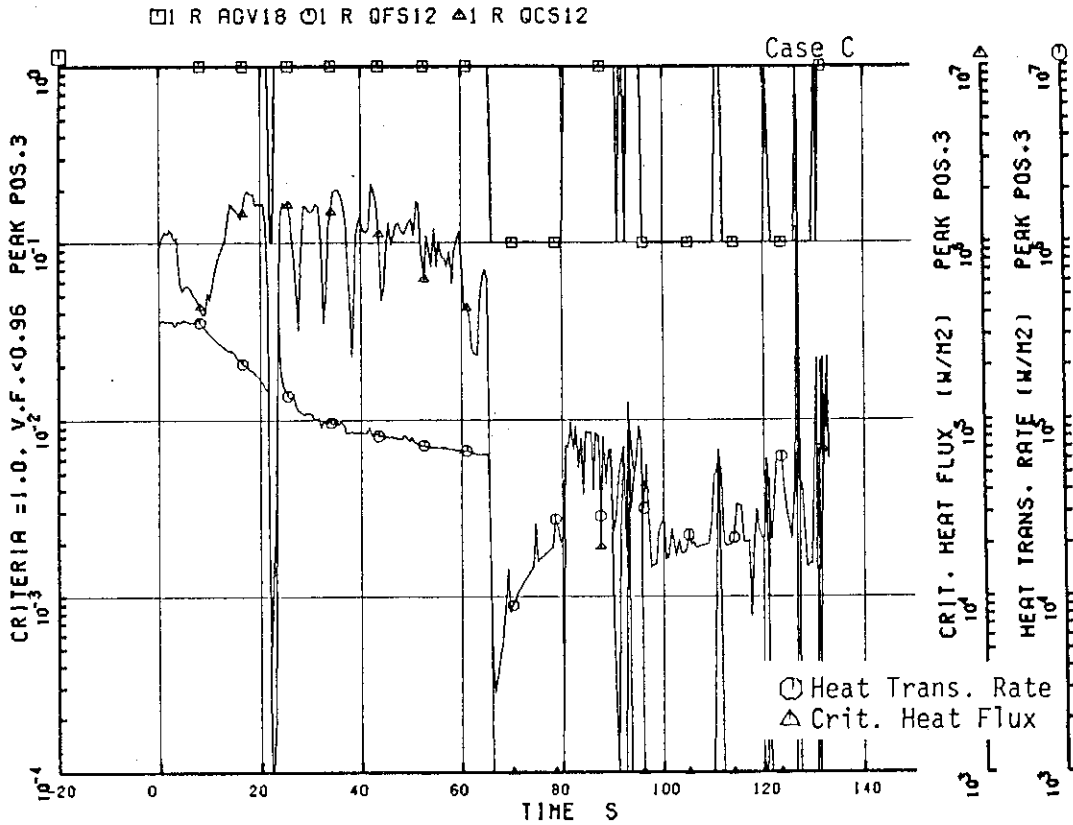


Fig. 4.81 CHF and Heat Transfer Rate at Position 3 in Peak-Power Channel (Case C)

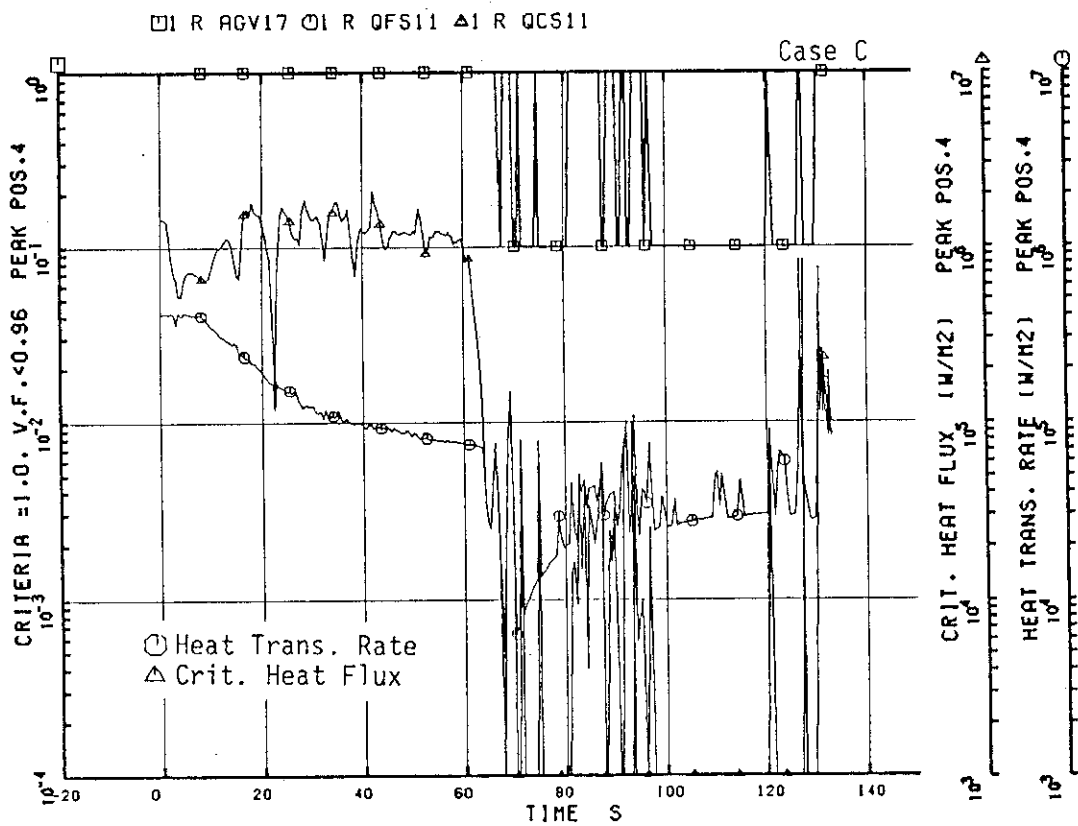


Fig. 4.82 CHF and Heat Transfer Rate at Position 4 in Peak-Power Channel (Case C)

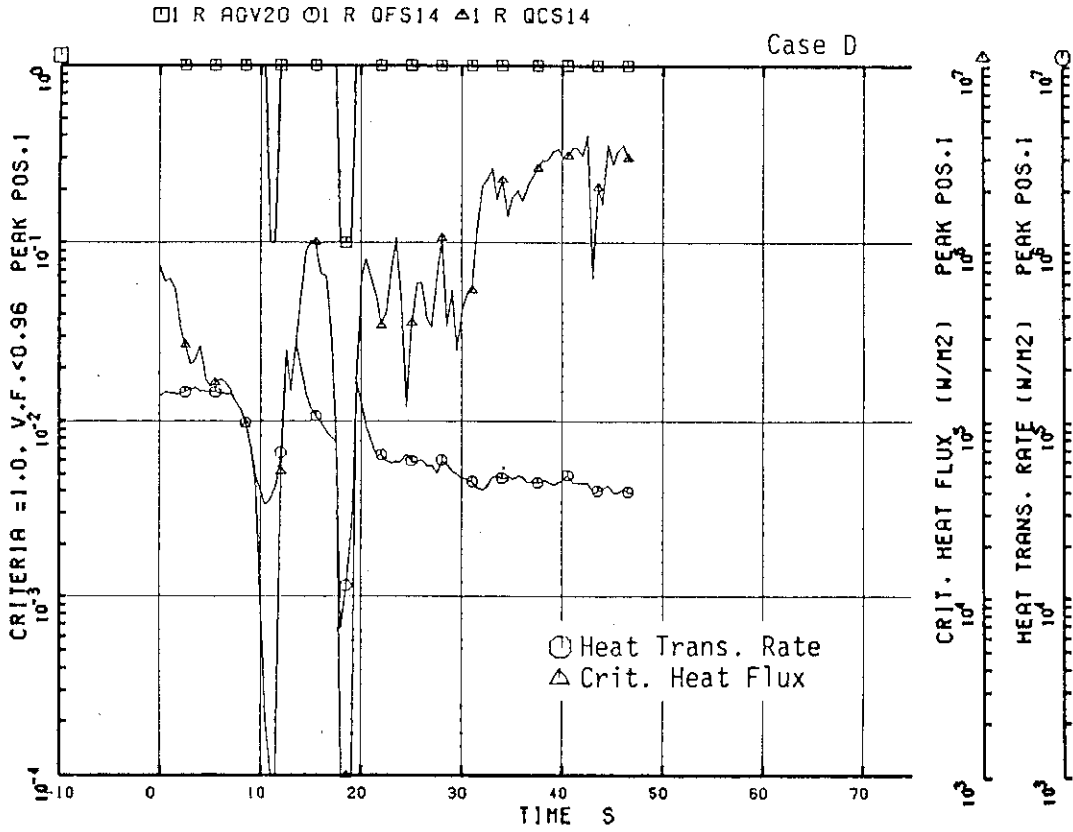


Fig. 4.83 CHF and Heat Transfer Rate at Position 1 in Peak-Power Channel (Case D)

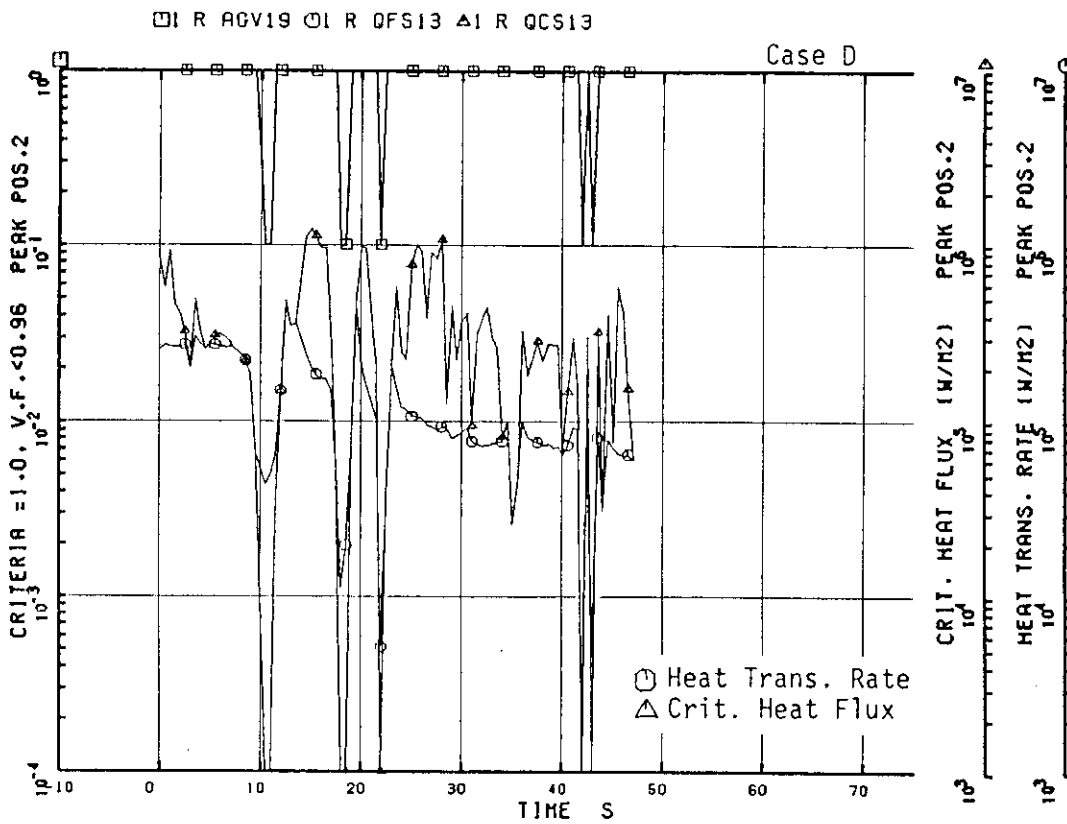


Fig. 4.84 CHF and Heat Transfer Rate at Position 2 in Peak-Power Channel (Case D)

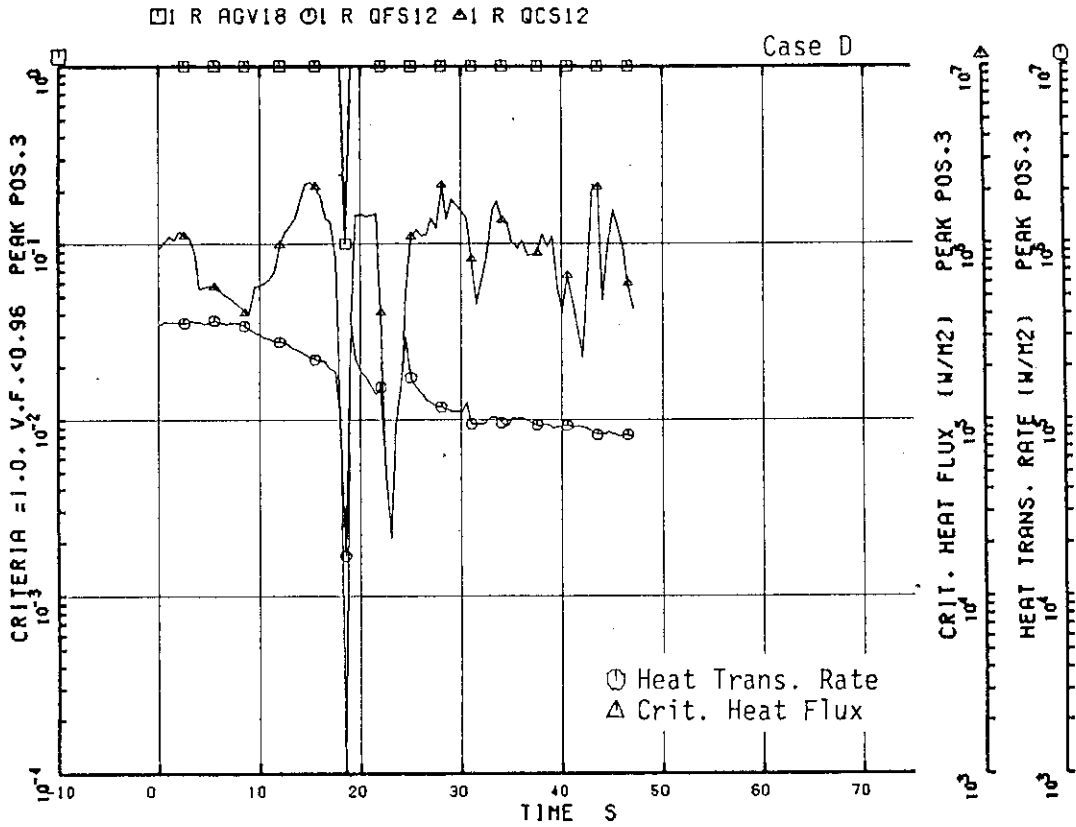


Fig. 4.85 CHF and Heat Transfer Rate at Position 3 in Peak-Power Channel (Case D)

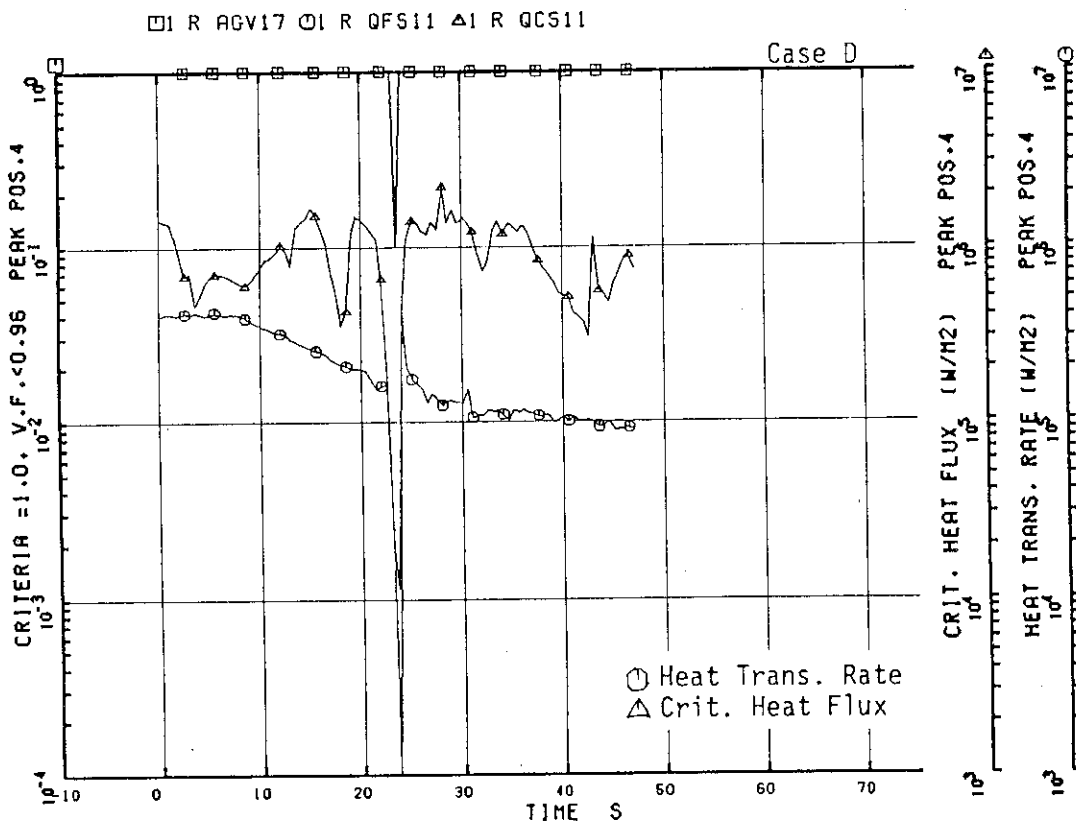


Fig. 4.86 CHF and Heat Transfer Rate at Position 4 in Peak-Power Channel (Case D)

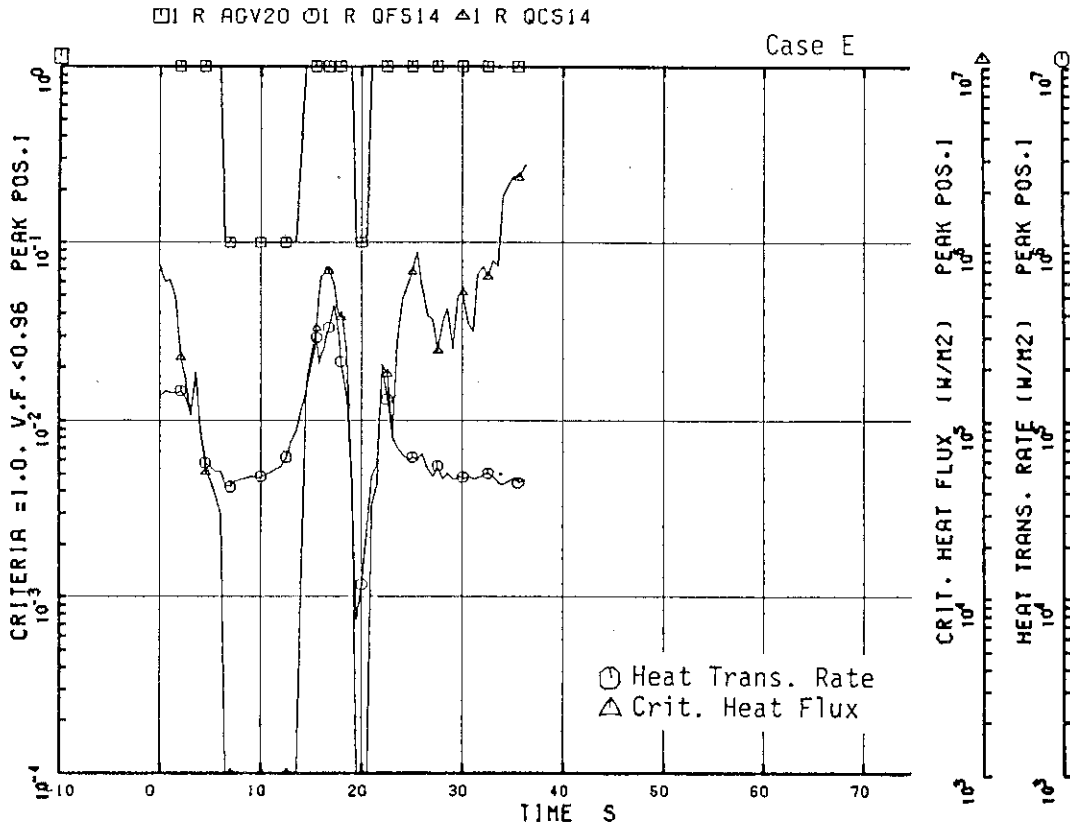


Fig. 4.87 CHF and Heat Transfer Rate at Position 1 in Peak-Power Channel (Case E)

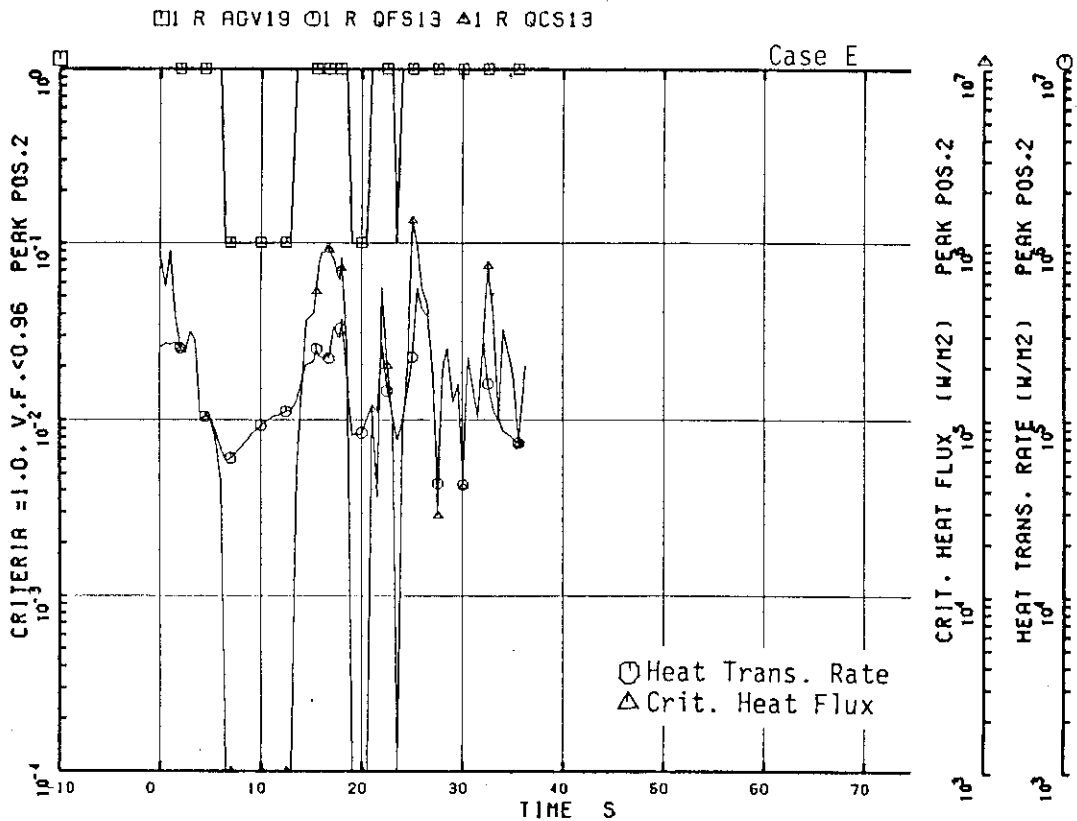


Fig. 4.88 CHF and Heat Transfer Rate at Position 2 in Peak-Power Channel (Case E)

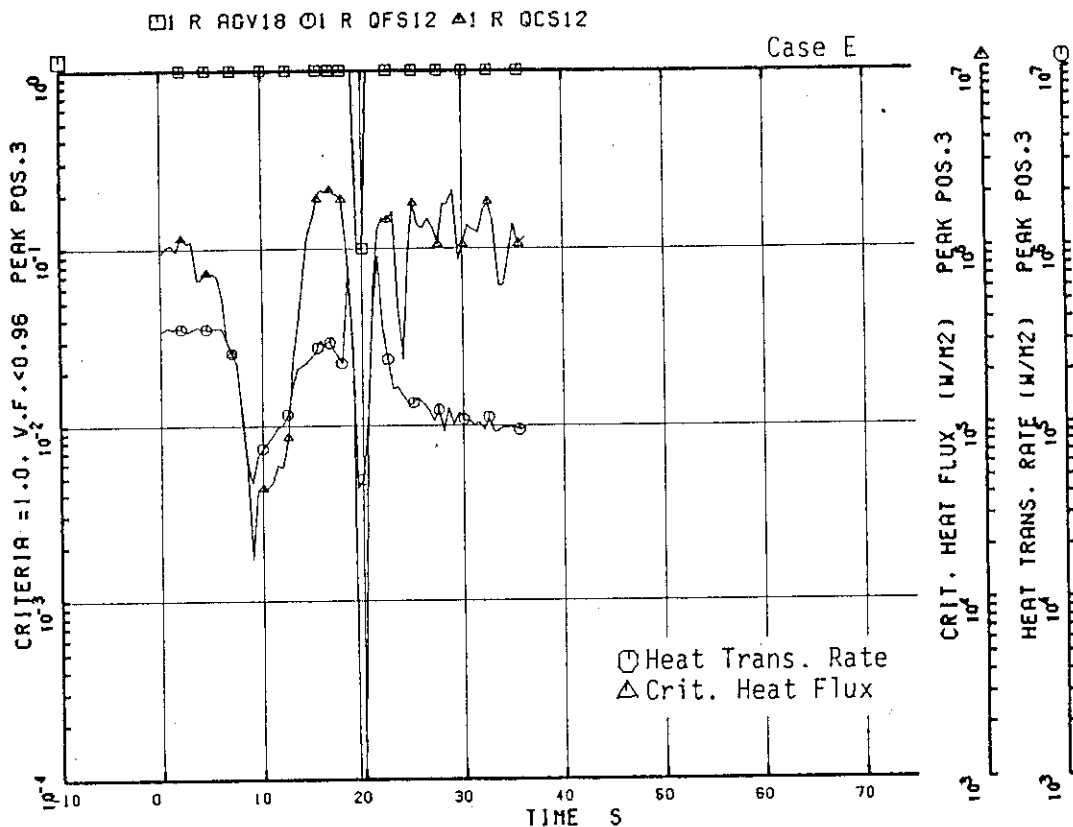


Fig. 4.89 CHF and Heat Transfer Rate at Position 3 in Peak-Power Channel (Case E)

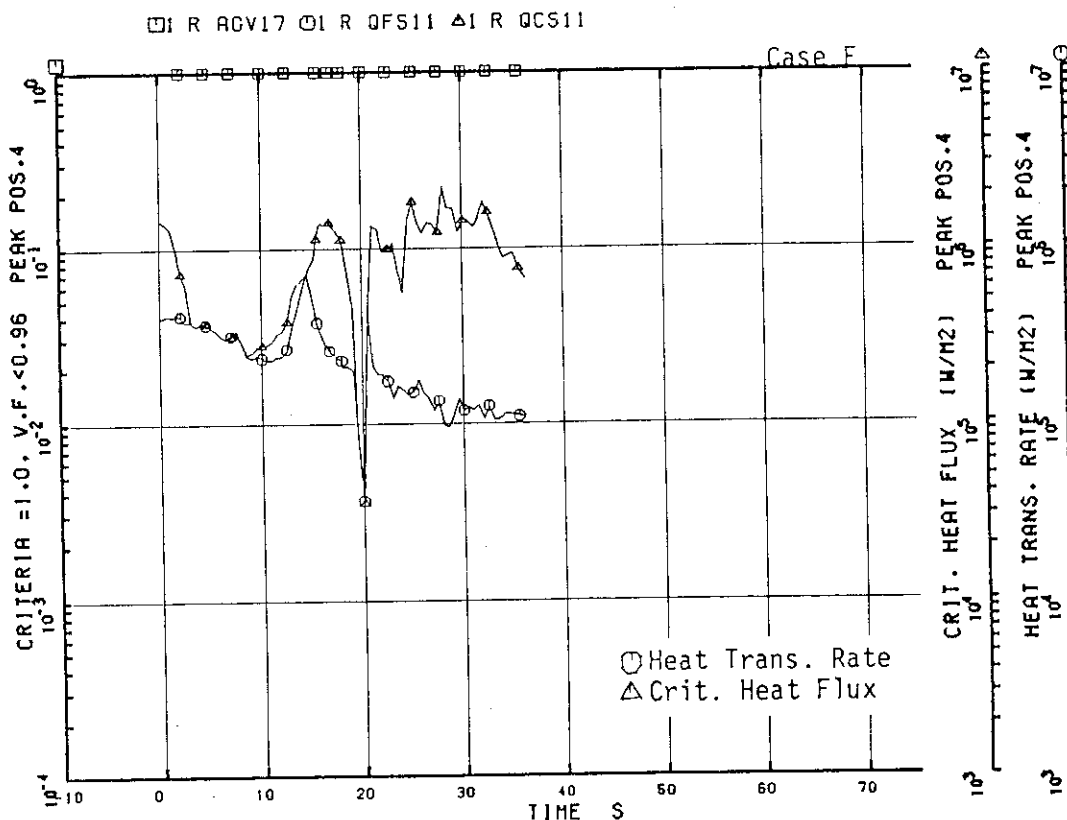


Fig. 4.90 CHF and Heat Transfer Rate at Position 4 in Peak-Power Channel (Case E)

5. CONCLUSIONS

The post test calculations of the ROSA-III large break test, RUN 901, were performed with the RELAP4J and the RELAP5/MOD1/001 codes and the following conclusions were obtained.

- (1) The system pressure calculated with the two codes agreed well with the data.
- (2) RELAP4J satisfactorily calculated the overall behavior of the mixture level in the core and the core inlet flow behavior until the beginning of the lower plenum flashing (LPF). However, the homogenous two-phase flow model was not able to predict the water penetration into the core through the upper tie plate. As a result, the spray water was calculated to accumulate in the upper plenum.
- (3) RELAP5 satisfactorily calculated the rewet in the core after the LPF. The top-down quench following the whole core uncovering was calculated by the advanced two-phase flow model in the code. However, the counter current flow calculation was inadequate and this resulted in the accumulation of the spray water in the upper plenum and a delay in the reflooding of the core. The beginning of the fall in core mixture level after the LPF was also delayed. Incorporation of the counter current flow limiting (CCFL) model and/or the improvement in the interphase drag correlation should enable more accurate calculation of the mixture level behavior.
- (4) The break flow rate was overpredicted with the RELAP5 characteristic analysis model. Therefore, an appropriate discharge coefficient or improvement in the break flow model is necessary.
- (5) The use of the jet pump model of the TRAC-BD1 code and the change in the moment of inertia and the rated liquid density data of the ROSA-III main recirculation pump, resulted in good agreement between the calculated and measured core inlet flow rate.

Acknowledgment

The authors wish to express their appreciation Ms. T. Kurosawa of Nihon Computer Bureau Corporation for her help in preparing the report.

References

- (1) H. Nakamura, et al., "ROSA-III 200% Double-ended Break Integral Test RUN 901 (Full ECCS Actuation)", JAERI-M 84-007, (1984).
- (2) Y. Anoda, et al., "ROSA-III System Description for Fuel Assembly No. 4", JAERI-M 9363, (1981).
- (3) N. Abe, et al., "Electric Power Transient Curve for ROSA-III Test", JAERI-M 8728 (1980).
- (4) "General Electric Standard Safety Analysis Report BWR/6", DOCKET-STN-50447-48, GE, Co. (1975).
- (5) Y. Motizuki, et al. "LOCA Analysis Program RELAP4J for Water Cooled Nuclear Reactors (Modification of RELAP4-Mod 2)", JAERI-M 7506 (1978).
- (6) J. F. Wilson, et al., "The Velocity of Rising Steam in a Bubbling Two-Phase Mixture", ANS Transaction 5(1), 151-152, (1962).
- (7) EG&G, "RELAP5/MOD1 Code Manual", NUREG/CO-1826 (Volume 1,2) (1980).
- (8) M. Katoh, et al., "ROSA-III Small Break Test Analysis by RELAP5/MOD1 Code", International Meeting on Thermal Nuclear Reactor Safety, Chicago, USA, (August 1982).
- (9) EG&G, "TRAC-BD1: An Advanced Best Estimate Computer Program for Boiling Water Reactor Loss-of-Coolant Accident Analysis", NUREG/CR-2178 EGG-2109 (Volume 1,2) (1981).
- (10) M. Okazaki, et al., "Development of JAERI Jet Pump Model for RELAP5/MOD1 Code", internal report, (1984).

Acknowledgment

The authors wish to express their appreciation Ms. T. Kurosawa of Nihon Computer Bureau Corporation for her help in preparing the report.

References

- (1) H. Nakamura, et al., "ROSA-III 200% Double-ended Break Integral Test RUN 901 (Full ECCS Actuation)", JAERI-M 84-007, (1984).
- (2) Y. Anoda, et al., "ROSA-III System Description for Fuel Assembly No. 4", JAERI-M 9363, (1981).
- (3) N. Abe, et al., "Electric Power Transient Curve for ROSA-III Test", JAERI-M 8728 (1980).
- (4) "General Electric Standard Safety Analysis Report BWR/6", DOCKET-STN-50447-48, GE, Co. (1975).
- (5) Y. Motizuki, et al. "LOCA Analysis Program RELAP4J for Water Cooled Nuclear Reactors (Modification of RELAP4-Mod 2)", JAERI-M 7506 (1978).
- (6) J. F. Wilson, et al., "The Velocity of Rising Steam in a Bubbling Two-Phase Mixture", ANS Transaction 5(1), 151-152, (1962).
- (7) EG&G, "RELAP5/MOD1 Code Manual", NUREG/CO-1826 (Volume 1,2) (1980).
- (8) M. Katoh, et al., "ROSA-III Small Break Test Analysis by RELAP5/MOD1 Code", International Meeting on Thermal Nuclear Reactor Safety, Chicago, USA, (August 1982).
- (9) EG&G, "TRAC-BD1: An Advanced Best Estimate Computer Program for Boiling Water Reactor Loss-of-Coolant Accident Analysis", NUREG/CR-2178 EGG-2109 (Volume 1,2) (1981).
- (10) M. Okazaki, et al., "Development of JAERI Jet Pump Model for RELAP5/MOD1 Code", internal report, (1984).


```

*** PUMP HEAD OR TORQUE DATA CARDS ***
HEAD= ROSA-III MRP PUMP
TORQUE= BINGHAM PUMP

IT IC N PHEAD(1) OR PTORK(1), PHEAD(2) OR PTORK(2) -----
* HEAD
103011 1 1 5 0.0 0.92 0.2 0.94 0.4 0.97
103012 1 2 5 0.0 1.0 1.0 0.0 0.4 0.12
103021 1 2 5 0.0 -0.2 0.25 0.0 0.4 0.12
103022 1 3 5 0.7' 0.5 1.0 1.0 0.0 0.0
103031 1 3 5 -1.0 1.2 -0.8 0.98 -0.6 0.94
103032 1 3 5 -0.3 0.92 0.0 0.92 0.0 0.0
103041 1 4 5 -1.0 1.2 -0.8 0.7 -0.5 0.34
103042 1 5 5 0.0 0.18 0.0 0.18 0.0 0.0
103051 1 5 5 0.0 0.62 0.20 0.69 0.40 0.77
103052 1 6 5 0.6 0.85 1.0 1.00 0.0 0.0
103061 1 6 5 0.0 0.18 0.20 0.22 0.40 0.32
103062 1 7 5 0.65 0.52 1.00 1.00 0.0 0.0
103071 1 7 5 -1.0 0.00 -0.80 0.16 -0.4 0.45
103072 1 8 5 -0.2 0.56 0.0 0.62 0.0 0.0
103081 1 8 5 -1.0 0.00 -0.80 -0.14 -0.50 -0.24
103082 1 8 5 -0.20 -0.24 0.0 -0.20 0.0 0.0
* TORQUE
103091 2 1 5 0.0 -0.46 -0.2 0.54 -0.5 -0.67
103092 2 2 5 0.8 -0.86 1.0 1.0 0.08 0.5 0.34
103101 2 2 5 0.0 -0.1 0.2 0.08 0.5 0.34
103102 2 3 5 0.8 0.65 1.0 1.0 0.68 -0.5 0.48
103111 2 3 5 -1.0 0.7 -0.8 0.68 -0.5 0.48
103112 2 4 5 -1.0 0.44 0.0 0.46 -0.4 0.38
103121 2 4 5 -1.0 0.7 -0.7 0.45 -0.4 0.38
103122 2 5 5 -0.2 0.32 0.0 0.28 -0.53 0.6 -0.3
103131 2 5 5 0.8 -0.2 1.0 -0.1 0.22 0.5 -0.1
103132 2 6 5 0.0 0.28 0.2 0.22 0.5 -0.1
103141 2 6 5 0.0 0.28 0.2 0.22 0.5 -0.1
103142 2 7 5 0.8 0.0 1.0 -0.1 0.22 0.5 -0.1
103151 2 7 5 -1.0 -1.4 -0.8 -1.25 -0.5 -1.0
103152 2 8 5 -0.2 -0.8 0.0 -0.66 -0.5 -0.66
103161 2 8 5 -1.0 -1.4 -0.6 -0.8 -0.5 -0.66
103162 2 8 5 -0.2 -0.3 0.0 -0.1 -0.5 -0.66
*** VALVE DATA CARDS ***
ITCV IACV LATCH PCV CV1 CV2 CV3
110010 13 0.0 0.0 0.0
110020 12 0.0 0.0 0.0
110030 3 0.0 0.0 0.0
110040 -15 0.0 0.0 0.0
* ITCV IACV LATCH PCV CV1 CV2 CV3
110010 13 0.0 0.0 0.0 * AV 127 TRIP
110020 12 0.0 0.0 0.0 * MSIV L2 TRIP
110030 3 0.0 0.0 0.0 * FW L2 TRIP
110040 -15 0.0 0.0 0.0 * NO USED
*** LEAK TABLE CARDS ***
NAREA SINK TAREA(1),TAREA(2),-----
ITLEAK (PSIA)
120100 -3 2 14.7 0.0 1.0 1000.0 1.0 * BREAK A START
120200 -3 2 14.7 0.0 1.0 1000.0 1.0 * BREAK B START
120300 -6 8 14.7 0.0 0.0 129.3 0.0 130.1 1.0 * MSIV L2 TRIP
120301 146.0 0.0 2000.0 0.0 * ADS
120401 -3 12 14.7 0.0 1.0 9.15 0.0 1000.0 0.0 * MSIV L2 TRIP
120501 -3 3 14.7 0.0 0.0 3.30 0.0 1000.0 0.0 * FW L2 TRIP
*HPCS,LEAK

```

```

* * * * *
* 180101 -5 572. 16.7 932. 16.2 1292. 15.7 1652. 15.2 * BN
* 180102 1832. 15.5
* 180201 -3 68. 10.1 212. 8. 4712. 6.72
* 180301 1 32. 3.36
* 180401 -9 70. 8.58 200. 9.08 400. 10.1 600. 11.1 *INCONEL 600
* 180402 800. 12.1 1000. 13.2 1200. 14.3 1400. 15.5
* 180403 1600. 16.7
* 180501 -2 32. 9.41 932. 12.1
* 180601 -11 392. 15.4 572. 11.9 752. 9.92 932. 8.13 *MGO
* 180602 1112. 6.77 1292. 5.81 1472. 5.08 1832. 3.99
* 180603 2192. 3.63 2252. 3.87 2912. 4.23
* 180701 1 32. 8.42
* * * * *
* *** VOLUMETRIC HEAT CAPACITY ***
* * * * *
* NCP TPC(1),TPC(2) -----
* (DEGF) (BTU/FF13)
* * * * *
* 190101 -4 680. 5.28 950. 5.98 1562. 7.55 2300. 9.47 * BN
* 190201 -3 68. 57.4 212. 55.6 4712. 57.4
* 190301 -4 680. 5.28 950. 5.99 1562. 7.56 2300. 9.47 * BN
* 190401 -9 70. 55.7 200. 58.3 400. 60.9 600. 63.6 * INCONEL 600
* 190402 800. 66.2 1000. 69.3 1200. 73.5 1400. 76.2
* 190403 1600. 78.3
* 190501 1 32. 59.3
* 190601 1 32. 50.3
* 190701 1 32. 54.3
* * * * *
* *** LINEAR EXPANSION COEFF., HEAT EXCHANGER DATA
* *** 20XXXX, 21XXXX ARE NOT USED.
* * * * *
* *** OTHER INPUT OPTIONS ARE NOT USED. ***
* * * * *
* *** END OF INPUT DATA CARDS ****
* * * * *
* 0 0
* * * * *

```

```

* * * * *
* 4.17 4.17 14.14 3.31 0.0
* 0.0 6.043 0.06083 0.0 0.04285
* 0.0 6.043 -0.6083 0.0 0.04285
* 0.0 6.043 0.06083 0.0 0.04285
* 0.0 12.09 -1217 0.0 0.04285
* 0.0 6.043 -0.6083 0.0 0.04285
* 0.0 6.043 0.06083 0.0 0.04285
* 0.0 6.043 -0.6083 0.0 0.04285
* 41.41 41.41 11.08 2.66 0.0
* 0.0 17.51 0.143 0.0 0.04718
* * * * *
* PFR HTC
* * * * *
* 150092 0.0264 8.74
* 150102 0.0015 8.74
* 150182 0.0155 8.74
* * * * *
* *** CORE SLAB DATA ***
* * * * *
* ISLB NODT1 NODT2 NODT3 CHAN(FT) CLTI HEDIAN GFRACT
* 160010 1 1 4 0 9 0.771 0.0 0.04718 0.04109
* 160020 2 1 4 0 9 0.771 0.0 0.04718 0.07690
* 160030 3 1 4 0 9 0.771 0.0 0.04718 0.10360
* 160040 4 1 4 0 9 1.541 0.0 0.04718 0.23860
* 160050 5 1 4 0 9 0.771 0.0 0.04718 0.10360
* 160060 6 1 4 0 9 0.771 0.0 0.04718 0.07690
* 160070 7 1 4 0 9 0.771 0.0 0.04718 0.04109
* 160080 11 1 4 0 9 0.771 0.0 0.04718 0.01918
* 160090 12 1 4 0 9 0.771 0.0 0.04718 0.03589
* 160100 13 1 4 0 9 0.771 0.0 0.04718 0.04833
* 160110 14 1 4 0 9 1.542 0.0 0.04718 0.11140
* 160120 15 1 4 0 9 0.771 0.0 0.04718 0.04833
* 160130 16 1 4 0 9 0.771 0.0 0.04718 0.03589
* 160140 17 1 4 0 9 0.771 0.0 0.04718 0.01918
* * * * *
* *** CORE SLAB FOR EM 16XXXX NOT USED ***
* * * * *
* *** SLAB GEOMETRY DATA ***
* * * * *
* O1 IG NR IGP IM NDX XR XR PF
* O2 IM NDX (FT) (FT) PF
* * * * *
* 170101 2 4 0 0 3 0.0 0.01001 0.0
* 170102 0 2 1 0.002297 1.0
* 170103 0 3 1 0.003557 0.0
* 170104 0 4 3 0.004265 0.0
* 170201 2 3 7 1 0.0 0.008203 0.0
* 170202 0 6 1 0.004922 0.0
* 170203 0 4 1 0.00328 0.0
* 170301 1 1 5 10 0.0 0.13 0.0
* 170401 1 1 5 10 0.0 0.509 0.0
* 170501 1 1 5 10 0.0 0.18 0.0
* * * * *
* *** THERMAL CONDUCTIVITY DATA
* * * * *
* * * * *
* NKP TPK(1),TPK(2) -----
* (DEGF) (BTU/FF13)
* * * * *

```


NO	NAME	LEN	VOL	HZ	VR	ELV	ROUG	HYD	FE	CTL	PRESSURE	TEMP	ZERO	FR	TO	AREA	F-LOSS	R-LOSS	CAHS	FLOW-F	FLOW-G	VELJ	JUN NO
0200101	0.07849	2																					
0200201	0.04366	1																					
0200301	0.2550	1																					
0200302	0.7819	2																					
0200401	0.0	2																					
0200501	0.0	2																					
0200601	90.0	2																					
0200701	0.2550	1																					
0200702	0.7819	2																					
0200801	0.00005	0.03714	2																				
0200901	2.77	2.77	1																				
0201001	0.0	2																					
0201101	0.0000	1																					
0201201	3	7.34788+6	551.7	0.0	0.0	1																	
0201202	3	7.34475+6	551.7	0.0	0.0	2																	
0201300	1																						
0201301	15.85	0.0	0.0	1																			
***** (VOLUME 3) ***** RELAP4J *****																							
* CORE INLET CHAMBER (2 VOLUMES) (VOLUME 3) RELAP4J																							
0300000	NAME	TYPE																					
0300000	C030	BRANCH																					
0300001	NO JUN	INITIAL C.C																					
0300001	3	1																					
0300101	AREA	LEN	VOL	HZ	VR	ELV	ROUG	HYD	FE														
0300101	0.029355	0.3350	0.0	0.0	90.0	0.2300	0.00005	9.795-3	0.0														
0300200	CTL	PRESSURE	TEMP	ZERO																			
0300200	3	7.34132+6	551.7	0.0																			
***** (VOLUME 3) ***** RELAP4J *****																							
0301101	FR	TO	AREA	F-LOSS	R-LOSS	CAHS																	
0301101	020010000	030000000	0.005352	4.38	4.38	0.0000																	
0302101	030010000	040000000	0.009498	1.75	1.75	0.0000																	
0303101	030010000	100000000	3.937-4	2.64	2.64	0.0000																	
***** (VOLUME 3) ***** RELAP4J *****																							
0301201	FLOW-F	FLOW-G	VELJ																				
0302201	11.8875	0.0	0.0																				
0302201	11.40	0.0	0.0																				
0303201	0.4875	0.0	0.0																				
0310000	C031	BRANCH																					
0310001	3	1																					
0310101	0.009785	0.335	0.0	0.0	90.0	0.23	0.00005	3.265-3	0.0														
0310200	3	7.34132+6	551.7	0.0																			
0311101	020010000	031000000	0.001784	4.38	4.38	0.0000																	
0312101	031010000	045000000	0.003166	1.75	1.75	0.0000																	
0313101	031010000	100000000	1.312-4	2.64	2.64	0.0000																	
0311201	3.9625	0.0	0.0																				
0312201	3.8	0.0	0.0																				
0313201	0.1625	0.0	0.0																				
***** (VOLUME 3) ***** RELAP4J *****																							
* CORE ***** AVERAGE POWER CHANNEL *****																							
0400000	NAME	C040	PIPE																				
0400000	0400000	C040	PIPE																				
0400001	NO.VOL	7																					
0400101	AREA	VOL NO																					
0400101	0.02936	7																					
0400201	AREA	JUN NO																					
0400201	0.0	6																					
0400301	LEN	VOL NO																					
0400301	0.308	1																					
0400302	0.235	3																					
0400303	0.470	4																					
0400304	0.235	6																					
0400305	0.308	7																					
0400401	VOL	VOL NO																					
0400401	0.0	7																					
0400501	HZ	VOL NO																					
0400501	0.0	7																					
0400601	VR	VOL NO																					
0400601	90.0	7																					
0400701	ELV	VOL NO																					
0400701	0.308	1																					
0400702	0.235	3																					
0400703	0.470	4																					
0400704	0.235	6																					
0400705	0.308	7																					
0400801	ROUGH	HYD	VOL NO																				
0400801	0.00005	0.01306	7																				
0400901	F-LOSS	R-LOSS	JUN NO																				
0400901	1.361	1.361	6																				
0401001	FE	VOL NO																					
0401001	0.0	7																					
0401101	CAHS	JUN NO																					
0401101	0.0000	6																					
0401201	CTL	PRESSURE	TEMP	ZERO	VOL																		
0401201	3	7.33881+6	553.1	0.0	0.0	1																	
0401202	3	7.33631+6	557.1	0.0	0.0	2																	
0401203	2	7.33255+6	0.00330	0.0	0.0	3																	
0401204	2	7.32879+6	0.04434	0.0	0.0	4																	
0401205	2	7.32503+6	0.08537	0.0	0.0	5																	
0401206	2	7.32128+6	0.10704	0.0	0.0	6																	
0401207	2	7.31752+6	0.12123	0.0	0.0	7																	
0401300	CTL	1																					
***** (VOLUME 3) ***** RELAP4J *****																							
* CORE ***** AVERAGE POWER CHANNEL *****																							


```

*****
* LOWER DOWNCOMER (JET PUMP INLET) (VOLUME11 .... RELAP4J)
*
* NAME TYPE
* C120 BRANCH
1200000
* NO JUN INITIAL C.C
* 4 1
1200001
*
* AREA LEN VOL HZ VR ELV ROUG HYD FE
* 0.022478 0.541 0.0 0.0 90.0 0.541 0.00005 0.030 00
1200101
*
* CTL PRESSURE TEMP ZERO
* 3 7.31093+6 551.7 0.0
1200200
*
* FR TO AREA F-LOSS R-LOSS CAHS
* 112000000 120010000 0.0 0.0 0.0 0.100
1201101
* 120000000 130010000 0.0 0.0 0.0 0.000
1202101
* 120000000 170000000 0.0 0.75 1.0 0.000
1203101
* 120000000 230000000 0.0 0.75 1.0 0.000
1204101
*
* FLOW-F FLOW-G VELJ
* 16.0 0.0 0.0
1201201
* 6.00 0.0 0.0
1202201
* 5.00 0.0 0.0
1203201
* 5.00 0.0 0.0
1204201
*
*****
* LOWER DOWNCOMER (VOLUME11 .... RELAP4J)
*
* NAME TYPE
* C130 PIPE
1300000
* 4
1300001
* 1
1300101
* 4
1300102
* 3
1300201
* 4
1300301
* 4
1300401
* 1
1300402
* 4
1300501
* 4
1300601
* 4
1300701
* 4
1300801
* 0.00005 0.070333 1
1300802
* 0.00005 0.030 4
1300901
* 0.0 0.0 3
1301001
* 00 4
1301101
* 0000 3
1301201
* 3 7.32447+6 551.7 0.0 0.0 1
1301202
* 3 7.32108+6 551.7 0.0 0.0 2
1301203
* 3 7.31770+6 551.7 0.0 0.0 3
1301204
* 3 7.31431+6 551.7 0.0 0.0 4
1301300
* 1
1301301
* -6.00 0.0 0.0 3
*****
* RECIRCULATION INLET PIPE TEE
* C131 BRANCH
1310000
* 1
1310001
* 2
1310001
* 1
1000901 0.0 0.0 2
1001001 00 0.0 3
1001101 0000 2
1001201 3 7.33424+6 551.7 0.0 0.0 1
1001202 3 7.33014+6 551.7 0.0 0.0 2
1001203 3 7.32195+6 551.7 0.0 0.0 3
1001300 1
1001301 0.80 0.0 0.0 2
*****
* UPPER DOWNCOMER-1 (VOLUME27 .... RELAP4J)
*
* NAME TYPE
* C110 SINGLVOL
1100000
* 0.0 0.2371 0.05588 0.0 90.0 0.2371 0.00005 0.5478 00
1100101
* 2 7.29410+6 0.0 0.0
1100200
*
*****
* UPPER DOWNCOMER (FEEDWATER SPARGER)
*
* NAME TYPE
* C111 BRANCH
1110000
*
1110001 2 1
1110101 0.0 0.328 0.081672 0.0 90.0 0.328 0.00005 0.56306 00
1110200 3 7.29739+6 551.7 0.0
1111101 110000000 111010000 0.0 0.0 0.0 0.000
1112101 111000000 112010000 0.08006 0.0 0.0 0.000
1111201 13.8881 0.0 0.0
1112201 16.00 0.0 0.0
*****
*
* C112 PIPE
1120000
* 3
1120101 0.0 1
1120102 0.08006 2
1120103 0.08006 3
1120201 0.0 2
1120301 0.189 1
1120302 0.356 2
1120303 0.35 3
1120401 0.013658 1
1120402 0.0 3
1120501 0.0 3
1120601 90.0 3
1120701 0.189 1
1120702 0.356 2
1120703 0.35 3
1120801 0.00005 0.303 1
1120802 0.00005 0.092 3
1120901 0.0 0.0 2
1121001 00 3
1121101 0000 2
1121201 3 7.30077+6 551.7 0.0 0.0 1
1121202 3 7.30416+6 551.7 0.0 0.0 2
1121203 3 7.30754+6 551.7 0.0 0.0 3
1121300 1
1121301 -16.00 0.0 0.0 2

```



```

1710202 1 5.00 0.0 0.0
1710301 150 150 150 -1 -1 509 1
1710302 376.99 0.5092 0.01250 26.0 184.24 1.9 765.76
1710303 0.0 0.0 0.0 0.0
1710310 0.0 0.0 0.0
*
*****
* INTACT JET PUMP
*
1800000 C180 BRANCH
*
1800001 2 1
*
1800101 0.000585 0.121 0.0 0.0 -90.0 -0.121 0.00005 0.0273 00
*
1800200 3 7.38813+6 551.7 0.0
*
1801101 160010000 180000000 0.000111 0.936 0.510 0000
1802101 180010000 185000000 0.000585 0.07 0.0 0000
*
18011201 3.00 0.0 0.0
1802201 8.00 0.0 0.0
*
*****
* INTACT JET PUMP OUTLET LINE (VOLUME22 .... RELAP4J)
*
1850000 NAME TYPE
1850001 C185 PIPE
1850101 0.0 1
1850102 0.003849 2
1850103 0.0 3
1850104 0.004289 5
1850201 0.003849 1
1850202 0.003849 2
1850203 0.004289 3
1850204 0.0 4
1850301 0.285 1
1850302 1.396 2
1850303 0.4243 3
1850304 2.0864 4
1850305 1.8464 5
1850401 0.0005636 1
1850402 0.0 2
1850403 0.003073 3
1850404 0.0 5
1850501 0.0 5
1850601 -90.0 5
1850701 -0.285 1
1850702 -1.396 2
1850703 -0.300 3
1850704 -0.240 4
1850705 -0.2729 5
1850801 0.00005 0.0502 1
1850802 0.00005 0.0700 2
1850803 0.00005 0.0960 3
1850804 0.00005 0.0739 4
*
*****
* BROKEN RECIRCULATION INLET LINE (VOLUME15 .... RELAP4J)
*
1900000 NAME TYPE
1900001 C190 PIPE
1900101 0.0019244 3
1900201 0.0 2
1900301 2.1317 1
1900302 2.5127 2
1900303 2.5424 3
1900401 0.0 3
1900501 0.0 3
1900601 -90.0 2
1900602 0.0 3
1900701 -0.154 1
1900702 -1.285 2
1900703 -0.0 3
1900801 0.00005 0.0495 3
1900901 0.185 1
1900902 0.345 2
1901001 0.0 3
1901101 0.000 2
1901201 3 7.33639+6 551.7 0.0 0.0 1
1901202 3 7.34492+6 551.7 0.0 0.0 2
1901203 3 7.35346+6 551.7 0.0 0.0 3
1901300 1
1901301 3.00 0.0 0.0 2
*
*****
* BROKEN RECIRCULATION INLET LINE (VOLUME16 .... RELAP4J)
*
2000000 NAME TYPE
2000001 C200 PIPE
2000101 0.0019244 3
2000201 0.0 2
2000301 2.0659 1
2000302 2.6398 2
2000303 2.3574 3
2000401 0.0 3
2000501 0.0 3

```



```

2310302 376.99 0.5344 0.01250 28.0 184.24 1.9 765.76
2310303 0.0 0.0 0.0 0.0 0.0 0.0
2310310 0.0 0.0 0.0
*****
* BROKEN JET PUMP
*
2400000 C240 BRANCH
2400001 2 1
2400101 0.000585 0.121 0.0 0.0 -90.0 -0.121 0.00005 0.0273 0.0
2400200 3 7.38813+6 551.7 0.0
2401101 220010000 240000000 0.000111 0.936 0.510 0000
2402101 240010000 245000000 0.000585 0.07 0.0 0000
2401201 3.00 0.0 0.0
2402201 8.00 0.0 0.0
*****
* BROKEN JET PUMP OUTLET LINE (VOLUME14 .... RELAP4J)
*
2450000 NAME TYPE
C245 PIPE
2450001 5
2450101 0.0 1
2450102 0.003849 2
2450103 0.0 3
2450104 0.004289 5
2450201 0.003849 1
2450202 0.003849 2
2450203 0.004289 3
2450204 0.0 4
2450301 0.285 1
2450302 1.396 2
2450303 0.4243 3
2450304 2.0864 4
2450305 1.8464 5
2450401 0.0005636 1
2450402 0.0 2
2450403 0.003073 3
2450404 0.0 5
2450501 0.0 5
2450601 -90.0 5
2450701 -0.285 1
2450702 -1.396 2
2450703 -0.3000 3
2450704 -0.240 4
2450705 -0.2729 5
2450801 0.00005 0.0502 1
2450802 0.00005 0.0700 2
2450803 0.00005 0.0960 3
2450804 0.00005 0.0739 5
2450901 0.0 0.46 1
2450902 5.369 5.369 2
*****
2450903 0.3 1.0 3
2450904 0.832 0.832 4
2451001 0.0 5
2451101 0.000 4
2451201 3 7.38000+6 551.7 0.0 0.0 1
2451202 3 7.37500+6 551.7 0.0 0.0 2
2451203 3 7.37000+6 551.7 0.0 0.0 3
2451204 3 7.36500+6 551.7 0.0 0.0 4
2451205 3 7.36000+6 551.7 0.0 0.0 5
2451300 1
2451301 8.00 0.0 0.0 4
*****
* QUICK SHUTT-OFF VALVE NOT USED IN THE SMALL BREAK TEST SERIES
*
2500000 C250 VALVE
2500101 190010000 200000000 2.0019244 2.0 2.0 0000
2500201 1 3.00 0.0 0.0
2500300 TRPVLV
2500301 513
*****
* VESSEL SIDE BREAK (BRK B) (JUNCTION55 .... RELAP4J)
*
2600000 NAME TYPE
C260 VALVE
2600101 190010000 280000000 5.391-4 0.0 0.0 0100
2600201 1 0.0 0.0 0.0
CTL FLOW-F FLOW-G VELJ
2600300 VALVE TYPE TRIP.NO
TRPVLV 502
2600301
*****
* PUMP SIDE BREAK ( BRK A) NOT USED IN THE SMALL BREAK TEST
*
2700000 C270 VALVE
2700101 200000000 281000000 5.391-4 0.0 0.0 0100
2700201 1 0.0 0.0 0.0
2700300 TRPVLV
2700301 502
*****
* CONTAINMENT
*
2800000 NAME TYPE
C280 TMDPVOL
2800101 AREA LEN VOL HZ VR ELV ROU HYD FE
1.0+3 0.0 1.0+6 0.0 0.0 0.0 0.0 11
CTL
2800200 3
2800201 TIME PRESSURE TEMP
0.0 9.8043+4 303.15 * CONSTANT
*****

```

```

*****
* MAIN STEAM RESERVOIR * ENTHALPY CALCULATION
*
* NAME TYPE
* C290 TMDPVOL
*
* 2900101 1.0+3 0.0 1.0+6 0.0 0.0 0.0 0.0 0.0 0.0 11
* CTL
* 2 0.0
*
* TIME PRESSURE TEMP
* 0.0 7.2900+6 1.0 * CONSTANT
*
*****
* MAIN STEAM
*
* NAME TYPE
* C300 TMDPJUN
*
* 3000101 290000000 080010000 3.141-4
* CTL
* 0
*
* TIME FLOW-F FLOW-G VELJ
* 0.0 -175.9 0.0
* 0.9 -139.3 0.0
* 2.1 -179.1 0.0
* 3.0 -179.4 0.0
* 3.9 -179.1 0.0
* 4.8 -179.6 0.0
* 5.7 -179.7 0.0
* 6.6 -178.9 0.0
* 7.8 -176.4 0.0
* 8.7 -62.4 0.0
* 9.6 -0.3 0.0
* 9.8 0.0 0.0
* 128.9 0.0 0.0
* 129.0 0.0 -74.7 0.0
* 130.2 0.0 -153.6 0.0
* 135.0 0.0 -205.7 0.0
* 144.6 0.0 -202.8 0.0
* 146.4 0.0 -153.0 0.0
* 150.0 0.0 -156.9 0.0
* 201.9 0.0 -1.7 0.0
* 202.0 0.0 0.0 0.0
* 1000.0 0.0 0.0 0.0
*
*****
* HPCS RESERVOIR
*
* 2920000 C292 TMDPVOL
* 2920101 1.0+3 0.0 1.0+6 0.0 0.0 0.0 0.0 0.0 0.0 11
*
*****
* MAIN STEAM RESERVOIR * ENTHALPY CALCULATION
*
* NAME TYPE
* C310 TMDPVOL
*
* 3100101 1.0+3 0.0 1.0+6 0.0 0.0 0.0 0.0 0.0 0.0 11
* CTL
* 3
*
* TIME PRESSURE TEMP
* 0.0 7.5001+6 489.0 * CONSTANT
*
*****
* FEEDWATER
*
* NAME TYPE
* C320 TMDPJUN
*
* 3200101 310000000 111010000 1.157-3
* CTL
* 0
*
* TIME FLOW-F FLOW-G VELJ
* 0.0 2.147 0.0 0.0
* 0.375 2.251 0.0 0.0
* 1.875 0.138 0.0 0.0
* 2.25 0.105 0.0 0.0
* 3.0 0.053 0.0 0.0
* 3.7 0.0 0.0 0.0
* 1000.0 0.0 0.0 0.0
*
*****
* HPCS
*
* 3020000 C302 TMDPJUN
* 3020101 292000000 050000000 1.157-3
* 0
*
* 3020201 0.0 0.0 0.0 0.0
* 3020202 31.5 0.0 0.0 0.0
* 3020203 33.8 0.628 0.0 0.0
* 3020204 34.3 0.670 0.0 0.0
* 3020205 35.6 0.681 0.0 0.0
* 3020206 37.5 0.686 0.0 0.0
* 3020207 60.0 0.696 0.0 0.0
* 3020208 90.0 0.702 0.0 0.0
* 3020209 180.0 0.712 0.0 0.0
* 3020210 1000.0 0.712 0.0 0.0
*
*****
* FEEDWATER RESERVOIR * ENTHALPY CALCULATION
*
* NAME TYPE
* C310 TMDPVOL
*
* 3100101 1.0+3 0.0 1.0+6 0.0 0.0 0.0 0.0 0.0 0.0 11
* CTL
* 3
*
* TIME PRESSURE TEMP
* 0.0 7.5001+6 489.0 * CONSTANT
*
*****
* FEEDWATER * JUNCTIONS1 .... RELAP4J
*
* NAME TYPE
* C320 TMDPJUN
*
* 3200101 310000000 111010000 1.157-3
* CTL
* 0
*
* TIME FLOW-F FLOW-G VELJ
* 0.0 2.147 0.0 0.0
* 0.375 2.251 0.0 0.0
* 1.875 0.138 0.0 0.0
* 2.25 0.105 0.0 0.0
* 3.0 0.053 0.0 0.0
* 3.7 0.0 0.0 0.0
* 1000.0 0.0 0.0 0.0
*
*****

```

```

*****
* LPCI
*
* 4010000 C401 TMDPJUN 1.923-3
4010101 331000000 100010000
4010200 0 0.0 0.0 0.0
4010201 0.0 0.0 0.0 0.0
4010202 90.9 0.0 0.0 0.0
4010203 93.0 0.0 0.0 0.0
4010204 94.9 1.259 0.0 0.0
4010205 95.8 1.337 0.0 0.0
4010206 97.5 1.357 0.0 0.0
4010207 103.1 1.498 0.0 0.0
4010208 118.1 1.742 0.0 0.0
4010209 120.0 1.789 0.0 0.0
4010210 135.0 1.867 0.0 0.0
4010211 150.0 1.914 0.0 0.0
4010212 165.0 1.940 0.0 0.0
4010213 180.0 1.961 0.0 0.0
4010214 195.0 1.966 0.0 0.0
4010215 210.0 1.981 0.0 0.0
4010216 1000.0 1.981 0.0 0.0
*****
* LPCS
*
* 4020000 C402 TMDPJUN
4020101 332000000 050000000 1.157-3
4020200 0
4020201 0.0 0.0 0.0 0.0
4020202 65.6 0.0 0.0 0.0
4020203 67.5 0.419 0.0 0.0
4020204 69.4 0.650 0.0 0.0
4020205 86.3 0.754 0.0 0.0
4020206 116.3 0.880 0.0 0.0
4020207 146.3 0.953 0.0 0.0
4020208 210.0 0.953 0.0 0.0
4020209 1000.0 0.953 0.0 0.0
*****
* CORE
*
* ***** COMPOSED OF BN,HEATER,BN,INC600 *****
* ***** HIGH POWER CHANNEL (A CHANNEL) 10010000 *****
* ***** AVERAGE POWER CHANNEL (B,C,D CHANNEL)10020000 *****
* ***** AVERAGE POWER CHANNEL HEAT STRUCTURE *****
*
* NH NP TYPE S-FLG L-COR
10010000 7 9 2 1 0.0
*
* LOC-F MESH-F
*****
10010100 0 1
*
* NO ITV R-COR NO ITV R-COR NO ITV R-COR
3 0.003051 1 0.0037511, 1 0.004835,
10010102 3 0.006135
*
* FLG
0
*
* CMP NO
1 3, 2 4, 3 5, 4 8
*
* FLG
0
*
* SOURCE
0.0 3, 1.0 4, 0.0 5, 0.0 8
*
* FLG
0
*
* TEMP NP
534.8 9
*
* B.V. INC BCT A-C AREA NH
0 0 0 0 0 7
*
* LEFT
10010501
*
* RIGHT
10010601 B.V INC BCT A-C SURFACE NH
040010000 10000 1 0 1.6849 3
10010602 040040000 0 1 0 3.3698 4
10010603 040050000 10000 1 0 1.6849 7
*
* TYPE IS MULTI L-D-H R-D-H NH
900 0.04109 0.0 0.0 1
900 0.07690 0.0 0.0 2
10010703 900 0.10360 0.0 0.0 3
10010704 900 0.23860 0.0 0.0 4
10010705 900 0.10360 0.0 0.0 5
10010706 900 0.07690 0.0 0.0 6
10010707 900 0.04109 0.0 0.0 7
*
* LEFT CHF HYD HEQ CHAN NH
10010801 0 0.0 0.0 0.0 7
*
* RIGHT CHF HYD HEQ CHAN NH
10010901 0 0.01306 0.01348 0.2350 3
10010902 0 0.01306 0.01348 0.4700 4
10010903 0 0.01306 0.01348 0.2350 7
*
* ***** HIGH POWER CHANNEL HEAT STRUCTURE *****
*
* 10020000 7 9 2 1 0.0
10020100 0010
*
* 10020300 0010
10020400 0010
10020501 0 0 0 0.0 7
10020601 045010000 10000 1 0 0.5616 3
10020602 045040000 0 1 0 1.1233 4
*****

```


Material ID	Weight (g)	Volume (cm ³)	Temperature (K)	Heat Capacity (BTU/(S*F))	Thermal Conductivity (BTU/(S*F))	Thermal Expansion (1/K)	Thermal Property Data	Material Name	Other Parameters
11500201	5	3	1173.15	26.2933	1273.15	26.8541		20100102	HEATER
11500300	0	0	293.15	17.5081	373.15	13.8320		20100201	HEATER
11500301	0	0	293.15	17.5081	373.15	13.8320		20100201	HEATER
11500400	0	0	293.15	17.5081	373.15	13.8320		20100201	HEATER
11500401	560.0	4	294.26	14.8289	366.48	15.7012		20100401	INCONEL600
11500501	0	0	294.26	14.8289	366.48	15.7012		20100401	INCONEL600
11500502	0	0	588.71	19.1904	699.82	20.9350		20100402	INCONEL600
11500601	9000.0	0	922.04	24.7357	1033.15	26.8541		20100403	INCONEL600
11500602	0	0	294.26	14.8289	366.48	15.7012		20100401	INCONEL600
11500701	0	0	294.26	14.8289	366.48	15.7012		20100401	INCONEL600
11500801	0	0	588.71	19.1904	699.82	20.9350		20100402	INCONEL600
11500901	0	0	922.04	24.7357	1033.15	26.8541		20100403	INCONEL600
11600000	1	4	273.15	16.2620	773.15	20.9350		20100501	SUS
11600100	0	1	273.15	16.2620	773.15	20.9350		20100501	SUS
11600101	3	0.180	273.15	16.2620	773.15	20.9350		20100501	SUS
11600200	0	0	293.15	26.6672	573.15	20.6234		20100601	MGO
11600201	5	3	293.15	26.6672	573.15	20.6234		20100601	MGO
11600300	0	0	773.15	14.0813	873.15	11.7136		20100602	MGO
11600301	0	0	1073.15	8.7852	1273.15	6.9160		20100603	MGO
11600400	0	0	1506.48	6.7291	1873.15	7.3522		20100604	MGO
11600401	560.0	4	293.15	26.6672	573.15	20.6234		20100601	MGO
11600501	9000.0	0	293.15	26.6672	573.15	20.6234		20100601	MGO
11600601	0	0	773.15	14.0813	873.15	11.7136		20100602	MGO
11600701	0	0	1073.15	8.7852	1273.15	6.9160		20100603	MGO
11600801	0	0	1506.48	6.7291	1873.15	7.3522		20100604	MGO
11600901	0	0	1506.48	6.7291	1873.15	7.3522		20100604	MGO
20100101	0	0	293.15	3.8496+6	373.15	3.7289+6		20100252	HEATER
20100102	0	0	293.15	3.8496+6	373.15	3.7289+6		20100252	HEATER
20100151	0	0	293.15	3.0716+5	783.15	4.0106+5		20100151	INNER BN
20100152	0	0	1533.15	6.3512+5	1533.15	6.3512+5		20100152	INNER BN
20100351	0	0	293.15	3.0649+5	783.15	4.0173+5		20100351	OUTER BN
20100352	0	0	1533.15	6.3512+5	1533.15	6.3512+5		20100352	OUTER BN
20100451	0	0	294.26	3.7355+6	366.48	3.9100+6		20100451	INCONEL600
20100452	0	0	588.71	4.2654+6	699.82	4.4398+6		20100452	INCONEL600
20100453	0	0	922.04	4.9294+6	1033.15	5.1104+6		20100453	INCONEL600
20100551	0	0	294.26	3.7355+6	366.48	3.9100+6		20100551	SUS
20100552	0	0	588.71	4.2654+6	699.82	4.4398+6		20100552	SUS
20100651	0	0	922.04	4.9294+6	1033.15	5.1104+6		20100651	MGO
20100751	0	0	922.04	4.9294+6	1033.15	5.1104+6		20100751	MGO
20290000	0	0	293.15	29.7824	773.15	28.0379		20290000	INNER BN
20100101	0	0	293.15	29.7824	773.15	28.0379		20100101	INNER BN

* * * * *

0000393 MFLOWJ 050010000
 0000394 MFLOWJ 050020000
 0000395 MFLOWJ 050030000
 0000396 MFLOWJ 050040000
 0000397 VELFJ 050010000
 0000398 VELGJ 050010000

* * * * *

0000334 VOIDG 040060000
 0000335 VOIDG 040070000
 0000336 VOIDGJ 050020000
 0000337 MFLOWJ 031020000
 0000338 HTEMP 002000109
 0000339 HTEMP 002000209
 0000340 HTEMP 002000309
 0000341 HTEMP 002000409
 0000342 HTEMP 002000509
 0000343 HTEMP 002000609
 0000344 HTEMP 002000709
 0000345 MFLOWJ 050010000
 0000346 VOIDGJ 031020000
 0000347 VOIDG 045010000
 0000348 VOIDG 045020000
 0000349 VOIDG 045030000
 0000350 VOIDG 045040000
 0000351 VOIDG 045050000
 0000352 VOIDG 045060000
 0000353 VOIDG 045070000
 0000354 VOIDGJ 050010000
 0000355 VOIDG 100010000
 0000356 VOIDG 100020000
 0000357 VOIDG 100030000
 0000358 VOIDG 090010000
 0000359 VOIDG 090020000
 0000360 VOIDG 090030000
 0000361 VOIDG 060040000
 0000362 VOIDG 060010000
 0000363 VOIDG 051020000
 0000364 VOIDG 050010000
 0000365 VOIDG 030010000
 0000366 VOIDG 020020000
 0000367 VOIDG 020010000
 0000368 VOIDG 010010000
 0000369 VOIDG 080010000
 0000370 VOIDG 070010000
 0000371 VOIDG 071010000
 0000372 VOIDG 110010000
 0000373 VOIDG 110010000
 0000374 VOIDG 111010000
 0000375 VOIDG 112030000
 0000376 VOIDG 112020000
 0000377 VOIDG 112010000
 0000378 VOIDG 120010000
 0000379 VOIDG 130040000
 0000380 VOIDG 130030000
 0000381 VOIDG 130020000
 0000382 VOIDG 130010000
 0000383 VOIDG 131010000
 0000384 MFLOWJ 010010000
 0000385 MFLOWJ 010020000
 0000386 MFLOWJ 010030000
 0000387 MFLOWJ 010040000
 0000388 MFLOWJ 010050000
 0000389 MFLOWJ 030010000
 0000390 MFLOWJ 030020000
 0000391 MFLOWJ 030030000
 0000392 MFLOWJ 031010000

***** (VOLUME15 RELAP4J) *****			
NAME	TYPE	INLET LINE	(VOLUME15 RELAP4J)
1851001	00		
1851101	0000		
1851201	3	7.37500+6	551.7 0.0 0.0 1
1851202	3	7.37000+6	0.0 0.0 2
1851203	3	7.36500+6	551.7 0.0 0.0 3
1851204	3	7.36000+6	551.7 0.0 0.0 4
1851300	1		
1851301	8.00	0.0 0.0 3	
***** (VOLUME16 RELAP4J) *****			
NAME	TYPE	INLET LINE	(VOLUME16 RELAP4J)
1900000	C190		
1900001	3		
1900101	0.0019244	3	
1900201	0.0	2	
1900301	2.1317	1	
1900302	2.5127	2	
1900303	2.5424	3	
1900401	0.0	3	
1900501	0.0	3	
1900601	-90.0	2	
1900602	0.0	3	
1900701	-0.154	1	
1900702	-1.285	2	
1900703	-0.0	3	
1900801	0.00005	0.0495 3	
1900901	0.185	0.185 1	
1900902	0.345	0.345 2	
1901001	0.0	3	
1901101	0.000	2	
1901201	3	7.33639+6	551.7 0.0 0.0 1
1901202	3	7.34492+6	551.7 0.0 0.0 2
1901203	3	7.35346+6	551.7 0.0 0.0 3
1901300	1		
1901301	3.00	0.0 2	
***** (VOLUME15 RELAP4J) *****			
NAME	TYPE	INLET LINE	(VOLUME15 RELAP4J)
2000000	C200		
2000001	3		
2000101	0.0019244	3	
2000201	0.0	2	
2000301	2.0659	1	
2000302	2.6398	2	
2000303	2.3574	3	
2000401	0.0	3	
2000501	0.0	3	
2000601	-90.0	1	
2000602	0.0	2	
2000603	-90.0	3	
2000701	-0.219	1	
2000702	-0.0	2	
2000703	-1.515	3	
***** (VOLUME16 RELAP4J) *****			
NAME	TYPE	INLET LINE	(VOLUME16 RELAP4J)
2200201	0.0		
2200202	0.0023162	3	
2200301	2.0046	4	
2200302	2.5762	1	
2200303	2.6315	2	
2200304	2.2613	3	
2200305	0.859	4	
2200401	0.0	4	
2200402	0.001776	5	
2200501	0.0	5	
2200601	90.0	1	
2200602	0.0	2	
2200603	90.0	4	
2200604	-90.0	5	
2200701	1.275	1	
2200702	0.0	2	
2200703	2.3485	3	
2200704	2.1715	4	
2200705	-0.559	5	
2200801	0.00005	0.0495 4	
2200802	0.00005	0.0513 5	
2200901	0.26	0.26 1	
2200902	13.903	13.903 2	
2200903	0.085	0.085 3	
2200904	0.414	0.414 4	
2201001	0.0	5	
2201101	0.000	4	
2201201	3	7.90790+6	551.7 0.0 0.0 1
2201202	3	7.86740+6	551.7 0.0 0.0 2
2201203	3	7.82700+6	551.7 0.0 0.0 3
2201204	3	7.78650+6	551.7 0.0 0.0 4
2201205	3	7.74600+6	551.7 0.0 0.0 5
2201300	1		
2201301	3.00	0.0 4	
***** (VOLUME16 RELAP4J) *****			
NAME	TYPE	INLET LINE	(VOLUME16 RELAP4J)
2300000	C230		
2300101	0.003048	1.304 0.0 0.0 0.0 0.0 0.0 0.00005 0.0623 0.0	
2300200	3	7.29093+6	551.7 0.0
***** (VOLUME16 RELAP4J) *****			
NAME	TYPE	INLET LINE	(VOLUME16 RELAP4J)
3100000	C231		
310101	0.0	0.973 0.002225 0.0 -90.0 -0.073 0	
310108	230010000	0.003048 0.6438 0.6438 0.000	
310109	240000000	0.000474 0.042 0.021 0.000	
310200	3	7.39435+6	551.7 0.0
310201	1	5.00 0.0 0.0	
310202	1	5.00 0.0 0.0	
310301	150	150 -1 -1 510 1	
310302	376.99	0.5344 0.01250 20.0 184.24 1.9 765.76	
310303	0.0	0.0 0.0 0.0	
310310	0.0	0.0 0.0	
2310000	C231		
2310101	6.743-4	0.203 0.0 0.0 90.0 -0.0605 0.00005 0.0 0.0	

```

2310200 3 7.29093+6 551.7 0.0
*
* BROKEN JET PUMP
*
2400000 C240 BRANCH
*
2400001 2 1
*
2400101 5.-851-4 0.406 0.0 0.0 -90.0 -0.406 0.00005 0.0273 00
*
2400200 3 7.38813+6 551.7 0.0
*
2401101 220010000 240000000 1.108-4 0.936 0.510 0000
2402101 240010000 245000000 5.851-4 0.07 0.01 0000
*
2401201 3.00 0.0 0.0
2402201 8.00 0.0 0.0
*
* BROKEN JET PUMP OUTLET LINE (VOLUME14 .... RELAP4J)
*
* NAME TYPE
* C245 PIPE
*
2450101 0.003849 1
2450102 0.0 2
2450103 0.004289 4
2450201 0.003849 1
2450202 0.004289 2
2450203 0.0 3
2450301 1.396 1
2450302 0.4243 2
2450303 2.0864 3
2450304 1.8464 4
2450401 0.0 1
2450402 0.003073 2
2450403 0.0 4
2450501 0.0 4
2450601 -90.0 4
2450701 -1.396 1
2450702 -0.3000 2
2450703 -0.240 3
2450704 -0.2729 4
2450801 0.00005 0.0700 1
2450802 0.00005 0.0960 2
2450803 0.00005 0.0739 4
2450901 5.369 5.369 1
2450902 0.3 1.0 2
2450903 0.832 0.832 3
2451001 00 4
2451101 0000 3
2451201 3 7.37500+6 551.7 0.0 0.0 1
2451202 3 7.37090+6 551.7 0.0 0.0 2
2451203 3 7.36500+6 551.7 0.0 0.0 3
2451204 3 7.36000+6 551.7 0.0 0.0 4
2451300 1
*
2451301 8.00 0.0 0.0 3
*
* QUICK SHUT-OFF VALVE NOT USED IN THE SMALL BREAK TEST SERIES
*
2500000 C250 VALVE
2500101 190010000 200000000 0.0019244 2.0 2.0 0000
2500201 1 3.00 0.0 0.0
2500300 TRPVLV
2500301 513
*
* VESSEL SIDE BREAK (BRK B) (JUNCTION55 .... RELAP4J)
*
* NAME TYPE
* C260 VALVE
*
2600101 190010000 280000000 3.2348-4 0.0 0.0 0100
*
* FR TO AREA F-LOS R-LOS CAHS
*
2600201 1 0.0 0.0 0.0
*
* CTL FLOW-F FLOW-G VELJ
*
2600300 TRPVLV
2600301 502
*
* VALVE TYPE TRIP.NO
*
2600000 C270 VALVE
2700000 C270 VALVE
2700101 200000000 281000000 3.2438-4 0.0 0.0 0100
2700201 1 0.0 0.0 0.0
2700300 TRPVLV
2700301 502
*
* PUMP SIDE BREAK ( BRK A) NOT USED IN THE SMALL BREAK TEST
*
* CONTAINMENT TYPE
* NAME TMDPVOL
*
2800000 C280
*
2800101 1.0+3 0.0 1.0+6 0.0 0.0 0.0 0.0 11
*
2800200 C280
*
2800201 0.0 9.8043+4 303.15 * CONSTANT
*
* MAIN STEAM RESERVOIR * ENTHALPY CALCULATION
*
* NAME TYPE
* C290 TMDPVOL
*
2900000 C290
*
2900101 1.0+3 0.0 1.0+6 0.0 0.0 0.0 0.0 11

```

```

20290011 100.0 0.506+6
20290012 150.0 0.413+6
20290013 210.0 0.311+6
20290014 300.0 0.251+6
20290015 480.0 0.227+6
20290016 600.0 0.214+6
20290017 1800.0 0.166+6
*
* *****
* CONTAINMENT
* NAME TYPE
* C281 TMDPVOL
*
* AREA LEN VOL HZ VR ELV ROU HYD FE
* 2810101 1.0+3 0.0 1.0+6 0.0 0.0 0.0 0.0 0.0 11
*
* CTL
* 2810200 3
*
* TIME PRESSURE TEMP
* 2810201 0.0 0.09804+6 303.15 * CONSTANT
*
* *****
* LPCI RESERVOIR * ENTHALPY CALCULATION
*
* NAME TYPE
* C331 TMDPVOL
*
* AREA LEN VOL HZ VR ELV ROU HYD FE
* 3310101 1.0+3 0.0 1.0+6 0.0 0.0 0.0 0.0 0.0 11
*
* CTL
* 3310200 3
*
* TIME PRESSURE TEMP
* 3310201 0.0 2.47+6 313.0 * CONSTANT
*
* *****
* LPCS RESERVOIR * ENTHALPY CALCULATION
*
* NAME TYPE
* C332 TMDPVOL
*
* AREA LEN VOL HZ VR ELV ROU HYD FE
* 3320101 1.0+3 0.0 1.0+6 0.0 0.0 0.0 0.0 0.0 11
*
* CTL
* 3320200 3
*
* TIME PRESSURE TEMP
* 3320201 0.0 3.76+6 313.0 * CONSTANT
*
* *****
* JET PUMP SUCTION AT BROKEN LOOP
* C530 SINGLJUN
* 5300000 23010000 231000000 4.743-4 0.1 0.1 0.000
*
* 5300101 170010000 171000000 4.743-4 0.1 0.1 0.000
*
* *****
* JET PUMP SUCTION AT INTACT LOOP
* C533 SINGLJUN
* 5330000 170010000 171000000 4.743-4 0.1 0.1 0.000
*
* 5330101 170010000 171000000 4.743-4 0.1 0.1 0.000
*
* 5330201 1 5.0 0.0
*
* 5340000 C534 SINGLJUN
* 5340101 171010000 180000000 4.743-4 0.042 0.021 0.000
*
* 5340201 1 5.0 0.0
*
* *****
* HEAT SINK FOR HEAT LOSS
*
* C900 TMDPVOL
* 9000000 1.3 0.0 1.6 0.0 90.0 10.0 0.0 0.0 11
*
* 9000101 3
* 9000200 0.0 0.09804+6 303.15 * CONSTANT
*
* *****
* C910 VALVE
* 9100000 080010000 900000000 1.0-3 0.0 0.0 0100
*
* 9100101 1 0.0 0.0 0.0
*
* 9100201 TRPVLV 527
*
* 9100300
* 9100301
*
* *****
* MINOR EDIT
*
* P 010010000
* 0000301 MFLOWJ 534000000
* 0000302 MFLOWJ 185010000
* 0000303 MFLOWJ 180010000
* 0000304 MFLOWJ 180020000
* 0000305 MFLOWJ 532000000
* 0000306 MFLOWJ 245010000
* 0000307 MFLOWJ 240010000
* 0000308 MFLOWJ 240020000
* 0000309 P 080010000
* 0000310 MFLOWJ 300000000
* 0000311 MFLOWJ 320000000
* 0000312 MFLOWJ 302000000
* 0000313 MFLOWJ 402000000
* 0000314 MFLOWJ 401000000
* 0000315 MFLOWJ 260000000
* 0000316 MFLOWJ 270000000
* 0000317 MFLOWJ 030010000
* 0000318 MFLOWJ 030020000
* 0000319 MFLOWJ 001000109
* 0000320 HTTEMP 001000209
* 0000321 HTTEMP 001000309
* 0000322 HTTEMP 001000409
* 0000323 HTTEMP 001000509
* 0000324 HTTEMP 001000609
* 0000325 HTTEMP 001000709
* 0000326 MFLOWJ 050020000
* 0000327 MFLOWJ 050020000
* 0000328 VOICG 050020000

```


* 2-PHASE HEAD DIFFERENCE TABLES										* BUILT-IN RELAP4J																			
ID	Q	Q	Q	Q	Q	Q	Q	Q	Q	ID	Q	Q	Q	Q	Q	Q	Q	Q	Q										
1503000	0	0.0	0.0	0.0	0.0	0.0	0.0	0.0	0.0	2000701	-0.219	1																	
1503001	0.0	0.0	0.1	0.0	0.15	0.05	0.24	0.8	0.3	2000702	-0.0	2																	
1503002	0.4	0.98	0.6	0.97	0.80	0.90	0.90	0.8	0.96	2000703	-1.515	3																	
1503003	1.0	1.0								2000801	0.00005	0.0495	3																
1503100	0									2000901	0.325	0.325	1																
1503101	0.0	0.0	0.125	0.07	0.165	0.125	0.24	0.56	0.80	2000902	0.17	0.17	2																
1503102	0.96	0.45	1.0	0.0						2001001	0.0	0.0	3																
* 2-PHASE TORQUE DIFFERENCE TABLES										* BUILT-IN RELAP4J																			
1504100	1	1								2001101	0.000	0.000	2																
1504101	0.00	0.00	0.10	0.67	0.25	0.91	0.50	1.12		2001201	3	7.36200+6	551.7	0.0	0.0	1													
1504102	0.75	1.28	1.00	1.34						2001202	3	7.37053+6	551.7	0.0	0.0	2													
1504200	1	2								2001203	3	7.37907+6	551.7	0.0	0.0	3													
1504201	0.00	0.31	0.25	0.42	0.50	0.57	0.75	0.97	1.00	2001300	1																		
1504300	1	3								2001301	3.00	0.0	0.0	2															
1504301	-1.00	-1.18	-0.75	-1.30	-0.50	-1.08	-0.25	-0.93		***** (VOLUME17 ... RELAP4J) *****																			
1504302	-0.10	-0.71	0.00	0.00						***** BROKEN RECIRCULATION PUMP *****																			
1504400	1	4								***** NAME TYPE *****																			
1504401	-1.00	-1.18	-0.75	-0.24	-0.50	-0.07	-0.25	-0.08	0.00	***** C210 PUMP *****																			
1504500	1	5								***** AREA LEN VOL HZ VR ELV CTL *****																			
1504501	0.00	0.00	0.10	-0.39	0.25	-0.71	0.50	-0.71		***** 0.0 0.26 0.005295 0.0 -90.0 -0.26 0 *****																			
1504502	0.75	-0.58	1.00	-0.47						***** VOL NO AREA F-LOSS R-LOSS CAHS *****																			
1504600	1	6								***** 200010000 0.00019244 5.28 5.28 0.000 *****																			
1504700	1	7								***** VOL NO AREA F-LOSS R-LOSS CAHS *****																			
1504701	-1.00	0.51	-0.75	0.55	-0.50	0.51	-0.25	0.39	0.00	***** 220000000 0.0002746 0.1 0.1 0.000 *****																			
1504800	1	8								***** CTL PRESSURE TEMP ZERO *****																			
1504801	-1.00	0.51	-0.75	0.31	-0.50	0.22	-0.25	0.21	0.00	***** 3 7.64350+6 551.7 0.0 *****																			
* 2-PHASE TORQUE DIFFERENCE TABLES										* BUILT-IN RELAP4J																			
1504900	2	1								***** CTL FLOW-F FLOW-G VELJ *****																			
1504901	0.00	0.00	0.10	0.67	0.25	0.91	0.50	1.12		***** 1 3.00 0.0 0.0 *****																			
1504902	0.75	1.28	1.00	1.34						***** CTL FLOW-F FLOW-G VELJ *****																			
1505000	2	2								***** 1 3.00 0.0 0.0 *****																			
1505100	2	3								***** TAB-D TWO-P DIF-T MOTOR TAB-S TRIP REVER *****																			
1505101	-1.00	-1.18	-0.75	-1.30	-0.50	-1.08	-0.25	-0.93		***** 150 150 150 -1 510 1 *****																			
1505102	-0.10	-0.71	0.00	0.00						***** R-SP I/R R-FL R-HD R-TOR M-IN R-DEN *****																			
1505200	2	4								***** 376.99 0.5344 0.0075 262.0 184.2 0.475 1000.0 *****																			
1505201	-1.00	-1.18	-0.75	-0.24	-0.50	-0.07	-0.25	-0.08	0.00	***** R-M-TR FR-TF2 FR-TFO FR-TF1 FR-TF3 *****																			
1505300	2	5								***** 0.0 7.56 0.001 0.0 4.2 *****																			
1505301	0.00	0.00	0.10	-0.39	0.25	-0.71	0.50	-0.71		***** ELS TM MX-R *****																			
1505302	0.75	-0.58	1.00	-0.47						***** 0.0 0.0 0.0 *****																			
1505400	2	6								***** ***** (VOLUME18,19... RELAP4J) *****																			
1505401	0.00	-0.19	0.25	-0.45	0.50	-0.55	0.75	-0.59	1.00	***** BROKEN RECIRCULATION OUTLET LINE *****																			
1505500	2	7								***** NAME TYPE *****																			
1505501	-1.00	0.51	-0.75	0.55	-0.50	0.51	-0.25	0.39	0.00	***** C220 PIPE *****																			
1505600	2	8								***** ***** NO.101 *****																			
1505601	-1.00	0.51	-0.75	0.31	-0.50	0.22	-0.25	0.21	0.00	***** ***** (VOLUME18,19... RELAP4J) *****																			

```

2451203 3 7.36500+6 551.7 0.0 0.0 3
2451204 3 7.36000+6 551.7 0.0 0.0 4
2451300 1
2451301 8.00 0.0 0.0 3
*
* *****
* QUICK SHUTT-OFF VALVE NOT USED IN THE SMALL BREAK TEST SERIES
* *****
2500000 C250 VALVE
2500101 190010000 200000000 0.0019244 2.0 2.0 0000
2500201 1 3.00 0.0 0.0
2500300 TRPVLV 513
2500301
*
* *****
* VESSEL SIDE BREAK (BRK B) (JUNCTION55 .... RELAP4J)
* *****
* NAME TYPE
* C260 VALVE
*
* FR TO AREA F-LOS R-LOS CAHS
* 2600101 190010000 550000000 19.24-4 0.0 0.0 0100
*
* CTL FLOW-F FLOW-G VELJ
* 2600201 1 0.0 0.0 0.0
*
* VALVE TYPE TRIP.NO
* 2600300 TRPVLV 502
* 2600301
*
* *****
5500000 C550 SINGLVOL
5500101 19.24-4 0.4 0.0 0.0 0.0 0.00005 0.0495 00
5500200 3 7.35346+6 511.7 0.0
*
5550000 C555 VALVE
5550101 550010000 560000000 5.391-4 0.0 0.0 0100
5550201 1 0.0 0.0 0.0
5550300 TRPVLV
5550301 502
*
5600000 C560 SINGLVOL
5600101 5.391-4 0.3 0.0 0.0 0.0 0.00005 0.0262 00
5600200 3 7.35346+6 511.7 0.0
*
5650000 C565 VALVE
5650101 560010000 280000000 5.391-4 0.0 0.0 0100
5650201 1 0.0 0.0 0.0
5650300 TRPVLV
5650301 502
*
* *****
* PUMP SIDE BREAK ( BRK A) NOT USED IN THE SMALL BREAK TEST
* *****
2700000 C270 VALVE
2700101 200000000 551000000 19.24-4 0.0 0.0 0100
2700201 1 0.0 0.0 0.0
2700300 TRPVLV
2700301 502
*
5510000 C551 SINGLVOL
5510101 19.24-4 0.4 0.0 0.0 0.0 0.00005 0.0495 00
5510200 3 7.35346+6 511.7 0.0
*
5600000 C556 VALVE
5600101 551010000 561000000 5.391-4 0.0 0.0 0100
560201 1 0.0 0.0 0.0
560300 TRPVLV
560301 502
*
5610000 C561 SINGLVOL
5610101 5.391-4 0.3 0.0 0.0 0.0 0.00005 0.0262 00
5610200 3 7.35346+6 511.7 0.0
*
5660000 C566 VALVE
5660101 561010000 281000000 5.391-4 0.0 0.0 0100
5660201 1 0.0 0.0 0.0
5660300 TRPVLV
5660301 502
*
* *****
* CONTAINMENT NAME TYPE
* C280 TMDPVOL
*
2800000
*
2800101 AREA LEN VOL HZ VR ELV ROU HYD FE
* 1.0+3 0.0 1.0+6 0.0 0.0 0.0 0.0 0.0 11
*
CTL
2800200 3
*
TIME PRESSURE TEMP
2800201 0.0 9.8043+4 303.15 * CONSTANT
*
* *****
* MAIN STEAM RESERVOIR * ENTHALPY CALCULATION
* *****
NAME TYPE
2900000 C290 TMDPVOL
*
2900101 1.0+3 0.0 1.0+6 0.0 0.0 0.0 0.0 11
*
CTL
2900200 2
*
TIME PRESSURE TEMP
2900201 0.0 7.2900+6 1.0 * CONSTANT
*
* *****
* MAIN STEAM NAME TYPE
* C300 TMDPVOL
*
3000101 FR TO AREA
* 290000000 080010000 3.141-4
*

```